Coordination chemistry of bulky alkyl substituted cyclopentadienyl and indenyl ligands with manganese, iron and cobalt

Von der Fakultät für Lebenswissenschaften

der Technischen Universität Carolo-Wilhelmina

zu Braunschweig

zur Erlangung des Grades einer

Doktorin der Naturwissenschaften

(Dr. rer. nat.)

genehmigte

D i s s e r t a t i o n

von Miyuki Maekawa
aus Tokyo / Japan

1. Referent:	Dr. Marc Daniel Walter
2. Referent:	Prof. Dr. Matthias Tamm
eingereicht am:	14.07.2014
mündliche Prüfung (Disputation) am:	10.10.2014

Druckjahr 2014

Dissertation an der Technischen Universität Braunschweig,
Fakultät für Lebenswissenschaften

Vorveröffentlichungen der Dissertation

Teilergebnisse aus dieser Arbeit wurden mit Genehmigung der Fakultät für Lebenswissenschaften, vertreten durch den Mentor der Arbeit, in folgenden Beiträgen vorab veröffentlicht:

Publikationen

Maekawa, M.; Daniliuc, C. G.; Jones, P. G.; Hohenberger, J.; Sutter, J.; Meyer, K.; Walter, M. D. Synthesis of [Cp'Fe(η^3-BH_4)] and its conversion to [Cp'Fe(BH_2)]$_3$. *Eur. J. Inorg. Chem.* **2013**, 4097–4104.

Maekawa, M.; Römelt, M.; Danilliuc, C. G.; Jones, P. G.; White, P. S.; Neese, F.; Walter, M. D. Reactivity Studies on [Cp'MnX(thf)]$_2$: Manganese Amide and Polyhydride Synthesis. *Chem. Sci.* **2012**, *3*, 2972–2979.

Maekawa, M.; Daniliuc, C. G.; Freytag, M.; Jones, P. G.; Walter, M. D. Complexes of Manganese, Iron and Cobalt with Sterically Demanding Indenyl Ligands. *Dalton Trans.* **2012**, *41*, 10317–10327.

Glöckner, A.; Bauer, H.; Maekawa, M.; Bannenberg, T.; Daniliuc, C. G.; Jones, P. G.; Sun, Y.; Sitzmann, H.; Tamm, M.; Walter, M. D. How big is a Cp? Cylcoheptatrienyl Zirconium Complexes with Bulky Cyclopentadienyl and Indenyl Ligands. *Dalton Trans.* **2012**, *41*, 6614–6624.

Tagungsbeiträge

Maekawa, M.; Daniliuc, C. G.; Jones, P. G.; Walter, M. D. Synthesis and Reactivity of [Cp'FeBH_4] (Poster). 2nd European Association for Chemical and Molecular Sciences Inorganic Chemistry Conference, Jerusalem, Israel, July 7–11, 2013.

Maekawa, M.; Daniliuc, C. G.; Freytag, M.; Jones, P. G.; Walter, M. D. Complexes of manganese, iron, and cobalt with sterically demanding indenyl ligands (Poster). 15th Jungchemikerforum Frühjahrssymposium, Berlin, Germany, March 6–9, 2013.

Maekawa, M.; Daniliuc, C. G.; Freytag, M.; Jones, P. G.; Walter, M. D. Complexes of Manganese, Iron and Cobalt with Sterically Demanding Indenyl Ligands (Vortrag). 11th Ferrocene Colloquium, Hanover, Germany, February 6–8, 2013.

Maekawa, M.; Hohenberger, J.; Sutter, J.; Meyer, K.; Daniliuc, C. G.; Jones, P. G.; White, P. S.; Walter, M. D. Reactivity of [Cp'FeI]$_2$ with pseudohalides (Poster). Japanese-German Symposium on Coordination Programming, Münster, Germany, October 25–27, 2012.

Maekawa, M.; Daniliuc, C. G.; Freytag, M.; Jones, P. G.; Walter, M. D. Complexes of manganese, iron, and cobalt with sterically demanding indenyl ligands (Poster). 16. Vortragstagung der Wöhler-Vereinigung, Göttingen, Germany, September 26–28, 2012.

Maekawa, M.; Hohenberger, J.; Sutter, J.; Meyer, K.; Daniliuc, C. G.; Jones, P. G.; White, P. S.; Walter, M. D. Reactivity of $[Cp'FeI]_2$ with pseudohalides (Poster). 244th American Chenmical Society National Meeting & Exposition, Philadelphia, USA, August 19–23, 2012.

Maekawa, M.; Daniliuc, C. G.; Freytag, M.; Jones, P. G.; Walter, M. D. Complexes of manganese, iron, and cobalt with sterically demanding indenyl ligands (Poster). 244th American Chenmical Society National Meeting & Exposition, Philadelphia, USA, August 19–23, 2012.

Maekawa, M.; Daniliuc, C. G.; Jones, P. G.; White, P. S., Walter, M. D. Reactivity of $[Cp'FeI]_2$ with pseudohalides (Poster). 8. Koordinationschemie-Treffen, Dortnund, Germany, February 26–28, 2012.

Maekawa, M.; Daniliuc, C. G.; Jones, P. G.; White, P. S., Walter, M. D. Reactivity of $[Cp'FeI]_2$ with pseudohalides (Poster). 10th Ferrocene Colloquium, Braunschweig, Germany, February 15–17, 2012.

Maekawa, M.; Daniliuc, C. G.; Jones, P. G.; White, P. S.; Walter, M. D. Reactivity of $[Cp'FeI]_2$ with pseudohalides (Vortrag). 14. Norddeutschland Doktrandenkolloquim, Walsrode, Germany, September 29–30, 2011.

Maekawa, M.; Daniliuc, C. G.; Jones, P. G.; Walter, M. D. Synthesis and Characterization of Manganese, Iron and Cobalt Complexes Containing Bulky Indenyl Ligands (Poster). 19th European Association for Chemical and Molecular Sciences Conference on Organometallic Chemistry, Toulouse, France, July 3–7, 2011.

Maekawa, M.; White, P. S.; Daniliuc, C. G.; Jones, P. G.; Walter, M. D. More Than Only Metallocenes – Low-coordinate Iron and Manganese Half-Sandwich Complexes (Poster). 13. Norddeutsches Doktorandenkolloquium, Greifswald, Germany, September 24–25, 2010.

Die vorliegende Arbeit wurde in der Zeit von Januar 2009 bis März 2010 unter Anleitung von Prof. Dr. Matthias Tamm und April 2010 bis Juli 2014 unter Anleitung von Dr. Marc D. Walter am Institut für Anorganische und Analytische Chemie der Technischen Universität Carolo-Wilhelmina zu Braunschweig angefertigt.

— 旧友へ —

Danksagung

Allen voran gilt mein aufrichtiger Dank Herrn Dr. Marc Walter. Seine stete Diskussionsbereitschaft, wissenschaftlichen Ratschläge, die kritischen und inspirierenden Fachdiskussionen sowie vor allem seine immerwährende Begeisterung für dieses Forschungsgebiet haben mich in besonderem Maße motiviert und gaben wichtige Impulse für das Voranschreiten dieser Arbeit.

Bei Herrn Prof. Dr. Matthias Tamm bedanke ich mich besonders für die Übernahme des Koreferates und für die Möglichkeit in Braunschweig zu promovieren.

Herrn Prof. Dr. Renji Okazaki möchte ich meine tiefe Dankbarkeit für seine hilfreichen Vorschläge und für das Ermutigen in schwierigen Situationen ausdrücken. Herrn Dr. Rainer Bartsch möchte ich für die Betreuung während der ersten Arbeitsphase in der präparativen anorganischen Chemie meinen Dank aussprechen.

Allen Mitarbeitern des Arbeitskreises Walter, Ann Christin Fecker, Markus Kreye und Matthias Reiners habe ich für die angenehme Arbeitsatmosphäre und unermüdliche Hilfsbereitschaft zu danken. Mein Dank geht auch allen ehemaligen und derzeitigen Mitarbeitern des Arbeitskreises Tamm für die wissenschaftlichen Gespräche. Besonders möchte ich mich hiermit bei Dr. Alexander R. Petrov, der seine Erfahrungen an mich weitergegeben und mir die präparativen Methoden beigebracht hat, für die Zusammenarbeit und für die wertvollen Ideen bedanken. Dr. Dirk Baabe und Peter Schweyen danke ich ganz herzlich für die hilfreichen Diskussionen über Mössbauer-Spektroskopie, SQUID-Magnetometrie und EPR-Spektroskopie. Òscar Àrias i Burguera, Dr. Adinarayana Doddi, Tobias Schnabel, Dr. Alain Charly Tagne Kuate und Dr. Xian Wu seien für das Korrekturlesen dieser Arbeit gedankt.

Des Weiteren möchte ich den Analytikabteilungen, den Mitarbeitern des Instituts und der Werkstätten, vor allem Herrn Prof. Dr. Jones und den Kristallographen für die Lösung zahlreicher Strukturen, Frau Dr. Ibrom und Frau Holba-Schulz für zahlreiche, technisch und zeitlich aufwendige NMR-Experimenten, Frau Miehe, Herrn Kurz, Herrn Gebhardt sowie Herrn Schröpfer für ihre kompetente Unterstützung danken.

Meinen Eltern bin ich zu großem Dank verpflichtet. Sie haben mir diese Berufsaufbildung ermöglicht und mich bei allen meinen Entscheidungen finanziell unterstützt.

It is a story of the greatest sculptor of ancient Greece, Phidias. He was commissioned around 440 b.c. to make the statues that to this day stand on the roof of the Parthenon, in Athens. They are considered among the greatest sculptures of the Western tradition, but when Phidias submitted his bill, the city accountant of Athens refused to pay it. "These statues," the accountant said, "stand on the roof of the temple, and on the highest hill in Athens. Nobody can see anything but their fronts. Yet you have charged us for sculpting them in the round – that is, for doing their back sides, which nobody can see."

"You are wrong," Phidias retorted. "The gods can see them."

Table of contents

Abbreviations

av.	average
equiv.	equivalent
cent.	centroid
M	molar
Me	methyl group
Et	ethyl group
*i*Pr	isopropyl group
*n*Bu	*n*-butyl group
*t*Bu	*tert*-butyl group
Ph	phenyl group
R	alkyl group
X	elements other than C, H and metals
ox.	oxidation
calcd	calculated
observd	observed
NMR	nuclear magnetic resonance
δ	chemical shift
ppm	parts per million
SQUID	superconducting quantum interference device
B.M.	Bohr magneton
T	temperature
K	kelvin
EPR	electron paramagnetic resonance
G	gauss
χ	molecular magnetic susceptibility
$\boldsymbol{B}$	magnetic field
T	tesla

T_{rel}	relative transmission
v	velocity
IR	infrared
T	transmittance
$\overline{\nu}$	wave number
UV-vis	ultraviolet-visible
ε	molar extinction coefficient
Norm. A	normalized absorbance
λ	wave length
i	electric current
A	ampere
E	voltage
V	volt
$E^{\circ\prime}$	redox potential
SCE	saturated calomel electrode
MS	mass spectrometry
GC	gas chromatography
EI	electron ionization / electron impact
ESI	electrospray ionization
LIFDI	liquid injection field desorption ionization

List of figures

Chapter 1.

Chapter 2.

Chapter 3.

Chapter 4.

Chapter 5.

Chapter 6.

List of schemes

Chapter 7.

List of tables

Chapter 1. Introduction

1.1 Ferrocene

Ferrocene is one of the iconic molecules in organometallic chemistry, which was independently discovered in 1951 by two research groups. Moreover, this discovery is considered as the beginning of modern organometallic chemistry.

Kealy and Pausen obtained orange crystals, which sublimed easily from the reaction of CpMgBr (Cp = C_5H_5) and $FeCl_3$ in an attempt to synthesis fulvalene (Scheme 1).[1]

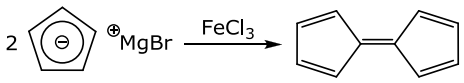

Scheme 1. The originally planned reaction of Kealy and Pausen.

Miller, Tebboth and Tremaine synthesized a yellow crystalline compound from the reaction of freshly reduced iron powder with a stream of nitrogen containing cyclopentadiene vapor at 300°C with the goal to prepare amine derivatives (Scheme 2).[2]

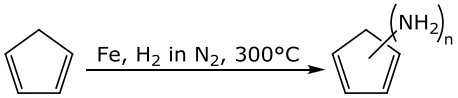

Scheme 2. The originally planned reaction of Miller, Tebboth and Tremaine.

This solid, "bis(cyclopentadienyl)iron", had notable properties and unusual stability for an organometallic compound, thus, the elucidation of its structure has attracted much attention. In 1952, Wilkinson *et al.* proposed a "sandwich" structure by IR spectroscopy,[3] while Fischer and Pfab proposed a "double cone" structure by single crystal analysis.[4] Eiland and Pepinsky also investigated crystallographically the structure of ferrocene and suggested a

sandwich structure.[5] Finally, Dunitz *et al.* confirmed the sandwich structure by a single crystal analysis.[6,7]

Wilkinson and Woodward, who were able to demonstrate the aromaticity of this new compound by electrophilic substitution reactions, proposed the name of "ferrocene" because of its similar behavior to benzene.[8]

Today, ferrocene is used not only as a ligand scaffold[9–11] especially for palladium-coupling reactions,[12] but also in various fields, *e.g.* as fuel additive,[13] in pharmaceuticals,[14,15] as catalyst for the production of carbon nanotubes,[16] or in new materials such as polymers,[17] electro-optical materials and thermotropic liquid crystals.[18] One of the reasons is that the properties of ferrocene (steric, electronic, magnetic, optical and redox) can be designed or fine tuned through the introduction of various substituents.

1.2 Metallocene

Originally, metallocenes referred to metal organic compounds in which a metal atom is placed between two parallel Cp ligands in a sandwich fashion. Thus, metallocenes are also often called sandwich compounds. Today, metallocenes can be defined as metal-organic compounds which contain two arene ligands such as cyclopentadienyl (Cp), cycloheptatrienyl or benzene, whereby the metal atom must have at least two of such ligands. In 1991 it was estimated that 80% of all organometallic complexes contain the cyclopentadienyl ligand or its substituted derivatives[19] because of their great abilities as stabilizing ligands.

Immediately after the discovery of ferrocene, Wilkinson reported the syntheses of $[Cp_2TiBr_2]$, $[Cp_2ZrBr_2]$ and $[Cp_2VCl_2]$.[20] In the following year, $[Cp_2Ni]$ and $[Cp_2Co]$,[4,21] $[Cp_2Ru]$,[22] $[Cp_2Cr]$,[23] $[Cp_2Rh]^+$ and $[Cp_2Ir]^+$ [24] were synthesized successively. Until today, metallocenes with various elements (s-elements,[25–32] p-elements,[33–45] d-elements,[24,46–74] rare-earth elements[75–82] and actinides[83–91]) were successfully synthesized and characterized. Nevertheless, metallocenes of rubidium, technetium, copper, silver and gold could not be prepared yet, although $[Cp_2Cu]$ and $[Cp_2Au]$ have been predicted by calculation.[92] Some metallocenes *e.g.* $[Cp_2Ti(CH_3)_2]$ (Petasis-reagent) and $[Cp_2Ti(\mu\text{-}CH_2)(\mu\text{-}Cl)Al(CH_3)_2]$ (Tebbe-reagent) behave as active catalysts for olefination of ketones, aldehydes, esters and lactones, and $[Cp_2TiCl_2]$, $[Cp_2ZrCl_2]$ and $[Cp_2HfCl_2]$ (Kaminsky-catalyst) for polymerization.

There are several types of metallocene complexes; such as linear and bent metallocenes,

multi-decker and half-sandwich complexes. Notably, new types of metallocenes such as *ansa*-metallocenes, open metallocenes and metallocenes with heterocycles have attracted attention because of their the reactivity. Metallocenes are often regarded as chemical "inert", although organic ring-substitution processes can occur.

1.3 Bonding in 3d-block metallocene[93]

Early on it was attempted to explain and predict the properties of metallocenes. The 18 valence electron (VE) rule can explain the high stability of ferrocene and the reactivity of cobaltocene and rhodocene to cobaltocenium- and rhodocenium-cations. The crystal field theory provides a qualitative understanding and the ligand field theory allows a quantitative prediction of properties, such as color and magnetism. However, none of the 18 VE rule, the crystal field theory and the ligand field theory can explaine the structure of metallocenes, because only the electron number is considered in the 18 VE rule, whereas only the orbital energy and the electronic count of the metal atom is taken into account in the crystal and ligand field theory.

In contrast, the molecular orbital (MO) theory can explain the structure of metallocenes. In the MO theory, as well as in the crystal or ligand field theory, interactions of the metal orbitals with the ligand orbitals are considered. When the degenerate orbitals of the metal and the ligand interact with each other, their energy levels are split and the bonding and anti-bonding MOs are formed. If no interaction occurs, the energy of the corresponding orbital does not change and a non-bonding MO is formed.

The more electrons are located in bonding MOs, the stronger the bond between the metal and the ligand, and thus the more stable is the complex. The complex with 18 VE exhibits the highest stability, because all bonding orbitals are occupied. The weak bonding character of e_{2g} and a'_{1g} MOs enables the access to metallocenes with a VE number less than 18 such as $[Cp_2Cr]$ (16 VE) and $[Cp_2V]$ (15 VE). The anti-bonding e^*_{1g} orbital with one or two electrons in cobaltocene and nickelocene explains the destabilization and the elongation of the M–Cp bond (V, 2.26 Å;[94] Cr, 2.15 Å;[95] Fe, 2.04 Å;[96] Co, 2.11 Å;[96] Ni, 2.18 Å[4]). The elongation of M–Cp bond in $[Cp_2Cr]$ and $[Cp_2V]$ can be explained by their bond order.

The MO diagram of ferrocene is shown in Figure 1. The MO diagrams of other sandwich complexes are very similar, although the individual energy levels of the orbitals differ from metal to metal.

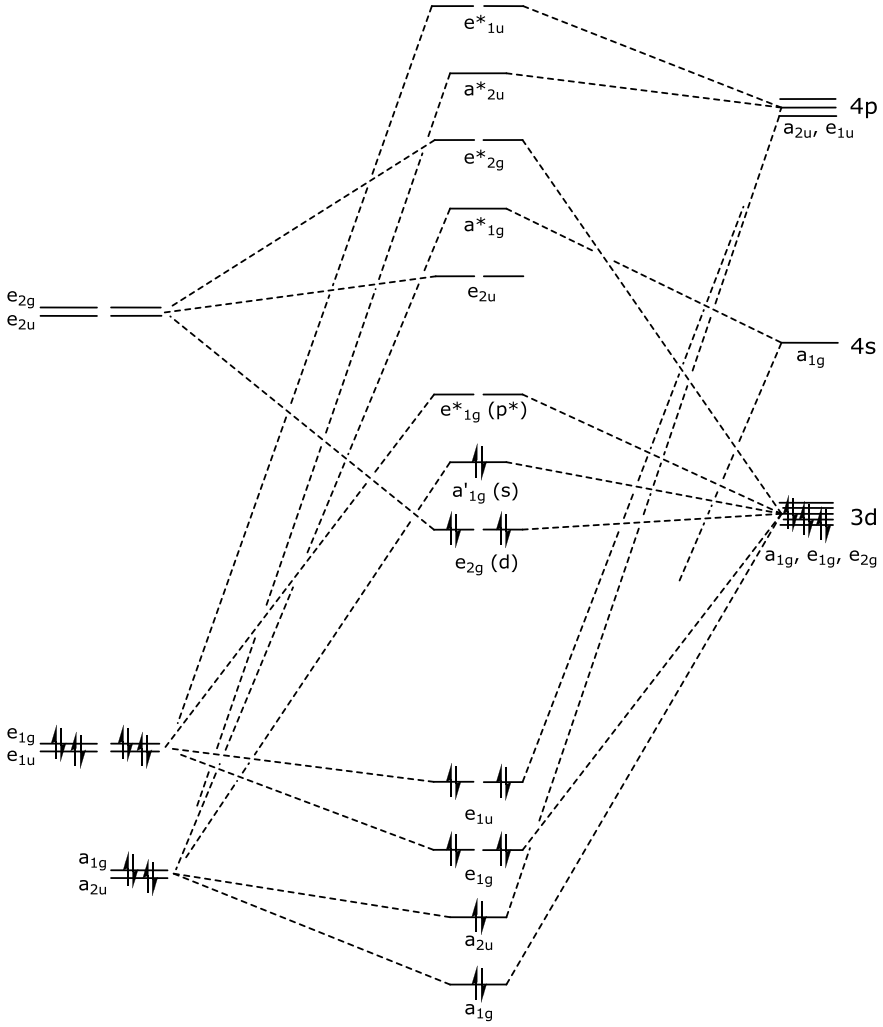

Figure 1. A quantitative MO diagram for ferrocene (D_{5d}).

1.4 *Ansa*-metallocenes

The word *ansa* means "handle" in Latin and it is used to describe a bridge between a ligand and a functional group in organometallic chemistry. *Ansa*-metallocenes are derivatives of metallocenes with an intramolecular bridge between two cyclopentadienyl rings. The first *ansa*-complexes, the *ansa*-ferrocenes showed in Figur 2 were synthesized by Lüttringhaus and Kullick in the late 1950s, and they used this term to describe $(CH_2)_n$-bridged ferrocenes.[97] The incorporation of an *ansa*-bridge changes the structure and increases the reactivity of the complex compared to the non-bridged analogues.[98–100]

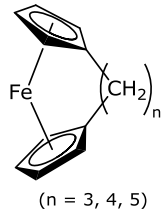

Figure 2. The first *ansa*-ferrocenes.

Today, *ansa*-metallocenes (metallocenophanes) with several metals such as hafnium,[101,102] rhenium,[103] scandium,[104] lanthanids,[105] vanadium[106] and chromium[107] were synthesized. Above all, titanium[108–113] and zirconium[101,114–118] complexes were the main focus. Although some homoleptic analogues *e.g. ansa*-hafnocenophane is able to cleave the dinitrogen and to functionalize it,[119] recent research in this area has shifted from homoleptic to heteroleptic species. Some metallocenophanes such as Me_2Si- and tBu_2Sn-bridged [1]troticenophane undergo thermal ring-opening polymerizations (ROP) to give polymers with transition metals in the polymer backbone (Scheme 3).[109,112]

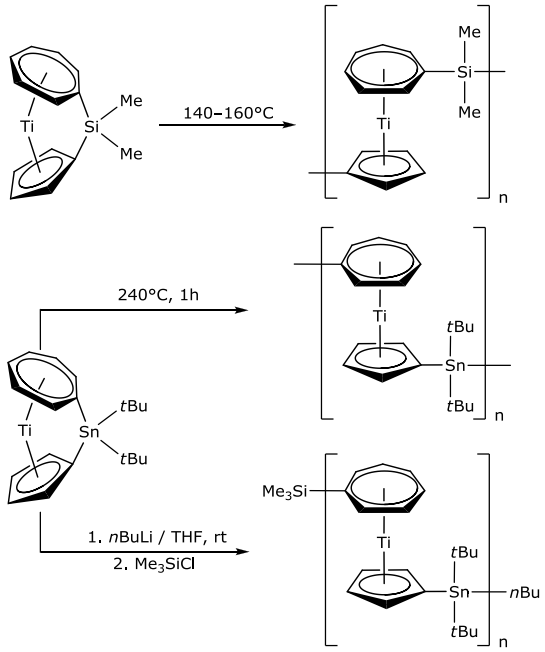

Scheme 3. The ROP of Si- (top) and Sn-bridged (bottom) *ansa*-troticenes.

The half-sandwich *ansa*-complexes are also accessible, *e.g.* tungsten half-sandwich

ansa-complexes[120] and iron half-sandwich *ansa*-complexes are known.[121] More specifically, a half-sandwich *ansa*-complex with an amido group is commonly called a constrained geometry complex. Both metallocenophanes and constrained geometry complexes are promising homogeneous catalyst precursors for the stereoselective polymerization of propene, ethylene and α-olefins.[122–124]

1.5 Open metallocenes

Besides Cp ligands, allyl ligands play an important role in organometallic chemistry. Pentadienyl ligands combine properties of the Cp and allyl ligands. Since the pentadienyl can be considered to be "opened" cyclopentadienyl ligands (Figure 3), metallocenes with pentadienyl ligands instead of Cp derivatives are called "open" metallocenes.

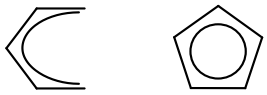

Figure 3. "Open" and "closed" pentadienyl ligands.

While the cyclopentadienyl ligand is one of the most widely used ligand in organometallic chemistry, the pentadienyl ligand is often employed in synthetic and catalytic applications[125] because of its noteworthy properties: an open Cp exhibits a shorter metal-ligand plane distance than a normal Cp, and as shown in Figure 4, can adopt κ*C*-, η^3- and η^5-coordination modes.

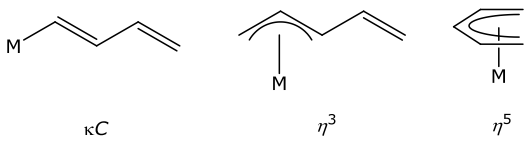

Figure 4. κ*C*, η^3 and η^5 coordination modes of the pentadienyl ligands.

Pentadienyls adopt an intermediate position between the allyl and the cyclopentadienyl

systems because of its binding modes, and their coordination chemistry with transition metals has been well established.[126–129] Recently, the coordination chemistry of enantiomerically pure pentadienyl ligands with early to late transition metals (M = Ti, V, Cr, Fe, Ir)[130] and open-metallocenes with the heavy alkaline-earth metals (M = Ca, Sr, Ba) were presented.[131]

An important pentadienyl subclass is the so-called edge-bridged open cyclopentadienyls, which have properties in between those of pentadienyl and cyclopentadienyl ligands, have also been used to prepare half-open trozircenes[132,133] and some iron and ruthenium complexes.[134]

1.6 Metallocenes with heterocycles

Replacing a CH group of the Cp by an electronically isovalence and isolobal group 15 element such as N, P, As, Sb or Bi, the resulting ligands behave differently from the original Cp ligand.

The first pyrrolyl complexes of iron and manganese were reported shortly after the discovery of ferrocene.[135,136] However, the pyrrolyl ligand acts as a highly flexible ligand that can readily undergo η^5–κ*N* haptotropic shifts, which makes bis(pyrrolyl)ferrocene instable and its synthesis very difficult.[137–140] The first stable diazaferrocene[141] and the first diphosphaferrocene[142] are illustrated in Figure 5.

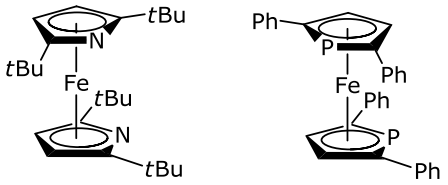

Figure 5. The first diazaferrocene and the first diphosphaferrocene.

In the early 1990s Kuhn *et al.* introduced several sterically encumbered pyrrolyls derivatives. Increasing the steric demand at the 2,5-positions of the pyrrolyl ligand and provided sufficient effective blocking of the κ*N* coordination mode to isolate its metal complexes. For instance, 2,5-di-*tert*-butyl pyrrolyl ligand (2,5-$(Me_3C)_2C_4H_2N$) has been used for the synthesis

of transition-,[141,143–147] rare-earth-,[148–151] and main-group-metal complexes.[152–155] Concerning their applications, the organometallic pyrrolyl derivatives are also relevant for the hydrodenitrogenation processes,[156,157] while a chromium pyrrolyl complex are active catalysts for the selective ethylene trimerization.[147] Although the research of pyrrolyl complexes with several metals[158–160] and phospholyl iron complexes[161–163] are being expanded now, the metal complexes with other heterocycle derivatives such as arsolyl (C_4H_4As), stibolyl (C_4H_4Sb) and bismolyl (C_4H_4Bi) ligands have been theoretical predicted,[164] synthesized and their structure and electrochemical property compared by Elschenbroich.[165,166] However, the heterocyclic derivatives have not been extensively investigated.

1.7 Half-sandwich complexes

Half-sandwich complexes contain only one Cp ligand which is bound in η^5-fashion, and the other coordination sites are occupied by other ligands e.g. CO or halides. These compounds are also referred to as piano-stool complexes due to their shape. Cp carbonyl complexes such as $[CpV(CO)_4]$, $[CpMn(CO)_3]$, $[CpCo(CO)_2]$ and [CpNi(CO)][167] are typical examples for this compound class and some of them are applied in industrial processes: $[(CH_3C_5H_4)Mn(CO)_3]$ as an antiknock agent[168,169] or $[CpCo(CO)_2]$ as a catalyst for the pyridine synthesis.[170–173]
The metal atoms in the half-sandwich complexes are often "coordinatively unsaturated", *i.e.* the half-sandwich complexes are often non-18 VE complexes, and thus unusual reactivities are expected as "coordinatively saturated" *i.e.* 18 VE complexes. The study in the reactivity of group 8 half-sandwich complexes is mainly based on the Cp*Ru-fragment, *e.g.* $[Cp^*Ru(ER)]_2$ or [Cp*Ru(ER)L],[174] and have shown to oligomerize to compensate the lack of valence electrons in the metal-centered bonding orbital. They exhibit different reactivity from corresponding ruthenocenes, which are 18 VE complexes. For instance, the Cp* ruthenium clusters show a series of interesting reactions,[175–178] above all, its polyhydride cluster can cleave the nitrogen-nitrogen single[179,180] and double[181] bond of hydrazine derivatives effectively and catalytically (Scheme 4).

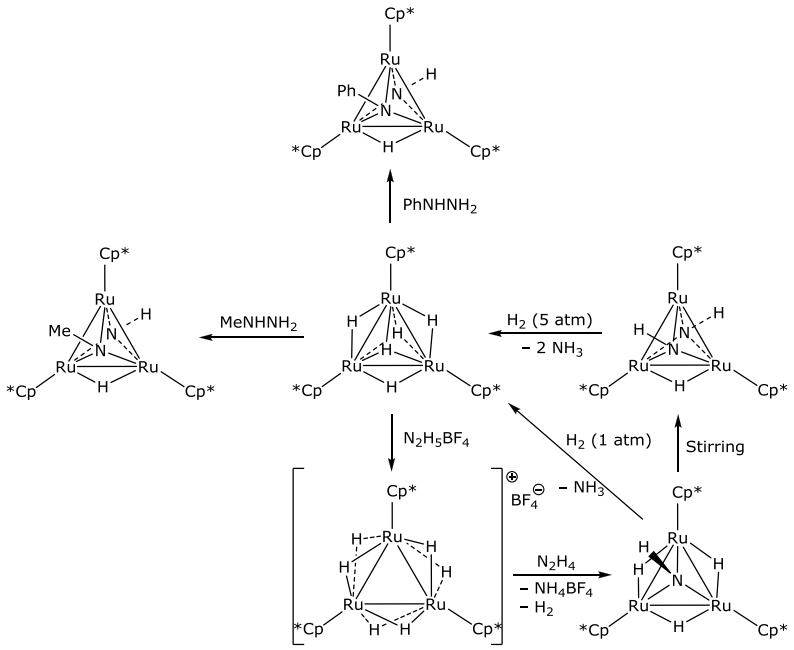

Scheme 4. The nitrogen-nitrogen bond cleavage cycle of Cp*Ru cluster.

1.8 Sterically demanding Cp ligands

In general, the introduction of substituents on the cyclopentadienyl ring can influence the steric and the electronic properties, *e.g.* chirality, solubility, stability or reactivity, the electron donor character or the spectral properties. Furthermore, sterically demanding ligands allow the isolation or the stabilization of thermodynamically unstable species and this is a common and well-established concept. For example, palladocene[67] and platinocene[66] are only accessible with sterically demanding Cp ligands such as pentamethylcyclopentadienyl (Cp*). Furthermore, the sterically demanding substituent in metallocene plays an important role in the investigation of ring rotation dynamics, because the bulky ligands are more likely to lock the Cp ring in certain positions.

Some bulky Cp derivatives such as Cp^{PRO} (C_5Ph_5), Cp^{bn} ($C_5(CH_2Ph)_5$), Cp^{BIG} ($C_5(4\text{-}n\text{BuC}_6H_4)_5$), ^4Cp ($((CH_3)_2CH)_4C_5H$) and ^5Cp ($C_5((CH_3)_2CH)_5$) are known and several complexes containing these ligands were prepared and characterized.

Cp^{PRO} and Cp^{bn} ligands are shown in Figure 6. Cp^{PRO} is known for about 90 years[182] but an improved synthesis was only published in 1986,[183] and Tikkanen *et al.* introduced the abbreviation "Cp^{PRO}" for this ligand.[184,185] The first metallocene with this ligand was a molybdocene reported in 1964 by Hübel and Merényi, in which Cp^{PRO} was formed as a

rearrangement product from diphenylacetylene.[51] The first intended synthesis of a Cp^{PRO} containing complex was reported by Wilke *et al.* in 1973.[186] Later, other sandwich complexes (Fe,[187] Sn,[188] Ge,[189] and Pb[190]) were also synthesized and characterized. Notably, Cp^{PRO} half-sandwich ruthenium complexes [$Cp^{PRO}Ru(CO)_2L$] (L = Cl or OtBu) exhibit catalytic activity for conversion of racemic *sec*-alcohols into enantiomerically pure acetates[191–193] and racemization of *sec*-alcohols.[194–197]

Cp^{bn} is also known for more than 30 years,[198] and germanocenes and stannocenes with this ligand can be stored in air for days or weeks without decomposition,[38,39] while their Cp or even Cp* analogues are unstable toward H_2O and O_2.[35–37,41,42] This ligand was also applied to stabilize the phosphaferrocene [(η^5-Cp^{bn})Fe(η^5-P_5)].[163]

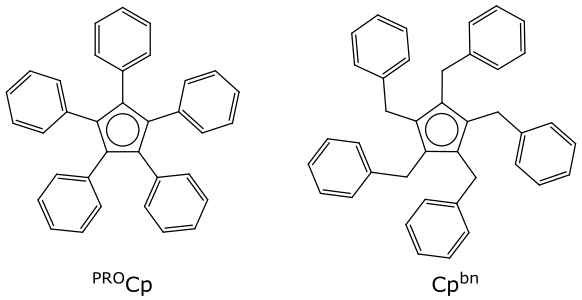

Figure 6. Cp^{PRO} (left) and Cp^{bn} (right) ligands.

Harder and coworkers have used the relatively new Cp^{BIG} ligand, which was first prepared in 2000[199] and shown in Figure 7, for the synthesis of metallocenes containing s-elements (K,[200] Ca,[201] Ba and Sr[202]), lanthanides (Eu,[43] Yb and Sm[201,203]) and p-elements (Ge[40] and Sn[43]) with Cp^{BIG}. Unfortunately, the synthesis of [$Cp^{BIG}{}_2Mg$] failed.[202] Some of these complexes exhibit interesting properties, such as the extraordinary luminescence of [$Cp^{BIG}{}_2Eu$].[204] The manganese complex [{$Cp^{BIG}Mn(CO)_2$}$_2$(P_4)] also shows an interesting reactivity.[205]

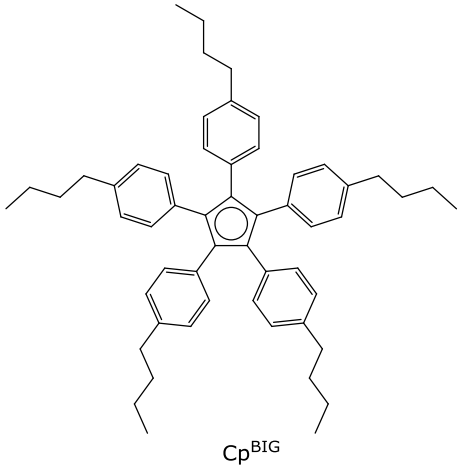

Figure 7. Cp^{BIG} ligand.

On the other hand, sterically demanding Cp derivatives without phenyl rings such as ^{4}Cp and ^{5}Cp are also employed[206,207] to stabilize nickel[208] and iron[209] half-sandwich complexes (Figure 8). The reactivity of $[^{4}CpFeBr]_2$,[208,210] $[^{5}CpFeBr(dme)]_2$[211] and $[^{4}CpNiBr]_2$[212,213] has been explored.

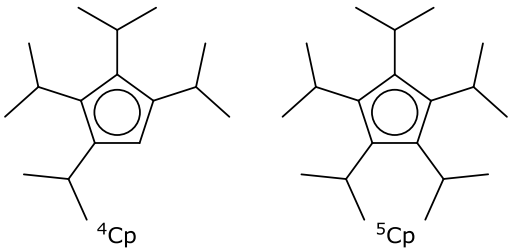

Figure 8. ^{4}Cp and ^{5}Cp ligands.

1.9 Objective

In this dissertation, the synthesis and reactivity of 1,2,4-$(Me_3C)_3C_5H_2$ (Cp') half-sandwich complexes of manganese, iron and cobalt will be investigated.

Today, iron is recognized as an attractive starting material in organometallic chemistry because of its low toxicity and high abundance. The application of iron complexes in organic synthesis and catalysis is becoming more and more important.[214–216]

Generally, low-coordinate, open shell mono(cyclopentadienyl) iron complexes have not been

explored extensively and will deserve special attention in this work, since they conceal various reactivities and may provide valuable contributions to various fields such as in material science, in theoretical and spectroscopic studies, for the development of new synthetic methods and in catalytic reactions. Some of these possible features and applications will be explored, partly using advanced analytic techniques such as Mössbauer and SQUID magnetometer.

Due to its advantages, the sterically demanding Cp' ligand has been chosen for the complexes studied in this project. On the one hand, it is easily synthesized in acceptable yield compared to the other sterically demanding Cp derivatives like Cp^{PRO}, Cp^{bn}, Cp^{BIG}, ^{4}Cp and ^{5}Cp, and it is also sufficiently sterically demanding to enable kinetic stabilization, *i.e.* to avoid metallocene formation. On the other hand, the ^{1}H NMR signals for this ligand can unambiguously be identified, which is especially helpful in paramagnetic compounds.

1.10 References

(1) Kealy, T. J.; Pauson, P. L. *Nature* **1951**, *168*, 1039–1040.

(2) Miller, S. A.; Tebboth, J. A.; Tremaine, J. F. *J. Chem. Soc.* **1952**, 632–635.

(3) Wilkinson, G.; Rosenblum, M.; Whiting, M. C.; Woodward, R. B. *J. Am. Chem. Soc.* **1952**, *74*, 2125–2126.

(4) Fischer, E. O.; Pfab, W. *Z. Naturforsch.* **1952**, *7b*, 377–379.

(5) Eiland, P. F.; Pepinski, R. *J. Am. Chem. Soc.* **1952**, *74*, 4971.

(6) Dunitz, J. D.; Orgel, L. E. *Nature* **1953**, *171*, 121–122.

(7) Dunitz, J. D.; Orgel, L. E.; Rich, A. *Acta Cryst.* **1956**, *9*, 373–375.

(8) Woodward, R. B.; Rosenblum, M.; Whiting, M. C. *J. Am. Chem. Soc.* **1952**, *74*, 3458–3459.

(9) Buergler, J. F.; Togni, A. *Organometallics* **2011**, *30*, 4742–4750.

(10) Madalska, M.; Lönnecke, P.; Hey-Hawkins, E. *Organometallics* **2013**, *32*, 2019–2025.

(11) Madalska, M.; Lönnecke, P.; Ivanovski, V.; Hey-Hawkins, E. *Organometallics* **2013**, *32*, 5852–5861.

(12) Nataro, C.; Fosbenner, S. M. *J. Chem. Educ.* **2009**, *86*, 1412.

(13) Chao, T. S.; Owston, E. H. Iron-containing motor fuel compositions and method for using same. US Patent 4,104,136, Aug. 1, 1978.

(14) Top, S.; Dauer, B.; Vaissermann, J.; Jaouen, G. *J. Organomet. Chem.* **1997**, *541*, 355–361.

(15) Top, S.; Vessières, A.; Leclercq, G.; Quivy, J.; Tang, J.; Vaissermann, J.; Huché, M.; Jaouen, G. *Chem. Eur. J.* **2003**, *9*, 5223–5236.

(16) Conroy, D.; Moisala, A.; Cardoso, S.; Windle, A.; Davidson, J. *Chem. Eng. Sci.* **2010**, *65*, 2965–2977.

(17) Liu, W.; Xu, Q.; Ma, Y.; Liang, Y.; Dong, N.; Guan, D. *J. Organomet. Chem.* **2001**, *625*, 128–131.

(18) *Ferrocenes: Ligands, Materials and Biomolecules*; Petr Štěpnička, Ed.; John Wiley & Sons, Ltd: West Sussex, 2008.

(19) Janiak, C.; Schumann, H. *Adv. Organomet. Chem.* **1991**, *33*, 291–393.

(20) Wilkinson, G. *J. Am. Chem. Soc.* **1952**, *74*, 6146–6147.

(21) Pfab, W.; Fischer, E. O. *Z. Anorg. Allg. Chem.* **1953**, *274*, 316–322.

(22) Wilkinson, G.; Pauson, P. L.; Birmingham, J. M.; Cotton, F. A. *J. Am. Chem. Soc.* **1953**, *75*, 1011–1012.

(23) Fischer, E. O.; Hafner, W. *Z. Naturforsch.* **1953**, *8b*, 444–445.

(24) Cotton, F. A.; Whipple, R. O.; Wilkinson, G. *J. Am. Chem. Soc.* **1953**, *75*, 3586–3587.

(25) Harder, S.; Prosenc, M. H. *Angew. Chem. Int. Ed. Engl.* **1994**, *33*, 1744–1746.

(26) Dinnebier, R. E.; Behrens, U.; Olbrich, F. *Organometallics* **1997**, *16*, 3855–3858.

(27) Harder, S.; Prosenc, M. H. *Angew. Chem. Int. Ed. Engl.* **1996**, *35*, 97–99.

(28) Del Mar Conejo, M.; Fernández, R.; Gutiérrez-Puebla, E.; Monge, Á.; Ruiz, C.; Carmona, E. *Angew. Chem. Int. Ed.* **2000**, *39*, 1949–1951.

(29) Fischer, E. O.; Hafner, W. *Z. Naturforsch.* **1954**, *9b*, 503–504.

(30) Pinkus, A. G. *J. Chem. Educ.* **1978**, *55*, 704.

(31) Fischer, E. O.; Stölzle, G. *Chem. Ber.* **1961**, *94*, 2187–2193.

(32) Andersen, R. A.; Blom, R.; Boncella, J. M.; Burns, C. J.; Volden, H. V. *Acta Chem. Scand.* **1987**, *41a*, 24–35.

(33) Jutzi, P. *J. Organomet. Chem.* **1990**, *400*, 1–17.

(34) Beswick, M. A.; Palmer, J. S.; Wright, D. S. *Chem. Soc. Rev.* **1998**, *27*, 225–232.

(35) Jutzi, P.; Kohl, F.; Hofmann, P.; Krüger, C.; Tsay, Y. *Chem. Ber.* **1980**, *113*, 757–769.

(36) Grenz, M.; Hahn, E.; du Mont, W.-W.; Pickardt, J. *Angew. Chem. Int. Ed. Engl.* **1984**, *23*, 61–63.

(37) Scibelli, J. V.; Curtis, M. D. *J. Am. Chem. Soc.* **1973**, *95*, 924–925.

(38) Schumann, H.; Janiak, C.; Hahn, E.; Loebel, J.; Zuckerman, J. J. *Angew. Chem. Int. Ed. Engl.* **1985**, *24*, 773.

(39) Schumann, H.; Janiak, C.; Hahn, E.; Kolax, C.; Loebel, J.; Rausch, M. D.; Zuckerman, J. J.; Heeg, M. J. *Chem. Ber.* **1986**, *119*, 2656–2667.

(40) Naglav, D.; Tobey, B.; Harder, S.; Schnepf, A. *Z. Anorg. Allg. Chem.* **2013**, *639*, 354–359.

(41) Fischer, E. O.; Grubert, H. *Z. Naturforsch.* **1956**, *11b*, 423–424.

(42) Dave, L. D.; Evans, D. F.; Wilkinson, G. *J. Chem. Soc.* **1959**, 3684–3688.

(43) Harder, S.; Naglav, D.; Schwerdtfeger, P.; Nowik, I.; Herber, R. H. *Inorg. Chem.* **2014**, *53*, 2188–2194.

(44) Fischer, E. O.; Grubert, H. *Z. Anorg. Allg. Chem.* **1956**, *286*, 237–242.

(45) Shapiro, P. J.; Lee, S.-J.; Perrotin, P.; Cantrell, T.; Blumenfeld, A.; Twamley, B. *Polyhedron* **2005**, *24*, 1366–1381.

(46) Friedman, L.; Irsa, A. P.; Wilkinson, G. *J. Am. Chem. Soc.* **1955**, *77*, 3689–3692.

(47) Birmingham, J. M.; Fischer, A. K.; Wilkinson, G. *Naturwissenschaften* **1955**, *42*, 96.

(48) Hitchcock, P. B.; Kerton, F. M.; Lawless, G. A. *J. Am. Chem. Soc.* **1998**, *120*, 10264–10265.

(49) Smirnov, A. S.; Alad'in, A. A.; Tatarnikov, A. N.; Kabarova, N. J. Method of synthesis of metallocene halides. Russian patents RU 2184739 C1, 2001.

(50) Hillman, M.; Weiss, A. J. *J. Organomet. Chem.* **1972**, *42*, 123–128.

(51) Hübel, W.; Merényi, R. *J. Organomet. Chem.* **1964**, *2*, 213–221.

(52) Hartwig, J. F.; He, X. *Angew. Chem. Int. Ed. Engl.* **1996**, *35*, 315–317.

(53) Francis, B. R.; Green, M. L. H.; Roberts, G. G. *J. Chem. Soc. D* **1971**, 1290.

(54) Green, M. L. H.; Knowles, P. J. *J. Chem. Soc. A* **1971**, 1508–1511.

(55) Thomas, J. L. *J. Am. Chem. Soc.* **1973**, *95*, 1838–1848.

(56) Wilkinson, G. *J. Am. Chem. Soc.* **1954**, *76*, 209–211.

(57) Wilkinson, G.; Birmingham, J. M. *J. Am. Chem. Soc.* **1954**, *76*, 4281–4284.

(58) Hill, J. N.; Perutz, R. N.; Rooney, A. D. *J. Phys. Chem.* **1995**, *99*, 531–537.

(59) Wilkinson, G.; Birmingham, J. M. *J. Am. Chem. Soc.* **1955**, *77*, 3421–3422.

(60) Fischer, E. O.; Grubert, H. *Chem. Ber.* **1959**, *92*, 2302–2309.

(61) Bobyens, J. C. A.; Levendis, D. C.; Bruce, M. I.; Williams, M. L. *J. Crystallogr. Spectrosc. Res.* **1986**, *16*, 519–524.

(62) Wilkinson, G.; Pauson, P. L.; Cotton, F. A. *J. Am. Chem. Soc.* **1954**, *76*, 1970–1974.

(63) El Murr, N.; Sheats, J. E.; Geiger, W. E.; Holloway, J. D. L. *Inorg. Chem.* **1979**, *18*, 1443–1446.

(64) Wilson, R. J.; Warren, L. F.; Hawthorne, M. F. *J. Am. Chem. Soc.* **1969**, *91*, 758–759.

(65) Werner, H.; Kraus, H.-J. *Angew. Chem. Int. Ed. Engl.* **1979**, *18*, 948–949.

(66) Gusev, O. V.; Peganova, T. A.; Peterleitner, M. G.; Peregudova, S. M.; Denisovich, L. I.; Ustynyuk, N. A.; Maitlis, P. M. *J. Organomet. Chem.* **1994**, *480*, C16–C17.

(67) Gusev, O. V.; Morozova, L. N.; Peterleitner, M. G.; Peregudova, S. M.; Petrovskii, P. V.; Ustynyuk, N. A.; Maitlis, P. M. *J. Organomet. Chem.* **1996**, *509*, 95–99.

(68) Budzelaar, P. H. M.; Boersma, J.; van der Kerk, G. J. M.; Spek, A. L.; Duisenberg, A. J. M. *J. Organomet. Chem.* **1985**, *281*, 123–130.

(69) Haaland, A.; Samdal, S.; Tverdova, N. V.; Girichev, G. V.; Giricheva, N. I.; Shlykov, S. A.; Garkusha, O. G.; Lokshin, B. V. *J. Organomet. Chem.* **2003**, *684*, 351–358.

(70) Cummins, C. C.; Schrock, R. R.; Davis, W. M. *Organometallics* **1991**, *10*, 3781–3785.

(71) Blom, R.; Stølevik, R.; Seip, R.; Volden, H. V.; Gundersen, S.; Lehrich, F.; Nielsen, C. J.; Powell, D. L.; Trætteberg, M. *Acta Chem. Scand.* **1988**, *42a*, 445–453.

(72) Fischer, E. O.; Hofmann, H. P.; Treiber, A. *Z. Naturforsch.* **1969**, *14b*, 599–600.

(73) Maslowsky, E.; Nakamoto, K. *Inorg. Chem.* **1969**, *8*, 1108–1113.

(74) Lorberth, J. *J. Organomet. Chem.* **1969**, *19*, 189–190.

(75) Wilkinson, G.; Birmingham, J. M. *J. Am. Chem. Soc.* **1954**, *76*, 6210.

(76) Birmingham, J. M.; Wilkinson, G. *J. Am. Chem. Soc.* **1956**, *78*, 42–44.

(77) Fischer, E. O.; Fischer, H. *J. Organomet. Chem.* **1965**, *3*, 181–187.

(78) Evans, W. J.; Hughes, L. A.; Hanusa, T. P. *J. Am. Chem. Soc.* **1984**, *106*, 4270–4272.

(79) Calderazzo, F.; Pappalardo, R.; Losi, S. *J. Inorg. Nucl. Chem.* **1966**, *28*, 987–999.

(80) Evans, W. J.; Hughes, L. A.; Hanusa, T. P. *Organometallics* **1986**, *5*, 1285–1291.

(81) Watt, G. W.; Gillow, E. W. *J. Am. Chem. Soc.* **1969**, *91*, 775–776.

(82) Evans, W. J.; Bloom, I.; Hunter, W. E.; Atwood, J. L. *J. Am. Chem. Soc.* **1981**, *103*, 6507–6508.

(83) Fischer, E. O.; Treiber, A. *Z. Naturforsch.* **1962**, *17b*, 276.

(84) Baumgärtner, F.; Fischer, E. O.; Kanellakopulos, B.; Laubereau, P. G. *Angew. Chem. Int. Ed. Engl.* **1969**, *8*, 202.

(85) Fischer, E. O.; Hristidu, Y. *Z. Naturforsch.* **1962**, *17b*, 275–276.

(86) Baumgärtner, F.; Fischer, E. O.; Kanellakopulos, B.; Laubereau, P. G. *Angew. Chem. Int. Ed. Engl.* **1968**, *7*, 634.

(87) Baumgärtner, F.; Fischer, E. O.; Kanellakopulos, B.; Laubereau, P. G. *Angew. Chem. Int. Ed. Engl.* **1965**, *4*, 878.

(88) Baumgärtner, F.; Fischer, E. O.; Kanellakopulos, B.; Laubereau, P. G. *Angew. Chem. Int. Ed. Engl.* **1966**, *5*, 134–135.

(89) Laubereau, P. G.; Burns, J. H. *Inorg. Nucl. Chem. Lett.* **1970**, *6*, 59–63.

(90) Laubereau, P. G. *Inorg. Nucl. Chem. Lett.* **1970**, *6*, 611–616.

(91) Laubereau, P. G.; Burns, J. H. *Inorg. Chem.* **1970**, *9*, 1091–1095.

(92) Carrascal, D.; Fernández-Seivane, L.; Ferrer, J. *Phys. Rev. B* **2009**, *80*, 184415.

(93) Mehrotra, R. C.; Singh, A. *Organometallic Chemistry: A Unified Approach*; Wiley-Interscience, 1991.

(94) Rogers, R. D.; Atwood, J. L.; Foust, D.; Rausch, M. D. *J. Cryst. Mol. Struct.* **1981**, *11*, 183–188.

(95) Flower, K. R.; Hitchcock, P. B. *J. Organomet. Chem.* **1996**, *507*, 275–277.

(96) Antipin, M. Y.; Boese, R.; Augart, N.; Schmid, G. *Struct. Chem.* **1993**, *4*, 91–101.

(97) Kreutzkamp, N.; Schindler, H.; Genser, M. *Angew. Chem.* **1958**, *70*, 438–438.

(98) Hughes, D. L.; Lazarowych, N. J.; Maguire, M. J.; Morris, R. H.; Richards, R. L. *J. Chem. Soc., Dalton Trans.* **1995**, 5–15.

(99) Chernega, A.; Cook, J.; Green, M. L. H.; Labella, L.; Simpson, S. J.; Souter, J.; Stephens, A. H. H. *J. Chem. Soc., Dalton Trans.* **1997**, *4*, 3225–3244.

(100) Conway, S. L. J.; Dijkstra, T.; Doerrer, L. H.; Green, J. C.; Green, M. L. H.; Stephens, A. H. H. *J. Chem. Soc., Dalton Trans.* **1998**, 2689–2696.

(101) Alt, H. G.; Jung, M. *J. Organomet. Chem.* **1998**, *568*, 127–131.

(102) Izmer, V. V.; Agarkov, A. Y.; Nosova, V. M.; Kuz'mina, L. G.; Howard, J. A. K.; Beletskaya, I. P.; Voskoboynikov, A. Z. *J. Chem. Soc., Dalton Trans.* **2001**, 1131–1136.

(103) Conway, S. L. J.; Doerrer, L. H.; Green, J. C.; Green, M. L. H.; Scottow, A.; Stephens, A. H. H. *J. Chem. Soc., Dalton Trans.* **2000**, *2*, 329–333.

(104) Fontaine, F.-G.; Tilley, T. D. *Organometallics* **2005**, *24*, 4340–4342.

(105) Paolucci, G.; Vignola, M.; Formenti, S.; Massa, W. *Eur. J. Inorg. Chem.* **2005**, 3472–3478.

(106) Honzíček, J.; Paláčková, H.; Císařová, I.; Vinklárek, J. *J. Organomet. Chem.* **2006**, *691*, 202–207.

(107) Braunschweig, H.; Breher, F.; Capper, S.; Dück, K.; Fuß, M.; Jimenez-Halla, J. O. C.; Krummenacher, I.; Kupfer, T.; Nied, D.; Radacki, K. *Chem. Eur. J.* **2013**, *19*, 270–281.

(108) Tamm, M.; Kunst, A.; Bannenberg, T.; Herdtweck, E.; Sirsch, P.; Elsevier, C. J.; Ernsting, J. M. *Angew. Chem. Int. Ed.* **2004**, *43*, 5530–5534.

(109) Tamm, M.; Kunst, A.; Herdtweck, E. *Chem. Commun.* **2005**, 1729–1731.

(110) Tamm, M.; Kunst, A.; Bannenberg, T.; Randoll, S.; Jones, P. G. *Organometallics* **2007**, *26*, 417–424.

(111) Braunschweig, H.; Fuss, M.; Kupfer, T.; Radacki, K. *J. Am. Chem. Soc.* **2011**, *133*, 5780–5783.

(112) Tagne Kuate, A. C.; Daniliuc, C. G.; Jones, P. G.; Tamm, M. *Eur. J. Inorg. Chem.* **2012**, 1727–1733.

(113) Tagne Kuate, A. C.; Alexandru, M.; Freytag, M.; Racles, C.; Cazacu, M.; Jones, P. G.; Tamm, M. *J. Organomet. Chem.* **2014**, *751*, 628–637.

(114) Noh, S. K.; Kim, S.; Lee, D.; Yoon, K.; Lee, H. *Bull. Korean Chem. Soc.* **1997**, *18*, 618–622.

(115) Lee, H.; Hascall, T.; Desrosiers, P. J.; Parkin, G. *J. Am. Chem. Soc.* **1998**, *120*, 5830–5831.

(116) Antiñolo, A.; López-Solera, I.; Orive, I.; Otero, A.; Prashar, S.; Rodríguez, A. M.; Villaseñor, E. *Organometallics* **2001**, *20*, 71–78.

(117) Antiñolo, A.; Fernández-Galán, R.; Gallego, B.; Otero, A.; Prashar, S.; Rodríguez, A. M. *Eur. J. Inorg. Chem.* **2003**, 2626–2632.

(118) Büschel, S.; Daniliuc, C. G.; Jones, P. G.; Tamm, M. *Acta Cryst.* **2010**, *C66*, m86–m88.

(119) Knobloch, D. J.; Lobkovsky, E.; Chirik, P. J. *Nat. Chem.* **2010**, *2*, 30–35.

(120) Bera, H.; Braunschweig, H.; Dörfler, R.; Kupfer, T.; Radacki, K.; Seeler, F. *Organometallics* **2010**, *29*, 5111–5120.

(121) Braunschweig, H.; Dörfler, R.; Mies, J.; Radacki, K.; Schmitt, M. *J. Organomet. Chem.* **2012**, *699*, 26–30.

(122) Möhring, P. C.; Coville, N. J. *J. Organomet. Chem.* **1994**, *479*, 1–29.

(123) Brintzinger, H. H.; Fischer, D.; Mülhaupt, R.; Rieger, B.; Waymouth, R. M. *Angew. Chem. Int. Ed. Engl.* **1995**, *34*, 1143–1170.

(124) Braunschweig, H.; Breitling, F. M. *Coord. Chem. Rev.* **2006**, *250*, 2691–2720.

(125) Hartwig, J. *Organotransition Metal Chemistry: From Bonding to Catalysis*; University Science books, 2009.

(126) Ernst, R. D. *Acc. Chem. Res.* **1985**, *18*, 56–62.

(127) Powell, P. *Adv. Organomet. Chem.* **1986**, *26*, 125–164.

(128) Ernst, R. D. *Chem. Rev.* **1988**, *88*, 1255–1291.

(129) Stahl, L.; Ernst, R. D. *Adv. Organomet. Chem.* **2007**, *55*, 137–199.

(130) Fecker, A. C.; Glöckner, A.; Daniliuc, C. G.; Freytag, M.; Jones, P. G.; Walter, M. D. *Organometallics* **2013**, *32*, 874–884.

(131) Reiners, M.; Fecker, A. C.; Freytag, M.; Jones, P. G.; Walter, M. D. *Dalton Trans.* **2014**, *43*, 6614–6617.

(132) Glöckner, A.; Bannenberg, T.; Tamm, M.; Arif, A. M.; Ernst, R. D. *Organometallics* **2009**, *28*, 5866–5876.

(133) Glöckner, A.; Arif, A. M.; Ernst, R. D.; Bannenberg, T.; Daniliuc, C. G.; Jones, P. G.; Tamm, M. *Inorg. Chim. Acta* **2010**, *364*, 23–29.

(134) Volbeda, J.; Daniliuc, C. G.; Jones, P. G.; Tamm, M. *Organometallics* **2013**, *32*, 5918–5925.

(135) Joshi, K. K.; Pauson, P. L.; Qazi, A. R.; Stubbs, W. H. *J. Organomet. Chem.* **1964**, *1*, 471–475.

(136) King, R. B.; Bisnette, M. B. *Inorg. Chem.* **1964**, *3*, 796–800.

(137) Seel, F.; Sperber, V. *Angew. Chem. Int. Ed. Engl.* **1968**, *7*, 70.

(138) Seel, F.; Sperber, V. *J. Organomet. Chem.* **1968**, *14*, 405–410.

(139) Efraty, A.; Jubran, N.; Goldman, A. *Inorg. Chem.* **1982**, *21*, 868–873.

(140) Janiak, C.; Kuhn, N.; Gleiter, R. *J. Organomet. Chem.* **1994**, *475*, 223–227.

(141) Kuhn, N.; Jendral, K.; Boese, R.; Bläser, D. *Chem. Ber.* **1991**, *124*, 89–91.

(142) De Lauzon, G.; Deschamps, B.; Fischer, J.; Mathey, F.; Mitschler, A. *J. Am. Chem. Soc.* **1980**, *102*, 994–1000.

(143) Kuhn, N.; Köckerling, M.; Stubenrauch, S.; Bläser, D.; Boese, R. *J. Chem. Soc., Chem. Commun.* **1991**, 1368–1370.

(144) Kuhn, N.; Stubenrauch, S.; Boese, R.; Bläser, D. *J. Organomet. Chem.* **1992**, *440*, 289–296.

(145) Kuhn, N.; Henkel, G.; Kreutzberg, J.; Stubenrauch, S.; Janiak, C. *J. Organomet. Chem.* **1993**, *456*, 97–106.

(146) Kuhn, N.; Jendral, K.; Stubenrauch, S.; Mynott, R. *Inorg. Chim. Acta* **1993**, *206*, 1–3.

(147) Licciulli, S.; Albahily, K.; Fomitcheva, V.; Korobkov, I.; Gambarotta, S.; Duchateau, R. *Angew. Chem. Int. Ed.* **2011**, *50*, 2346–2349.

(148) Schumann, H.; Winterfeld, J.; Hemling, H.; Kuhn, N. *Chem. Ber.* **1993**, *126*, 2657–2659.

(149) Schumann, H.; Rosenthal, E. C. E.; Winterfeld, J.; Kociok-Köhn, G. *J. Organomet. Chem.* **1995**, *495*, C12–C14.

(150) Schumann, H.; Rosenthal, E. C. E.; Winterfeld, J.; Weimann, R.; Demtschuk, J. *J. Organomet. Chem.* **1996**, *507*, 287–289.

(151) Nishiura, M.; Mashiko, T.; Hou, Z. *Chem. Commun.* **2008**, 2019–2021.

(152) Kuhn, N.; Henkel, G.; Stubenrauch, S. *J. Chem. Soc., Chem. Commun.* **1992**, 760–761.

(153) Kuhn, N.; Henkel, G.; Stubenrauch, S. *Angew. Chem. Int. Ed. Engl.* **1992**, *31*, 778–779.

(154) Westerhausen, M.; Wieneke, M.; Nöth, H.; Seifert, T.; Pfitzner, A.; Schwarz, W.; Schwarz, O.; Weidlein, J. *Eur. J. Inorg. Chem.* **1998**, 1175–1182.

(155) Schumann, H.; Gottfriedsen, J.; Demtschuk, J. *Chem. Commun.* **1999**, *376*, 2091–2092.

(156) Eisenstadt, A.; Giandomenico, C. M.; Frederick, M. F.; Laine, R. M. *Organometallics* **1985**, *4*, 2033–2039.

(157) Zhu, G.; Tanski, J. M.; Churchill, D. G.; Janak, K. E.; Parkin, G. *J. Am. Chem. Soc.* **2002**, *124*, 13658–13659.

(158) Kreye, M.; Glöckner, A.; Daniliuc, C. G.; Freytag, M.; Jones, P. G.; Tamm, M.; Walter, M. D. *Dalton Trans.* **2013**, *42*, 2192–2200.

(159) Kreye, M.; Baabe, D.; Schweyen, P.; Freytag, M.; Daniliuc, C. G.; Jones, P. G.; Walter, M. D. *Organometallics* **2013**, *32*, 5887–5898.

(160) Kreye, M.; Runyon, J. W.; Freytag, M.; Jones, P. G.; Walter, M. D. *Dalton Trans.* **2013**, *42*, 16846–16856.

(161) Mathey, F.; Mitschler, A.; Weiss, R. *J. Am. Chem. Soc.* **1977**, *99*, 3537–3538.

(162) Herber, R. H.; Nowik, I.; Loginov, D. A.; Starikova, Z. A.; Kudinov, A. R. *Eur. J. Inorg. Chem.* **2004**, 3476–3483.

(163) Dielmann, F.; Merkle, R.; Heinl, S. *Z. Naturforsch.* **2009**, *64b*, 3–10.

(164) Su, M. Der; Chu, S. Y. *J. Phys. Chem.* **1989**, *93*, 6043–6051.

(165) Ashe, A. J.; Kampf, J. W.; Pilotek, S.; Rousseau, R. *Organometallics* **1994**, *13*, 4067–4071.

(166) Ashe, A. J.; Al-Ahmad, S.; Pilotek, S.; Puranik, D. B.; Elschenbroich, C.; Behrendt, A. *Organometallics* **1995**, *14*, 2689–2698.

(167) Ross, S. D.; Bassin, M.; Kuntz, I. *J. Am. Chem. Soc.* **1954**, *76*, 4179.

(168) Brown, J. E.; Lovell, W. G. *Ind. Eng. Chem.* **1958**, *50*, 1547–1550.

(169) Gibb, B. C. *Nat. Chem.* **2012**, *4*, 769–70.

(170) Wakatsuki, Y.; Yamazaki, H. *Tetrahedron Lett.* **1973**, *14*, 3383–3384.

(171) Bönnemann, H. *Angew. Chem. Int. Ed. Engl.* **1978**, *17*, 505–515.

(172) Vollhardt, K. P. C. *Angew. Chem. Int. Ed. Engl.* **1984**, *23*, 539–556.

(173) Bönnemann, H. *Angew. Chem. Int. Ed. Engl.* **1985**, *24*, 248–262.

(174) Kölle, U. *Chem. Rev.* **1998**, *98*, 1313–1334.

(175) Takao, T.; Suzuki, H. *Coord. Chem. Rev.* **2012**, *256*, 695–708.

(176) Nakajima, Y.; Sakaki, S.; Nakao, Y.; Suzuki, H. *Organometallics* **2012**, *31*, 5342–5348.

(177) Tahara, A.; Kajigaya, M.; Takao, T.; Suzuki, H. *Organometallics* **2013**, *32*, 260–271.

(178) Yanagi, T.; Suzuki, H.; Oishi, M. *Chem. Lett.* **2013**, *42*, 1403–1405.

(179) Nakajima, Y.; Suzuki, H. *Organometallics* **2003**, *22*, 959–969.

(180) Nakajima, Y.; Inagaki, A.; Suzuki, H. *Organometallics* **2004**, *23*, 4040–4046.

(181) Nakajima, Y.; Suzuki, H. *Organometallics* **2005**, *24*, 1860–1866.

(182) Ziegler, K.; Schnell, B. *Liebigs Ann. Chem.* **1925**, *445*, 266–282.

(183) Chambers, J. W.; Baskar, A. J.; Bott, S. G.; Atwood, J. L.; Rausch, M. D. *Organometallics* **1986**, *5*, 1635–1641.

(184) Greene, D. L.; Villalta, O. A.; Macias, D. M.; Gonzalez, A.; Tikkanen, W.; Schick, B.; Kantardjieff, K. *Inorg. Chem. Commun.* **1999**, *2*, 311–314.

(185) Greene, D. L.; Villalta, O. A.; Macias, D. M.; Gonzalez, A.; Tikkanen, W.; Schick, B.; Kantardjieff, K. *Inorg. Chem. Commun.* **1999**, *2*, 381.

(186) Schott, A.; Schott, H.; Wilke, G.; Brandt, J.; Hoberg, H.; Hoffmann, E. G. *Liebigs Ann. Chem.* **1973**, 508–530.

(187) Brown, K. N.; Field, L. D.; Lay, P. A.; Lindall, C. M.; Masters, A. F. *J. Chem. Soc., Chem. Commun.* **1990**, 408–410.

(188) Heeg, M. J.; Janiak, C.; Zuckerman, J. J. *J. Am. Chem. Soc.* **1984**, *106*, 4259–4261.

(189) Heeg, M. J.; Herber, R. H.; Janiak, C.; Zuckerman, J. J.; Schumann, H.; Manders, W. F. *J. Organomet. Chem.* **1988**, *346*, 321–332.

(190) Lowack, R. H.; Peter, K.; Vollhardt, C. *J. Organomet. Chem.* **1994**, *476*, 25–32.

(191) Martín-Matute, B.; Edin, M.; Bogár, K.; Bäckvall, J.-E. *Angew. Chem. Int. Ed.* **2004**, *43*, 6535–6539.

(192) Martín-Matute, B.; Edin, M.; Bogár, K.; Kaynak, F. B.; Bäckvall, J.-E. *J. Am. Chem. Soc.* **2005**, *127*, 8817–8825.

(193) Träff, A.; Bogár, K.; Warner, M. C.; Bäckvall, J.-E. *Org. Lett.* **2008**, *10*, 4807–4810.

(194) Martín-Matute, B.; Aberg, J. B.; Edin, M.; Bäckvall, J.-E. *Chem. Eur. J.* **2007**, *13*, 6063–6072.

(195) Aberg, J. B.; Warner, M. C.; Bäckvall, J.-E. *J. Am. Chem. Soc.* **2009**, *131*, 13622–13624.

(196) Warner, M. C.; Verho, O.; Bäckvall, J.-E. *J. Am. Chem. Soc.* **2011**, *133*, 2820–2823.

(197) Stewart, B.; Nyhlen, J.; Martín-Matute, B.; Bäckvall, J.-E.; Privalov, T. *Dalton Trans.* **2013**, *42*, 927–934.

(198) Hirsch, S. S.; Bailey, W. J. *J. Org. Chem.* **1978**, *43*, 4090–4094.

(199) Dyker, G.; Heiermann, J.; Miura, M.; Inoh, J.-I.; Pivsa-Art, S.; Satoh, T.; Nomura, M. *Chem. Eur. J.* **2000**, *6*, 3426–3433.

(200) Harder, S.; Ruspic, C. *J. Organomet. Chem.* **2009**, *694*, 1180–1184.

(201) Ruspic, C.; Moss, J. R.; Schürmann, M.; Harder, S. *Angew. Chem. Int. Ed.* **2008**, *47*, 2121–2126.

(202) Orzechowski, L.; Piesik, D. F.-J.; Ruspic, C.; Harder, S. *Dalton Trans.* **2008**, 4742–4746.

(203) Meyer, G. *Angew. Chem. Int. Ed.* **2008**, *47*, 4962–4964.

(204) Harder, S.; Naglav, D.; Ruspic, C.; Wickleder, C.; Adlung, M.; Hermes, W.; Eul, M.; Pöttgen, R.; Rego, D. B.; Poineau, F.; Czerwinski, K. R.; Herber, R. H.; Nowik, I. *Chem. Eur. J.* **2013**, *19*, 12272–12280.

(205) Heinl, S.; Peresypkina, E. V.; Timoshkin, A. Y.; Mastrorilli, P.; Gallo, V.; Scheer, M. *Angew. Chem. Int. Ed.* **2013**, *52*, 10887–10891.

(206) Sitzmann, H. *J. Organomet. Chem.* **1988**, *354*, 203–214.

(207) Sitzmann, H. *Z. Naturforsch.* **1989**, *44b*, 1293–1297.

(208) Weismann, D.; Saurenz, D.; Boese, R.; Bläser, D.; Wolmershäuser, G.; Sun, Y.; Sitzmann, H. *Organometallics* **2011**, *30*, 6351–6364.

(209) Weismann, D.; Sun, Y.; Lan, Y.; Wolmershäuser, G.; Powell, A. K.; Sitzmann, H. *Chem. Eur. J.* **2011**, *17*, 4700–4744.

(210) Wallasch, M. W.; Wolmershäuser, G.; Sitzmann, H. *Angew. Chem. Int. Ed.* **2005**, *44*, 2597–2599.

(211) Sitzmann, H.; Dezember, T.; Kaim, W.; Baumann, F.; Stalke, D.; Kärcher, J.; Dormann, E.; Winter, H.; Wachter, C.; Kelemen, M. *Angew. Chem. Int. Ed. Engl.* **1996**, *35*, 2872–2875.

(212) Sitzmann, H.; Saurenz, D.; Wolmershäuser, G.; Klein, A.; Boese, R. *Organometallics* **2001**, *20*, 700–705.

(213) Schär, M.; Saurenz, D.; Zimmer, F.; Schädlich, I.; Wolmershäuser, G.; Demeshko, S.; Meyer, F.; Sitzmann, H.; Heigl, O. M.; Köhler, F. H. *Organometallics* **2013**, *32*, 6298–6305.

(214) Bolm, C.; Legros, J.; Le Paih, J.; Zani, L. *Chem. Rev.* **2004**, *104*, 6217–6254.

(215) Czaplik, W. M.; Mayer, M.; Cvengros, J.; von Wangelin, A. J. *ChemSusChem* **2009**, *2*, 396–417.

(216) Morris, R. H. *Chem. Soc. Rev.* **2009**, *38*, 2282–2291.

Chapter 2. Complexes of manganese, iron and cobalt with sterically demanding indenyl ligands

Abstract

A series of manganese, iron and cobalt complexes bearing sterically demanding 1,3-disubstituted indenyl ligands, 1,3-$(Me_3C)_2C_9H_5$ ($^{2t\mathrm{Bu}}$Ind) and 1,3-$(c\text{-}C_6H_{11})_2C_9H_5$ ($^{2\mathrm{Cy}}$Ind) has been prepared and investigated. These complexes have been characterized by various spectroscopic techniques, elemental analyses, and X-ray diffraction analyses. In addition the electronic properties and steric influences of these ligands have been evaluated. Although the cone angles and electronic properties are similar to 1,2,4-$(Me_3C)_3C_5H_2$ (Cp'), indenyl iron half-sandwich complexes are only stable at low temperature. This has been demonstrated for [($^{2t\mathrm{Bu}}$Ind)FeI] using suitable trapping experiments such as NaCp' or CO addition to yield [($^{2t\mathrm{Bu}}$Ind)(Cp')Fe] and [($^{2t\mathrm{Bu}}$Ind)Fe$(CO)_2$I], respectively. Overall the metal–ligand bonds in these indenyl compounds are weaker than in the corresponding cyclopentadienyl derivatives. In addition, it was established that the both homoleptic bis(indenyl)manganese complexes, [($^{2t\mathrm{Bu}}$Ind)$_2$Mn] and [($^{2\mathrm{Cy}}$Ind)$_2$Mn], are high-spin, as established by solid state magnetic susceptibility studies in the temperature range of 5 – 300 K.

2.1 Introduction

In this chapter, the coordination chemistry of sterically demanding *tert*-butyl (*t*Bu) and cyclohexyl (Cy) substituted indenyl ligands with manganese, iron and cobalt is described. Previous studies have shown that the cone angles of these ligands are comparable to that in of 1,2,4-$(Me_3C)_3C_5H_2$ (Cp').[1] This bulky cyclopentadienyl ligand has gained some prominence in the isolation of extraordinary and kinetically stabilized molecules, such as those with low-coordinated metal centers in low oxidation states and displaying unusual spin states or novel reactivity patterns.[2–4] By replacing the bulky indenyl ligand, unique properties might be expected, *e.g.* rate enhancement of ligand substitution[5–7] and enhanced catalytic activites[8–11].

Indenyl ligands are often considered close analogues to the cyclopentadienyl anion, which

has dominated organometallic chemistry since the discovery of the iconic molecule ferrocene, [(η^5-C_5H_5)$_2$Fe].[12,13] Both indenyl and cyclopentadienyl ligands are monoanionic, formally six-electron ligands and can be readily functionalized for many applications such as polymerization and small molecule activation.

The main factor that distinguishes indenyl ligands from cyclopentadienyl ligands is the haptropic shift and the change in the electron count at the metal center. In general, the five-membered ring can easily slip from η^5- to η^3-coordination in indenyl complexes. This phenomenon was first observed by Hart-Davis and Mawby,[14] and named "indenyl effect" by Basolo *et al.*[7] The reason for this effect can be ascribed to thermodynamic difference in the ground state[15] and Cp–metal bond strength[16] arising mainly from the nodal properties of indenyl's π-orbitals.[17] In addition, the η^9-indenyl-metal-interaction is a variant thereof, which masks and stabilizes low-valent zirconium centers.[18–24]

The differences between the indenyl and cyclopentadienyl ligands are also evident in first-row transition metal sandwich complexes, especially when the properties of substituted Cp- and Ind-ligands are compared, *e.g.* in the case of chromium and manganese.[25,26] In contrast to the well-established bis(cyclopentadienyl) manganese chemistry,[27–31] only few of bis(indenyl)manganese complexes have been reported.[26] Ring substituents can also influence the compound's properties, *e.g.* conformation and spin state.[32]

However, the synthetic route to bulky alkyl substituted indenyl ligands has not been optimized in contrast to Cp ligands. Hence, examples with sterically demanding *e.g.* *i*Pr-,[33–35] *t*Bu-,[36–39] Cy-,[40] or tms-[26,41–43] (tms = $SiMe_3$) indenyl complexes are limited, but they exhibit interesting properties.[44] Therefore, better synthetic protocols would be desirable to provide synthetically useful quantities of these ligands and to facilitate the exploration of the corresponding coordination chemistry.

2.2 Ligand synthesis

1,3-Di-*tert*-butyl substituted indenyl ligand ($^{2t\text{Bu}}$Ind) was prepared with a new two-step method, using classical phase-transfer catalysis with alkylation followed by a Grignard-reaction (Scheme 1). An alkylation method using phase-transfer catalysis, which has already successfully been applied in the synthesis of tri-*tert*-butyl cyclopentadiene (Cp'),[31] was chosen instead of the fulvene protocol,[36,39,45–48] or the one-pot reaction *via* lithium organyls which has showed the highest total yield (11%) of 1,3-di-*tert*-butyl-indene to date.[37]

The use of Grignard-reagent, here $^{t\text{Bu}}$IndMgBr, significantly increased the yield for the introduction of the second *tert*-butyl group (51%) and the total yield is now 42%.

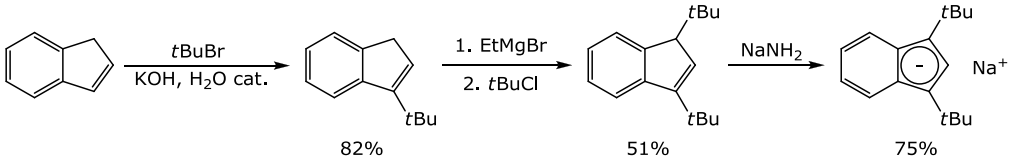

Scheme 1. Preparation of $^{2t\text{Bu}}$Ind ligand and its deprotonation.

The first *tert*-butyl group was installed by the classical alkylation method using a phase transfer catalyst.[31] Indene was deprotonated in a 50% KOH solution at *ca.* 85°C, and *tert*-butyl bromide was slowly added into the reaction mixture. The reaction progress was monitored by GC. Since the reaction occurred under biphasic condition, it should be stirred vigorously for several days. When the addition rate of *tert*-butyl bromide is too high, the side reaction dominants which leads to the formation of di-*tert*-butyl ether. The product was extracted with diethyl ether and then distilled under reduced pressure.

1,3-Di-*tert*-butylindene ($^{2t\text{Bu}}$IndH) was prepared using ethylmagnesium bromide for the deprotonation of 3-*tert*-butylindene.[49] Deprotonation of 1-*tert*-butylindene was carried out in toluene under reflux. After the deprotonation, the reaction mixture was cooled to 0°C and *tert*-butyl chloride was added dropwise. The product was extracted with diehtyl ehter and then distilled under reduced pressure. Unreacted 3-*tert*-butylindene was recovered as a mixed fraction with 1,3-di-*tert*-butylindene. The product was further purified by vacuum-distillation.

The deprotonation of di-1,3-*tert*-butylindene succeeds with sodium amide in tetrahydrofuran in 75% yield.

2.3 Attempted synthesis of indenyl half-sandwich complexes

Half-sandwich complexes of manganese, iron and cobalt with sterically demanding Cp ligands like Cp' have been reported.[50–53] Therefore the synthesis of half-sandwich complexes with bulky indenyl ligand were attempted. As mentioned above, the steric demands of Cp' and $^{2t\text{Bu}}$Ind are very similar.[1] Hence, it might be expected that the Ind ligands would also

stabilize the half-sandwich species.

When one equivalent of Na$^{2t\text{Bu}}$Ind is added to a solution of one equivalent of [$FeI_2(thf)_2$] at low temperature, the reaction mixture turnes red-brown, which is an indication for the iron half-sandwich derivative (**1**).[23] However, the homoleptic metallocene (**2**) is formed when the reaction mixture is allowed to warm to approximately –10°C as indicated by a color change from red-brown to blue-green. The indenyl ligand is not sterically demanding enough to stabilize the half-sandwich complexes at room temperature (Scheme 2).

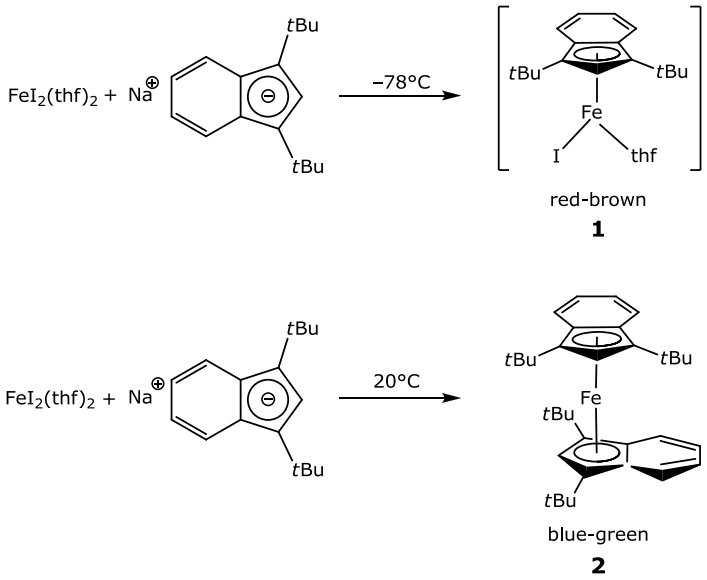

Scheme 2. Reaction of [$FeI_2(thf)_2$] and $^{2t\text{Bu}}$IndNa at different temperatures.

To prove the formation of an iron half-sandwich intermediate, trapping experiments were tried with NaCp' and CO (Scheme 3). The reaction between one equivalent of [$FeI_2(thf)_2$] and one equivalent of Na$^{2t\text{Bu}}$Ind at –78°C and sequential addition of one equivalent of NaCp' ligands or exposure to CO (1 atm) gave the mixed ferrocene (**3**), [($^{2t\text{Bu}}$Ind)(Cp')Fe], and the iron dicarbonyl complex (**4**), [($^{2t\text{Bu}}$Ind)Fe$(CO)_2$I], respectively.

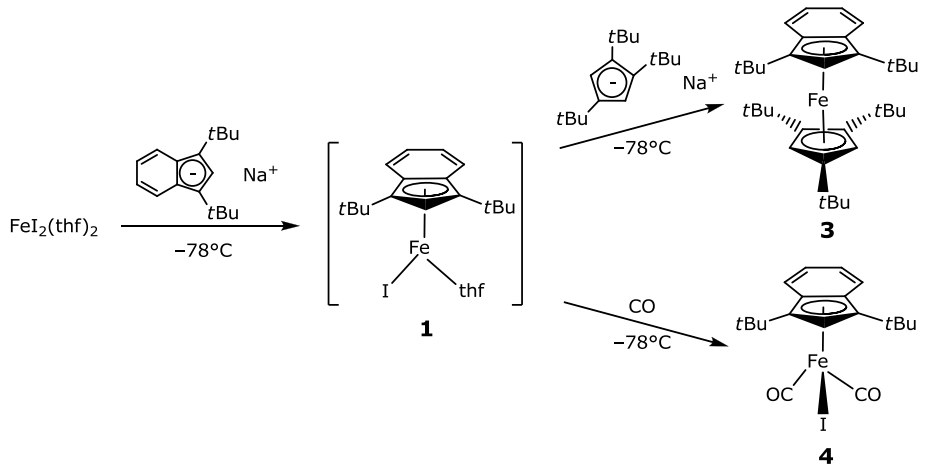

Scheme 3. Trapping experiments of the iron half-sandwich intermediates.

The solid state molecular structures of compounds **3** and **4** were determined by X-ray single crystal diffraction analysis. ORTEP diagrams of these molecules are drawn in Figure 1. The mixed ferrocene **3** has a very similar centroid (Cp_{cent})–metal distance (av. 1.71 Å) and Cp_{cent}–metal–Cp_{cent} angle (177.1°) as bis(tri-*tert*-butyl)ferrocene, [Cp'$_2$Fe] (av. 1.71 Å, 175°).[51] The Cp_{cent}–metal distances of both dicarbonyl structures are also comparable (1.75 Å for compound **4** and 1.73 Å for [Cp'Fe(CO)$_2$I]). This result confirms experimentally that Cp' and $^{2t\text{Bu}}$Ind have similar steric demands.

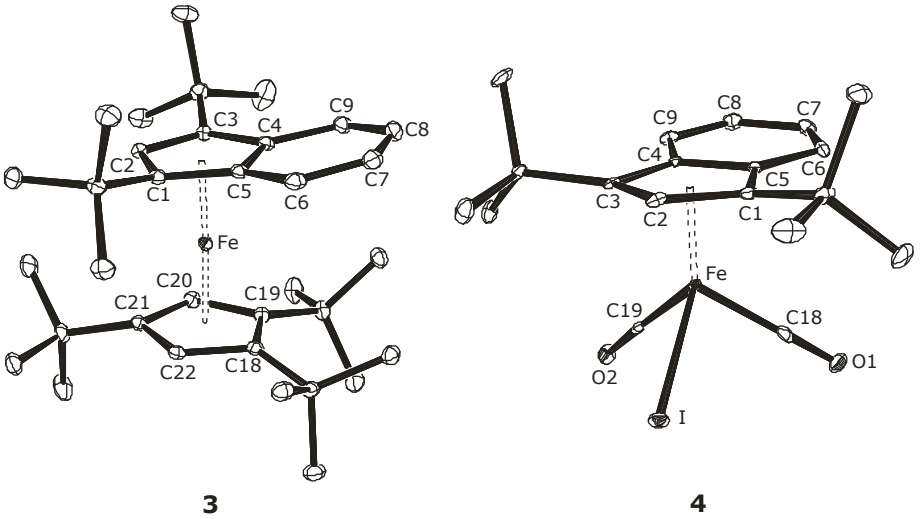

Figure 1. ORTEP diagrams of [(Cp')($^{2t\text{Bu}}$Ind)Fe] (**3**) and [($^{2t\text{Bu}}$Ind)Fe(CO)$_2$I] (**4**) with 30% probability ellipsoids. Hydrogen atoms are omitted for clarity.

The electron donating abilities of the Cp'- and $^{2t\mathrm{Bu}}$Ind-ligands were also evaluated by infrared spectroscopy. A comparison of the average CO stretching frequencies of 1991 and 1989 cm^{-1} for compound **4** and [Cp'Fe(CO)$_2$I], respectively, shows that both ligand have also very similar electron donating abilities.

2.4 Synthesis of bis(indenyl)metal complexes

To investigate the influence of these new ligands on the molecular structures, physical and electronic properties, the corresponding complexes of manganese, iron and cobalt were synthesized. Their indenyl complexes were prepared by the salt metathesis reactions of the appropriate indenide sodium salts with [MnI$_2$(thf)$_2$], [FeI$_2$(thf)$_2$] or [Co(acac)$_2$] (acac = acetylacetonate) in tetrahydrofuran (Scheme 4) followed by extraction and crystallization.

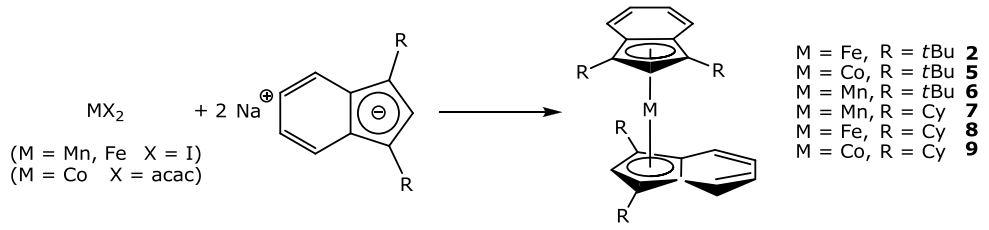

Scheme 4. Synthesize of $^{2t\mathrm{Bu}}$Ind and $^{2\mathrm{Cy}}$Ind complexes.

These metallocene were usually obtained in moderate yields, only for [$^{2t\mathrm{Bu}}$Ind$_2$Co] (**5**) the highest yield was only 10%. This might indicate the formation of a cobalt half-sandwich complex, such as [$^{2t\mathrm{Bu}}$IndCo(acac)], but no definite evidence can be provided. Moreover, [Co(acac)$_2$] was chosen to prevent an undesirable coupling reaction of the indenyl ligands. Bradley *et al.* reported that lithium fluorenide and $CoCl_2$ result in the formation of the corresponding bifluorenes.[54] Although the indenyl ligands are less reducing than the fluorenyl derivative,[55] [Co(acac)$_2$], which is more resistant to reduction than $CoCl_2$,[54] might be a better starting material. Whereas, several substituted bis(indenyl)iron and -cobalt complexes are known, there was no examples of the corresponding manganese complexes until a recent repot by Hanusa.[26] They pointed out that the purity of the manganese starting

material strongly affects the quality of the resulting manganocene.[26] In this study, the use of $[MnI_2(thf)_2]$ increased not only the yield, but also the purity.

All metallocenes are soluble in coordinating solvent such as tetrahydrofuran, moderately soluble in aromatic solvents such as toluene and poorly soluble in aliphatic solvent such as pentane. However, both manganocenes decomposed in acetonitrile immediately. [$^{2t\text{Bu}}$Ind$_2$Mn] (**6**) formed a green solid in dichloromethane while [$^{2\text{Cy}}$Ind$_2$Mn] (**7**) completely decomposed in dichloromethane within one week.

To investigate the comformational dynamics of the indenyl ligands in the diamagnetic iron complex **2** and **8**, the solution behavior was examined by variable temperature ^{1}H NMR spectroscopy. The ^{1}H NMR spectra of compound **2** are shown in Figure 2.

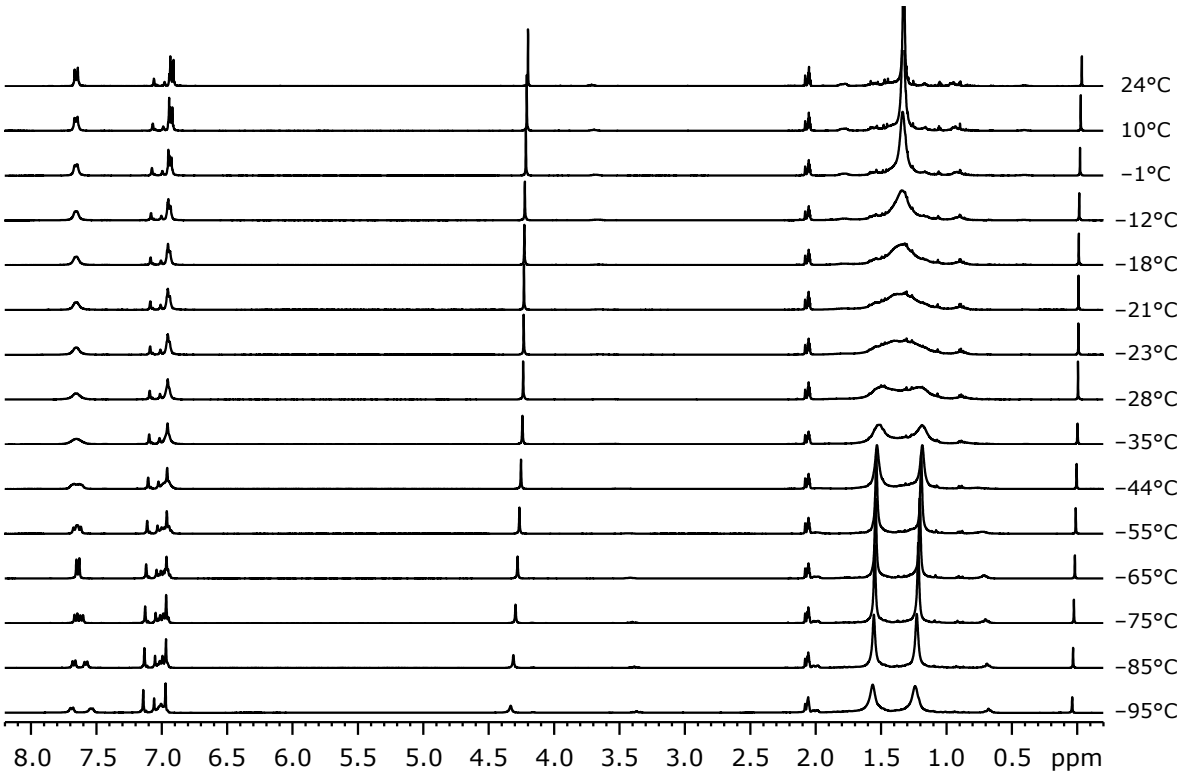

Figure 2. Variable temperature ^{1}H NMR spectroscopy of [$^{2t\text{Bu}}$Ind$_2$Fe] (**2**) in C_6D_6.

At 24°C, the ^{1}H NMR spectrum of compound **2** exhibits equivalent *tert*-butyl groups and a benzo doublet, suggesting a time-averaged C_{2v} symmetric metallocene arising from fast ring rotation on the time scale of the NMR experiment. Cooling the sample resulted in broadening of the *tert*-butyl and indenyl resonances (T_c = –23°C), at –85°C the peaks of two *tert*-butyl groups and benzene ring are completely resolved. The determined activation

barrier for compound **2** is 11.8 kcal mol^{-1}, which is comparable to that obtained for [^{2tms}Ind$_2$Fe], but lower than the rotation barriers of 14.2 kcal mol^{-1} for [Cp'$_2$Fe] and 13.1 kcal mol^{-1} for [(1,3-(Me$_3$C)C$_5$H$_3$)$_2$Fe] ([$^{2t\text{Bu}}$Cp$_2$Fe]). Compound **3** ([($^{2t\text{Bu}}$Ind)Fe(CO)$_2$I]), **6** and [$^{2\text{Cy}}$Ind$_2$Fe] (**8**) showed only line broadening in toluene-d_8 solution even at –90°C. Because the rotation barrier was not observed in compound **6**, low-temperature ^{1}H NMR experiments were not performed for compound **7**.

A reaction between **2** and [Cp'FeI]$_2$ was attempted in order to probe for ligand exchange behavior. When one equivalent of [Cp$_2$Fe] is mixed with one equivalent of [Cp'FeI]$_2$, the mixed ferrocene, [(Cp')(Cp)Fe], and FeI$_2$ are formed. However, no reaction was observed between compound **2** and [Cp'FeI] $_2$ (Scheme 5).

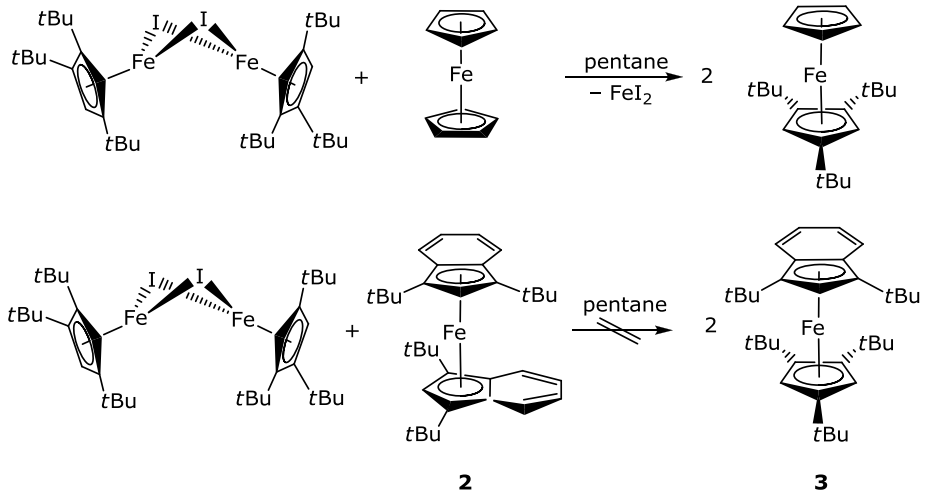

Scheme 5. Reactivity of [$^{2t\text{Bu}}$Ind$_2$Fe] (**2**) toward [Cp'FeI]$_2$.

2.5 Solid state molecular structures

The solid state molecular structures of the bis(indenyl) complexes were determined by X-ray single crystal diffraction analysis at 100 K. Single crystals of **8** suitable for structural determination were grown by sublimation under static vacuum. All other compounds were crystallized from saturated solutions at –30°C. The structures of bis(di-*tert*-butylindenyl) complexes are isostructual and crystallize in the space group $P2_1/c$. In contrast, **7** ([$^{2\text{Cy}}$Ind$_2$Mn]) crystallizes with two independent molecules in the triclinic space group $P\bar{1}$ and **8** ([$^{2\text{Cy}}$Ind$_2$Fe]) with one independent molecule in $P2_1/c$, whereas [$^{2\text{Cy}}$Ind$_2$Co] (**9**)

crystallizes with imposed inversion symmetry in $P2_1/c$ with three deuterobenzene molecules in the crystal lattice. ORTEP diagrams of compounds **6** and **7** are shown in Figure 3.

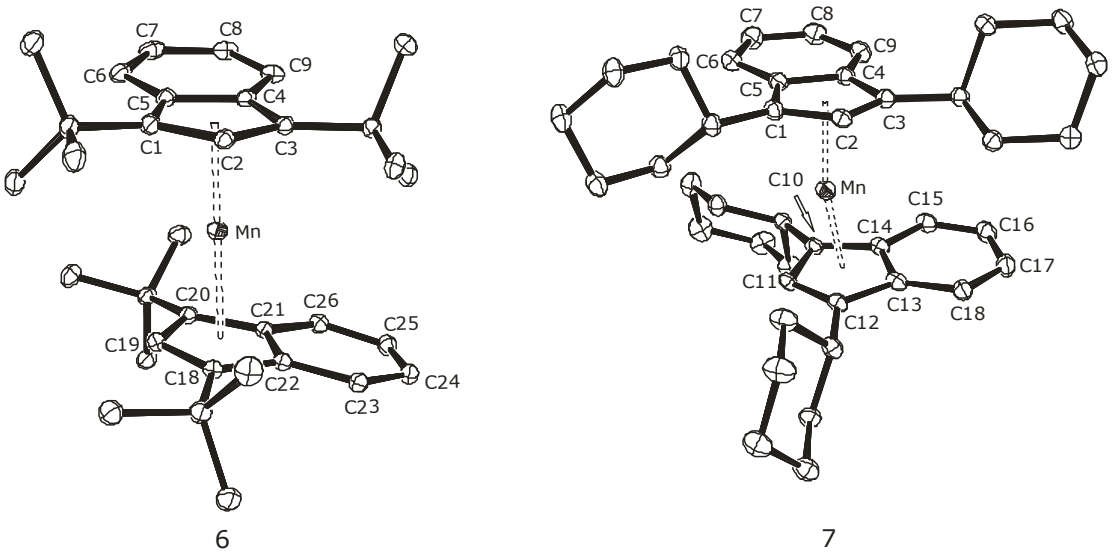

Figure 3. ORTEP diagrams of compound [^{2fBu}Ind$_2$Mn] (**6**) and [^{2Cy}Ind$_2$Mn] (**7**) with 30% probability ellipsoids. Hydrogen atoms are omitted for clarity.

To evaluate the morphology of the molecular structure, the following parameters (rotation angle Θ,[37,56] centroid-metal distance, ring slippage Δ_{M-C}[56,61] and hinge angle Ψ[56,61,63]) were defined and calculated (Figure 4).

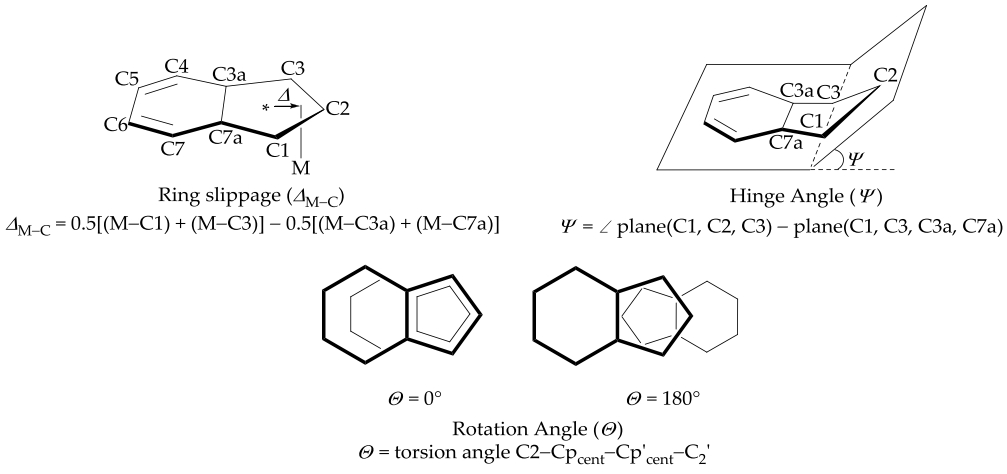

Figure 4. Parameter definition for ring slippage Δ_{M-C}, hinge angle Ψ and rotation angle Θ.

One of the structural features of bis(indenyl)metal complexes is the conformational preference of the two indenyl ligands. For simple [Ind_2M], the conformation in the solid state adopted by the two indenyl ligands can be described by the rotation angle Θ, defined as the torsion angle between C2–Cp_{cent}–Cp'_{cent}–C2'. A rotation angle of 0° indicates a completely eclipsed geometry, whereas an angel of 180° corresponds to the fully staggered arrangement of the two rings.

Table 1. Selected bond lengths [Å] and angles [°]of compounds **1** and **5 – 9**.

	Cent–M	Ring slippage (Δ_{M-C})	Hinge angle (Ψ)	Rotation angle (Θ)
[($^{2t\text{Bu}}$Ind)$_2$Mn] (6)	2.08 / 2.12	0.14 / 0.18	2.7 / 3.4	86.0
[($^{2\text{Cy}}$Ind)$_2$Mn] (7)	2.03 / 2.05 2.04 / 2.07	0.11 / 0.15 0.14 / 0.22	2.7 / 2.8 2.2/ 4.0	93.8 / 85.9
[($^{2t\text{Bu}}$Ind)$_2$Fe] (1)	1.72 / 1.72	0.05 / 0.06	3.0 / 3.3	87.0
[($^{2\text{Cy}}$Ind)$_2$Fe] (8)	1.68 / 1.68	0.03 / 0.03	3.5 / 3.7	–96.9
[($^{2t\text{Bu}}$Ind)$_2$Co] (5)	1.79 / 1.82	0.04 / 0.19	1.1 / 6.8	86.2
[($^{2\text{Cy}}$Ind)$_2$Co] (9)	1.76 / 1.76	0.16 / 0.16	7.3 / 7.3	180.0

The bisindenyl complex with bulky substituents such as tms-,[26,37,41] *t*Bu- and Cy-groups adopt a gauche conformation with the exception of compound **8**, which shows a fully staggered arrangement with its imposed inversion symmetry. In these complexes, substituents of the upper ring are arranged so that they interlock between the substituents of the lower ring. In contrast, small substituents like methyl- or isopropyl-groups seem not to affect the conformation. For example, the ligands in Cr[34] and Mn[26] complexes are almost fully staggered, while Fe[24] complexes adopt a gauche conformation.

The number of the substituents also influence the conformation of these complexes. Therefore, its influence was investigated by comparison with already known compounds. In unsubstituted indenyl complexes (Fe,[56] Co[56] and Cr[57]) the ligands are almost eclipsed, or fully staggered (Ni).[56] In mono-substituted indenyl ligand Cr,[37,58] Co[38] and Ni[59] complexes only the *meso* diastereomer is formed independent of the substituent, whereas Fe complexes behave differently, here the *rac*-diastereomer is formed predominantely to minimize steric replusion between the substituents. With a *t*Bu-group the product is a mixture of *meso*- and *rac*-diastereomers. The *rac*-diastereomers are formed exclusively for $SiMe_2$(*t*Bu)[35] and PPh_2[60] substituted indenyl ligands according to ^{1}H NMR spectroscopy.

Cp_{cent}–M distance is a reliable indicator of the spin state at the metal atom since the population of metal-ligand antibonding orbital leads to weaker metal–carbon bonds.[30] This is nicely illustrated by the comparison of the corresponding iron (S = 0), cobalt (S = 1/2) and

manganese (S = 5/2) complexes.

The centroid–iron distances of 1.72 Å and 1.68 Å for compounds **2** ([($^{2t\text{Bu}}$Ind)$_2$Fe]) and **8** ([($^{2\text{Cy}}$Ind)$_2$Fe]), respectively, are in agreement with a low-spin (S = 0) d^6 electron configuration, and can be compared to [Cp'$_2$Fe] (1.71 Å)[51] and the unsubstituted [Ind$_2$Fe] (1.67 Å / 1.66 Å).[56] The slight elongation in the case of complex **2** might be attributed to the strain imposed by the sterically demanding *t*Bu-groups.

The addition of one electron to the metal–ligand antibonding orbital leads to an elongation of the centroid–metal distance of *ca.* 0.08 Å as shown for compounds **5** ([($^{2t\text{Bu}}$Ind)$_2$Co]) and **9** ([($^{2\text{Cy}}$Ind)$_2$Fe]).

However, for the corresponding manganese complexes **6** and **7** this distance increased even further by *ca.* 0.4 Å consistent with a high-spin manganese (II) atom. The averaged centroid-manganese values of 2.07 Å can be compared to the values observed for [Cp'$_2$Mn] (2.11 Å)[31]. The less-heavily substituted derivative, [$^{2t\text{Bu}}$Cp$_2$Mn], is a low-spin molecule with a Cp$_{cent}$–Mn distance of 1.75 Å.[31]

2.6 Evaluation of hapticity

In contrast to the cyclopentadienyl complexes, a perfect η^5-coordination of the indenyl ligand is rarely observed, but slightly distorted η^3:η^2-mode due to its orbital asymmetry. To account for this behavior, several structural parameters have been introduced to define the indenyl coordination such as the slippage parameter Δ_{M-C} and the hinge angle Ψ (Figure 4). All synthesized complexes have distorted η^3:η^2-geometry in the solid state. According to a comparison with similar complexes [($^{2\text{R}}$Ind)$_2$M] (M = Cr, Mn, Fe and Co; R = tms, *i*Pr and *t*Bu),[24,26,34,37,41,43] substituents seem not to affect the hapticity significantly.

Several methods have been suggested to describe the ring slippage, but here the parameter Δ_{M-C} is defined as the difference between the average distance from metal to the two hinge carbon (C3a and C7a) and the metal to adjacent carbon (C1 and C3) of the five membered ring[56,61] (Figure 4). Some authors define the slip distortion Δ as the distance between the perpendicular projection of heavy atom on the least-squares plane of the ring and ring centroid.[62,63] This parameter can also be given as an angle.[64] Originally, those parameters were introduced to quantify the slip distortion in carborane complexes. Therefore, it is less exact for indenyl complexes because the pentagon is folded in indenyl ligands, while it remains planar in carboranes. The values of slip distortion Δ are 20 – 45% larger than the slip

parameters Δ_{M-C} depending on the type of metal. Other authors calculated the slip distortion as Δ_{M-C} = [av. of M–C(3a, 7a)] – [av. of M–C(1, 2, 3)].[61,63,64] This is also not appropriate because C2 is not in the plane defined by C(7a, 1, 3, 3a).

The relative weakness of the metal-carbon bonds in these complexes is reflected in the averaged ring slippage parameters Δ_{M-C}. These values vary from 0.04 Å for Fe, to 0.13 Å for Co and 0.15 Å for Mn. For comparison, the slippage parameter Δ_{M-C} varies between 0.08 Å ≤ Δ_{M-C} ≤ 0.23 Å for indenyl complexes with nearly unperturbed η^3:η^2-mode and 0.75 Å ≤ Δ_{M-C} ≤ 1.00 Å for true η^3-coordination (as recalculated from published crystallographic data).[65–77]

The parameter Ψ is defined as a dihedral angle between the normals of the planes (C1, C2, C3) and (C1, C3, C3a, C7a), where the three carbon fragments includes the carbon with the shortest metal carbon bond length.[56,61,63] The hinge angle increases with the ring slippage. For all compounds $\Psi < 10°$ is found. This angle is close to 0° for the "true" η^5-coordination. The values were commonly found $\Psi < 10°$ for η^3:η^2-mode and $20° < \Psi < 30°$ for η^3-modes, respectively (this angle is referred to as the fold angle[16]).

Hapticity can also be evaluated by the chemical shift of C3a and C7a in the ^{13}C NMR spectrum. There is a strong correlation between the solid state structure parameter Δ_{M-C} and δ_{13C}(3a, 7a).[56] In [(η^3-Ind)Fe(CO)$_2$][N(PPh$_3$)$_2$], the resonances of C(3a, 7a) appear at 157.3 ppm.[78] For η^3:η^2-indenyl ligand the resonances of C(3a, 7a) should be found upfield-shifted and indeed, the resonances of [(η^5-Ind)$_2$Fe] were observed at 87.0 ppm for C(3a, 7a).[79] The ^{13}C NMR data of C(3a, 7a) for compound **1** ([($^{2t\text{Bu}}$Ind)$_2$Fe]), δ_{13C}(3a, 7a) = 86.0 ppm, and for compound **9** ([($^{2\text{Cy}}$Ind)$_2$Fe]), δ_{13C}(3a, 7a) = 82.6 ppm, respectively. The values of δ_{13C}(3a, 7a) = 100.0 ppm for iron dicarbonyl complex **4** ([($^{2t\text{Bu}}$Ind)Fe(CO)$_2$I]) indicate that it has a η^3:η^2-coordination, but not η^3. No ^{13}C NMR data could be obtained for Mn and Co complexes due to their strong paramagnetic properties.

As η^3:η^2-geometry, Mn complexes have large Δ_{M-C}, but small Ψ values; Cr and Co complexes have on the contrary large Ψ and small Δ_{M-C} values. In the Fe complexes both values are rather small.

2.7 Solid state magnetic susceptibility studies

Cyclopentadienyl complexes of manganese are unique among the first-row transition metallocenes since they possess two thermally accessible spin states, $^2E_{2g}$ (low-spin) and $^6A_{1g}$

(high-spin), which can readily interconvert depending on the substitution pattern on the cyclopentadienyl ligands. So far, only the solid state magnetic susceptibility of [(1,3-(Me_2CH)$_2C_9H_6$)$_2$Mn] ([$^{2i\mathrm{Pr}}$Ind$_2$Mn]) has been reported,[26] hence the magnetic susceptibility of compound **6** ([$^{2t\mathrm{Bu}}$Ind$_2$Mn]) and **7** ([$^{2\mathrm{Cy}}$Ind$_2$Mn]) were investigated (Figure 5).

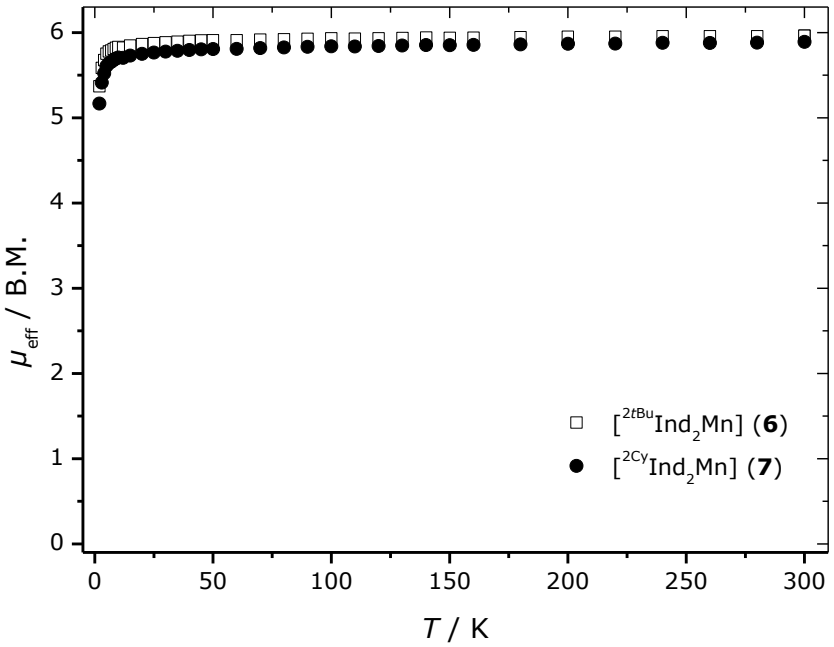

Figure 5. Solid state magnetic moment μ_{eff} *vs.* T plot for [$^{2t\mathrm{Bu}}$Ind$_2$Mn] (**6**) and [$^{2\mathrm{Cy}}$Ind$_2$Mn] (**7**).

For complex **6** and **7** the magnetic moment of *ca.* 5.9 B.M. is temperature independent, consistent with high-spin manganese (II) centers (S = 5/2). No indication of a spin crossover was detected in the range between 5 – 300 K.

The chemical shift δ of *t*Bu-group is temperature dependent and the δ *vs.* T^{-1} plot is linear in the temperature range 233 – 353 K (Figure 6), *i.e.* exhibits the relationship of $\delta \sim T^{-1}$. From Curie's law, $\chi = \mathrm{C} \cdot T^{-1}$ where χ is the magnetic susceptibilty, C is the material-specific Curie constant and T is temperature, if $\delta \sim T^{-1}$ then $\delta \sim \chi$ is also satisfied.

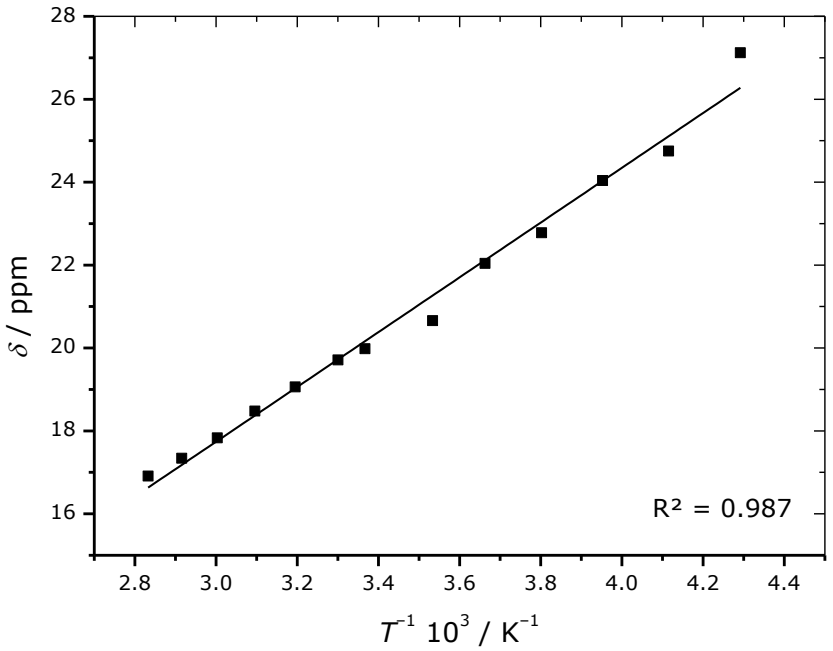

Figure 6. δ *vs.* T^{-1} plot for [$^{2t\text{Bu}}$Ind$_2$Mn] (**6**) in C_7D_8 at temperature from 233 to 353 K.

2.8 Electrochemistry

Little is known about the electrochemistry of manganocenes, and even less on bis(indenyl)manganese with very few exceptions. Therefore, electrochemical data on these complexes were collected (Table 2) and compared with the results of previous studies on related indenyl and cyclopentadienyl compounds.

Table 2. Electrochemical potentials of selected metallocenes *vs.* SCE.

	***E*°′ / V *vs.* SCE**	**Solvent / Supporting electrolyte**	**Ref.**
[(^{2tms}Ind)$_2$Mn]	–0.58	THF / *	26
[(^{2tBu}Ind)$_2$Mn] (6)	–0.833	THF / [(*n*Bu)$_4$N][PF$_6$]	this work
[(^{2Cy}Ind)$_2$Mn] (7)	–0.842	THF / [(*n*Bu)$_4$N][PF$_6$]	this work
[Cp$_2$Fe]	0.460	CH_2Cl_2 / [(*n*Bu)$_4$N][PF$_6$]	80
[Cp$_2$Fe]	0.560	THF / [(*n*Bu)$_4$N][PF$_6$]	80
[^{3iPr}Cp$_2$Fe]	0.25	CH_2Cl_2 / *	81
[^{3tms}Cp$_2$Fe]	0.356	CH_2Cl_2 / [(*n*Bu)$_4$N][PF$_6$]	82
[^{3tBu}Cp$_2$Fe]	0.096	CH_2Cl_2 / [(*n*Bu)$_4$N][PF$_6$]	this work
[^{3Cy}Cp$_2$Fe]	0.18	CH_2Cl_2 / *	83
[Ind$_2$Fe]	0.21	CH_2Cl_2 / [(*n*Bu)$_4$N][ClO_4]	84
[(^{2iPr}Ind)$_2$Fe]	0.28	THF / [(*n*Bu)$_4$N][PF$_6$]	24
[(^{2tms}Ind)$_2$Fe]	0.102	CH_2Cl_2 / [(*n*Bu)$_4$N][PF$_6$]	41
[(^{2tBu}Ind)$_2$Fe] (2)	–0.069	CH_2Cl_2 / [(*n*Bu)$_4$N][PF$_6$]	this work
[(^{2Cy}Ind)$_2$Fe] (8)	–0.043	CH_2Cl_2 / [(*n*Bu)$_4$N][PF$_6$]	this work
[(Ind)(Cp)Fe]	0.350	CH_2Cl_2 / [(*n*Bu)$_4$N][ClO_4]	84
[(^{2tBu}Ind)(^{3tBu}Cp)Fe] (3)	–0.024	CH_2Cl_2 / [(*n*Bu)$_4$N][PF$_6$]	this work
[Cp$_2$Co]	–0.86	CH_2Cl_2 / *	85
[^{3tBu}Cp$_2$Co]	–1.06	CH_2Cl_2 / [(*n*Bu)$_4$N][PF$_6$]	86
[Ind$_2$Co]	–0.51	MeCN / *	87
[(^{2tms}Ind)$_2$Co]	–0.29 / –1.24	THF / [(*n*Bu)$_4$N][PF$_6$]	43
[(^{2tBu}Ind)$_2$Co] (5)	–0.730 / –1.788	CH_2Cl_2 / [(*n*Bu)$_4$N][PF$_6$]	this work
[(^{2Cy}Ind)$_2$Co] (9)	–0.690	CH_2Cl_2 / [(*n*Bu)$_4$N][PF$_6$]	this work

*not given

The cyclic voltammetry experiments show an irreversible Mn(II)/Mn(III) redox process for both manganocene **6** and **7**. The irreversible oxidation most probably arises from the inherent instability of these high-spin Mn(II) complexes.

As expected, the bis(indenyl)iron complexes, **2** and **8**, show a reversible single-electron Fe(II)/Fe(III) redox process (Table 2). The oxidation potentials of [^{2tBu}Ind$_2$Fe] (**2**), [(^{2tBu}Ind)(Cp′)Fe] (**3**) and [Cp′$_2$Fe] have also been compared. A comparison with unsubstituted [Ind$_2$Fe], [(Ind)(Cp)Fe] and [Cp$_2$Fe][84] shows that the exchange of a Cp′ group by ^{2tBu}Ind facilitates the metallocene oxidation. Cobaltocene, [Cp$_2$Co], undergoes two reversible redox processes, the first, (a) corresponding to the cobaltocenium/cobaltocene redox couple and the second, (b) to the reduction wave of cobaltocene to the cobaltocene anion. Two reversible redox processes have also been observed for compound **5** (Figure 7),

and the observed redox-potentials compare very well with previous literature reports for [^{2tms}Ind$_2$Co] (Table 2). In contrast, compound **9** exhibits only one reversible oxidation under the given conditions.

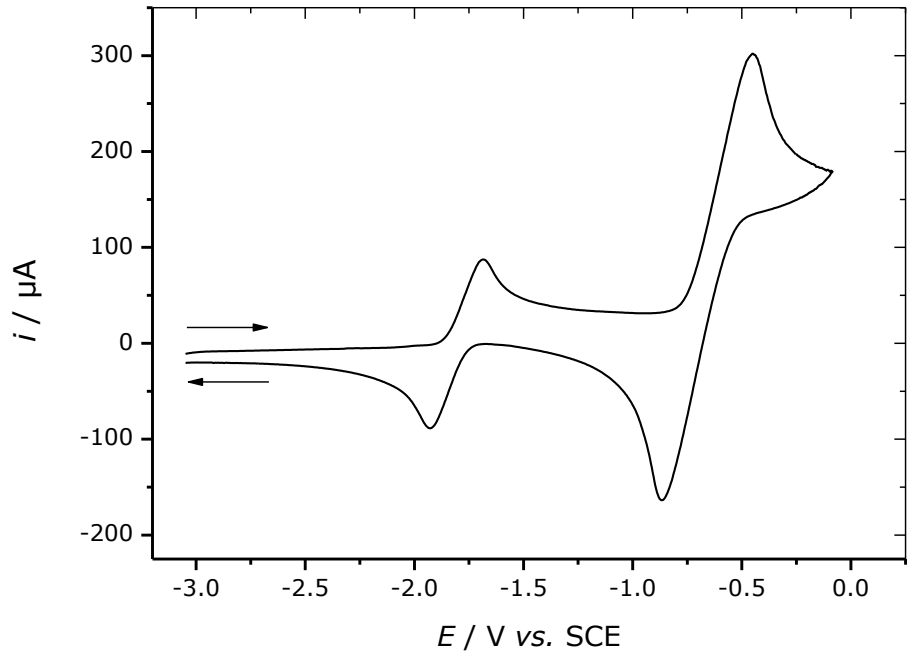

Figure 7. Cyclic voltammogram of [^{2tBu}Ind$_2$Co] (**5**) measured in dichlormethane with 0.1 M [*n*Bu$_4$N][PF$_6$]. Sweep rate: 100 mV s^{-1}. External calibration.

From these studies it is clear that the substituents also affect the redox potential. Cyclopentadienyl derivatives are susceptible to oxidation in order of *t*Bu > Cy > *i*Pr > tms (Table 2), whereas in indenyl derivatives the order is *t*Bu > Cy > tms > *i*Pr. This difference might be caused by a change in solvents used for the electrochemical study (tetrahydrofuran *vs.* dichloromethane).

2.9 Conclusion

The sterically demanding 1,3-disubstituted indenyl ligands, 1,3-$(Me_3C)_2C_9H_5$ ($^{2t\text{Bu}}$Ind) and 1,3-(c-$C_6H_{11})_2C_9H_5$ ($^{2\text{Cy}}$Ind), have been employed to prepare a series of bis(indenyl)manganese, iron and cobalt complexes. In the case of iron, indenyl ligand $^{2t\text{Bu}}$Ind stabilizes an iron half-sandwich species at low temperature, which has been confirmed by suitable trapping experiments.

In addition, although $^{2t\text{Bu}}$Ind exhibits similar electronic and steric properties to those of 1,2,4-tri-*tert*-butylcyclopentadienyl (Cp'), the reduced stability of the half-sandwich complex can be attributed to weak metal–carbon bonds in the metal indenyl compounds. The bis(indenyl)manganocenes, [$^{2t\text{Bu}}Ind_2Mn$] (**6**) and [$^{2\text{Cy}}Ind_2Mn$] (**7**), contain high-spin d^5 manganese(II) centers as established by solid state magnetic susceptibility studies, and no spin-cross-over behavior has been observed. Electrochemical studies on [$^{2t\text{Bu}}Ind_2Co$] (**5**) show two reversible redox-processes which suggest that compound **5** can be chemically reduced and might offer an interesting entry into the low-valent cobalt half-sandwich chemistry.

2.10 References

(1) Glöckner, A.; Bauer, H.; Maekawa, M.; Bannenberg, T.; Daniliuc, C. G.; Jones, P. G.; Sun, Y.; Sitzmann, H.; Tamm, M.; Walter, M. D. *Dalton Trans.* **2012**, *41*, 6614–6624.

(2) Walter, M. D.; Grunenberg, J.; White, P. S. *Chem. Sci.* **2011**, *2*, 2120–2131.

(3) Walter, M. D.; White, P. S. *Dalton Trans.* **2012**, *41*, 8506–8508.

(4) Walter, M. D.; White, P. S. *Inorg. Chem.* **2012**, *51*, 11860–11872.

(5) Rerek, M. E.; Basolo, F. *J. Am. Chem. Soc.* **1984**, *106*, 5908–5912.

(6) Kakkar, A. K.; Taylor, N. J.; Marder, T. B.; Shen, J. K.; Hallinan, N.; Basolo, F. *Inorg. Chim. Acta* **1992**, *198-200*, 219–231.

(7) Rerek, M. E.; Ji, L.-N.; Basolo, F. *J. Chem. Soc., Chem. Commun.* **1983**, 1208–1209.

(8) Garrett, C. E.; Fu, G. C. *J. Org. Chem.* **1998**, *63*, 1370–1371.

(9) Brunner, H.; Fisch, K. *Angew. Chem. Int. Ed. Engl.* **1990**, *29*, 1131–1132.

(10) Ready, T. E.; Chien, J. C. W.; Rausch, M. D. *J. Organomet. Chem.* **1999**, *583*, 11–27.

(11) Marder, T. B.; Roe, D. C.; Milstein, D. *Organometallics* **1988**, *7*, 1451–1453.

(12) Janiak, C.; Schumann, H. *Adv. Organomet. Chem.* **1991**, *33*, 291–393.

(13) Werner, H. *Angew. Chem. Int. Ed.* **2012**, *51*, 6052–6058.

(14) Hart-Davis, A. J.; Mawby, R. J. *J. Chem. Soc. A* **1969**, 2403–2407.

(15) Kubas, G. J.; Kiss, G.; Hoff, C. D. *Organometallics* **1991**, *10*, 2870–2876.

(16) Calhorda, M. J.; Veiros, L. F. *Coord. Chem. Rev.* **1999**, *185-186*, 37–51.

(17) Calhorda, M. J.; Romão, C. C.; Veiros, L. F. *Chem. Eur. J.* **2002**, *8*, 868–875.

(18) Bradley, C. A.; Keresztes, I.; Lobkovsky, E.; Young, V. G.; Chirik, P. J. *J. Am. Chem. Soc.* **2004**, *126*, 16937–16950.

(19) Bradley, C. A.; Veiros, L. F.; Pun, D.; Lobkovsky, E.; Keresztes, I.; Chirik, P. J. *J. Am. Chem. Soc.* **2006**, *128*, 16600–16612.

(20) Bradley, C. A.; Veiros, L. F.; Chirik, P. J. *Organometallics* **2007**, *26*, 3191–3200.

(21) Pun, D.; Bradley, C. A.; Lobkovsky, E.; Keresztes, I.; Chirik, P. J. *J. Am. Chem. Soc.* **2008**, *130*, 14046–14047.

(22) Chirik, P. J. *Organometallics* **2010**, *29*, 1500–1517.

(23) Glöckner, A.; Bannenberg, T.; Ibrom, K.; Daniliuc, C. G.; Freytag, M.; Jones, P. G.; Walter, M. D.; Tamm, M. *Organometallics* **2012**, *31*, 4480–4494.

(24) McGovern, G. P.; Hung-Low, F.; Tye, J. W.; Bradley, C. A. *Organometallics* **2012**, *31*, 3865–3879.

(25) Heinemann, O.; Jolly, P. W.; Krüger, C.; Verhovnik, G. P. J. *Organometallics* **1996**, *15*, 5462–5463.

(26) Crisp, J. A.; Meier, R. M.; Overby, J. S.; Hanusa, T. P.; Rheingold, A. L.; Brennessel, W. W. *Organometallics* **2010**, *29*, 2322–2331.

(27) Fischer, E. O.; Jira, R. *Z. Naturforsch.* **1954**, *9b*, 618–619.

(28) Köhler, F. H.; Hebendanz, N. *Chem. Ber.* **1983**, *116*, 1261–1263.

(29) Hays, M. L.; Burkey, D. J.; Overby, J. S.; Hanusa, T. P.; Sellers, S. P.; Yee, G. T.; Young, V. G. *Organometallics* **1998**, *17*, 5521–5527.

(30) Sitzmann, H. *Coord. Chem. Rev.* **2001**, *214*, 287–327.

(31) Walter, M. D.; Sofield, C. D.; Booth, C. H.; Andersen, R. A. *Organometallics* **2009**, *28*, 2005–2019.

(32) Meredith, M. B.; Crisp, J. A.; Brady, E. D.; Hanusa, T. P.; Yee, G. T.; Pink, M.; Brennessel, W. W.; Young, V. G. *Organometallics* **2008**, *27*, 5464–5473.

(33) Overby, J. S.; Hanusa, T. P. *Organometallics* **1996**, *15*, 2205–2212.

(34) Overby, J. S.; Hanusa, T. P.; Sellers, S. P.; Yee, G. T. *Organometallics* **1999**, *18*, 3561–3562.

(35) Bradley, C. A.; Flores-Torres, S.; Lobkovsky, E.; Abruña, H. D.; Chirik, P. J. *Organometallics* **2004**, *23*, 5332–5346.

(36) Ready, T. E.; Chien, J. C. W.; Rausch, M. D. *J. Organomet. Chem.* **1996**, *519*, 21–28.

(37) Brady, E. D.; Overby, J. S.; Meredith, M. B.; Mussman, A. B.; Cohn, M. A.; Hanusa, T. P.; Yee, G. T.; Pink, M. *J. Am. Chem. Soc.* **2002**, *124*, 9556–9566.

(38) Guo, S.; Hauptmann, R.; Belaj, F.; Schneider, J. J. *Z. Kristallogr. NCS* **2007**, *222*, 363–364.

(39) Honzíček, J.; Romão, C. C.; Calhorda, M. J.; Mukhopadhyay, A.; Vinklárek, J.; Padeľková, Z. *Organometallics* **2011**, *30*, 717–725.

(40) Krüger, C.; Lutz, F.; Nolte, M.; Erker, G.; Aulbach, M. *J. Organomet. Chem.* **1993**, *452*, 79–86.

(41) Fern, G. M.; Klaib, S.; Curnow, O. J.; Lang, H. *J. Organomet. Chem.* **2004**, *689*, 1139–1144.

(42) Hung-Low, F.; Bradley, C. A. *Organometallics* **2011**, *30*, 2636–2639.

(43) Hung-Low, F.; Bradley, C. A. *Inorg. Chem.* **2013**, *52*, 2446–2457.

(44) Peruzzini, M.; Abdreimova, R. R.; Budnikova, Y.; Romerosa, A.; Scherer, O. J.; Sitzmann, H. *J. Organomet. Chem.* **2004**, *689*, 4319–4331.

(45) Howie, R. A.; McQuillan, G. P.; Thompson, D. W.; Lock, G. A. *J. Organomet. Chem.* **1986**, *303*, 213–220.

(46) Crane, G.; Boord, C. E.; Henne, A. L. *J. Am. Chem. Soc.* **1945**, *67*, 1237–1239.

(47) Thiele, J. *Ber. Dtsch. Chem. Ges.* **1900**, *33*, 666–673.

(48) Thiele, J.; Balhorn, H. *Liebigs Ann. Chem.* **1906**, *348*, 1–15.

(49) Sitzmann, H.; Zhou, P.; Wolmershäuser, G. *Chem. Ber.* **1994**, *127*, 3–9.

(50) Maekawa, M.; Römelt, M.; Daniliuc, C. G.; Jones, P. G.; White, P. S.; Neese, F.; Walter, M. D. *Chem. Sci.* **2012**, *3*, 2972–2979.

(51) Walter, M. D.; White, P. S. *New J. Chem.* **2011**, *35*, 1842–1854.

(52) Baumann, F.; Dormann, E.; Ehleiter, Y.; Kaim, W.; Kärcher, J.; Kelemen, M.; Krammer, R.; Saurenz, D.; Stalke, D.; Wachter, C.; Wolmershäuser, G.; Sitzmann, H. *J. Organomet. Chem.* **1999**, *587*, 267–283.

(53) Schneider, J. J.; Specht, U. *Z. Naturforsch.* **1995**, *50b*, 684–686.

(54) Al-Afyouni, M. H.; Huang, T. A.; Hung-Low, F.; Bradley, C. A. *Tetrahedron Lett.* **2011**, *52*, 3261–3265.

(55) Lochert, P.; Federlin, P. *Tetrahedron Lett.* **1973**, *14*, 1109–1112.

(56) Webott, S. A.; Kakkar, A. K.; Stringer, G.; Taylor, N. J. *J. Organomet. Chem.* **1990**, *394*, 777–794.

(57) Chekkal, F.; Zendaoui, S.-M.; Zouchoune, B.; Saillard, J.-Y. *New J. Chem.* **2013**, *37*, 2293–2302.

(58) Meredith, M. B.; Crisp, J. A.; Brady, E. D.; Hanusa, T. P.; Yee, G. T.; Brooks, N. R.; Kucera, B. E.; Young, V. G. *Organometallics* **2006**, *25*, 4945–4952.

(59) Bauer, H.; Sun, Y.; Sitzmann, H. *Acta Cryst.* **2011**, *E67*, m1184.

(60) Curnow, O. J.; Fern, G. M. *Organometallics* **2002**, *21*, 2827–2829.

(61) O'Hare, D.; Murphy, V. J.; Kaltsoyannis, N. *J. Chem. Soc., Dalton Trans.* **1993**, 383–392.

(62) Mingos, D. M. P.; Forsyth, M. I.; Welch, A. J. *J. Chem. Soc., Dalton Trans.* **1978**, 1363–1374.

(63) Faller, J. W.; Crabtree, R. H.; Habib, A. *Organometallics* **1985**, *4*, 929–935.

(64) Honan, M. B.; Atwood, J. L.; Bernal, I.; Herrmann, W. A. *J. Organomet. Chem.* **1979**, *179*, 403–410.

(65) Cadierno, V.; Díez, J.; Pilar Gamasa, M.; Gimeno, J.; Lastra, E. *Coord. Chem. Rev.* **1999**, *193-195*, 147–205.

(66) Ascenso, J. R.; de Azevedo, C. G.; Gonçalves, I. S.; Herdtweck, E.; Moreno, D. S.; Pessanha, M.; Romão, C. C. *Organometallics* **1995**, *14*, 3901–3919.

(67) Kowaleski, R. M.; Rheingold, A. L.; Trogler, W. C.; Basolo, F. *J. Am. Chem. Soc.* **1986**, *108*, 2460–2461.

(68) Ascenso, J. R.; Gonçalves, I. S.; Herdtweck, E.; Romão, C. C. *J. Organomet. Chem.* **1996**, *508*, 169–181.

(69) Drew, M. G. B.; Félix, V.; Gonçalves, I. S.; Romão, C. C.; Royo, B. *Organometallics* **1998**, *17*, 5782–5788.

(70) Merola, J. S.; Kacmarcik, R. T.; Van Engen, D. *J. Am. Chem. Soc.* **1986**, *108*, 329–331.

(71) Husebo, T. Le; Jensen, C. M. *Organometallics* **1995**, *14*, 1087–1088.

(72) Carl, R. T.; Hughes, R. P.; Rheingold, A. L.; Marder, T. B.; Taylor, N. J. *Organometallics* **1988**, *7*, 1613–1624.

(73) Marder, T. B.; Calabrese, J. C.; Roe, D. C.; Tulipg, T. H. *Organometallics* **1987**, *6*, 2012–2014.

(74) Li, W.-F.; Sun, H.-M.; Shen, Q.; Zhang, Y.; Yu, K.-B. *Polyhedron* **2004**, *23*, 1473–1478.

(75) Alías, F. M.; Belderrain, T. R.; Carmona, E.; Graiff, C.; Paneque, M.; Tiripicchio, A. *J. Organomet. Chem.* **1999**, *577*, 316–322.

(76) Huber, T. A.; Bayrakdarian, M.; Dion, S.; Dubuc, I.; Bélanger-Gariépy, F.; Zargarian, D. *Organometallics* **1997**, *16*, 5811–5815.

(77) Groux, L. F.; Zargarian, D. *Organometallics* **2001**, *20*, 3811–3817.

(78) Forschner, T. C.; Cutler, A. R.; Kullnig, R. K. *Organometallics* **1987**, *6*, 889–891.

(79) Köhler, F. H. *Chem. Ber.* **1974**, *107*, 570–574.

(80) Connelly, N. G.; Geiger, W. E. *Chem. Rev.* **1996**, *96*, 877–910.

(81) Burkey, D. J.; Hays, M. L.; Duderstadt, R. E.; Hanusa, T. P. *Organometallics* **1997**, *16*, 1465–1475.

(82) Okuda, J.; Albach, R. W.; Herdtweck, E.; Wagner, F. E. *Polyhedron* **1991**, *10*, 1741–1748.

(83) Burman, J. A.; Hays, M. L.; Burkey, D. J.; Tanner, P. S.; Hanusa, T. P. *J. Organomet. Chem.* **1994**, *479*, 135–139.

(84) Treichel, P. M.; Johnson, J. W.; Wagner, K. P. *J. Organomet. Chem.* **1975**, *88*, 227–230.

(85) Kölle, U.; Khouzami, F. *Angew. Chem. Int. Ed. Engl.* **1980**, *19*, 640–641.

(86) Schneider, J. J.; Czap, N.; Spickermann, D.; Lehmann, C. W.; Fontani, M.; Laschi, F.; Zanello, P. *J. Organomet. Chem.* **1999**, *590*, 7–14.

(87) Knizhnikov, V. A.; Shirokii, V. L.; Dikusar, E. A.; Ryabtsev, A. N.; Maier, N. A. *Russ. J. Gen. Chem.* **1997**, *67*, 1634–1637.

Chapter 3. Synthesis and reactivity of cobalt half-sandwich complexes with sterically demanding Cp′ ligand

Abstract

The series of halide-bridged Cp′Co half-sandwich complexes (Cp′ = 1,2,4-$(Me_3C)_3C_5H_2$) $[Cp'CoCl]_2$, $[Cp'CoBr]_2$ and $[Cp'CoI]_2$ were synthesized. The single crystal X-ray analyses, EPR spectroscopy and solid state magnetic susceptibility measurements were investigated.

The reactions of $[Cp'CoI]_2$ toward $KHBEt_3$ and MeLi to yield $[Cp'CoH]_2$ $[(Cp'Co)_2(\mu\text{-CH})(\mu\text{-H})]$, respectively, were studied.

3.1 Introduction

Metals in low oxidation states can cleave strong bonds in small molecules such as N_2, CO_2 and alkanes resulting in stoichiometric[1–9] and catalytic[10–12] transformations. Today, H^+ reduction attracts attention for energy storage.

Cobalt is one of the potential candidates for catalytic H^+ reduction catalysts because of the strong basicity of low-valent cobalt complexes.[13–19] For instance, Kölle *et al.* described the electrochemical H^+ reduction utilizing $[CpCo(PR_3)_2]$ ($Cp = C_5H_5$) and showed spectroscopically that hydride complexes are intermediates in this reaction.[20]

CpCo half-sandwich complexes have long been known. For example, $[CpCo(\eta^2\text{-}\eta^2\text{-1,3-diene})]$ complex is a catalyst for pyridine synthesis[21–23] and $CpCo(CO)_2$ for alkyne trimerization.[24–26] Common CpCo half-sandwich complexes can be described as $[CpCoL_2]$ or $[CpCoL_nX_{3-n}]^{(2-n)+}$ ($L = PR_3$, X = halogen, n = 0 – 3) with Co(I) or Co(III). The first examples of CpCo half-sandwich complexes with Co(II) were stabilized by phosphine ligands.[27–29]

Replacement of Cp by Cp* (Cp* = C_5Me_5) allows the syntheses of Cp* half-sandwich complexes with Co(II) under suitable conditions, which serve as starting compounds for a

wide variety of Cp*Co complexes. The reactivity of $[(Cp^R)CoX]_n$ (R = Me_5, Me_4Et; X = Cl, Br, I, NH_2, acetylacetonate (acac); n = 1, 2) in ligand exchange reactions or with donor ligands such as CO and pyridine were investigated intensively.[30–33] The reaction between $[Cp^*CoCl]_2$ (or $[Cp^*CoCl_2]_2$) and $LiAlH_4$ resulted a mixture of black $[(Cp^*Co)_3H_4]$ and purple $[(Cp^*Co)_2H_3]$.[34] $[(Cp^*Co)_2H_3]$ can be sublimed under reduced pressure at 50°C, while $[(Cp^*Co)_3H_4]$ was crystalized from *n*-hexane solution.

$[(Cp^*Co)_3H_4]$ shows a rich chemistry with small molecules such as CO[34] and various organic and inorganic substrates. $[(Cp^*Co)_3H_4]$ can be converted to *e.g.* $[Cp^*CoBr_2]$ and $[Cp^*CoI_2]$, $[Cp^*CoBr]_2$, [Cp*Co(acac)] (acac = acetylacetonate) and $[Cp^*Co(PEt_2)_2]^+$ with Br_2, I_2, $(CH_2)_2Br_2$, H(acac) / $AgBF_4$ and PEt_3 / HBF_4, respectively.[35] As mensioned above, [Cp*Co(acac)] is also useful as a source for the Cp*Co-fragment.[33,36] $[(Cp^*Co)_3H_4]$ was successfully prepared from $[Cp^*CoBr]_2$ using $LiAlH_4$.[35] In contrast, the reactivity of $[(Cp^*Co)_2H_3]$ was less investigated than $[(Cp^*Co)_3H_4]$,[34] and the determination of its molecular structure required several attempts. [37] However, $[Cp^*CoI]_2$ could not be isolated even at low temperature (–10°C)[30] and its existence was inferred from trapping experiments with CO and I_2/NH_4PF_6.[38]

In the previous chapter, the coordination chemistry of steric demanding indenyl ligand with manganese, iron and cobalt was investigated. From the reaction with 1,3-di-*tert*-butyl substituted indenyl ligand ($^{2t\text{Bu}}$Ind) and $Co(acac)_2$, $[^{2t\text{Bu}}IndCo_2]$ was obtained only in low yield presumably because of the formation of a cobalt half-sandwich complex, such as $[^{2t\text{Bu}}IndCo(acac)]$. Nevertheless, Bradley *et al.* showed the formation of cobalt half-sandwich complexes when the 1,3-di-(trimethylsilyl) substituted indenyl ligand was employed.[39,40]

The steric demanding 1,2,4-$(Me_3C)_3C_5H_2$ (Cp') ligand, could also stabilize intermediates, which were not feasible to isolate for Cp* or bulky alkyl substituted indenyl ligands. Moreover, while the coordination chemistry of the Cp' ligand was examined with Mn,[41] Fe[42–45] and Ni,[46,47] only a few examples with Co have been reported, such as the thermal and photochemical reaction of $[Cp'Co(CO)_2]$ with P_4[48] and the cobaltocen formation from $[Cp'CoCl]_2$.[49]

In this chapter, the coordination chemistry of Cp' ligands with cobalt and the reactivity of obtained $[Cp'CoI]_2$ are described.

3.2 Synthesis of the series $[Cp'CoX]_2$ (X = Cl, Br, I)

The series of μ-halide bridged cobalt half-sandwich complexes were synthesized. $CoCl_2$,

$CoBr_2(thf)_2$ or $CoI_2(thf)_3$ were reacted with NaCp′ of KCp′ in THF at room temperature (*ca.* 23°C). After complete removal of the solvent the raw products were extracted with pentane and filtered to remove the formed metal halides. Concentration and cooling of the solution to –30°C resulted brown/dark-turquoise dichroic blocks ([Cp′CoCl]$_2$), black red needles ([Cp′CoBr]$_2$) and black red tablets ([Cp′CoI]$_2$).

[Cp′CoI]$_2$ was obtained with moderate yield (60%) while [Cp′CoCl]$_2$ and [Cp′CoBr]$_2$ were only isolated in low yields (18% and 26%, respectively). The reason might the unoptimized reaction conditions. Sitzmann *et al.* synthesized [Cp′CoCl]$_2$ at –45°C (yield: 54%).[50] Schneider and Specht have obtained [Cp′CoBr]$_2$ in about 80% yield by the reaction at 0°C.[51] The yield of [Cp′CoI]$_2$ might also be increased if the reaction was carried out at low temperature.

The IR spectra of [Cp′CoCl]$_2$, [Cp′CoBr]$_2$ and [Cp′CoI]$_2$ were recorded (Figure 1). All spectra are as expected very similar. The peak shift of Co–X bond was not detected in the recorded window. UV-vis spectra of [Cp′CoCl]$_2$, [Cp′CoBr]$_2$ and [Cp′CoI]$_2$ were also measured and shown in Figure 2. Only a weak band in the visible region was observed in the spectrum of [Cp′CoI]$_2$.

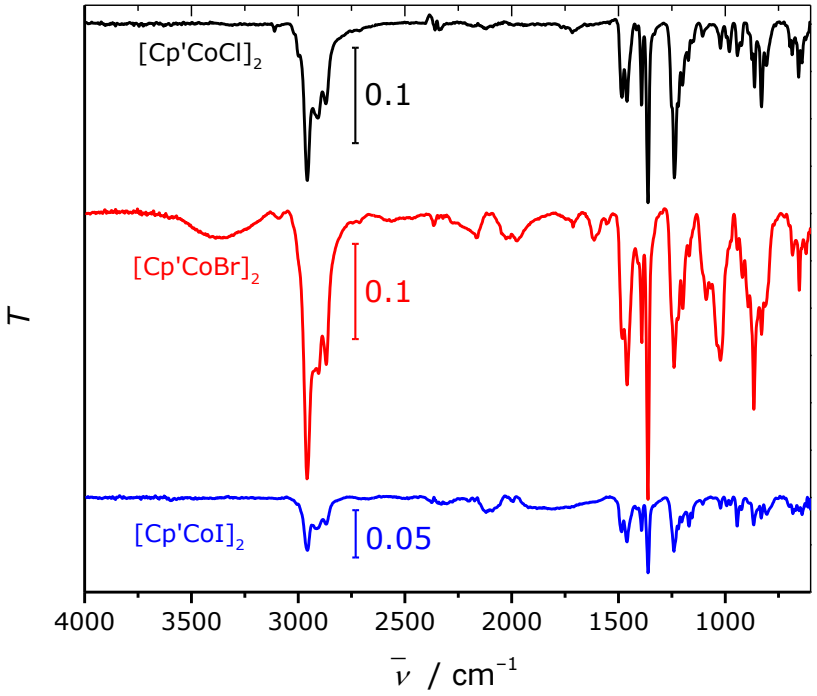

Figure 1. IR spectra of [Cp′CoCl]$_2$, [Cp′CoBr]$_2$ and [Cp′CoI]$_2$.

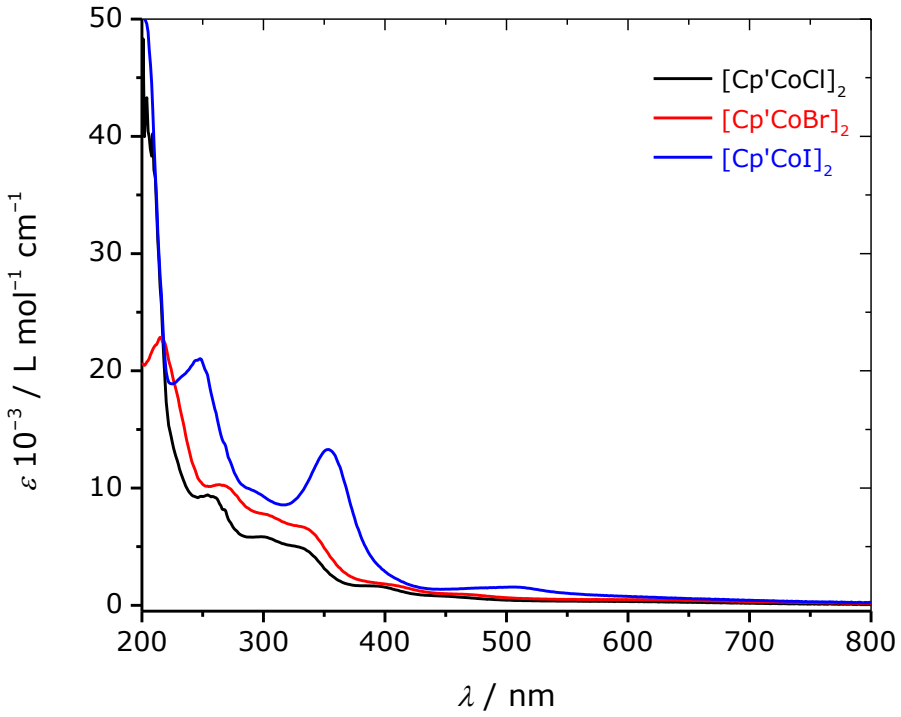

Figure 2. UV-vis spectra of [Cp′CoCl]$_2$, [Cp′CoBr]$_2$ and [Cp′CoI]$_2$ in *n*-hexane.

3.3 Solid state molecular structures

The molecular structures of the series [Cp′CoX]$_2$ (X = Cl, Br, I) were determined by X-ray single crystal diffraction at 100 K. [Cp′CoCl]$_2$ and [Cp′CoBr]$_2$ are known,[50,51] however, their molecular structures were not determined. The single crystals were grown from saturated pentane solutions ([Cp′CoCl]$_2$ and [Cp′CoI]$_2$), or dichloromethane solution ([Cp′CoBr]$_2$) at –30°C. [Cp′CoBr]$_2$ and [Cp′CoI]$_2$ are isostructual and crystallize in the triclinic space group $P\bar{1}$. In contrast, [Cp′CoCl]$_2$ crystallizes with two independent molecules in the monoclinic space group *P*n. ORTEP diagrams of [Cp′CoCl]$_2$, [Cp′CoBr]$_2$ and [Cp′CoI]$_2$ are shown in Figure 3. The Selected bond lengths and angles are summerized in Table 1. For [Cp′CoCl]$_2$, the following discussion focuses on the molecule shown in Figure 3.

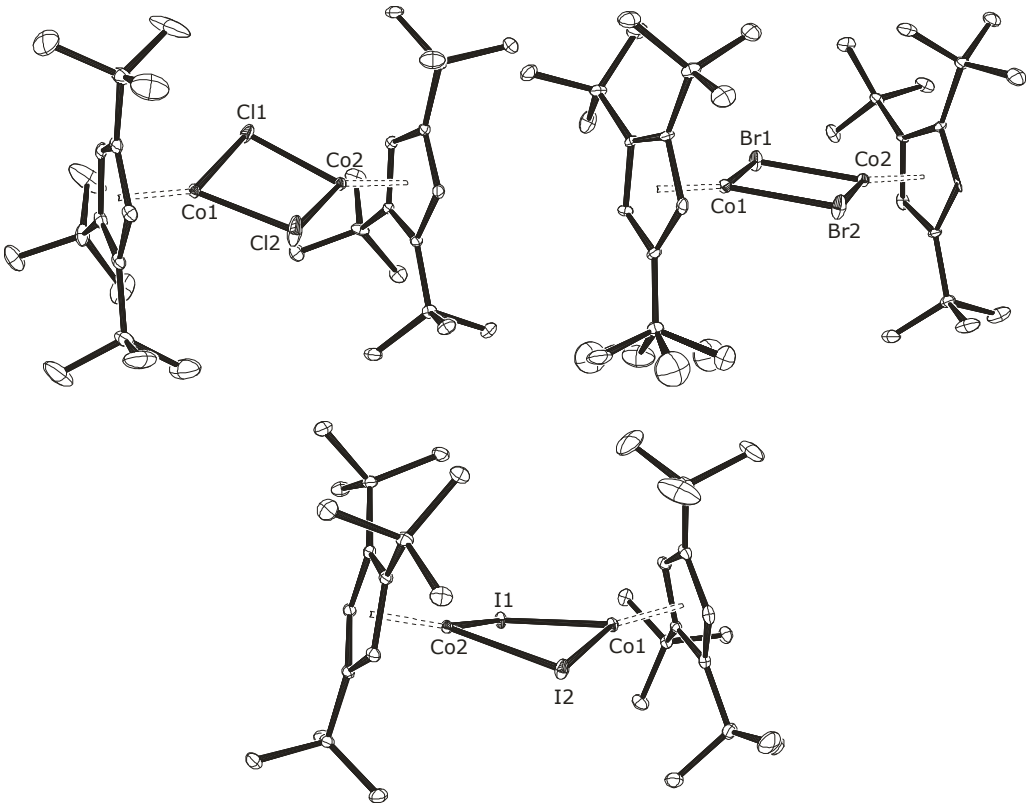

Figure 3. ORTEP diagram of $[Cp'CoCl]_2$ (top-left), $[Cp'CoBr]_2$ (top-right) and $[Cp'CoI]_2$ (bottom) with 30 % probability ellipsoids. Hydrogen atoms are omitted for clarity

Table 1. Selected bond lengths [Å] and angles [°] of $[Cp'CoCl]_2$, $[Cp'CoBr]_2$ and $[Cp'CoI]_2$.

	$[Cp'CoCl]_2$	**$[Cp'CoBr]_2$**	**$[Cp'CoI]_2$**
Cp'_{cent}–Co	1.68 / 1.68 / 1.69 / 1.68	1.68 / 1.68	1.70 / 1.70
Co–Co (calcd)	3.21 / 3.24	3.39	3.57
Co–X (av.)	2.2442(9) / 2.2487(9)	2.3745(10)	2.5564(2)
Co–X–Co′–X	8.55(4) / 0.24(3)	0.10(4)	16.511(8)

$[Cp'CoI]_2$ adopts a butterfly conformation, while the Co_2Br_2 core in $[Cp'CoBr]_2$ is almost planar. A *tert*-butyl group is disordered in $[Cp'CoBr]_2$.

The average Cp_{cent}–Co distances of 1.69 Å, 1.68 Å and 1.70 Å for $[Cp'CoCl]_2$, $[Cp'CoBr]_2$ and $[Cp'CoI]_2$, respectively, is consistent with low-spin Co(II) atoms. These values can be comparable to related structures of $[^4CpCoCl]_2$ ($^4Cp = i Pr_4C_5H$) (1.68 Å),[50] $[Cp^*CoBr]_2$ (1.68 Å)[35] and $[Cp^*CoBr_2]_2$ (1.69 Å),[52] although $[Cp^*CoBr_2]_2$ has Co(III) as a metal center.

The Co–Co distances are 3.22 Å ([Cp′CoCl]$_2$), 3.39 Å ([Cp′CoBr]$_2$) and 3.57 Å ([Cp′CoI]$_2$), *i.e.* the Co–Co distance becomes longer when the size of the bridging halide increases. The Co–Co distance in the related complexes [^{4}CpCoCl]$_2$, [Cp*CoBr]$_2$ and [Cp*CoBr$_2$]$_2$ are 3.183(2) Å,[50] 2.762(3) Å[35] and 3.616(2) Å[52], respectively. The steric demand of the Cp ligand also affects the Co–Co distance.

The average Co–μ-X distances are 2.2442(9) Å for [Cp′CoCl]$_2$, 2.3745(10) Å for [Cp′CoBr]$_2$ and 2.5564(2) Å for [Cp′CoI]$_2$, those reflects the ion radius of the halides. The Co–μ-X distance in relevant complexes [^{4}CpCoCl]$_2$, [Cp*CoBr]$_2$ and [Cp*CoBr$_2$]$_2$ are 2.217(3) Å,[50] 2.372(1) Å[35] and 2.4549(14) Å[52], respectively.

3.4 Spin behavior and solid state magnetic susceptibility

To investigate the spin behavior and the magnetic moment in these complexes, EPR spectra for [Cp′CoCl]$_2$, [Cp′CoBr]$_2$ and [Cp′CoI]$_2$ were recorded at 87 K in frozen toluene glass and solid state magnetic susceptibility measurements were carried out at 1 kG from 2 to 300 K. The EPR parameters are summarized in Table 2, and the EPR spectra and simulation are shown in Figure 4.

Table 2. EPR parameters in frozen toluene glass at 87 K and μ_{eff} in solid state at 300 K of [Cp′CoCl]$_2$, [Cp′CoBr]$_2$ and [Cp′CoI]$_2$.

	[Cp′CoCl]$_2$	**[Cp′CoBr]$_2$**	**[Cp′CoI]$_2$**
g_x	2.289	2.301	2.317
g_y	2.082	2.076	2.068
g_z	1.979	2.002	2.037
A_x [G]	270.0	248.4	220.0
A_y [G]	0	0	0
A_z [G]	112.6	87.0	90.0
μ_{eff} [B.M.]	2.75	2.66	2.49

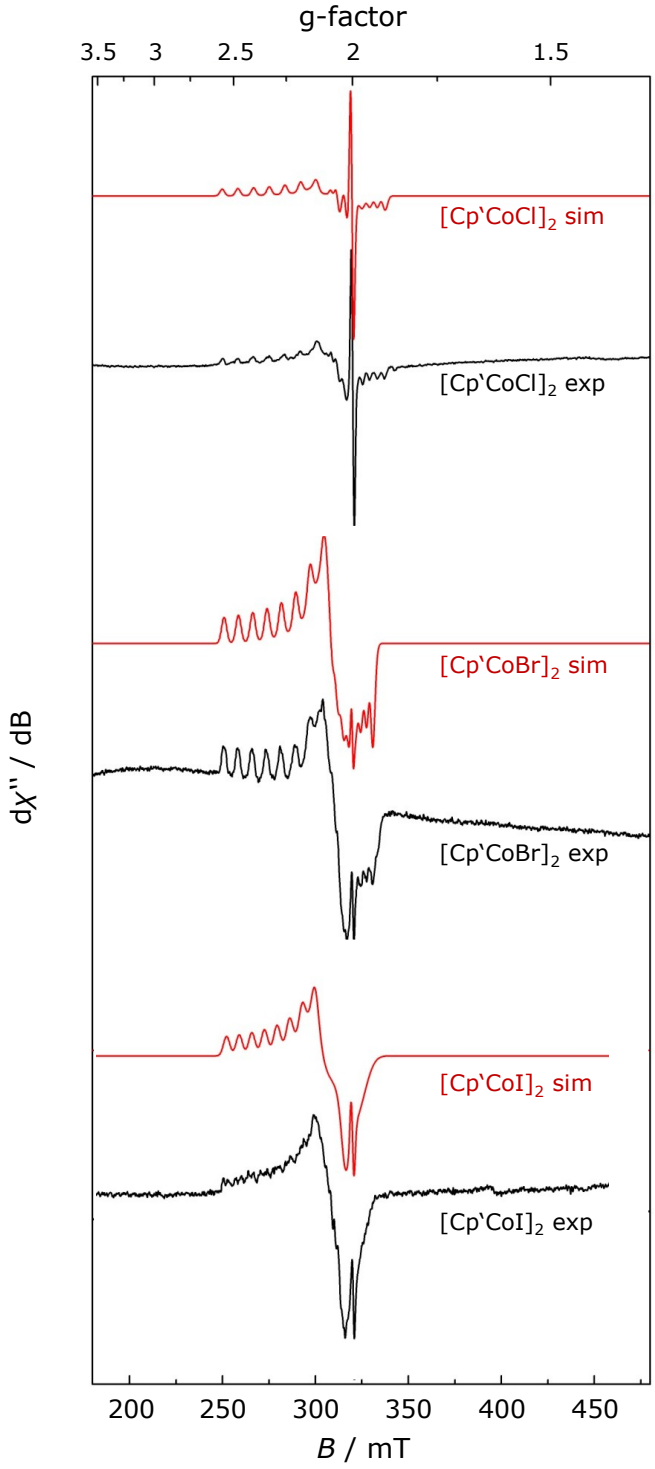

Figure 4. EPR spectra of [Cp′CoCl]$_2$, [Cp′CoBr]$_2$ and [Cp′CoI]$_2$ in toluene at 87 K.

The EPR spectra suggest that the Cp′Co-complexes have Co(II) center and exist in the solution as monomers or as dimers without any Co–Co interaction, since only eight lines are observed. Cobalt has one stable isotop with $I\{^{59}\text{Co}\} = 7/2$, thus, the typical splitting pattern consists of eight lines. If the complexes are dimers in the solution, fifteen lines would be

expected. The halides have also nuclear spins ($I\{^{35}Cl\} = 3/2$, $I\{^{37}Cl\} = 3/2$, $I\{^{79}Br\} = 3/2$, $I\{^{81}Br\} = 3/2$ and $I\{^{127}I\} = 5/2$). Therefore, the coupling between cobalt and halides should also be observed. The reason that no Co–X coupling was observed might be very small coupling constants. Only $[Cp'CoI]_2$ exhibit the hyperfine splitting by cobalt–halide coupling, however, its coupling constant could not be determined. In all compounds the signal at 2.000 was detected, which might be caused by an organic radical.

The μ_{eff} *vs. T* plots for $[Cp'CoCl]_2$, $[Cp'CoBr]_2$ and $[Cp'CoI]_2$ are shown in Figure 5. The Co(II) low-spin centers in $[Cp'CoCl]_2$, $[Cp'CoBr]_2$ and $[Cp'CoI]_2$ are also confirmed by the effective magnetic moments of 2.75 B.M. for $[Cp'CoCl]_2$, 2.66 B.M. for $[Cp'CoBr]_2$ and 2.49 B.M. for $[Cp'CoI]_2$ at 300 K. The cobalt centers in all complexes are antiferromagnetically coupled and a spin-crossover can be excluded, since only one species was detected in each EPR spectrum at 87 K. The magnetic moment for all compounds are comparable to relevant complex $[^4CpCoCl]_2$ (2.26 B.M.) at 300 K.[50] The effective magnetic moments for Cp*Co hydride complexes $[(Cp^*Co)_2H_3]$ and $[(Cp^*Co)_3H_4]$ were also determined (2.2(2) B.M. at room temperature and 3.9 ± 0.2 B.M. by Evans method, respectively).[34]

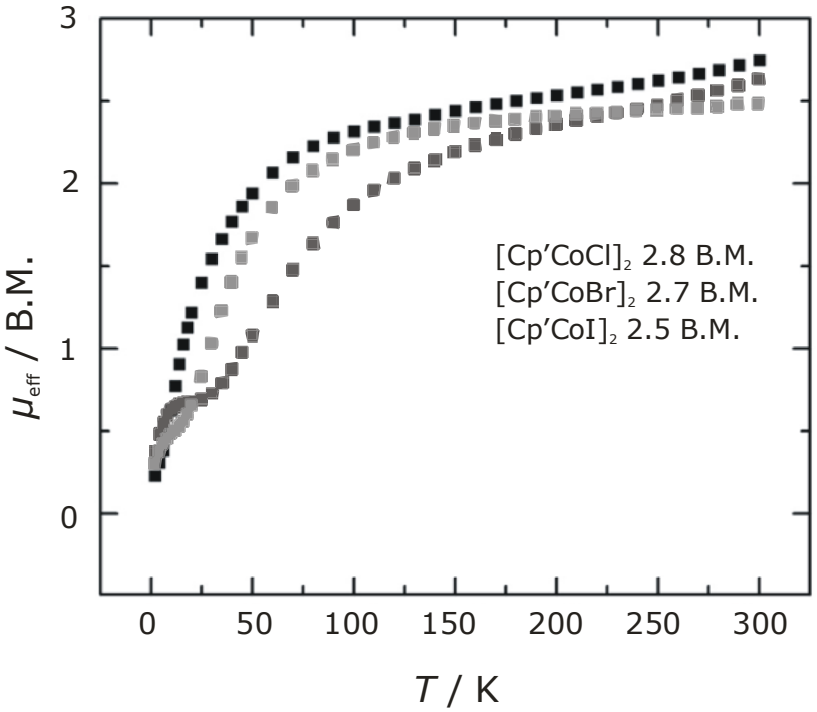

Figure 5. The plots of solid state magnetic moment μ_{eff} *vs. T* for $[Cp'CoCl]_2$, $[Cp'CoBr]_2$ and $[Cp'CoI]_2$.

3.5 Attempetd syntheses of $[Cp'CoH]_n$

The synthesis of cobalt hydride complex $[Cp'CoH]_n$ was investigated using $[Cp'CoI]_2$ as starting material which was reacted with $KHBEt_3$ and KBH_4 were chosen as a hydride source.

$[Cp'CoCl]_2$, $[Cp'CoBr]_2$ and $[Cp'CoI]_2$ are all paramagnetic, accordingly no Co–Co interaction is expected in those complexes and therefore the dimer should dissociate readily. This property can increase the reactivity of the complexes. Above all, $[Cp'CoI]_2$ is expected to be a more suitable starting material because of the good leaving group properties of iodide. The stability of the relevant Cp* complexes increases in the order $[Cp^*CoCl]_2 > [Cp^*CoBr]_2 > [Cp^*Co(NH_2)]_2 >> [Cp^*CoI]_2$.[38]

The reaction between $[Cp'CoI]_2$ and $KHBEt_3$ gave the expected cobalt dihydride complex $[Cp'CoH]_2$. In contrast, the reactions of $[Cp^*CoCl]_2$ or $[Cp'CoBr]_2$ with $LiAlH_4$ yielded the cobalt trihydride complexes $[(Cp^*Co)_2H_3]$[34] and $[(Cp'Co)_2H_3]$,[51] respectively. However, the formation of $[(Cp'Co)_3H_4]$ was not described. Reactions of relevant Cp′ half-sandwich complexes, $[Cp'FeI]_2$ and $[Cp'MnI(thf)]_2$, with KBH_4 formed the bimetallic iron polyhydrides $[Cp'FeH_2]_2$ and $[(Cp'Fe)_2H_3]$,[43] and manganese hydride cluster $[Cp'Mn]_4[MnH_6]$.[41]

The molecular structure of $[Cp'CoH]_2$ is illustrated in Figure 6. The selected bond lengths and angles of $[Cp'CoH]_2$ and related CpCo hydride derivatives are summerized in Table 3.

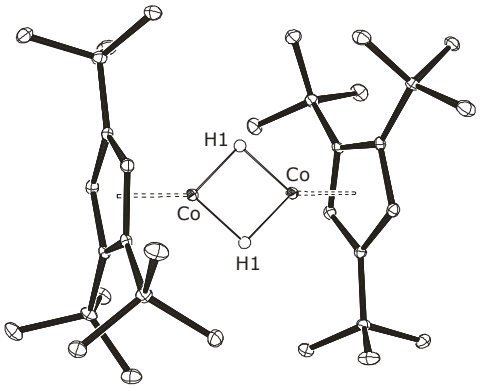

Figure 6. ORTEP diagram of $[Cp'CoH]_2$ with 30% probability ellipsoids. Hydrogen atoms of the Cp′ ring and *t*Bu group are omitted for clarity.

Table 3. Selected bond lengths [Å] and angles [°] of $[Cp'CoH]_2$ and related CpCo hydride derivatives.

	$[Cp'CoH]_2$	$[(Cp'Co)_2H_3]$	$[(^{2tBu}CpCo)_2H_3]$ (^{2tBu}Cp = 1,3-$(Me_3C)_2C_5H_3$)	$[(Cp^*Co)_2H_3]$	$[(Cp^*Co)_3H_4]$
space group	$P4_12_12$	$P4_32_12$	$P\bar{1}$	$P2/c$	$P2_1/n$
Cp_{cent}–Co (av.)	1.67	1.66	1.69	1.68	1.72
Co–Co	2.2344(5)	2.275(9)	2.244(2)	2.254(4)	2.476(5) (av.)
Co–H (av.)	1.48(3)	1.64(1)	—	1.642(5)	—
Co–H–Co′ (av.)	98(1)	88.1(6)	—	86.7(2)	—
ref.	this work	53	54	37	34

With the expection of $[(Cp^*Co)_3H_4]$, the Cp_{cent}–Co bond lengths in these four complexes are not much different. Unlike the bimetallic iron polyhydrides $[Cp'FeH_2]_2$ (1.71 Å) and $[(Cp'Fe)_2H_3]$ (1.66 Å), the steric demand or the number of bridging hydride atomes appear to not affect Cp_{cent}–Co bond lengths. The distance between the two Co atoms (2.2344(5) Å) is shorter than the typical value for Co–Co double bond (2.3 – 2.4 Å).[55,56] The Co–Co distance (2.2344(5) Å) and the average Co–H bond length (1.48(3) Å) in $[Cp'CoH]_2$ is shorter than in $[(Cp'Co)_2H]_3$ (2.275(9) Å and 1.64(1) Å, respectively), whereas, the average angle Co–H–Co′ in $[Cp'CoH]_2$ (98(1)°) is also larger than these in $[(Cp'Co)_2H]_3$ (av. 88.1(6)°). In contrast, $[(Cp'Fe)_2H_3]$ exhibits a longer Fe–Fe distance (2.2205(6) Å) and slightly shorter Fe–H bond lengths (av. 1.58(4) Å) than $[Cp'FeH_2]_2$ (2.1989(5) Å and av. 1.60(3) Å, respectively).[57] $[Cp'CoH]_2$ and $[(Cp'Co)_2H]_3$ crystallize in the tetragonal space groups $P4_12_12$ and $P4_32_12$, respectively, and their unit cell volumes are also very similar, whereas to $[Cp'FeH_2]_2$ and $[(Cp'Fe)_2H_3]$ crystallize in different space groups, triclinic $P\bar{1}$ or tetragonal $P4_12_12$, respectively.[43]

Hydrogenation of a $[Cp'CoR]_n$ precursor can also be considered as a synthetic pathway to $[Cp'CoH]_n$ complexes, thus, the reaction $[Cp'CoI]_2$ with two equivalent of CH_3Li was also attempted. However, unexpectedly the methylene- and hydride-bridged cobalt complex $[(Cp'Co)_2(\mu\text{-}CH)(\mu\text{-}H)]$ was isolated. The solid state molecular structure of $[(Cp'Co)_2(\mu\text{-}CH)(\mu\text{-}H)]$ is depicted in Figure 7.

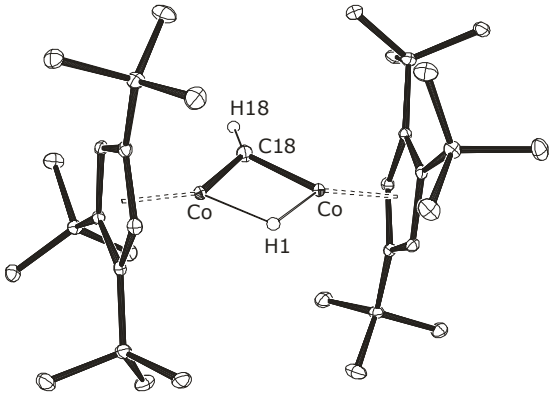

Figure 7. ORTEP diagram of [(Cp′Co)$_2$(μ-CH)(μ-H)] with 30% probability ellipsoids. Hydrogen atoms on the Cp′ ring and *t*Bu group are omitted for clarity. Selected bond lengths [Å] and angles [°]: Cp′$_{cent}$–Co 1,68, Co–Co′ 2.3614(4), Co–H1 1.58(2), Co–C18 1.7583(18), C18–H18 0.97(3), Co–C18–Co′ 84.36(10), Co–H1–Co′ 97(1).

The single crystal of [(Cp′Co)$_2$(μ-CH)(μ-H)] was grown from concentrated Et$_2$O solution at –30°C with imposed inversion symmetry in tetragonal space group $P4_32_12$. Co–Co distance (2.3614(4) Å) is longer than these in [Cp′CoH]$_2$, however, it is also shorter than the typical value for Co–Co double bond (2.3 – 2.4 Å).[55,56]

A possible reaction mechanisms are that 1) [Cp′CoMe] was formed as an intermediate, or 2) [Cp′CoMe]$_2$ was formed, then an elimination of CH$_4$ was occurred (Scheme 1).

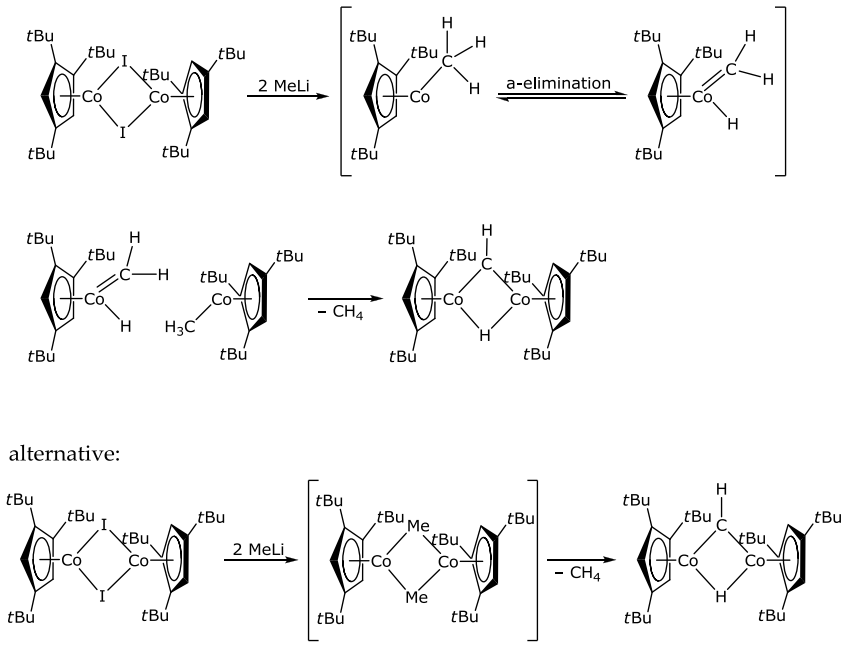

Scheme 1. Possible reaction mechanisms of the formation of [(Cp′Co)$_2$(μ-CH)(μ-H)].

The similar reactions of [Cp*Co(acac)] or [Cp′FeI]$_2$ with MeLi, and [^{4}CpNiBr]$_2$ with MeMgCl were also investigated. [Li(OEt$_2$)][Cp′] was formed from [Cp′FeI]$_2$ and MeLi,[45] while the reaction of [^{4}CpNiBr]$_2$ and MeMgCl yielded [(^{4}CpNi)$_2$(CH$_2$)][58] and [(Cp*Co)$_3$(μ^3-CH)(μ^3-H)] was isolated from [Cp*Co(acac)] and MeLi,[59] however, the [Cp′FeMe]$_2$, [^{4}CpNiMe]$_2$ and [Cp*CoMe]$_2$ were not obtained.

3.6 Conclusion

A series of halide-bridged Cp′Co half-sandwich complexes [Cp′CoI]$_2$, [Cp′CoI]$_2$ and [Cp′CoI]$_2$ were synthesized and characterized. Their molecular structures were determined and EPR and solid state magnetic susceptibility studies are consistent with low-spin Co(II) atoms.

The synthesis of [Cp′CoH]$_2$ from [Cp′CoI]$_2$ was also attempted. Using KHBEt$_3$ as a hydride source, [Cp′CoH]$_2$ was obtained, while the reaction of [Cp′CoI]$_2$ and MeLi yielded methylidyne bridged complex [(Cp′Co)$_2$(μ-CH)(μ-H)]. The reaction of [Cp′CoI]$_2$ with NaBH$_4$ is still under investigation.

In future, the reactivity of [Cp′CoI]$_2$ will be further investigated, *e.g.* regarding the alkylation with Mg(CH$_2$SiMe$_3$)$_2$ or Mg(CH$_2$CMe$_2$Ph)$_2$ or ligand exchange with pseudohalides.

3.7 References

(1) LaPointe, R. E.; Wolczanski, P. T.; Mitchell, J. F. *J. Am. Chem. Soc.* **1986**, *108*, 6382–6384.

(2) Hay-Motherwell, R. S.; Wilkinson, G.; Hussain-Bates, B.; Hursthouse, M. B. *Polyhedron* **1993**, *12*, 2009–2012.

(3) Laplaza, C. E.; Johnson, M. J. A.; Peters, J. C.; Odom, A. L.; Kim, E.; Cummins, C. C.; George, G. N.; Pickering, I. J. *J. Am. Chem. Soc.* **1996**, *118*, 8623–8638.

(4) Negishi, E.; Takahashi, T. *Bull. Chem. Soc. Jpn.* **1998**, *71*, 755–769.

(5) Rosenthal, U.; Burlakov, V. V.; Arndt, P.; Baumann, W.; Spannenberg, A. *Organometallics* **2003**, *22*, 884–900.

(6) Pool, J. A.; Lobkovsky, E.; Chirik, P. J. *Nature* **2004**, *427*, 527–530.

(7) Konnick, M. M.; Guzei, I. a; Stahl, S. S. *J. Am. Chem. Soc.* **2004**, *126*, 10212–10213.

(8) Knobloch, D. J.; Lobkovsky, E.; Chirik, P. J. *Nat. Chem.* **2010**, *2*, 30–35.

(9) Cai, X.; Majumdar, S.; Fortman, G. C.; Cazin, C. S. J.; Slawin, A. M. Z.; Lhermitte, C.; Prabhakar, R.; Germain, M. E.; Palluccio, T.; Nolan, S. P.; Rybak-Akimova, E. V; Temprado, M.; Captain, B.; Hoff, C. D. *J. Am. Chem. Soc.* **2011**, *133*, 1290–1293.

(10) Kiplinger, J. L.; Richmond, T. G. *J. Am. Chem. Soc.* **1996**, *118*, 1805–1806.

(11) Sanford, M. S.; Love, J. a; Grubbs, R. H. *J. Am. Chem. Soc.* **2001**, *123*, 6543–6554.

(12) Barder, T. E.; Biscoe, M. R.; Buchwald, S. L. *Organometallics* **2007**, *26*, 2183–2192.

(13) Rakowski, M. C.; Muetterties, E. L. *J. Am. Chem. Soc.* **1977**, *99*, 739–743.

(14) Carter, S. J.; Stuhl, L. S. *Organometallics* **1988**, *7*, 1909–1918.

(15) Li, H. L.; Anderson, W. C.; Chambers, J. Q.; Hobbs, D. T. *Inorg. Chem.* **1989**, *28*, 863–868.

(16) Basallote, M. G.; Hughes, D. L.; Jiménez-Tenorio, M.; Leigh, G. J.; Vizcaíno, M. C. P.; Jiménez, P. V. *J. Chem. Soc., Dalton Trans.* **1993**, 1841–1847.

(17) Klein, H.; Mager, M.; Schmidt, A.; Hüber, M.; Haase, W.; Flörke, U.; Haupt, H.-J.; Boca, R. *Inorg. Chem.* **1997**, *36*, 4303–4306.

(18) Lee, H. K.; Lam, C. H.; Li, S. L.; Zhang, Z. Y.; Mak, T. C. *Inorg. Chem.* **2001**, *40*, 4691–4695.

(19) Hu, X.; Castro-Rodriguez, I.; Meyer, K. *J. Am. Chem. Soc.* **2004**, *126*, 13464–13473.

(20) Koelle, U.; Paul, S. *Inorg. Chem.* **1986**, *25*, 2689–2694.

(21) Bönnemann, H. *Angew. Chem. Int. Ed. Engl.* **1978**, *17*, 505–515.

(22) Vollhardt, K. P. C. *Angew. Chem. Int. Ed. Engl.* **1984**, *23*, 539–556.

(23) Bönnemann, H. *Angew. Chem. Int. Ed. Engl.* **1985**, *24*, 248–262.

(24) Nehl, H. *Chem. Ber.* **1993**, *126*, 1519–1527.

(25) Chebny, V. J.; Dhar, D.; Lindeman, S. V; Rathore, R. *Org. Lett.* **2006**, *8*, 5041–5044.

(26) Agenet, N.; Gandon, V.; Vollhardt, K. P. C.; Malacria, M.; Aubert, C. *J. Am. Chem. Soc.* **2007**, *129*, 8860–8871.

(27) Pfeiffer, E.; Kokkes, M. W.; Vrieze, K. *Transit. Met. Chem.* **1979**, *4*, 393–396.

(28) McKinney, R. J. *Inorg. Chem.* **1982**, *21*, 2051–2056.

(29) Broadley, K.; Connelly, N. G.; Geiger, W. E. *J. Chem. Soc., Dalton Trans.* **1983**, 121–125.

(30) Kölle, U.; Fuss, B. *Chem. Ber.* **1984**, *117*, 743–752.

(31) Kölle, U.; Fuss, B. *Chem. Ber.* **1984**, *117*, 753–762.

(32) Kölle, U.; Fuss, B.; Belting, M.; Raabe, E. *Organometallics* **1986**, *5*, 980–987.

(33) Takemoto, S.; Honma, T.; Matsuzaka, H. *Organometallics* **2011**, *30*, 1013–1020.

(34) Kersten, J. L.; Rheingold, A. L.; Theopold, K. H.; Casey, C. P.; Widenhoefer, R. A.; Hop, C. E. C. A. *Angew. Chem. Int. Ed. Engl.* **1992**, *31*, 1341–1343.

(35) Schneider, J. J.; Goddard, R.; Krüger, C. *Z. Naturforsch.* **1995**, *50b*, 448–459.

(36) Manriquez, J. M.; Ward, M. D.; Calabrese, J. C.; Fagan, P. J.; Epstein, A. J.; Miller, J. S. *Mol. Cryst. Liq. Cryst. Inc. Nonlinear Opt.* **1989**, *176*, 527–534.

(37) Lutz, F.; Bau, R.; Wu, P.; Koetzle, T. F.; Krüger, C.; Schneider, J. J. *Inorg. Chem.* **1996**, *35*, 2698–2700.

(38) Kölle, U.; Khouzami, F.; Fuss, B. *Angew. Chem. Int. Ed. Engl.* **1982**, *21*, 230–240.

(39) Hung-Low, F.; Bradley, C. A. *Organometallics* **2011**, *30*, 2636–2639.

(40) Hung-Low, F.; Bradley, C. A. *Inorg. Chem.* **2013**, *52*, 2446–2457.

(41) Maekawa, M.; Römelt, M.; Daniliuc, C. G.; Jones, P. G.; White, P. S.; Neese, F.; Walter, M. D. *Chem. Sci.* **2012**, *3*, 2972–2979.

(42) Walter, M. D.; White, P. S. *New J. Chem.* **2011**, *35*, 1842–1854.

(43) Walter, M. D.; Grunenberg, J.; White, P. S. *Chem. Sci.* **2011**, *2*, 2120–2130.

(44) Walter, M. D.; White, P. S. *Dalton Trans.* **2012**, *41*, 8506–8508.

(45) Walter, M. D.; White, P. S. *Inorg. Chem.* **2012**, *51*, 11860–11872.

(46) Wallasch, M. W.; Rudolphi, F.; Wolmershäuser, G.; Sitzmann, H. *Z. Naturforsch.* **2009**, *64b*, 11–17.

(47) Schär, M.; Saurenz, D.; Zimmer, F.; Schädlich, I.; Wolmershäuser, G.; Demeshko, S.; Meyer, F.; Sitzmann, H.; Heigl, O. M.; Köhler, F. H. *Organometallics* **2013**, *32*, 6298–6305.

(48) Scherer, O. J.; Berg, G.; Wolmershäuser, G. *Chem. Ber.* **1995**, *128*, 635–639.

(49) Schneider, J. J.; Czap, N.; Spickermann, D.; Lehmann, C. W.; Fontani, M.; Laschi, F.; Zanello, P. *J. Organomet. Chem.* **1999**, *590*, 7–14.

(50) Baumann, F.; Dormann, E.; Ehleiter, Y.; Kaim, W.; Kärcher, J.; Kelemen, M.; Krammer, R.; Saurenz, D.; Stalke, D.; Wachter, C.; Wolmershäuser, G.; Sitzmann, H. *J. Organomet. Chem.* **1999**, *587*, 267–283.

(51) Schneider, J. J.; Specht, U. *Z. Naturforsch.* **1995**, *50b*, 684–686.

(52) Stoll, C.; Lorenz, I.-P.; Polborn, K.; Paulus, E. F. *Z. Naturforsch.* **1999**, *54b*, 583.

(53) Bortz, M.; Bau, R.; Schneider, J. J.; Mason, S. A. *J. Clust. Sci.* **2001**, *12*, 285–291.

(54) Schneider, J. J.; Specht, U.; Goddard, R.; Krüger, C. *Chem. Ber.* **1997**, *130*, 161–170.

(55) Jones, R. A.; Stuart, A. L.; Atwood, J. L.; Hunter, W. E. *Organometallics* **1983**, *2*, 1437–1441.

(56) Enders, M.; Ludwig, G.; Pritzkow, H. *Organometallics* **2001**, *20*, 827–833.

(57) Walter, M. D.; Grunenberg, J.; White, P. S. *Chem. Sci.* **2011**, *2*, 2120–2130.

(58) Weismann, D.; Saurenz, D.; Boese, R.; Bläser, D.; Wolmershäuser, G.; Sun, Y.; Sitzmann, H. *Organometallics* **2011**, *30*, 6351–6364.

(59) Smith, M. E.; Andersen, R. A. *Organometallics* **1996**, *15*, 2680–2682.

La vérité, ce n'est point ce qui se démontre, c'est ce qui simplifie.
<Terre des hommes>
– Antoine de Saint-Exupéry (1900 – 1944)

Chapter 4. Reaction of the half-sandwich iron complex [Cp'FeI]$_2$ toward pseudohalides

Abstract

Reactions of [Cp'FeI]$_2$ (Cp' = 1,2,4-(Me_3C)$_3$$C_5H_2$) (**1**) and [Cp'MnI(thf)]$_2$ (**2**) with pseudohalides were investigated. In contrast to the halides, the pseudohalides behave as reaction partners. A series of nitrido-, sulfido-, cyanato-, diselenido- and thiocyanato-bridged iron and manganese complexes [Cp'FeN]$_2$ (**5**), [Cp'FeS]$_2$ (**6**), [Cp'Fe(NCO)]$_2$ (**3**), [Cp'Fe(Se_2)]$_2$ (**7**) and [Cp'Mn(NCS)(thf)]$_2$ (**4**) were prepared and spectroscopically and crystallographically characterized.

These new scomplexes exhibit different oxidation states, thus their electronic structures were also investigated by Mössbauer spectroscopy and SQUID magnetometry. These results suggest a rich redox chemistry of the Cp'Fe-fragment.

4.1 Introduction

Metal-element multiple bonds M=E or M≡E (E = CR_2, CR, NR, N or O) are proposed key intermediates in a number of catalytic transformations such as oxygen-, sulfur- and nitrogen-transfer reaction by cytochrom P450, and their properties and reactivities are under intensive investigations.[1–8] Although the nitrido complexes of early and middle transition metals are stable, those of the late transition metals have only been successfully synthesized with Fe, Ru Os and Ir.[9] Some examples of metal-nitrido complexes are shown in Figure 1.[10–13]

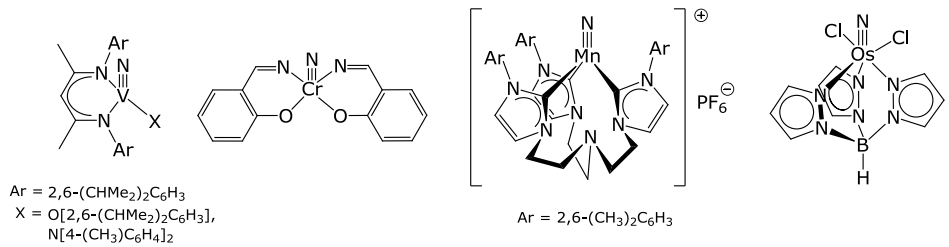

Figure 1. Some examples for metal-nitrido-complex.

Much attention has been paid to iron nitridos, which are possible intermediates in the biological[14–18] and the industrial (*e.g.* Haber-Bosch)[19] nitrogen fixation processes. Biological N_2 fixation occurs by the enzyme nitrogenase, which can also activate small molecules such as CS_2, SCN^- or OCN^-,[20] and CO_2 or COS.[21] Molecular systems with an Fe(V)≡N functionality are difficult to obtain,[22] but a molecular model system with very strongly σ-donating *N*-heterocyclic carbene (NHC) ligands was recently prepared. This complex reacts with water and releases ammonia in high yield under reducing conditions at low temperature (Scheme 1).[15]

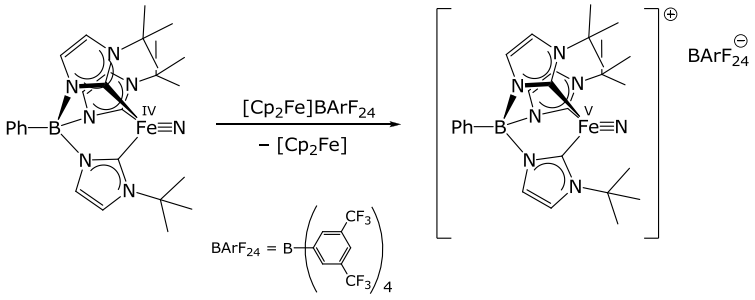

Scheme 1. Preparation of an Fe(V)≡N complex.

Some N_2 activation reactions to yield iron nitrido complexes have also been reported. Recently, a catalytic reduction of N_2 to NH_3 by an Fe–N_2 complex was demonstrated by Peters *et al.*[23,24] Holland *et al.* showed that an iron potassium complex supported by a β-diketiminato (nacnac) ligand is able to reduce dinitrogen to ammonia (Scheme 2).[25]

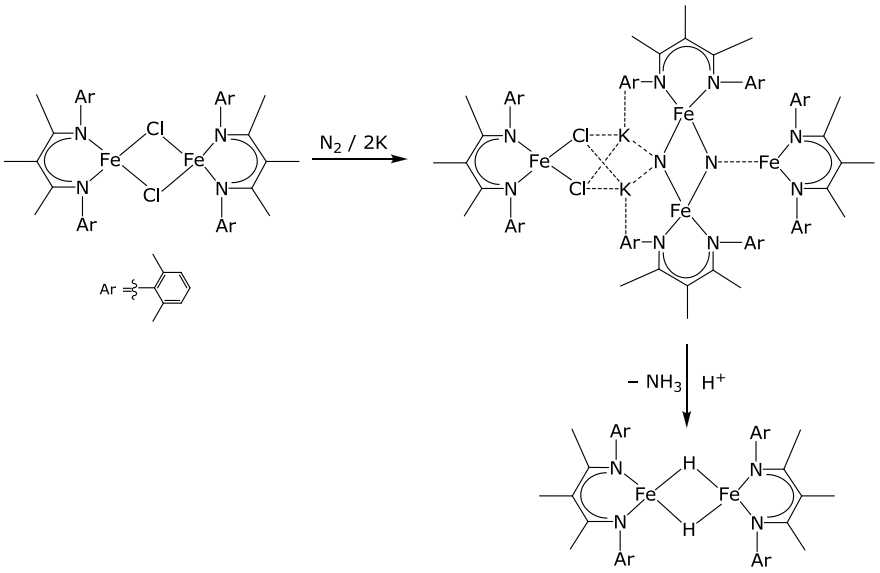

Scheme 2. Reduction of N_2 to ammonia by iron potassiumat complex supported by *N*-bonding ligand.

In this chapter, the use of the sterically demanding 1,2,4-$(Me_3C)_3C_5H_2$ (Cp') ligand for the stabilization of various oxidation states of iron will be explored. For this purpose, the half-sandwich complex $[Cp'FeI]_2$ (**1**) has shown promising synthetic potential in previous studies.[26–28] The iodide in **1** is readily exchanged by salt-metathesis reactions to give monomeric iron anilido and amido complexes that can be further converted into more highly functionalized complexes.[27] The halogen exchanges in $[Cp'FeI]_2$ and its analogeous compound $[Cp'FeBr]_2$ with aryl anions were also investigated. The Cp'Fe-fragment favors a η^5 coordination mode, but not κ^1 for the steric less demanding aryl ligands.[27,29–32]

Complex **1** can be reduced to the Fe(I) complex $[Cp'Fe(CO)_2]_2$ in several ways,[27] whose reactivity toward phosphorus and arsenic has been explored by Scherer *et al.* (Scheme 3).[33–35]

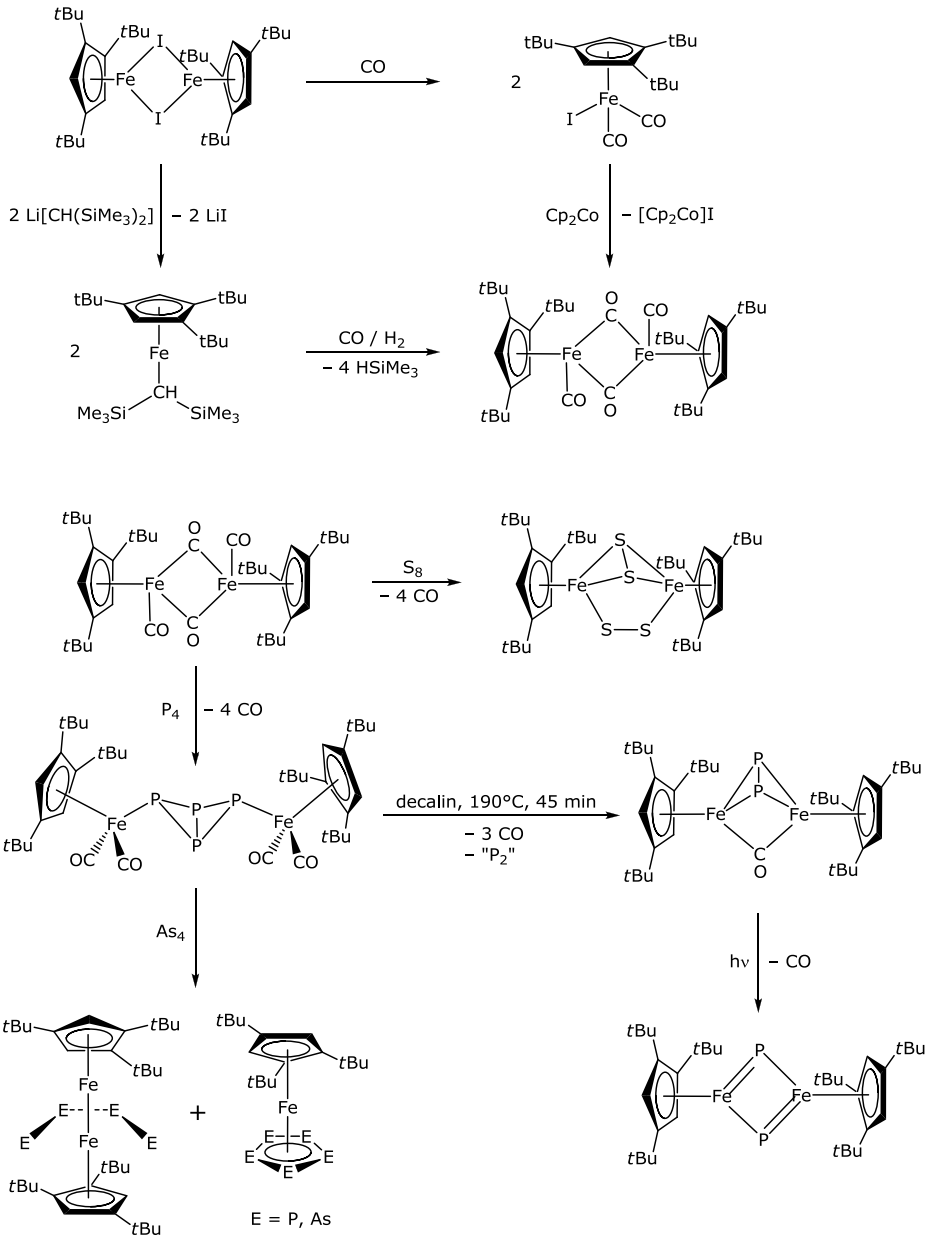

Scheme 3. Synthetic pathways to [Cp'Fe(CO)$_2$] and its further reactivity.

As shown in Scheme 4, [Cp'FeI]$_2$ can be oxidized by 1,2-diiodoethane to give the iron(III) complex [Cp'FeI$_2$][26] (**2**) that opens the possibility for further investigation of its reactivity. Additionally, the reaction of [Cp'FeI]$_2$ with KHBEt$_3$ has been reported to give either [Cp'FeH$_2$]$_2$ or [Cp'$_2$Fe$_2$H$_3$] depending on the reaction conditions.[36]

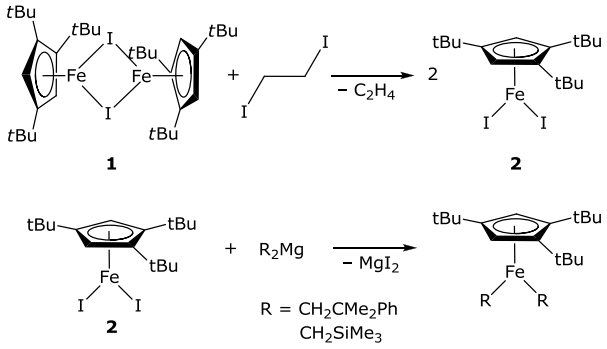

Scheme 4. Oxidation of [Cp'FeI]$_2$ (**1**) and its further reactions.

On the other hand, the Cp' ligand can also be used for the preparation of Mn(II) half-sandwich complexes such as [Cp'MnI(thf)]$_2$ (**3**), which is a 17 valence-electron (VE) complex. Furthermore, complex **3** can be converted to a 13 VE manganese pogo-stick compound [Cp'MnN(SiMe$_3$)$_2$] and to polyhydride cluster [{Cp'Mn}$_4${MnH$_6$}].[37]
To study low coordinate M≡E multiple bonds, especially M≡N complexes as the models for the nitrogenase active center, the reactivity of [Cp'FeI]$_2$ and [Cp'MnI(thf)]$_2$ towards pseudohalides is investigated.

4.2 The reactvity of [Cp'FeI]$_2$ and [Cp'MnI(thf)]$_2$ toward pseudohalides

The result of reactivity studies of [Cp'FeI]$_2$ (**1**) and [Cp'MnI(thf)]$_2$ (**3**) toward pseudohalides such as azide (N_3^-), cyanide (CN^-), cyanate (OCN^-), thiocyanate (SCN^-), selenocyanate ($SeCN^-$) and tellurocyanate ($TeCN^-$), are reported in this section. The starting materials **1** and **3** were reacted with the pseudohalide salts in tetrahydrofuran at room temperature and after removal of the solvent, the remaining residues were extracted with pentane. In the case of NaN_3, a color change from orange to green was observed when the solvent was removed.
From the reactions of [Cp'FeI]$_2$ with KOCN and [Cp'MnI(thf)]$_2$ with KSCN, the anticipated products, [Cp'Fe(NCO)]$_2$ (**4**) and [Cp'Mn(NCS)(thf)]$_2$ (**5**), respectively, were isolated while the reactions of [Cp'FeI]$_2$ with NaN_3, KSCN and KSeCN yielded [Cp'FeN]$_2$ (**6**), [Cp'FeS]$_2$ (**7**) and [Cp'Fe(Se_2)]$_2$ (**8**), respectively. The products were purified by recrystallization from the concentrated *n*-pentane (**4**, **5** and **6**) or diethyl ether (**7** and **8**) solutions at –30°C. The reaction

pathways are shown in Scheme 5.

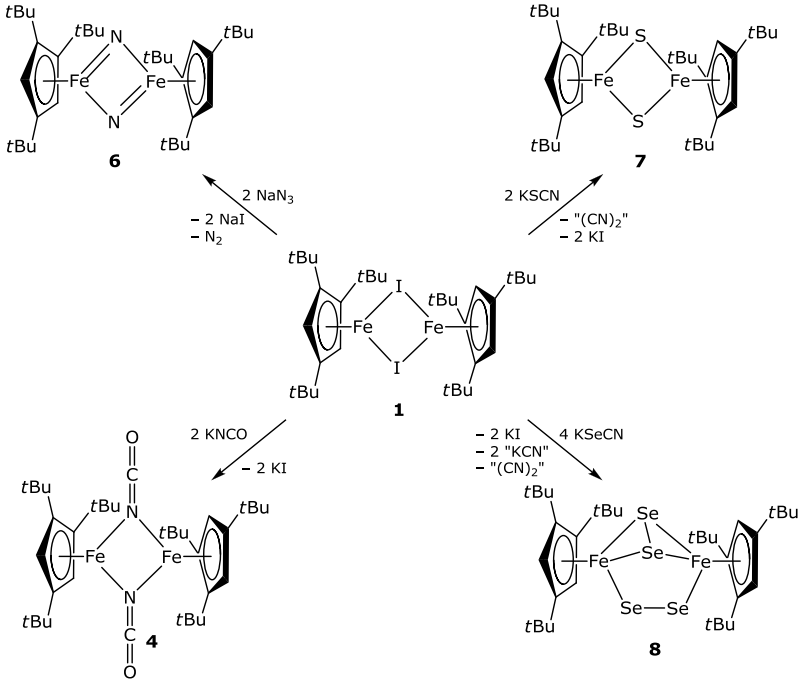

Scheme 5. The reactivity of [Cp'FeI]$_2$ toward pseudohalides.

Compound **4** is stable and no CO loss was detected in the EI-MS spectrum, *i.e.* the CO group is not released, whereby CN radical and N_2 are formed from the reaction of KSCN and NaN_3, respectively (discussed below). [Cp'FeS]$_2$ and [Cp'Fe(Se)$_2$]$_2$ could be obtained in *ca.* 20% yield. The reason for the low yields might be the CN radical which is formed during the synthesis of [Cp'FeS]$_2$ and [CpFe(Se$_2$)]$_2$. We proposed the formation of [Cp'Fe(Se$_2$)]$_2$ as below: The end-on fashion mono selenide-bridged complex is formed in a first step. In a second step, the selenide in this complex serves as a selenide acceptor and accepts a selenide from a second $SeCN^-$ anion (Scheme 6).

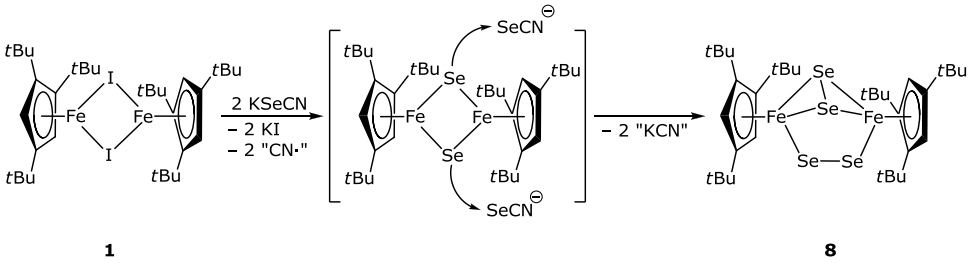

Scheme 6. The proposed process of [Cp'Fe(Se)$_2$]$_2$ (**8**) formation.

The elucidation of the reaction mechanisms was attempted by the analysis of the volatile part of the reaction mixture using GC-MS and IR, however, no evidence for CN• radical such as (CN)$_2$ or HCN as radical reaction products was found. In contrast, much better yields (around 50%) were obtained for the complexes **4**, **5** and **6**. Complex **4** is not stable in an aromatic solvent such as benzene or toluene for an extended period of time (≈ one week) and ferrocene is formed on degradation of **4**. In contrast, the other compounds **6**, **7** and **8** are stable under these conditions.

The reactions of [Cp'FeI]$_2$ with KCN or KTeCN and of [Cp'MnI(thf)] with NaN_3 or KOCN were also investigated, however, the starting materials either decomposed or were recovered unreacted.

In view of its potential, further reactivity of [Cp'FeN]$_2$ was explored, although not always successfully. This nitrido-bridged complex is extraordinary, because it is formed under reduced pressure at room temperature. To form a nitrido-bridged complexes, harsh reaction conditions such as heat or light radiation are usually required. No reaction was observed on addition of $B(C_6F_5)_3$ to form a frustrated Lewis pair, which can activate small molecules like P_4,[38] sulfur and selenium,[39] H_2,[40,41] or CO_2.[42,43] Furthermore, [Cp'FeN]$_2$ does not react with pyridine-*N*-oxide to give a ligand exchange from N to O as reported previously.[27] Fe–N bond splitting by 1,3-di-*tert*-butylimidazol-2-ylidene (I*t*Bu) and 1,3,4,5-tetramethyl-imidazol-2-ylidene (IMeMe$_2$) were also attempted. These NHCs ligands could also be used to trap the proposed intermediate for the formation of the nitrido-bridged complex **6**, the monomeric [Cp'Fe(N_3)(thf)] complex **9**, which was detected by IR and ^{1}H NMR spectroscopy (Scheme 7). However, no reaction occurred according to ^{1}H NMR spectroscopy.

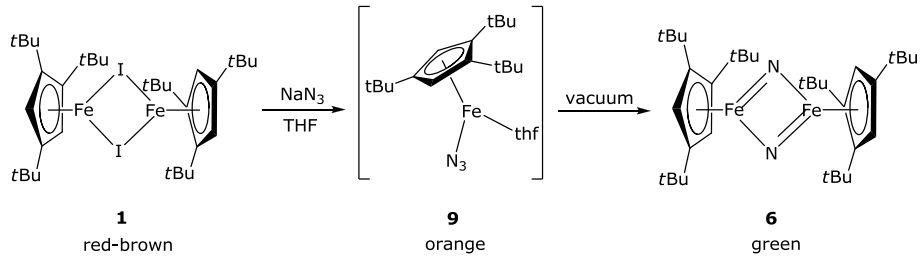

Scheme 7. Formation of [Cp'FeN]$_2$ (**6**) *via* a proposed intermediate (**9**).

NHC (I*t*Bu or IMeMe$_2$) was added when the reaction mixture turned orange. In case of I*t*Bu, the nitrido-bridged complex **6** was formed as monitored by ^{1}H NMR spectroscopy. In case of IMeMe$_2$, an NHC adduct was obtained in which two NHC molecules coordinate to the iron center with iodide acts as a counter anion. This might be explained by the lower solubility of NaN_3 in THF relative to NaI. The reason for that the smaller NHC stabilizes more effectively the cationе and electrophil Fe^{2+} atom could be the stronger electron donating property of the NHCs in comparison to N_3^-, which is replaced by the NHC as shown in Scheme 8.

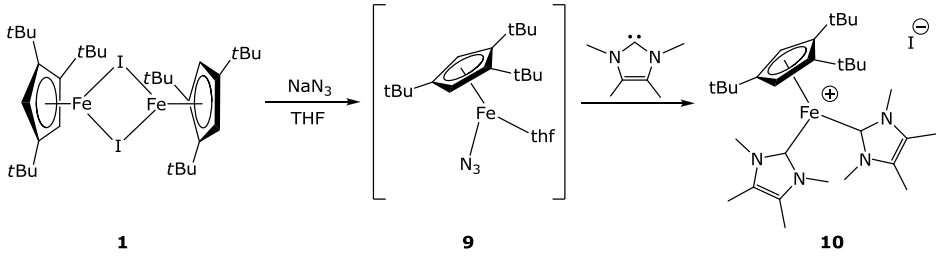

Scheme 8. Attempted trapping reaction of the proposed intermediate **9** by IMeMe$_2$.

4.3 Coordination chemistry toward *N*-heterocyclic carbenes

As discussed above, *N*-heterocyclic carbenes (NHCs) are used to trap the azide-adducts (Scheme 9), which could further react to nitrido-species or a pogo stick molecule (Scheme 10). The pogo stick molecule of Cp'Fe-fragment with the imidazolin-2-iminato ligand was successfully synthesized (Scheme 11)[44] and this complex could be obtained by a different way, *e.g.* by the reduction of the imidazolin-2-imine ligand.

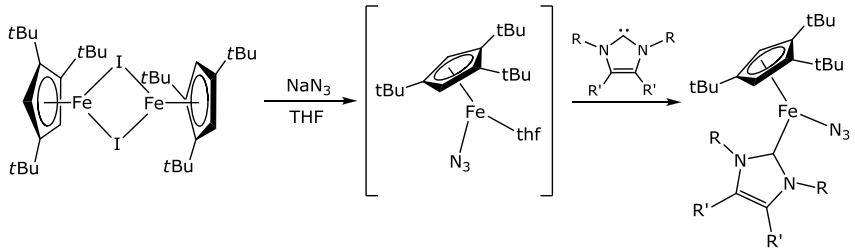

Scheme 9. The anticipated trapping reaction of the azide adduct.

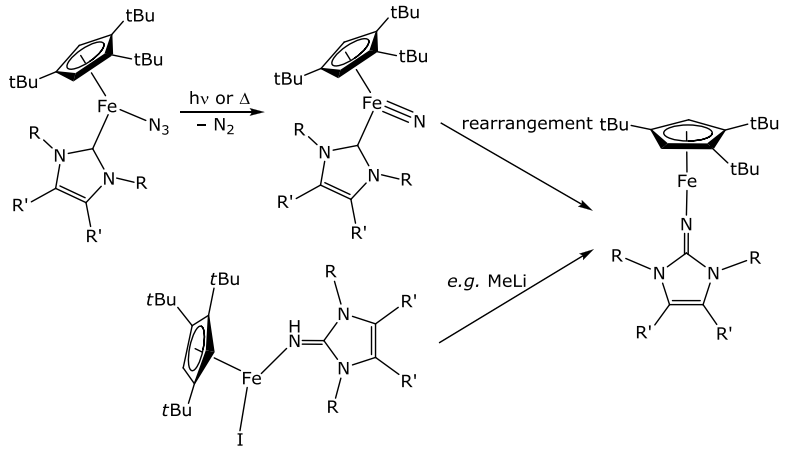

Scheme 10. Possible synthesis ways of the pogo stick molecule.

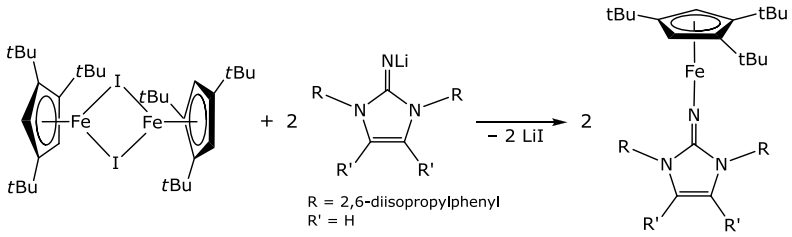

Scheme 11. The established synthesis method of the pogo stick molecule.

NHCs are sterically easily tunable ligands and are strong σ-donors, but only moderate π acceptors. Therefore, they can stabilize metals in high oxidation states.[45–48] Fe-NHC-complexes [FeL$_2$R$_2$] or [FeLR$_2$] (L = neutral 2e$^-$ donor; R = alkyl, aryl or hydride) are 12 or 14 VE "open-shell" complexes which lie the borderline between Werner-type complexes and closed shell 18 VE organometallic compounds. This is important for catalytic processes since these require a coordinatively unsaturated Fe center during the catalytic cycle. Iron complexes with NHCs are known since 1970s,[49,50] however, this field has not been thoroughly investigated in the last century.[51] However a series of reports in the last 10 years

has shown that Fe complexes based on NHC ligands have considerable potential for homogeneous catalysis,[52–54] and they exhibit the catalytic activity in C–C bond formation,[55–59] cyclization,[60–62] and polymerization.[63,64]

Most Fe-NHC complexes that are known today are four-coordinate tetrahedral complexes, however, a few examples of three-coordinate Fe-NHC complexes are known. Recently, three-coordinate Fe-NHC complexes have been recognized an single molecular magnets.[65] Three-coordinate Fe-NHC complexes can be easily realized with Cp.[66,67] The research area for the catalytic applications using CpFe-NHC compounds has also been expanded, *e.g.* in reduction of amide and nitriles,[68] imines,[69] sulfoxide[70,71], hydrosilylation of aldehyde[70,72–74] and ketons[70,72,73] and C–H bond activation/borylation of furans and thiophenes.[75]

To design more active and selective catalysts, information concerning the structure and reactivity of the Fe-NHC complexes is very important. However, recent publication have focused on the catalytic applications whereas the physical properties have so far more or less been neglected. Here, the coordination chemistry of $FeI_2(thf)_2$ and $[Cp'FeI]_2$ toward NHCs and their electronic and magnetic properties were investigated.

The NHC and imidazolin-2-imine Fe adducts were obtained from the reaction of $[FeI_2(thf)_2]$ and NHC or imidazolin-2-imine in tetrahydrofuran and the series of Cp'Fe-NHC adducts was prepared by NHC addition to the pentane solution of $[Cp'FeI]_2$. The NHC and imidazolin-2-imine adducts prepared are illustrated in Figure 2. The NHC adduct crystallized immediately from the reaction mixture. The following NHCs were used in this study: 1,3-di-*tert*-butyl-imidazol-2-ylidene (I*t*Bu), 1,3-diisopropyl-4,5-dimethyl-imidazol-2-ylidene (I*i*PrMe$_2$), 1,3-di(2,6-diisopropylphenyl)imidazol-2-ylidene (IPr) and 1,3-dimesityl-imidazol-2-ylidene (IMes). The yield varied from moderate (40%, I*i*PrMe$_2$, compound **13**) to almost quantitative (97%, IMes, compound **14**). However, the yield and quality (purity and stability) of the product depend on the purity of the starting material, especially that of the NHCs.

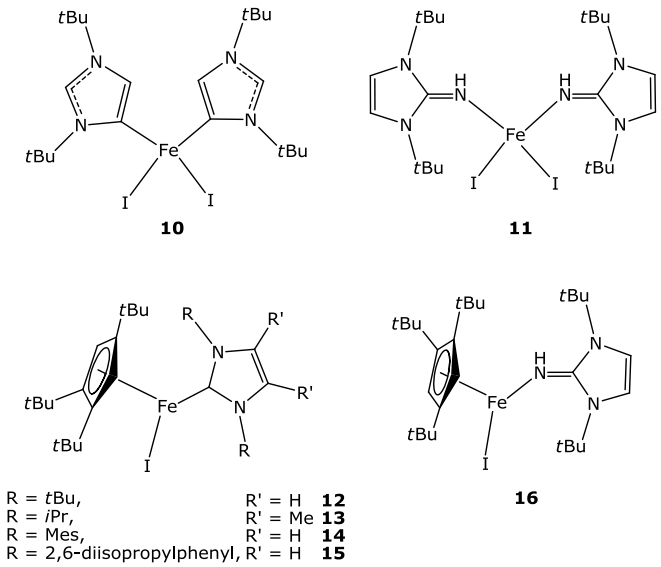

Figure 2. The NHC and imidazolin-2-imine Fe adducts.

4.4 NMR studies

The ^{1}H NMR spectra of [Cp'FeN]$_2$, [Cp'FeS]$_2$, [Cp'Fe(Se$_2$)]$_2$, [Cp'Fe(NCO)]$_2$, [Cp'Mn(NCS)(thf)]$_2$, NHC adducts [Cp'Fe(I*t*Bu)I], [Cp'Fe(*i*PrMe$_2$)I], [Cp'Fe(IMes)I], [Cp'Fe(IPr)I] and imidazolin-2-imin adduct were recorded. [Cp'FeN]$_2$ and [Cp'Fe(Se$_2$)]$_2$ are diamagnetic as judged by their ^{1}H and ^{13}C NMR spectra. All NHC adducts and imidazolin-2-imin adduct are paramagnetic.

In the ^{1}H NMR spectrum, the sulfur-bridged complex **6** exhibits an unusual downfield shift of the ring-C*H* resonance of the Cp' at $\delta = 10.95$ ppm at ambient temperature, while the corresponding resonance in [Cp'FeN]$_2$ and [Cp'Fe(Se$_2$)]$_2$ are observed at $\delta = 6.46$ and 5.89 ppm, respectively. To investigate this interesting downfield shift, variable temperature ^{1}H NMR measurements from 183 to 363 K were performed and the chemical shift of ring-C*H* is plotted against the reciprocal temperature. The temperature dependence of the chemical shift and its linear fit are shown in Figure 3.

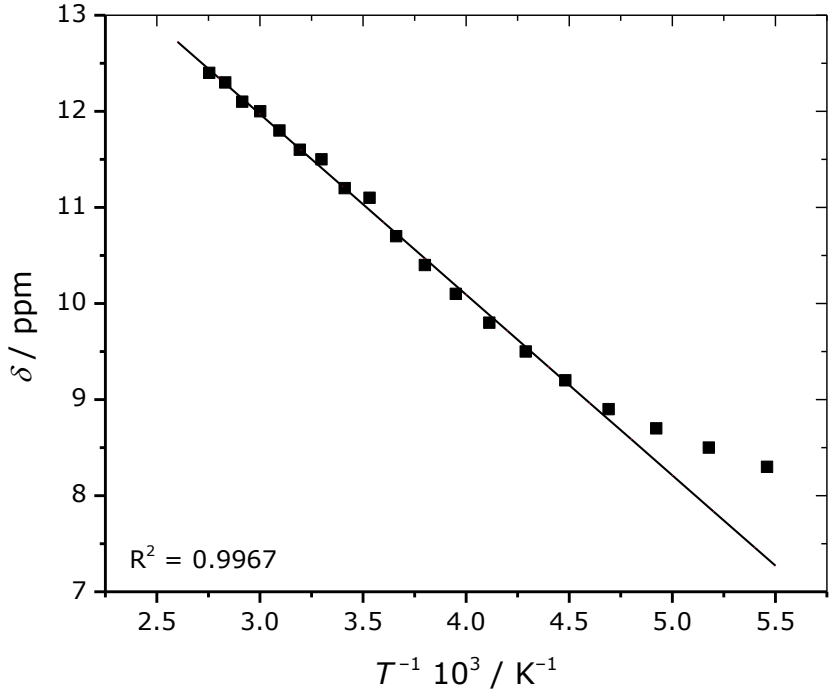

Figure 3. Dependence plot of δ of the ring-C*H* *vs.* T^{-1} for [Cp'FeS]$_2$ (**6**) in toluene-d_8 at temperatures from 183 to 363 K.

The ring-C*H* resonance in [Cp'FeS]$_2$ is temperature dependent. At 203 K ($T^{-1} = 4.92 \cdot 10^3$), the linear fit starts deviating and at large T^{-1} values (*i.e.* at low temperatures). This fact indicates a temperature-dependent magnetic property of [Cp'FeS]$_2$. On the contrary, the ring-C*H* resonance of [Cp'Fe(Se$_2$)]$_2$ does not show any significant temperature dependence, which supports the results of the SQUID measurement (discussed below).

For [Cp'Fe(NCO)]$_2$, a variable temperature ^{1}H NMR study was undertaken from 179 to 298 K in toluene-d_8. The chemical shift of the ring-C*H*, of the two equivalent *t*Bu groups and of the other *t*Bu group is plotted against the reciprocal temperature, the temperature-dependence of the chemical shift and the linear fit are shown in Figure 4. All resonances are temperature dependent and exhibit the relationship of $\delta \sim T^{-1}$. From Curie's law, $\chi = C \cdot T^{-1}$ where χ is the magnetic susceptibilty, C is the material-specific Curie constant and T is temperature, if $\delta \sim T^{-1}$ then $\delta \sim \chi$ is also satisfied. In contrast to [Cp'FeI]$_2$, which shows a monomer-dimer equilibrium in non-coordinating solvent,[26] [Cp'Fe(NCO)]$_2$ behaves as a dimer in a non-coordinating solvent.

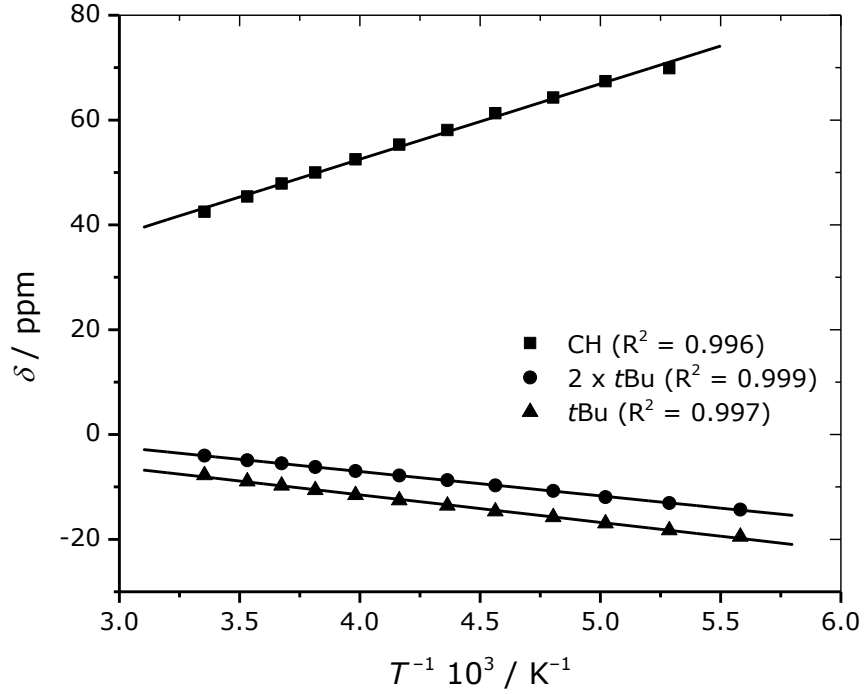

Figure 4. Dependence plot of δ *vs.* T^{-1} for [Cp'Fe(NCO)]$_2$ in toluene-d_8 at temperatures from 179 to 298 K.

The ^{77}Se NMR spectrum of [Cp'Fe(Se$_2$)]$_2$ exhibits two resonances at δ = 2103 and 493 ppm corresponding to the [Se$_2$]$^{2-}$ units in different coordination environments. The resonances for side-on fashion [Se$_2$]$^{2-}$ were found in the range of –202 to –265 ppm.[76] Likewise, the seleno-bridged nickel complex [{(1,2,3,4-(CH$_3$)$_2$CH)$_4$C$_5$H}NiSe]$_2$, the resonance of the selenium atom appeared at 880 ppm.[77] Moreover, the resonances in seleno-cuban complexes were observed at 1009 – 1241 ppm, which corresponds to the μ^3-Se atoms.[78] In contrast, ^{77}Se NMR resonances in Cr≡Se triple bond were shifted downfield to *ca*. 2550 ppm.[76] Nevertheless, the selenium resonances in ^{77}Se NMR spectroscopy are not yet predictable.

4.5 Solid state molecular structures

The solid state structures of [Cp'Fe(NCO)]$_2$ (**4**), [Cp'Mn(NCS)(thf)]$_2$ (**5**), [Cp'FeN]$_2$ (**6**), [Cp'FeS]$_2$ (**7**) and [Cp'FeSe$_2$]$_2$ (**8**) were determined by X-ray single crystal diffraction analyses at 100 K. All compounds were crystallized from saturated *n*-pentane or diethyl ether solutions at –30°C.

[Cp'FeN]$_2$ and [Cp'FeS]$_2$ are isostructual, but [Cp'FeN]$_2$ crystallizes in the tetragonal space group $P4_12_12$ and [Cp'FeS]$_2$ in the monoclinic Pn with two crystallographically independent molecules in the asymmetric unit cell. [Cp'FeSe$_2$]$_2$ and [Cp'Fe(NCO)]$_2$ crystallize in the space group $P2_1/n$, whereas [Cp'Fe(NCO)]$_2$ exhibits imposed inversion symmetry. [Cp'Mn(NCS)(thf)]$_2$ crystallizes with crystallographically imposed inversion symmetry in the space group $P2_1/c$. The selected bond lengths and angles are summarized in Table 1.

Table 1. Selected bond lengths [Å] and angles [°] of complex **1** and **4 – 8**.

	Cp_{cent}–M (av.)	M–X	M–M	X–X	M–X–M′–X′
[Cp'FeI]$_2$ (1)[26]	1.92	2.6764(6) (av.) 2.7104(7) (av.)	3.53 (calcd)	——	16.174(16)
[Cp'Fe(NCO)]$_2$ (4)	1.92	2.0425(12) 2.0840(12)	3.00 (calcd)	——	0.001(2)
[Cp'Mn(NCS)(thf)]$_2$ (5)	2.10	2.1182(12) 2.5995(5)	5.61 (calcd)	——	——
[Cp'FeS]$_2$ (7)	1.83 1.84	2.1292(15) (av.) 2.1373(14) (av.) 2.1333(15) (av.) 2.1448(14) (av.)	2.5757(10) 2.5905(10)	——	0 (calcd) 0.65 (calcd)
[Cp'FeSe$_2$]$_2$ (8)	1.71	2.2473(6) (av.) (end-on) 2.4099(6) (av.) (side-on)	3.72 (calcd)	2.2993(5) (end-on) 2.3255(5) (side-on)	——
[Cp'FeN]$_2$ (6)	1.74	1.734(2) 1.744(2)	2.2325(7)	——	0.0

[Cp'Fe(NCO)]$_2$ and [Cp'Mn(NCS)(thf)]$_2$

ORTEP diagrams of [Cp'Fe(NCO)]$_2$ (**4**) and [Cp'Mn(NCS)(thf)]$_2$ (**5**) are drawn in Figure 5. In [Cp'Fe(NCO)]$_2$, the geometry of Fe–N–Fe–N is planar and almost rectangular (the dihedral angle Fe–N–Fe–N is 0.001(2)°, ∠ Fe–N–Fe is 93.35(5)° and ∠ N–Fe–N is 86.65(5)°).

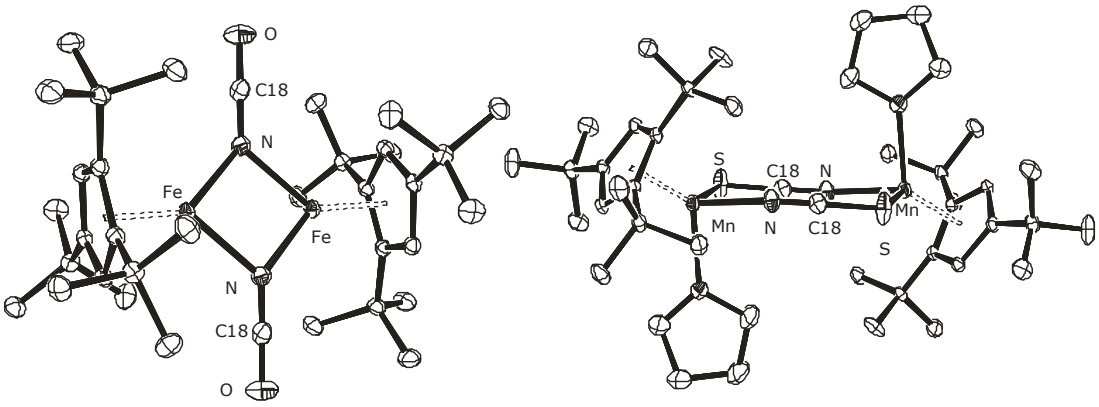

4 **5**

Figure 5. ORTEP diagrams of [Cp'Fe(NCO)]$_2$ (**4**) and [Cp'Mn(NCS)(thf)]$_2$ (**5**) at 30% probability level. Hydrogen atoms are omitted for clarity.

Dinuclear *N*-end-on bridged cyanato complexes are also known for Rh,[79] Mo[80] and Cu[81–88], but here it is compared to a crystallographically characterized NCO-bridged iron tetranuclear complex with a similar motif, [Fe$_2$(pypentO)(NCO)$_3$]$_2$ (pypentOH = 1,5-bis[(2-pyridylmethyl)amino]pentan-3-ol) will be discussed.[89] The selected bond lengths are summerized in Table 2.

Table 2-1. Selected bond lengths [Å] of complexes related to [Cp'Fe(NCO)]$_2$ (**4**) and [Cp'Mn(NCS)(thf)]$_2$ (**5**).

	M–X	M–M (calcd)	N–C	C–O / C–S
[Cp'Fe(NCO)]$_2$ (4)	2.0425(12) 2.0840(12)	3.00	1.1904(19)	1.1824(19)
[Fe$_2$(pypentO)(NCO)$_3$]$_2$	2.180(3) (av.) 2.255(4) (av.)	3.46	1.181(3)	1.182(3)
[Cu(L)(OCN)]$_2$[PF$_6$] (17)	1.94(1) 2.777(1)	3.51	1.16(2)	1.21(2)
[Cd(dmpp)(OCN)$_2$]$_2$ (18)	2.225(3) 2.5319(3)	3.70	1.17(1)	1.178(8)
[{Ni(Me$_6$[14]aneN$_4$)}(NCO)$_2$][ClO$_4$] (19)	2.076(4) 2.212(3)	5.45	1.158(3)	1.208(5)
[Ni(L)(NCO)]$_2$[PF$_6$]$_2$ (20)	1.982(7) 2.189(7)	5.09	1.17(1) (av.)	1.22(1) (av.)

Table 2-2. Selected bond lengths [Å] of complexes related to [Cp'Fe(NCO)]$_2$ (**4**) and [Cp'Mn(NCS)(thf)]$_2$ (**5**).

	M–X	M–M (calcd)	N–C	C–O / C–S
[Cp'Mn(NCS)(thf)]$_2$ (5)	2.1182(12) (Mn–N) 2.5995(5) (Mn–S)	5.61	1.1531(19)	1.6450(15)
[Cd(dmpp)(NCS)$_2$]$_2$	2.300(4) 2.7124(8)	6.03	1.146(5)	1.636(4)

The average Fe–μ-N bond length and Fe–Fe distances in [Cp'Fe(NCO)]$_2$ are 2.0633(12) and 3.00 Å, respectively, which are relatively short compared to [Fe$_2$(pypentO)(NCO)$_3$]$_2$ (2.218(4) and 3.46 Å).

The solid state structure is also compared to the structures of *O*-end-on bridged complexes [Cu(L)(OCN)]$_2$[PF$_6$]$_2$ (L = *N*,*N*-bis(3,5-dimethylpyrazol-1-ylmethyl) aminomethylpyridine)[90] (**17**) and [Cd(dmpp)(OCN)$_2$]$_2$ (dmpp = bis(2,6-(3,5- dimethylpyrazolyl)pyridine)[91] (**18**) (Figure 6) to confirm, whether the coordination mode affects the bond lengths of C–N and N–O. The selected bond lengths are given in Table 2.

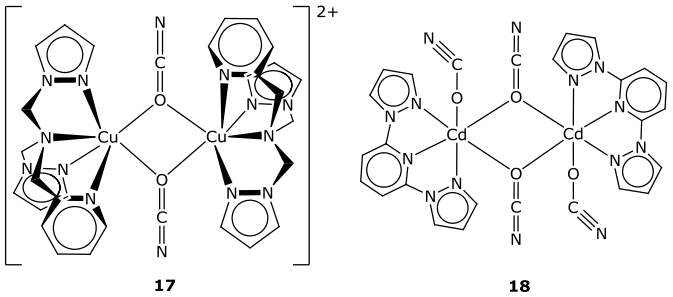

17 **18**

Figure 6. [Cu(L)(OCN)]$_2^{2+}$ (**17**, left) and [Cd(dmpp)(OCN)$_2$]$_2$ (**18**, right).

In *O*-end-on fashion, the M–μ-O distances are different (Cu1–O 1.94(1) Å and Cu2–O 2.777(1) Å in the complex **17**; Cd1–O 2.5319(3) Å and Cd2–O 2.225(3) Å in complex **18**), while M–μ-N bond lengths in *N*-end-on fashion complexes are relatively similar (Fe1–N 2.0425(12) Å / Fe2–N 2.0840(12) Å in [Cp'Fe(NCO)]$_2$ and Fe1-N 2.180(3) Å / Fe2-N 2.255(4) Å in [Fe$_2$(pypentO)(NCO)$_3$]$_2$). The M–M distances in these complexes (Cu–Cu 3.51 Å and Cd–Cd 3.70 Å) are slightly larger than the Fe–Fe distance (3.00 Å). The coordination mode, whether *N*- or *O*-end-on, seems not to affect the bond lengths between C–N and N–O in the cyanate group.

End-to-end coodinated NCO nickel complexes such as [{Ni(Me$_6$[14]aneN$_4$)}$_2$(NCO)$_2$][ClO$_4$]$_2$

(Me$_6$[14]aneN$_4$ = *D*,*L*-5,5,7,12,12,14-hexa-methyl- 1,4,8,11-tetraazacyclotetradecane)[92] (**19**) and [Ni(L)(NCO)]$_2$[PF$_6$]$_2$ (L = *N*,*N*-bis(3,5-dimethylpyrazol-1-ylmethyl)aminomethylpyridine)[90] (**20**) are also known (Figure 7). The selected bond lengths are given in Table 2.

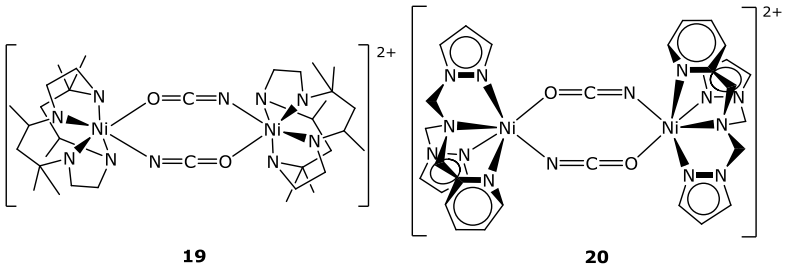

19 **20**

Figure 7. [{Ni(Me$_6$[14]aneN$_4$)}$_2$(NCO)$_2$]$^{2+}$ (**19**, left) and [Ni(L)(NCO)]$_2^{2+}$ (**20**, right).

Ni–N distances (2.076(4) Å and 1.982(7) Å in complex **19** and **20**, respectively) are shorter than the Ni–O distances (2.212(3) Å and 2.189(7) Å in complex **19** and **20**, respectively), however, it could not be clearly distinguished between Ni–N or Ni–O. As for the previous compounds, the Ni–Ni distances are also too large (5.45 Å in complex **19** and 5.09 Å in complex **20**) for a direct bond. The coordination mode, whether end-on or end-to-end, seems also not to affect the bond lengths between C–N and N–O in the cyanate group.

In [Cp'Mn(NCS)(thf)]$_2$, two NCS$^-$ ions bridges two manganese centers by adopting an end-to-end coordination, in which the Mn–N distance is 2.1182(12) Å and the Mn–S distance is 2.5995(5) Å. The NCS-group coordinates to the manganese centers of the *N*-site. The Mn–Mn distance is 5.61 Å, therefore too long for a direct metal–metal bond.

An end-to-end coordinate dicadmium complex [Cd(dmpp)(μ-NCS)(NCS)]$_2$ (dmpp = bis(2,6-(3,5-dimethylpyrazolyl)pyridine) was also crystallographically characterized[91] and can be used for comparison (Figure 8). The selected bond lentghs are summerized in Table 2.

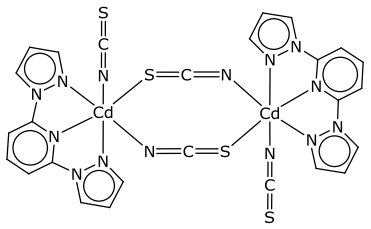

Figure 8. [Cd(dmpp)(NCS)$_2$]$_2$.

The Cd–N distance is 2.300(4) Å and the Cd–S distance is 2.7124(8) Å, suggesting that the NCS-group coordinates to the cadmium atom from the *N*-side. Here, the Cd–Cd distance is 6.03 Å, and again, no direct metal–metal bond is expected.

Some 3d-metal SCN complexes with the *N*-end-on fashion are also known.[93–95] [(18-C-6)K]$_2$[Hg(CF$_3$)$_2$(SCN)]$_2$ is the only one example for the SCN complex with the *S*-end-on fashion which does not exhibit a polymer structure.[96]

[Cp'FeS]$_2$ and [Cp'Fe(Se$_2$)]$_2$

The ORTEP diagrams of [Cp'FeS]$_2$ (**6**) and [Cp'Fe(Se$_2$)]$_2$ (**7**) are depicted in Figure 9. The complex **6** crystallized with two independent molecules in the asymmetric unit, thus, the following discussion for the complex **6** focuses on the molecule shown in Figure 9. The Fe–Fe distance and the average Fe–S bond length in [Cp'FeS]$_2$ are 2.5757(10) Å and 2.1333(15) Å, respectively, and they are shorter than those in the related [2Fe–2S] cluster (2.72 Å and av. 2.30 Å, respectively).[97] In contrast to the synthesized [2Fe–2S] cluster, the dihedral angle in [Cp'FeS]$_2$ is 0°.[98] The distance between the two iron atoms (av. 2.5831(10) Å) lies in the range for Fe–Fe single bond (2.6 – 2.8 Å).[99,100] The structure of [Cp'FeS]$_2$ is also compared to the sulfido-bridged nickel complex [^{4}CpNiS]$_2$ (^{4}Cp = C$_5$-1,2,3,4-((CH$_3$)$_2$CH)$_4$H).[101] The Ni–Ni distance and the average Ni–S bond length in [^{4}CpNiS]$_2$ are 3.241(2) Å and 2.124(3) Å.

In the structure of [Cp'Fe(Se$_2$)]$_2$, the Fe–Fe distance is rather long (3.72 Å) because one of the diselenides fragment coordinates to the metal center in an end-on fashion. The Fe–Se distances are 2.25 Å to end-on Se$_2$ and 2.41 Å to side-on Se$_2$, and the Se–Se distances are 2.2993(5) Å for end-on fashion and 2.3255(5) Å for side-on fashion.

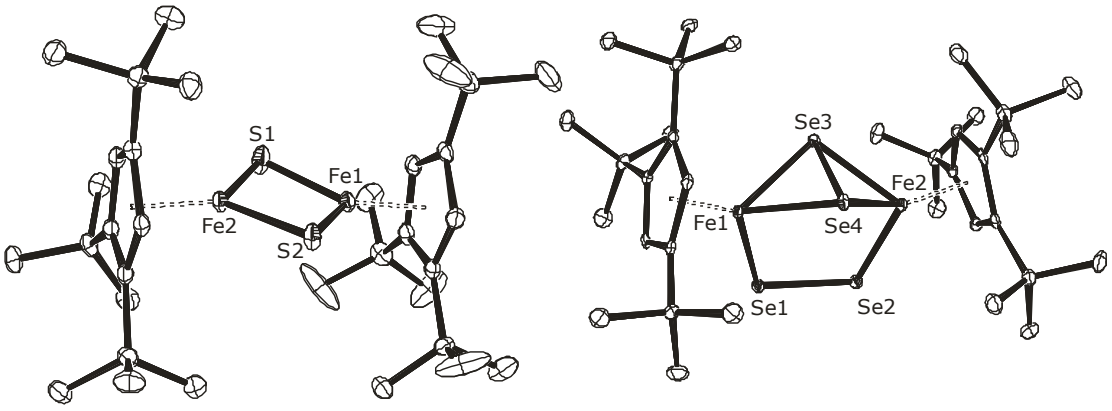

6 **7**

Figure 9. ORTEP diagrams of [Cp'FeS]$_2$ (**6**) and [Cp'Fe(Se$_2$)]$_2$ (**7**) at 30% probability level.

Some bond lengths can be compared to the already known diselenido-bridged complexes such as [$Fe_2(CO)_6(Se_2)$] and [$(MeC_5H_4)_2V_2(Se_2)_2Se$]. The selected bond lenghts are given in Table 3.

Table 3. Selected bond lengths [Å] of complexes related to [Cp'FeS]$_2$ (**6**), [Cp'FeSe$_2$]$_2$ (**7**) and [Cp'FeS$_2$]$_2$.

	M–M	M–X (av.)	X–X
[Cp'FeS]$_2$ (6)	2.5757(10)	2.1292(15)	—
	2.5905(10)	2.1373(14)	
		2.1448(14)	
		2.1333(15)	
[^{4}CpNiS]$_2$	3.241(2)	2.119(2) (found)	—
		2.129(3) (found)	
[Cp'FeSe$_2$]$_2$ (7)		2.2473(6) (end-on)	2.2993(5) (end-on)
		2.4099(6) (side-on)	2.3255(5) (side-on)
[$Fe_2(CO)_6(Se_2)$]	2.575(2)	2.361(2) (end-on)	2.293(2) (end-on)
[$(MeC_5H_4)_2V_2(Se_2)_2Se$]	2.780(4)	2.448(3) (end-on)	2.291(3) (end-on)
		2.528(3) (side-on)	2.294(2) (side-on)
[Cp'FeS$_2$]$_2$	3.51 (calcd)	2.1206(5) (end-on)	2.0121(6) (end-on)
		2.2670(5) (side-on)	2.0437(6) (side-on)
[CpFeS$_2$]$_2$	3.49 (calcd)	2.106(6) (end-on)	1.999(8) (end-on)
		2.263(6) (side-on)	2.043(8) (side-on)
[Cp*FeS$_2$]$_2$	3.53 (calcd)	2.126(2) (end-on)	2.021(2) (end-on)
		2.273(1) (side-on)	2.055(2) (side-on)
[{$(Me_3Si)_2C_5H_3$}FeS$_2$]$_2$	3.50 (calcd)	2.109(1) (end-on)	1.997(1) (end-on)
		2.259(1) (side-on)	2.033(2) (side-on)

The Fe–Se and Se–Se distances are comparable to the diselenido-bridged iron carbonyl complex [$Fe_2(CO)_6(Se_2)$] (Fe–Se distance 2.361(2) Å for side-on fashion and Se–Se distance 2.293(2) Å).[102] In addition, the Se–Se distances are similar to the reported diselenido-bridged Cp-vanadium complex [$(MeC_5H_4)_2V_2(Se_2)_2Se$], 2.291(3) Å for end-on Se_2 and 2.294(2) Å for side-on Se_2. On the other hand, the V–Se distances in the vanadium complex are larger than

the Fe–Se distances in [Cp'Fe(Se$_2$)]$_2$, 2.448(3) Å to end-on Se$_2$ and 2.528(3) Å to side-on Se$_2$, and the V–V distance is smaller (2.780(4) Å).[103] The reason for that may be that the V–Se bridge reduces the V–V distance.

[Cp'FeS$_2$]$_2$ was obtained from the reaction of [Cp'Fe(CO)$_2$]$_2$ with S$_8$, and its solid state molecular structure is shown in Figure 10.

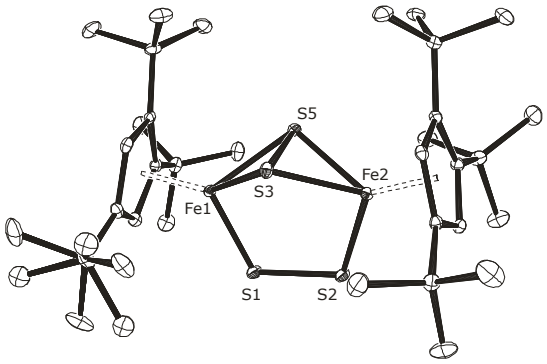

Figure 10. ORTEP diagrams of [Cp'FeS$_2$]$_2$ at 30% probability level. Hydrogen atoms are omitted for clarity. A *tert*-butyl group is disordered. Selected bond lenghs [Å]: Cp'$_{cent}$–Fe (av.) 1.70, Fe–Fe 3.51, Fe–S (av.) 2.1206(5) (end-on) / 2.2670(5) (side-on), S–S 2.0121(6) (end-on) / 2.0437(6) (side-on).

In the structue of [Cp'FeS$_2$]$_2$, Fe–Fe distance (3.51 Å) is longer than that in [Cp'FeS]$_2$ (av. 2.5831(10) Å) but shorter than in [Cp'Fe(Se$_2$)]$_2$ (3.72 Å) as expected. The average S–S bond lengths are 2.0121(6) Å for end-on S$_2$ and 2.0437(6) Å for side-on S$_2$. The bond length for side-on S$_2$ is longer than that for end-on S$_2$ as in [Cp'Fe(Se$_2$)]$_2$.

The similar disulfide-bridged iron complexes, [CpFeS$_2$]$_2$[104,105], [Cp*FeS$_2$]$_2$[106] (Cp* = Me$_5$C$_5$) and [(1,3-(Me$_3$Si)$_2$C$_5$H$_3$)FeS$_2$]$_2$[107] were reported and can be compared with [Cp'FeS$_2$]$_2$. The selected bond lengths are summerized in Table 3. The Fe–Fe distance of [Cp'FeS$_2$]$_2$ is almost identical with those of the related complexes (3.49 Å for [CpFeS$_2$]$_2$, 3.53 Å for [CpFeS$_2$]$_2$ and 3.50 Å for [(1,3-(Me$_3$Si)$_2$C$_5$H$_3$)FeS$_2$]$_2$). The average Fe–Se distances of [Cp'FeS$_2$]$_2$ (2.1206(5) Å to end-on S$_2$ and 2.2670(5) Å to side-on S$_2$) are also comparable to the complex [CpFeS$_2$]$_2$ (2.106(6) Å to end-on S$_2$ and 2.263(6) Å to side-on S$_2$)[104], [Cp*FeS$_2$]$_2$ (2.126(2) Å to end-on S$_2$ and 2.273(1) Å to side-on S$_2$)[106] and to [(1,3-(Me$_3$Si)$_2$C$_5$H$_3$)FeS$_2$]$_2$ (2.109(1) Å to end-on S$_2$ and 2.259(1) Å to side-on S$_2$).[107] The S–S bond lengths (1.999(8) Å (end-on) / 2.043(8) Å (side-on) in [CpFeS$_2$]$_2$, 2.021(2) Å (end-on) / 2.055(2) Å (side-on) in [Cp*FeS$_2$]$_2$ and 1.997(1) Å (end-on) / 2.033(2) Å (side-on) in [(1,3-(Me$_3$Si)$_2$C$_5$H$_3$)FeS$_2$]$_2$) are also similar. Interestingly, the coordination mode of the side-on S$_2$ in [Cp*FeS$_2$]$_2$ is changed to an end-on fashion, when the complex is oxidized

with NH_4PF_6.[108]

[Cp'FeN]$_2$

The ORTEP diagram of [Cp'FeN]$_2$ (**5**) is shown in Figure 11. The observed Fe–Fe distance of 2.2325(7) Å is smaller than that of a Fe=Fe double bond (2.316(1) Å).[109] It indicate that the two iron atoms in [Cp'FeN]$_2$ likely interact with each other and a multiple bond between two iron atoms is expected. The average value of the Fe–N distance (1.739(2) Å) in [Cp'FeN]$_2$ lies between those of a Fe–N single bond (in range of 1.9 – 2.0 Å) and that of an Fe=N double bond (in range of 1.6 – 1.7 Å).[110–117] The structure of [Cp'FeN]$_2$ suggests multiple bonding of the nitrido ligand to the two iron atoms.

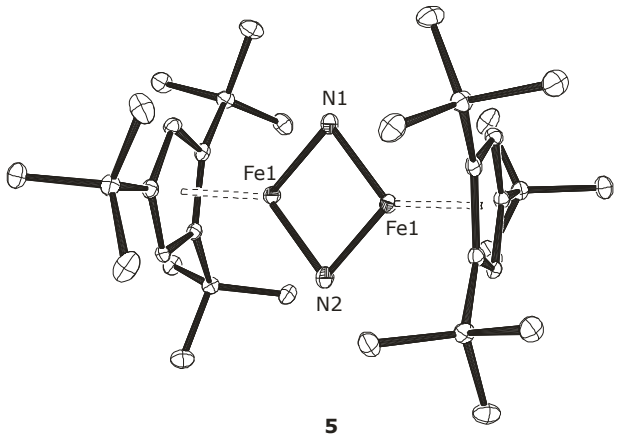

5

Figure 11. ORTEP diagram of [Cp'FeN]$_2$ (**5**) with 30% probability ellipsoids. Hydrogen atoms are omitted for clarity.

The structure of [Cp'FeN]$_2$ can also be compared to [Cp'FeP]$_2$,[34] which is isostructural to [Cp'FeN]$_2$. The Fe–Fe distance of 2.5005(4) Å in [Cp'FeP]$_2$ is larger than that in [Cp'FeN]$_2$ and that of a Fe=Fe double bond, but shorter than a Fe–Fe single bond (2.6 – 2.8 Å).[100] The average Fe–P distance is 2.1037(7) Å, *ca.* 0.37 Å longer than the average Fe–N distance, which can be ascribed to the difference of the ionic radius of each element (N^{3-}: 1.73 Å, P^{3-}: 2.25 Å).[118]

Some nitrido-bridged metal complexes are also obtained from different synthetic routes (Scheme 12).[119–124]

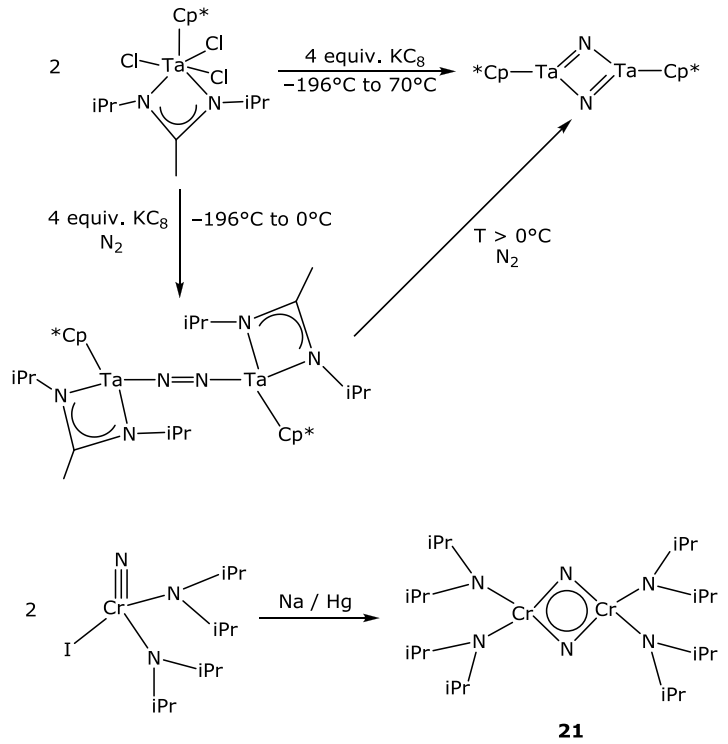

21

Scheme 12. Syntheses of nitrido-bridged complexes.[120,123]

In some complexes,[121,123,124] the M–N and M'–N bond lengths are slightly different (0.04 – 0.20 Å) in contrast to [Cp'FeN]$_2$ (0.01 Å). The typical bond length for the Fe–N single bond are in range between 1.9 – 2.0 Å and for the Fe=N double in range between bond 1.6 – 1.7 Å.[110–117] In many cases, the two bonds between the metal and the nitrogen atoms in dinuclear nitrido-bridged complexes are described by a single bond (M–N) and a double bond (M=N) (Figure 12).

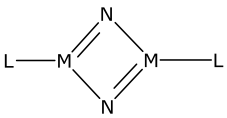

Figure 12. A nitrido-bridged dinuclear complex.

For Cp containing complexes, the M–N and M=N bond distances are nearly identical ($\Delta \leq 0.04$ Å).[119,122,123] In contrast, the difference between the localized M–N and M=N bonds is large ($\Delta \approx 0.20$ Å) in the tungsten[124] (**22**) and the vanadium[121] (**23**) complexes (Figure 13).

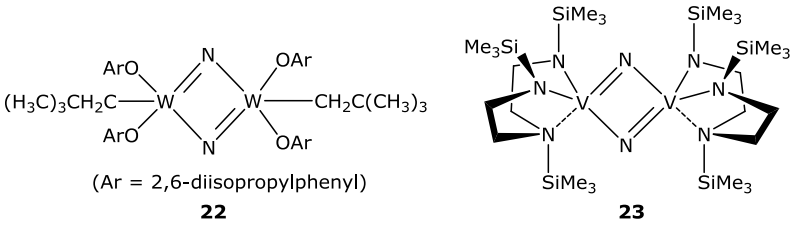

Figure 13. Nitrido-bridged tungsten (**22**) and vanadium (**23**) complexes with different M–N distances.

The difference between the bond lengths seems not to be affected by the oxidation number of the metal atom, and the absence of an inversion center in solid state molecular structure. The vanadium atom has the formal oxidation number of +5 in all Cp* complexes (**24**) and in the silylamino(disilylamino) complex (**25**) (Figure 14). However, the difference of bond lengths in complexes **24** are close to zero,[119,122] while it in compex **25** is *ca*. 0.15 – 0.20 Å.

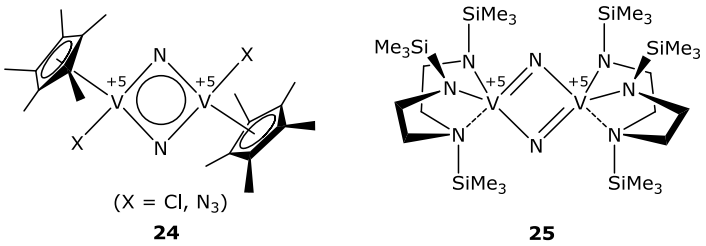

Figure 14. Two nitrido-bridged vanadium complexes with different bond types.

When the complex **25** is reduced by KC_8, the M–N and M=N bond lengths become almost identical since the negative charge is delocalized over the V_2N_2-fragment (Scheme 13).[121]

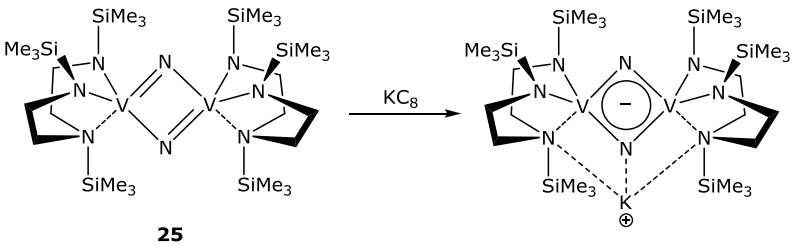

Scheme 13. Change of the bond type in nidrido-bridged vanadium complex **25**.

NHC and imidazolin-2-imine Fe adducts, and Cp'Fe-NHC adducts

The solid state molecular structures of the NHC and imidazolin-2-imine Fe adducts were also determined by X-ray single crystal diffraction analysis at 100 K. [FeI$_2$(I*t*Bu)$_2$] (**10**) crystallizes in the space group *P*2$_1$/n and [FeI$_2$(HNI*t*Bu)$_2$] (**11**) whose crystals are obtained from pentane solution in the monoclinic C2/*c* with imposed inversion symmetry and three tetrahydrofuran molecules are included in the crystal lattice. Complex **11** also crystallized from benzene or toluene solutions in the monoclinic space group C2 with imposed inversion symmetry. When the crystals are grown in benzene, one benzene molecule co-crystallizes. The Cp'Fe-NHC adducts crystallize in the space group C2/*c* ([Cp'Fe(I*t*Bu)I] (**12**)), P2$_1$/*n* ([Cp'Fe(I*i*PrMe$_2$)I] (**13**)), *P*2$_1$/*c* ([Cp'Fe(IMes)I] (**14**)) or *Pbca* ([Cp'Fe(IPr)I] (**15**)). In contrast, compound **16** crystallizes with two independent molecules in the orthorhombic space group *Pca*2$_1$. ORTEP diagrams of compounds **10**, **11**, **12** and **16** are shown in Figure 15 and 16.

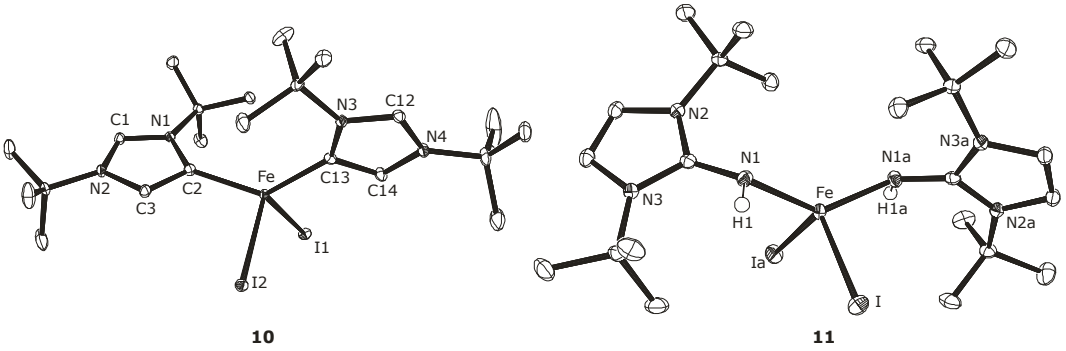

Figure 15. ORTEP diagrams of complex **10** (left) and complex **11** (right) at the 30% probability level. Hydrogen atoms on the Cp' and $C_3H_2N_2$ rings are omitted for clarity. Selected bond lengths [Å] and angles [°] for **10** and **11**: **10**, Fe–C2 2.083(2), Fe–C13 2.0884(19), Fe–I1 2.7060(3), Fe–I2 2.7712(3), C2–Fe–C13 133.37(8), C2–Fe–I1 108.85(5), C2–Fe–I2 101.12(5), C13–Fe–I1 103.94(5), C13–Fe–I2 100.95(5), I1–Fe–I2 105.562(10); **11**, Fe–N1 2.0329(11), Fe–I 2.7056(3), N1–Fe–N1 137.67(6), N1–Fe–I 97.72(3), N1–Fe–I' 105.32(3), I–Fe–I' 113.016(12).

Complexes **10** and **11** adopt a distorted tetrahedral geometry with angles in the range 100.95(5) – 133.37(8)° for complex **10** and 97.72(3) – 137.67(6)° for complex **11**. In both complexes, the $C_3H_2N_2$ rings are situated nearly perpendicular to each other (81.0° for complex **10** and 80.3° for complex **11**). Interestingly, the reaction between FeI$_2$(thf)$_2$ and 2 equivalents of I*t*Bu results in an abnormal NHC adduct while a normal NHC adduct was formed from the reaction of FeCl$_2$ and 2 equivalents IMes.[125] The Fe–C(carbene) distances found in [FeI$_2$(I*t*Bu)$_2$] are comparable to those distance in [FeCl$_2$(I*i*PrMe)$_2$] (2.1363(15) and

2.1298(16) Å).[63] The Fe–C(carbene) and Fe–I bond lengths can be compared to those in [FeI$_2$(CO)$_2$(IMes)$_2$]. The Fe–C(carbene) (2.002(6) Å) and Fe–I bond lengths (2.674(1) and 2.636(1) Å) in [FeI$_2$(CO)$_2$(IMes)$_2$] are shorter than those in **10**.[126]

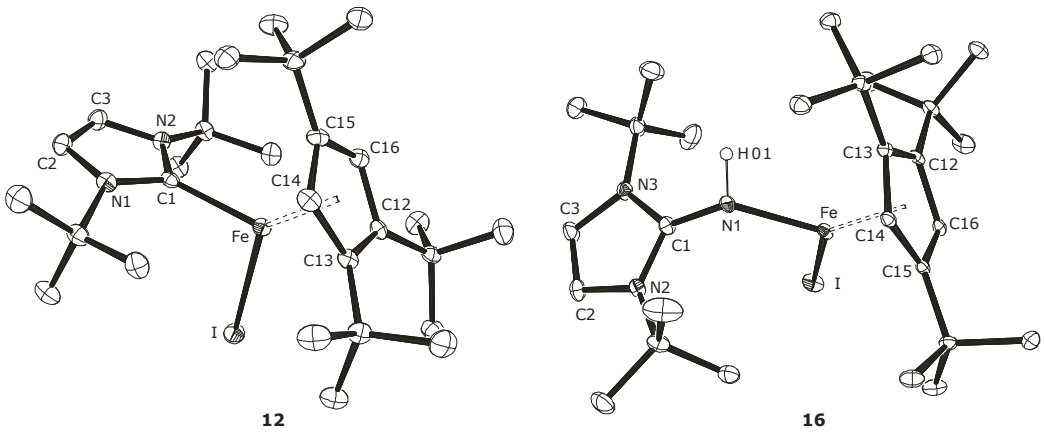

Figure 16. ORTEP diagrams of compound **12** (left) and compound **16** (right) at the 30% probability level. Hydrogen atoms on the Cp' and $C_3H_2N_2$ rings are omitted for clarity. Selected bond lengths [Å] for **16**: Cp$_{cent}$–Fe 1.98, Cp'$_{cent}$–Fe' 2.01, Fe–N1 2.031(4), Fe'–N1' 2.033(4), Fe–I2.6790(9), Fe'–I'2.6705(8).

Selected bond lengths are summarized in Table 4. All Cp'Fe-NHC adducts adopt a distorted trigonal-planar geometry at the Fe atom. For Cp', the Cp$_{cent}$–Fe distances range between 2.00 – 2.02 Å consistent with the high-spin configuration of the Fe(II) atom in these complexes. However, for the related Cp* complexes such as [Cp*Fe(I*i*PrMe$_2$)Cl] and [Cp*Fe(IMes)Cl], the Cp$_{cent}$–Fe distances are significantly shorter (1.78 – 1.93Å), which indicates a different spin state in these complexes. Appearently, the Cp*ligand is capable to induce an intermediate spin configuration (S = 1) in these systems.[66]

Table 4. The selected bond lengths of Cp'Fe-NCH adducts **12** – **14** and **15** [Å].

	Cp$_{cent}$–Fe	**Fe–C(carbene)**	**Fe–I**
[Cp'Fe(I*t*Bu)I] (12)	2.02	2.151(5)	2.7659(9)
[Cp'Fe(I*i*PrMe$_2$)I] (13)	2.00	2.1244(12)	2.71042(19)
[Cp'Fe(IMes)I] (14)	2.02	2.162(4)	2.7128(6)
[Cp'Fe(IPr)I] (15)	2.00	2.1718(19)	2.6883(3)

4.6 Solid state magnetism and Mössbauer investigations

To further investigate the oxidation states in these complexes, zero-field Mössbauer spectra for [Cp'FeI]$_2$ (**1**), [Cp'FeI$_2$] (**2**), [Cp'Fe(NCO)]$_2$ (**4**), [Cp'FeN]$_2$ (**6**), [Cp'FeS]$_2$ (**7**) and [Cp'Fe(Se$_2$)]$_2$ (**8**) were recorded at 77 K and magnetic susceptibility measurements for complexes **1**, **2**, **4**, **5**, **6** and **7** were carried out at 1 kG from 2 to 300 K. The fits of Mössbauer spectra were obtained by using Lorenzian line doublets with isomer shifts δ, quadrupole splittings ΔE_Q and line width Γ_{FWHM}. These results are summarized in Table 5 whereas the μ_{eff} *vs.* T plots are shown in Figure 17. Consistent with the ^{1}H NMR data, these measurements confirm the formal oxidation state of each complex, as discussed below.

Table 5. Results of Mössbauer measurement of compound **1**, **2**, **4**, **7** and **8** at 77 K. Two different line widths were fitted to the data of complex **1**.

	formal ox. state	δ / mm s^{-1}	ΔE_Q / mm s^{-1}	Γ_{FWHM} / mm s^{-1}
[Cp'FeI]$_2$ (1)	Fe(II)	1.08	1.98	0.49 / 0.86
[Cp'Fe(NCO)]$_2$ (4)	Fe(II)	1.05	1.49	0.31
[Cp'FeI$_2$] (2)	Fe(III)	0.47	0.80	0.52
[Cp'FeS]$_2$ (7)	Fe(III)	0.45	1.85	0.29
[Cp'Fe(Se$_2$)]$_2$ (8)	Fe(III)	0.49	1.26	0.28
[Cp'FeN]$_2$ (6)	Fe(IV)	–0.02	0.71	0.31

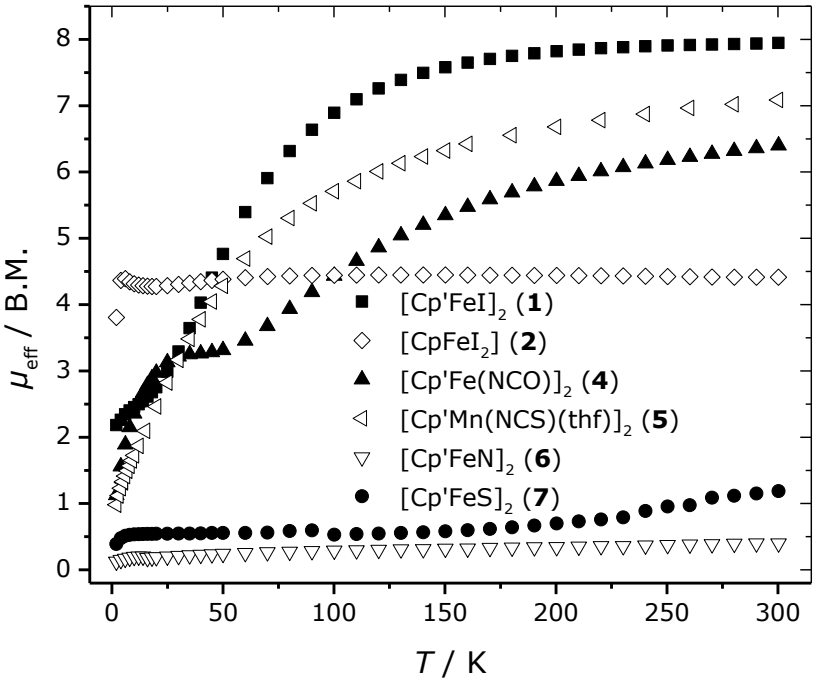

Figure 17. The plots of solid state magnetic moment μ_{eff} *vs.* T of compound **1**, **2** and **4** – **7**.

The spectra show that each complex contains only one type of iron atoms in the same electronic environment. The isomer shifts are *ca*. 1.0 mm s^{-1} for [Cp'FeI]$_2$ and [Cp'Fe(NCO)]$_2$, *ca*. 0.5 mm s^{-1} for [Cp'FeI$_2$], [Cp'FeS]$_2$ and [Cp'FeSe$_2$]$_2$ and *ca*. 0 mm s^{-1} for [Cp'FeN]$_2$. The Mössbauer spectra of [Cp'Fe(NCO)]$_2$ (**4**), [Cp'FeS]$_2$ (**7**) and [Cp'FeN]$_2$ (**6**) are shown in Figure 18.

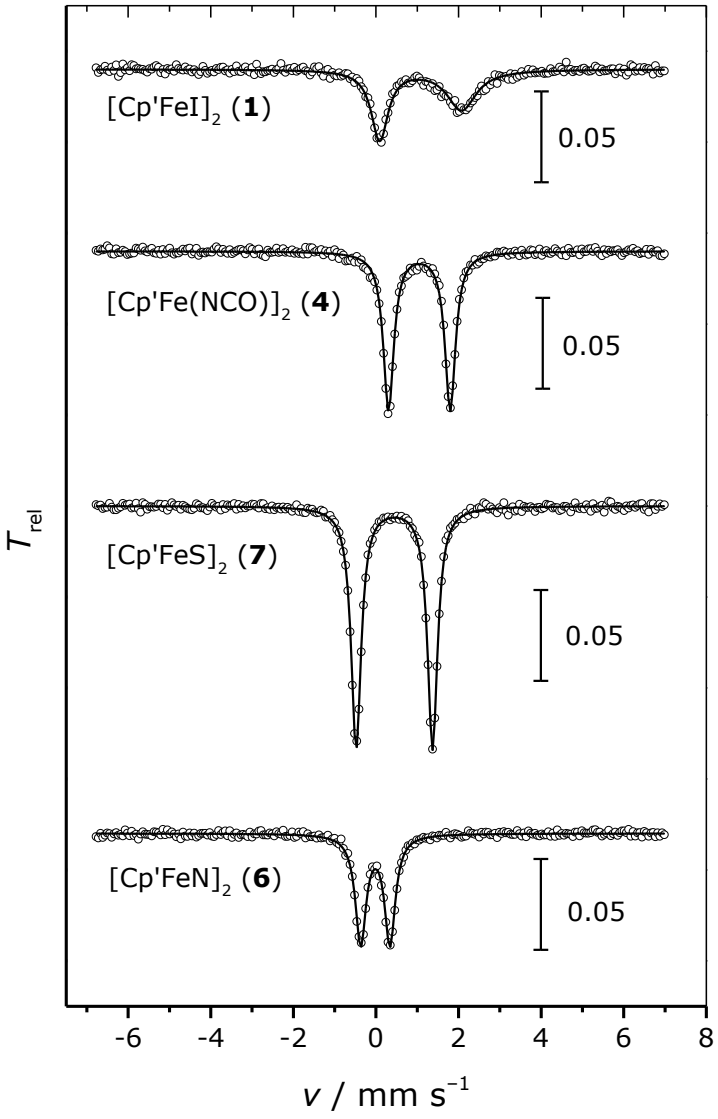

Figure 18. Mössbauer spectra of [Cp'FeI]$_2$ (**1**), [Cp'Fe(NCO)]$_2$ (**4**), [Cp'FeS]$_2$ (**7**) and [Cp'FeN]$_2$ (**6**). The solid lines are Lorenzian doublet fit to the experimental data (dots).

Except for [Cp'FeI]$_2$, all compounds show a symmetric quadrupole doublet. This significant asymmetry and the different line width for both lines observed for [Cp'FeI]$_2$ is caused by dynamic relaxation with fluctuation rates within the experimental time window of the method. The origin of these paramagnetic relaxation might be attributed to spin-lattice-relaxation as observed for ferrocenium compound.[127] Further studies of the temperature dependence might be useful to elucidate their observation.

The Fe(II) high-spin centers in [Cp'FeI]$_2$ (**1**) and [Cp'Fe(NCO)]$_2$ (**4**) are also confirmed by the magnetic moments of *ca*. 7.9 B.M. for complex **1** and *ca*. 6.4 B.M. for **4** at room temperature.

The magnetic moment for [Cp'FeI]$_2$ is larger than the theoretical value for two uncoupled Fe(II) atoms (6.9 B.M.), which may be caused by zero-field splitting.

The values of the magnetic moments in both complexes **1** and **3** decrease to almost zero at low temperatures, suggesting weak antiferromagnetic coupling between the two iron atoms, which is broken at elevated temperatures. The form of these curves could also be caused by spin-crossover effect, but then two different types of iron atoms must be observed in the Mössbauer spectra of **1** and **3**. However, both spectra at 77 K show only one type of iron atoms and thus, the spin-crossover can be excluded. In the case of complex **4**, The μ_{eff} *vs. T* plot showed a plateau at *ca.* 50 K in several independent measurements, however, no reasonable explanation has been found yet.

The isomer shifts of [Cp'FeI$_2$], [Cp'FeS]$_2$ and [Cp'Fe(Se$_2$)]$_2$ are of 0.47, 0.45 and 0.49 mm s^{-1}, as expected for an Fe(III) center.[128–130] From the value of the effective magnetic moment, which is temperature-independent (4.4 B.M. experimental *vs.* 3.9 B.M. theoretical value for $S = 3/2$), [Cp'FeI$_2$] appears to have an intermediate spin configuration. The half width of [Cp'FeI$_2$] is large (0.52 mm s^{-1}), as possible reasons for that might be inhomogeneity of the sample. The iodide containing complexes seem to have the μ_{eff} which differs from the theoretical value and to have a large half width in Mössbauer spectrum. For [Cp'FeS]$_2$ and [Cp'Fe(Se$_2$)]$_2$, the Fe(III) atom adopt a low spin or an intermediate spin configuration based on the quadrupole splitting.

The effective magnetic moment μ_{eff} of [Cp'FeS]$_2$ increases at *ca.* 200 K and reaches 1.2 B.M. at 300 K. This value is relatively low for a complex with two uncoupled Fe(III) atoms. This behavior is in accordance with strong antiferromagnetic coupling between the two iron centers to give an $S = 0$ ground state, as is usually observed for [2Fe–2S] clusters.[97] Since [Cp'Fe(Se$_2$)]$_2$ behaves as a diamagnetic compound, a much stronger antiferromagnetic coupling can be expected for this complex.

In comparison to the related [2Fe–2S] clusters, [Cp'FeS]$_2$ shows a significantly different isomer shift (0.45 mm s^{-1}) and quadrupole splitting (1.85 mm s^{-1}). For synthetic *S*-coordinated [2Fe–2S] clusters, the isomer shift is found at *ca.* 0.29 mm s^{-1} and the quadrupole splitting at *ca.* 0.40 and 0.6 mm s^{-1}.[131–137] The isomer shift and quadrupole splitting for [Cp'FeS]$_2$ differs significantly from natural Rieske-protein ($\delta = 0.2 – 0.3$ mm s^{-1} and $\Delta E_Q = 0.4 – 1.0$ mm s^{-1}).[138–141] These differences could be due to the charge of the complexes. [2Fe–2S] clusters are usually dications, while [Cp'FeS]$_2$ is a neutral molecule.

As for the Fe(III) center, Mn(II) also has d^5 configuration and a paramagnetic behavior as expected. The effective magnetic moment of [Cp'Mn(NCS)(thf)]$_2$ is 7.0 B.M. at ambient temperature, confirming the high-spin state, and only a very weak antiferromagnetic

coupling is observed (the theoretical value for two uncoupled Mn(II) high-spin center is 8.37 B.M.).

The Mössbauer spectrum of [Cp'FeN]$_2$ shows the isomer shift at –0.02 mm s^{-1} consistent with an Fe(IV) atom.[128–130] This value differs from the value of previously reported Fe(IV)≡N complexes (δ = –0.27 mm s^{-1} [142] and –0.34 mm s^{-1} [143]). Complex [Cp'FeN]$_2$ contains two iron atoms with d^4 electron configuration, however, the magnetic moment for [Cp'FeN]$_2$ is *ca*. 0.4 B.M., which is much lower than expected for two uncoupled Fe(IV) ions and it is almost temperature-independent. This can be explained by very strong antiferromagnetic coupling between the two iron atoms, and thus the antiferromagnetic coupling does not break at ambient temperature.

The magnetic susceptibility of compound **10**, **12**, **13**, **14** and **16** were also investigated (Figure 19), since only the solid state magnetic susceptibility of [FeCl$_2$(IMes)$_2$][125] and [FeCl(IPr)(CH$_2$SiMe$_3$)][144] have been reported so far. The NHC-ligands are considered as a strong-field ligand such as CO or NO. However, Fe-NHC[145] and CpFe-NHC[66] complexes reported to date exhibit typically paramagnetic behavior.

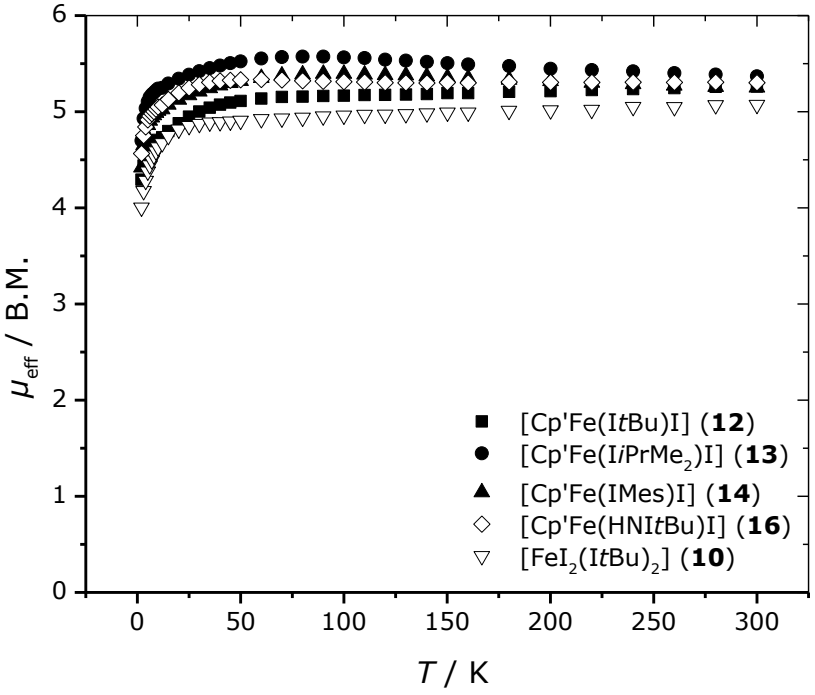

Figure 19. Solid state magnetic moment μ_{eff} *vs*. *T* plot for [Cp'Fe(I*t*Bu)I] (**12**), [Cp'Fe(I*i*PrMe$_2$)I] (**13**), [Cp'Fe(IMes)I] (**14**) [Cp'Fe(HNI*t*Bu)I] (**16**) and [FeI$_2$(I*t*Bu)$_2$] (**10**).

For all complexes the magnetic moment of *ca*. 5.2 B.M. is temperature independent,

consistent with high-spin iron (II) centers ($S = 2$). This result agrees the previous measurements of [FeCl(IPr)(CH_2SiMe_3)] and [Fe_2Cl_2(IMes)$_2$] (5.4 B.M.[144] and 5.2 B.M.[125], respectively).

To investigate the correlation between the Cp_{cent}–metal distances ($d(Cp_{cent}–M)$) and the spin states S for the complexes studied here and elsewhere,[26] the Cp_{cent}–metal distances of these complexes were plotted against their spin states and the linear fit is shown in Figure 20.

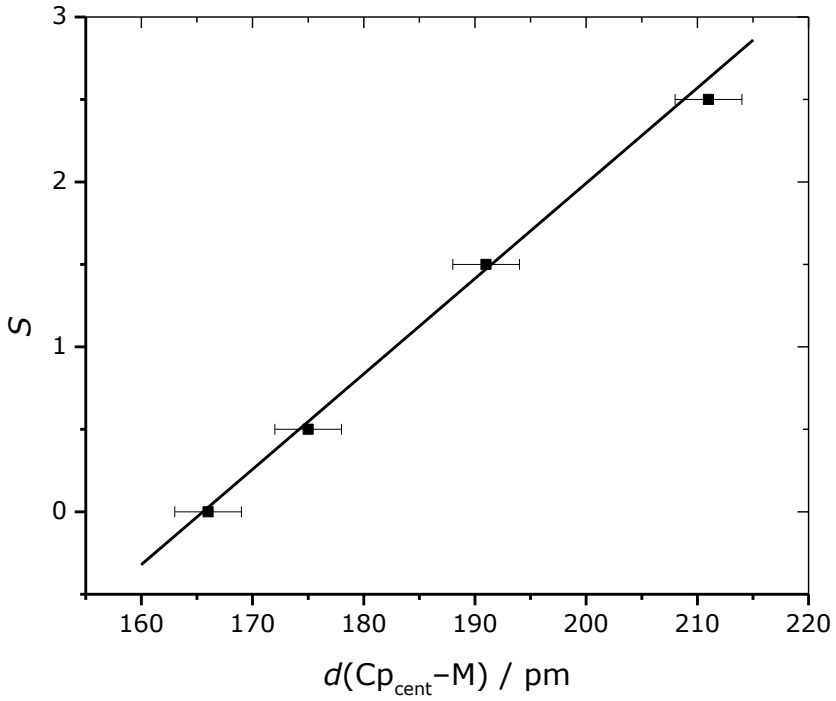

Figure 20. Dependance plot of spin state S *vs.* Cp_{cent}–metal distance $d(Cp_{cent}–M)$ and least squares linear fit.

The linear-fit suggests a strong correlation between the Cp_{cent}–metal distance and the spin state. Hence the spin state of the Cp complexes can be inferred from the Cp_{cent}–M distance.

Finally, the isomer shifts of iron complexes were also plotted against the oxidation states to investigate the correlation between them, and the linear-fit is shown in Figure 21.

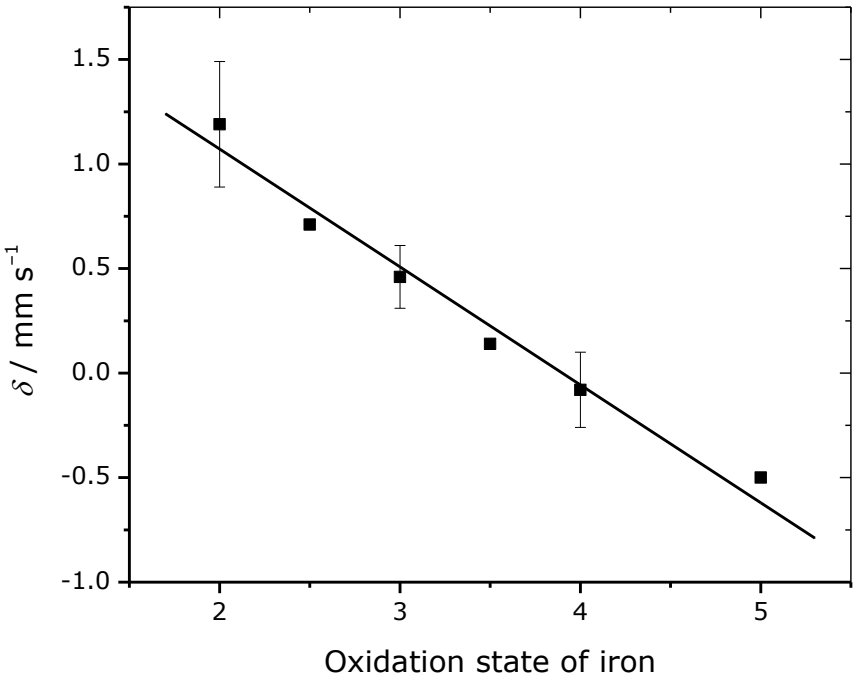

Figure 21. Dependance plot of oxidation state *vs.* isomer shift δ and least squares linear fit. The values with error bars are taken from Ref. 15 and 130.

Although the isomer shift is also affected by the coordination mode and the coordination number, the linear-fit shows a strong correlation between the isomer shifts and the oxidation states of the Cp complexes.

4.7 Electrochemistry and spectroscopic studies

Electrochemistry

In order to understand the electrochemical behavior of the complexes [Cp'FeI]$_2$ (**1**), [Cp'FeI$_2$] (**2**), [Cp'Fe(NCO)]$_2$ (**4**) and [Cp'FeN]$_2$ (**6**), their cyclic voltammogramms were explored. As shown in Figure 22 and 23, compounds **1**, **4** and **6** do not exhibit a reversible redox wave, while compound **2** shows a quasi-redox reaction.

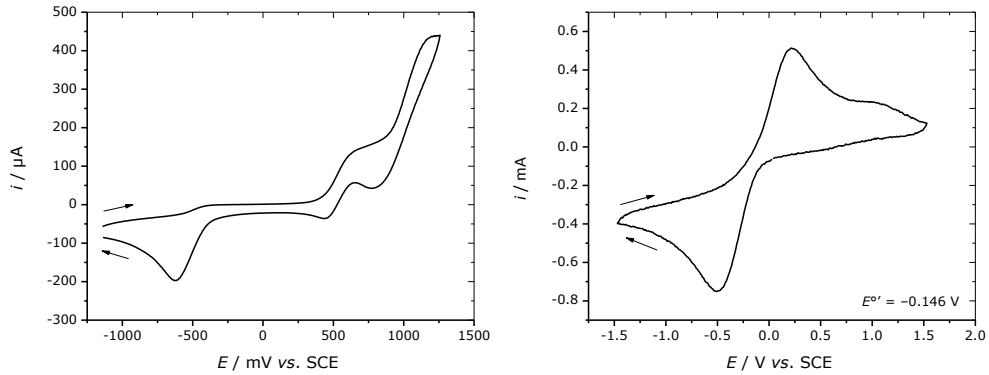

Figure 22. Cyclic voltammogram of [Cp'FeI]$_2$ (**1**) (left) and [Cp'FeI$_2$] (**2**) (right) measured in tetrahydrofuran (**1**) or dichloromethane (**2**) with 0.1 M [nBu$_4$N][PF$_6$]. Sweep rate: 500 mV s^{-1} (**1**) or 100 mV s^{-1} (**2**). External calibration.

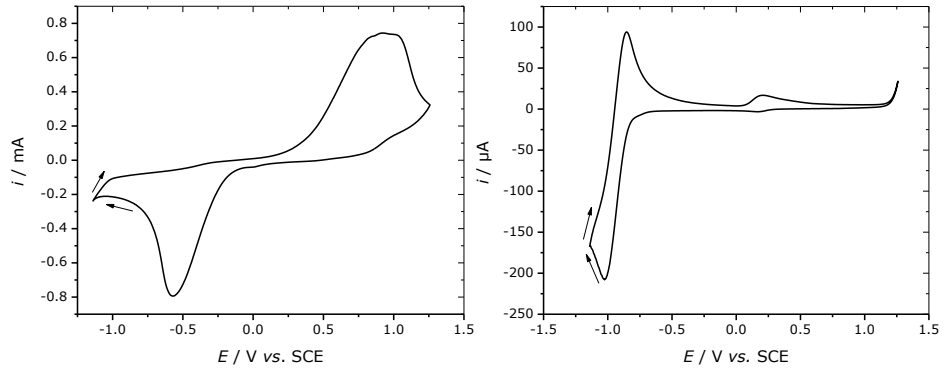

Figure 23. Cyclic voltammogram of [Cp'Fe(NCO)]$_2$ (**4**) (left) and [Cp'FeN]$_2$ (**6**) (right) measured in tetrahydrofuran with 0.1 M [nBu$_4$N][PF$_6$]. Sweep rate: 100 mV s^{-1}. External calibration.

The cyclic voltammogramms of the complexes [Cp'Fe(ItBu)I] (**12**), [Cp'Fe(IiPrMe$_2$)I] (**13**) and [Cp'Fe(IMes)I] (**14**) were also explored. As shown in Figure 24, 25 and 26, compound **13** shows a quasi-redox reaction in tetrahydrofuran and reacts in dichloromethane less than other derivatives. Compoud **12** exhibits also quasi-redox behavior in tetrahydrofuran. Presumably the double bond of the carbene ring is attacked by chlorine atom generated from dichloromethane.

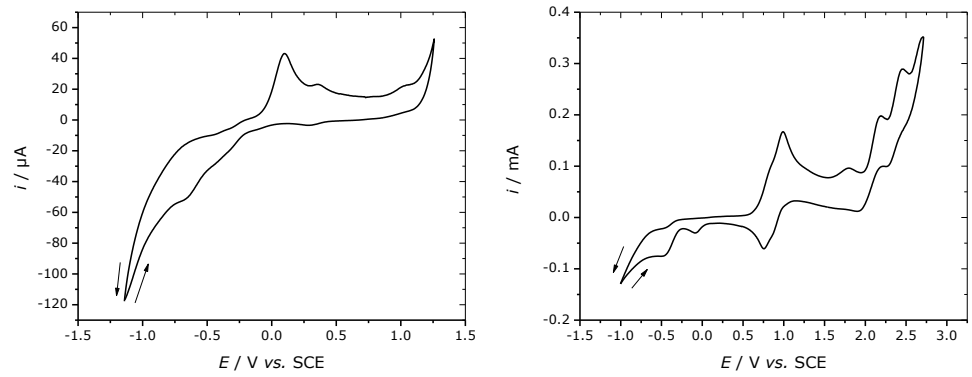

Figure 24. Cyclic voltammograms of [Cp'Fe(I*t*Bu)I] (**12**) measured in tetrahydrofuran (left) and in dichloromethane (right) with 0.1 M [*n*Bu$_4$N][PF$_6$]. Sweep rate: 100 mV s^{-1}. External calibration.

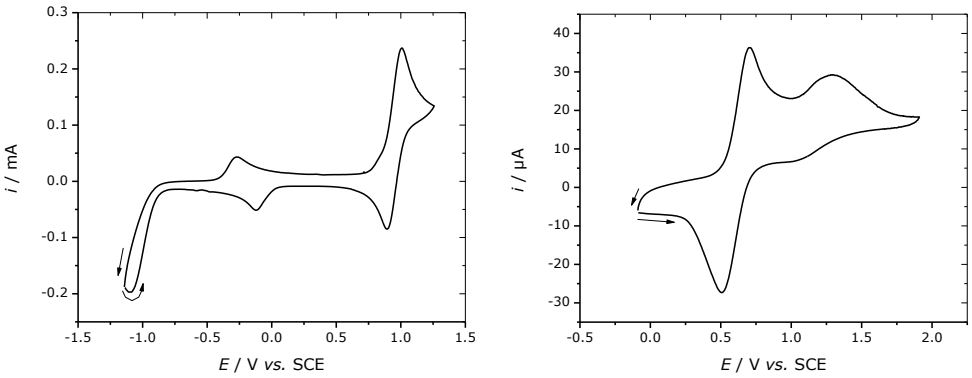

Figure 25. Cyclic voltammogram of [Cp'Fe(I*i*PrMe$_2$)I] (**13**) measured in tetrahydrofuran (left) and in dichloromethane (right) with 0.1 M [*n*Bu$_4$N][PF$_6$]. Sweep rate: 100 mV s^{-1}. External calibration.

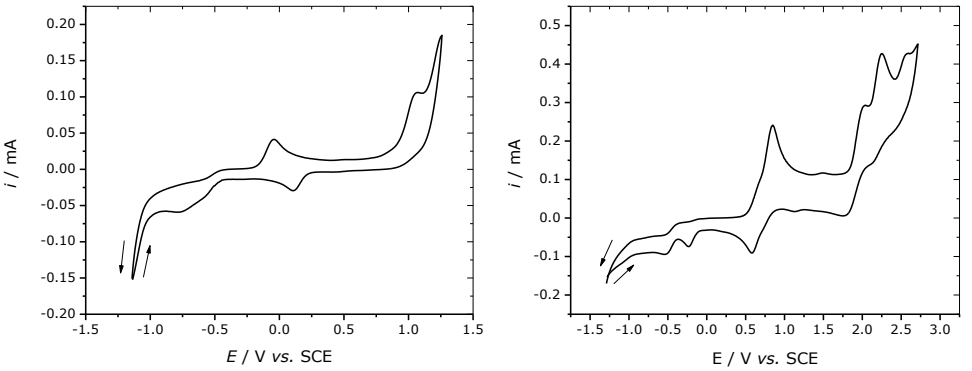

Figure 26. Cyclic voltammograms of [Cp'Fe(IMes)I] (**14**) measured in tetrahydrofuran (left) and in dichloromethane (right) with 0.1 M [*n*Bu$_4$N][PF$_6$]. Sweep rate: 100 mV s^{-1}. External calibration.

IR spectra

In the case of NCO-ligand, three coordination modes to the iron center are possible (Figure 27).

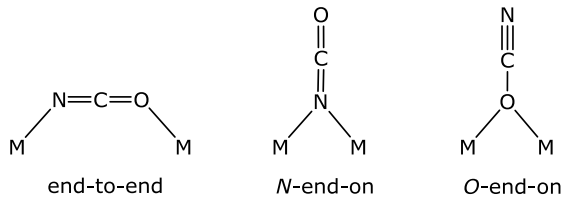

Figure 27. Possible coordination modes of the cyanate ion.

To distinguish the coordination mode of the cyanate ligand, an IR spectrum of [Cp'Fe(NCO)]$_2$ (**4**) was recorded (Figure 28).

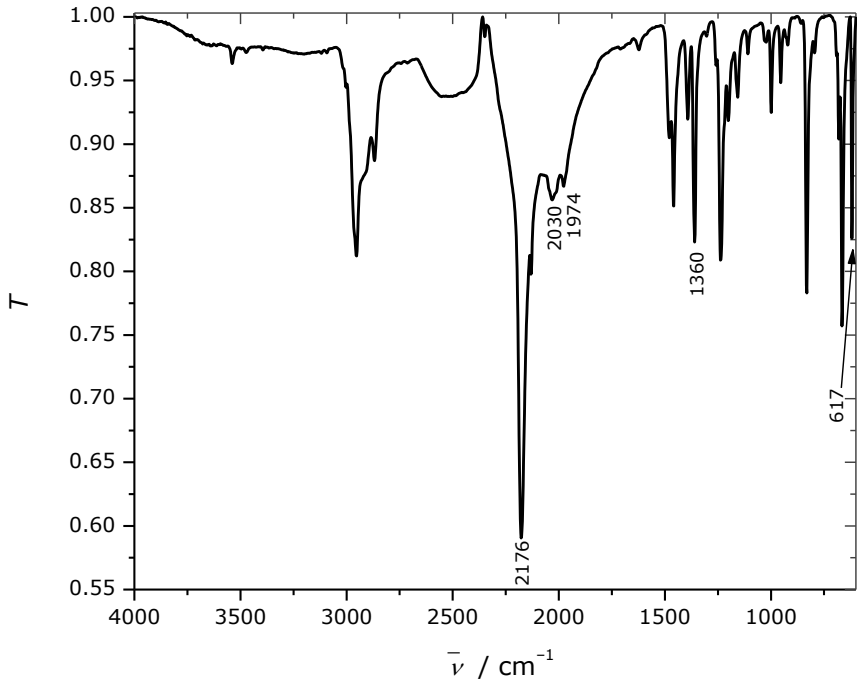

Figure 28. IR spectrum of [Cp'Fe(NCO)]$_2$ (**4**).

The characteristic IR absorptions for a cyanate group at 2176, 2030, 1974 cm^{-1} ($\nu_{C=N}$), 1360 cm^{-1} ($\nu_{C=O}$) and 617 cm^{-1} (δ_{OCN}) were observed for [Cp'Fe(NCO)]$_2$. This suggests a

bridging N-end-on coordination mode and these peaks are comparable to those of the known *N*-end-on bridged iron tetranuclear complex [Fe$_2$(pypentO)(NCO)$_3$]$_2$ (pypentOH = 1,5-bis[(2-pyridylmethyl)amino]pentan-3-ol) (2205 cm^{-1} and 2168 cm^{-1} for the asymmetric stretching vibration of CN, $\nu_{C=N}$; 1348 cm^{-1} for the asymmetric stretching vibration of CO, $\nu_{C=O}$; and 623 cm^{-1} for the deformation, δ_{OCN}; respectively).[89] IR spectra were corrected for *O*-end-on bridged [Cu(L)(OCN)]$_2$[PF$_6$]$_2$ (**17**) and end-to-end coordinated [Ni(L)(NCO)]$_2$[PF$_6$]$_2$ (**20**) (L = *N*,*N*-bis(3,5-dimethylpyrazol-1-ylmethyl)aminomethylpyridine) (Figure 29). The peak of $\nu_{C=N}$ at 2213 cm^{-1} for complex **17** and 2243 cm^{-1} for complex **20** were assigned,[90] but not for $\nu_{C=O}$ and for δ_{OCN} which were not reported for those compounds.

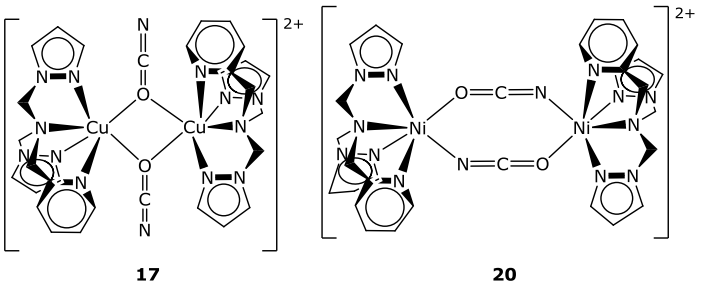

17 **20**

Figure 29. [Cu(L)(OCN)]$_2^{2+}$ (**17**) and [Ni(L)(NCO)]$_2^{2+}$ (**20**).

The IR spectra of [Cp'Fe(I*t*Bu)I] (**12**), [Cp'Fe(I*i*PrMe$_2$)I] (**13**), [Cp'Fe(IMes)I] (**14**), [Cp'Fe(IPr)I] (**15**) and [Cp'Fe(HNI*t*Bu)I] (**16**) were also recorded and the spectra of **12** and **16** are shown in Figure 30. Both complexes exhibit similar spectra. The NH (3371 cm^{-1}) and C=N bands (2148, 2031 and 1968 cm^{-1}) reflect the difference between both molecules.

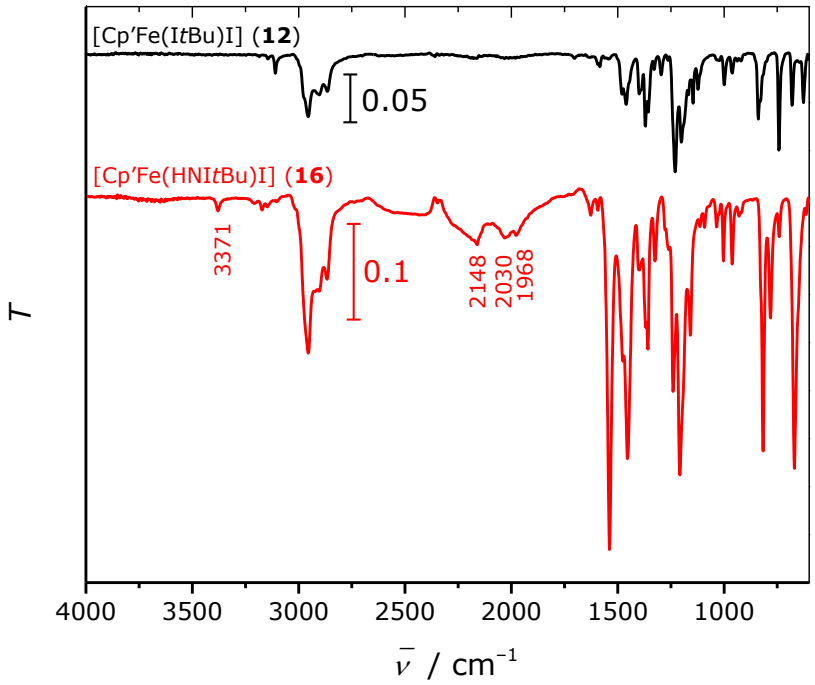

Figure 30. IR spectra of [Cp'Fe(I*t*Bu)I] (**12**) and [Cp'Fe(HNI*t*Bu)I] (**16**).

UV-vis spectra

Electronic spectra of [Cp'Fe(NCO)]$_2$ (**3**), [Cp'FeN]$_2$ (**5**) and [Cp'FeS]$_2$ (**6**) are shown in Figure 31. The UV-Vis spectrum of [Cp'Fe(NCO)]$_2$ is measured in tetrahydrofuran because of its low solubility in *n*-hexane, whereas the spectra of [Cp'FeN]$_2$ and [CpFeS]$_2$ were recorded in *n*-hexane at room temperature. For [Cp'Fe(I*t*Bu)I] (**12**), [Cp'Fe(I*i*PrMe$_2$)I] (**13**), [Cp'Fe(IMes)I] (**14**), [Cp'Fe(IPr)I] (**15**) and [Cp'Fe(HNI*t*Bu)I] (**16**), the UV-vis spectra are also corrected and shown in Figure 32, which are all measured in tetrahydrofuran at room temperature. As shown in Figure 31 and 32, complexes **3**, **5**, **13**, **14** and **16** exhibit bands at 705, 520, 775, 795 and 780 nm, respectively, which may be attributed due to the d–d transitions.

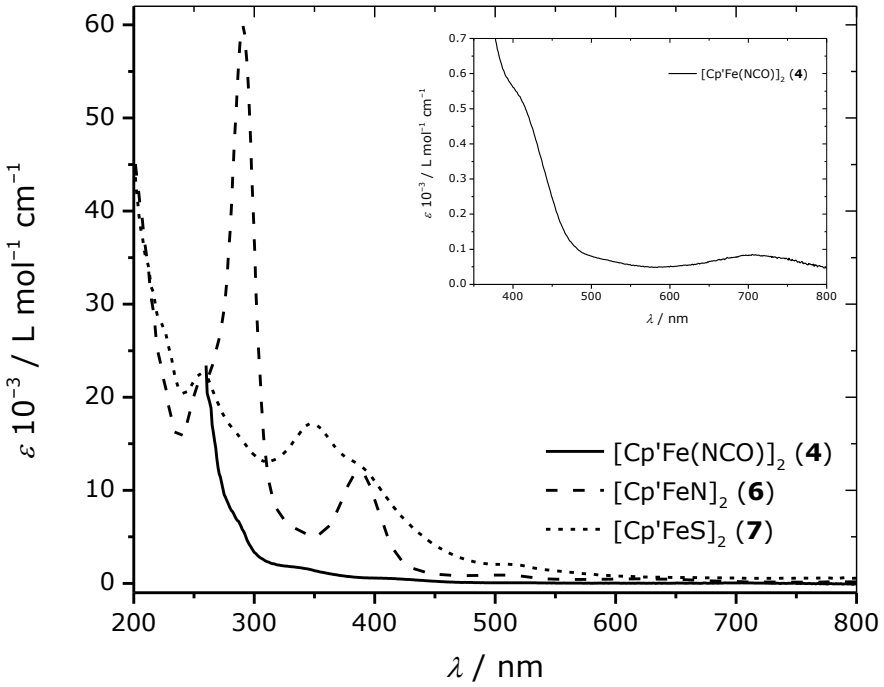

Figure 31. UV-vis spectra of [Cp'Fe(NCO)]$_2$ (**4**), [Cp'FeN]$_2$ (**6**) and [Cp'FeS]$_2$ (**7**).

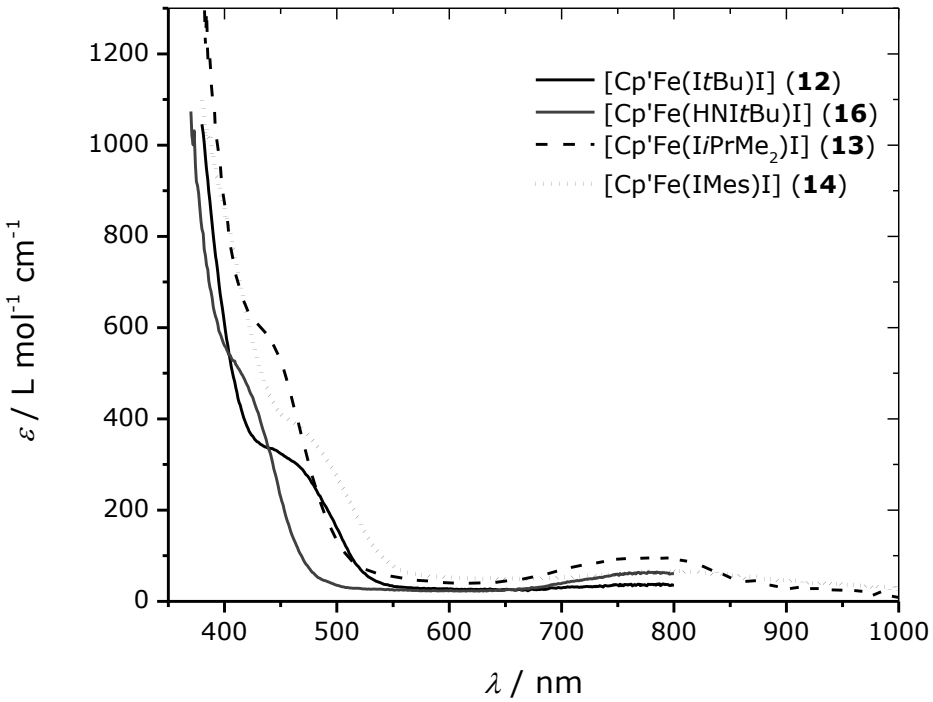

Figure 32. UV-vis spectra of [Cp'Fe(I*t*Bu)I] (**12**), [Cp'Fe(HNI*t*Bu)I] (**16**), [Cp'Fe(I*i*PrMe$_2$)I] (**13**) and [Cp'Fe(IMes)I] (**14**) in tetrahydrofuran.

4.8 Conclusion

Reactions of [Cp'FeI]$_2$ (**1**) and [Cp'MnI(thf)]$_2$ (**2**) with pseudohalides were investigated and a series of nitrido-, sulfido-, cyanato-, diselenido- and thiocyanato-bridged iron and manganese complexes [Cp'Fe(NCO)]$_2$ (**4**), [Cp'Mn(NCS)(thf)]$_2$ (**5**), [Cp'FeN]$_2$ (**6**), [Cp'FeS]$_2$ (**7**) and [Cp'Fe(Se$_2$)]$_2$ (**8**) were formed.

The pseudohalides either coordinate to the metal centers without participating in a redox reaction (in case of complex **4** and **5**), they coordinate in an end-on fashion with the splitting of small molecules (in case of complex **6** and **7**) or coordinate after further reaction (in case of complex **8**).

In SQUID magnetometry, **6** and **7** exhibit a very strong antiferromagnetic coupling whereas **1** and **4** show a weak antiferromagnetic coupling, but no spin-crossover. The Mössbauer spectroscopy was also carried out for the iron complexes. Compound **1** and **4** contain Fe(II) atoms, **7** and **8** Fe(III) atoms and **6** Fe(IV) atom. All complexes contain only one type of iron atoms in the same electronic environment.

In addition, a correlation between Cp$_{cent}$–metal distance and the spin state, and the Mössbauer isomer shift and oxidation state of iron atom were suggested.

In the future, the reactivity of these complexes will be investigated, *e.g.*, the modification of the sulfur atom in [Cp'FeS]$_2$ or selenium splitting in [Cp'Fe(Se$_2$)]$_2$ induced by UV light, or by reagents like PPh$_3$, KCN, Ag-compounds like AgNO$_3$ or NHCs.

4.5 References

(1) Doyle, M. P. *Acc. Chem. Res.* **1986**, *19*, 348–356.

(2) Woo, L. K. *Chem. Rev.* **1993**, *93*, 1125–1136.

(3) Saouma, C. T.; Peters, J. C. *Coord. Chem. Rev.* **2011**, *255*, 920–937.

(4) Costas, M.; Mehn, M. P.; Jensen, M. P.; Que, L. *Chem. Rev.* **2004**, *104*, 939–986.

(5) Shan, X.; Que, L. *J. Inorg. Biochem.* **2006**, *100*, 421–433.

(6) Klinker, E. J.; Kaizer, J.; Brennessel, W. W.; Woodrum, N. L.; Cramer, C. J.; Que, L. *Angew. Chem. Int. Ed.* **2005**, *44*, 3690–3694.

(7) Svastits, E. W.; Dawson, J. H.; Breslow, R.; Gellman, S. H. *J. Am. Chem. Soc.* **1985**, *107*, 6427–6428.

(8) Cummins, C. C. *Chem. Commun.* **1998**, *29*, 1777–1786.

(9) Yi, X.-Y.; Liang, Y.; Li, C. *RSC Adv.* **2013**, *3*, 3477–3486.

(10) Crevier, T. J.; Lovell, S.; Mayer, J. M.; Rheingold, A. L.; Guzei, I. A. *J. Am. Chem. Soc.* **1998**, *120*, 6607–6608.

(11) Kropp, H.; King, A. E.; Khusniyarov, M. M.; Heinemann, F. W.; Lancaster, K. M.; DeBeer, S.; Bill, E.; Meyer, K. *J. Am. Chem. Soc.* **2012**, *134*, 15538–15544.

(12) Du Bois, J.; Tomooka, C. S.; Hong, J.; Carreira, E. M. *Acc. Chem. Res.* **1997**, *30*, 364–372.

(13) Tran, B. L.; Krzystek, J.; Ozarowski, A.; Chen, C.-H.; Pink, M.; Karty, J. A.; Telser, J.; Meyer, K.; Mindiola, D. J. *Eur. J. Inorg. Chem.* **2013**, 3916–3929.

(14) Mehn, M. P.; Peters, J. C. *J. Inorg. Biochem.* **2006**, *100*, 634–643.

(15) Scepaniak, J. J.; Vogel, C. S.; Khusniyarov, M. M.; Heinemann, F. W.; Meyer, K.; Smith, J. M. *Science* **2011**, *331*, 1049–1052.

(16) Anderson, J. S.; Rittle, J.; Peters, J. C. *Nature* **2013**, *501*, 84–87.

(17) Chiang, K. P.; Bellows, S. M.; Brennessel, W. W.; Holland, P. L. *Chem. Sci.* **2014**, *5*, 267–274.

(18) Whited, M. T.; Mankad, N. P.; Lee, Y.; Oblad, P. F.; Peters, J. C. *Inorg. Chem.* **2009**, *48*, 2507–2517.

(19) Ertl, G. *Angew. Chem. Int. Ed. Engl.* **1990**, *29*, 1219–1227.

(20) Rasche, M. E.; Seefeldt, L. C. *Biochemistry* **1997**, *36*, 8574–8585.

(21) Seefeldt, L. C.; Rasche, M. E.; Ensign, S. A. *Biochemistry* **1995**, *34*, 5382–5389.

(22) Rohde, J.-U.; Betley, T. A.; Jackson, T. A.; Saouma, C. T.; Peters, J. C.; Que, L. *Inorg. Chem.* **2007**, *46*, 5720–5726.

(23) Anderson, J. S.; Moret, M.-E.; Peters, J. C. *J. Am. Chem. Soc.* **2013**, *135*, 534–537.

(24) Creutz, S. E.; Peters, J. C. *J. Am. Chem. Soc.* **2014**, *136*, 1105–1115.

(25) Rodriguez, M. M.; Bill, E.; Brennessel, W. W.; Holland, P. L. *Science* **2011**, *334*, 780–783.

(26) Walter, M. D.; White, P. S. *New J. Chem.* **2011**, *35*, 1842–1854.

(27) Walter, M. D.; White, P. S. *Inorg. Chem.* **2012**, *51*, 11860–11872.

(28) Walter, M. D.; White, P. S. *Dalton Trans.* **2012**, *41*, 8506–8508.

(29) Wallasch, M. W.; Rudolphi, F.; Wolmershäuser, G.; Sitzmann, H. *Z. Naturforsch.* **2009**, *64b*, 11–17.

(30) Wallasch, M. W.; Vollmer, G. Y.; Kafiyatullina, A.; Wolmershäuser, G.; Jones, P. G.; Mang, M.; Meyer, W.; Sitzmann, H. *Z. Naturforsch.* **2009**, *64b*, 18–24.

(31) Pammer, F.; Sun, Y.; Weismann, D.; Sitzmann, H.; Thiel, W. R. *Chem. Eur. J.* **2010**, *16*, 1265–1270.

(32) Wallasch, M. W.; Weismann, D.; Riehn, C.; Ambrus, S.; Wolmershäuser, G.; Lagutschenkov, A.; Niedner-Schatteburg, G.; Sitzmann, H. *Organometallics* **2010**, *29*, 806–813.

(33) Scherer, O. J.; Hilt, T.; Wolmershäuser, G. *Organometallics* **1998**, *17*, 4110–4112.

(34) Eichhorn, C.; Scherer, O. J.; Sögding, T. *Angew. Chem. Int. Ed.* **2001**, *40*, 2859–2861.

(35) Schwarzmaier, C.; Bodensteiner, M.; Timoshkin, A. Y.; Scheer, M. *Angew. Chem. Int. Ed.* **2014**, *53*, 290–293.

(36) Walter, M. D.; Grunenberg, J.; White, P. S. *Chem. Sci.* **2011**, *2*, 2120–2130.

(37) Maekawa, M.; Römelt, M.; Daniliuc, C. G.; Jones, P. G.; White, P. S.; Neese, F.; Walter, M. D. *Chem. Sci.* **2012**, *3*, 2972–2979.

(38) Holschumacher, D.; Bannenberg, T.; Ibrom, K.; Daniliuc, C. G.; Jones, P. G.; Tamm, M. *Dalton Trans.* **2010**, *39*, 10590–10592.

(39) Holschumacher, D.; Daniliuc, C. G.; Jones, P. G.; Tamm, M. *Z. Naturforsch.* **2011**, *66b*, 371–377.

(40) Kronig, S.; Theuergarten, E.; Holschumacher, D.; Bannenberg, T.; Daniliuc, C. G.; Jones, P. G.; Tamm, M. *Inorg. Chem.* **2011**, *50*, 7344–7359.

(41) Theuergarten, E.; Schlüns, D.; Grunenberg, J.; Daniliuc, C. G.; Jones, P. G.; Tamm, M. *Chem. Commun.* **2010**, *46*, 8561–8563.

(42) Theuergarten, E.; Schlösser, J.; Schlüns, D.; Freytag, M.; Daniliuc, C. G.; Jones, P. G.; Tamm, M. *Dalton Trans.* **2012**, *41*, 9101–9110.

(43) Theuergarten, E.; Bannenberg, T.; Walter, M. D.; Holschumacher, D.; Freytag, M.; Daniliuc, C. G.; Jones, P. G.; Tamm, M. *Dalton Trans.* **2014**, *43*, 1651–1662.

(44) Wu, X. New Tungsten Alkylidyne Complexes as Catalysts for Alkyne Metathesis. Dissertation, Technische Universität Braunschweig, 2011.

(45) Hu, X.; Tang, Y.; Gantzel, P.; Meyer, K. *Organometallics* **2003**, *22*, 612–614.

(46) Radius, U.; Bickelhaupt, F. M. *Coord. Chem. Rev.* **2009**, *253*, 678–686.

(47) Gusev, D. G. *Organometallics* **2009**, *28*, 6458–6461.

(48) Clavier, H.; Nolan, S. P. *Chem. Commun.* **2010**, *46*, 841–861.

(49) Öfele, K.; Kreiter, C. G. *Chem. Ber.* **1972**, *105*, 529–540.

(50) Huttner, G.; Gartzke, W. *Chem. Ber.* **1972**, *105*, 2714–2725.

(51) Toerien, J. G.; Desmet, M.; Kruger, G. J.; Raubenheimer, H. G. *J. Organomet. Chem.* **1994**, *479*, C12–C15.

(52) Herrmann, W. A. *Angew. Chem. Int. Ed.* **2002**, *41*, 1290–1309.

(53) Díez-González, S.; Marion, N.; Nolan, S. P. *Chem. Rev.* **2009**, *109*, 3612–3676.

(54) Ingleson, M. J.; Layfield, R. A. *Chem. Commun.* **2012**, *48*, 3579–3589.

(55) Bedford, R. B.; Betham, M.; Bruce, D. W.; Danopoulos, A. A.; Frost, R. M.; Hird, M. *J. Org. Chem.* **2006**, *71*, 1104–1110.

(56) Yamagami, T.; Shintani, R.; Shirakawa, E.; Hayashi, T. *Org. Lett.* **2007**, *9*, 1045–1048.

(57) Hatakeyama, T.; Nakamura, M. *J. Am. Chem. Soc.* **2007**, *129*, 9844–9845.

(58) Hatakeyama, T.; Hashimoto, S.; Ishizuka, K.; Nakamura, M. *J. Am. Chem. Soc.* **2009**, *131*, 11949–11963.

(59) Gao, H.; Yan, C.; Tao, X.-P.; Xia, Y.; Sun, H.-M.; Shen, Q.; Zhang, Y. *Organometallics* **2010**, *29*, 4189–4192.

(60) Hilt, G.; Bolze, P.; Kieltsch, I. *Chem. Commun.* **2005**, *2*, 1996–1998.

(61) Saino, N.; Kogure, D.; Okamoto, S. *Org. Lett.* **2005**, *7*, 3065–3067.

(62) Plietker, B.; Dieskau, A.; Möws, K.; Jatsch, A. *Angew. Chem. Int. Ed.* **2008**, *47*, 198–201.

(63) Louie, J.; Grubbs, R. H. *Chem. Commun.* **2000**, *1363*, 1479–1480.

(64) Chen, M.-Z.; Sun, H.-M.; Li, W.-F.; Wang, Z.-G.; Shen, Q.; Zhang, Y. *J. Organomet. Chem.* **2006**, *691*, 2489–2494.

(65) Lin, P.-H.; Smythe, N. C.; Gorelsky, S. I.; Maguire, S.; Henson, N. J.; Korobkov, I.; Scott, B. L.; Gordon, J. C.; Baker, R. T.; Murugesu, M. *J. Am. Chem. Soc.* **2011**, *133*, 15806–15809.

(66) Ohki, Y.; Hatanaka, T.; Tatsumi, K. *J. Am. Chem. Soc.* **2008**, *130*, 17174–17176.

(67) Hatanaka, T.; Ohki, Y.; Tatsumi, K. *Eur. J. Inorg. Chem.* **2013**, 3966–3971.

(68) Bézier, D.; Venkanna, G. T.; Sortais, J.-B.; Darcel, C. *ChemCatChem* **2011**, *3*, 1747–1750.

(69) Castro, L. C. M.; Sortais, J.-B.; Darcel, C. *Chem. Commun.* **2012**, *48*, 151–153.

(70) Kandepi, V. V. K. M.; Cardoso, J. M. S.; Peris, E.; Royo, B. *Organometallics* **2010**, *29*, 2777–2782.

(71) Cardoso, J. M. S.; Royo, B. *Chem. Commun.* **2012**, *48*, 4944–4946.

(72) Jiang, F.; Bézier, D.; Sortais, J.-B.; Darcel, C. *Adv. Synth. Catal.* **2011**, *353*, 239–244.

(73) Buitrago, E.; Zani, L.; Adolfsson, H. *Appl. Organomet. Chem.* **2011**, *25*, 748–752.

(74) Bézier, D.; Jiang, F.; Roisnel, T.; Sortais, J.-B.; Darcel, C. *Eur. J. Inorg. Chem.* **2012**, 1333–1337.

(75) Hatanaka, T.; Ohki, Y.; Tatsumi, K. *Chem. Asian J.* **2010**, *5*, 1657–1666.

(76) Song, L.-C.; Cheng, H.-W.; Hu, Q.-M. *J. Organomet. Chem.* **2004**, *689*, 1849–1855.

(77) Yao, S. A.; Lancaster, K. M.; Götz, A. W.; DeBeer, S.; Berry, J. F. *Chem. Eur. J.* **2012**, *18*, 9179–9183.

(78) Song, L.-C.; Cheng, H.-W.; Chen, X.; Hu, Q.-M. *Eur. J. Inorg. Chem.* **2004**, 3147–3153.

(79) Han, W. S.; Lee, S. W. *Bull. Korean Chem. Soc.* **2003**, *24*, 641–644.

(80) Fischer, E. O.; Wittmann, D.; Himmelreich, D.; Cai, R.; Ackermann, K.; Neugebauer, D. *Chem. Ber.* **1982**, *115*, 3152–3166.

(81) Parker, O. J.; Wolther, M. P.; Breneman, G. L. *Acta Cryst.* **1996**, *C52*, 1089–1091.

(82) Banerjee, S.; Sen, S.; Basak, S.; Mitra, S.; Hughes, D. L.; Desplanches, C. *Inorg. Chim. Acta* **2008**, *361*, 2707–2714.

(83) Gargano, M.; Ravasio, N.; Rossi, M.; Tiripicchio, A.; Camellini, M. T. *J. Chem. Soc., Dalton Trans.* **1989**, 921–925.

(84) Youngme, S.; Phatchimkun, J.; Suksangpanya, U.; Pakawatchai, C.; van Albada, G. A.; Reedijk, J. *Inorg. Chem. Commun.* **2005**, *8*, 882–885.

(85) Zukerman-Schpector, J.; Castellano, E. E.; De Simone, C. A.; Oliva, G.; Mauro, A. E. *Acta Cryst.* **1991**, *C47*, 957–959.

(86) Mauro, A. E.; Klein, S. I.; Saldaña, J. S.; De Simone, C. A.; Zukerman-Schpector, J.; Castellano, E. E. *Polyhedron* **1990**, *9*, 2937–2939.

(87) Carranza, J.; Sletten, J.; Lloret, F.; Julve, M. *J. Mol. Struct.* **2008**, *890*, 31–40.

(88) Chung, Y.-H.; Lin, H.-H.; Wei, H.-H. *J. Chin. Chem. Soc.* **2005**, *52*, 877–884.

(89) Clemente-Juan, J. M.; Mackiewicz, C.; Verelst, M.; Dahan, F.; Bousseksou, A.; Sanakis, Y.; Tuchagues, J.-P. *Inorg. Chem.* **2002**, *41*, 1478–1491.

(90) Mahendrasinh, Z.; Ankita, S.; Kumar, S. B.; Escuer, A.; Suresh, E. *Inorg. Chim. Acta* **2011**, *375*, 333–337.

(91) Ercan, F.; Arıcı, C.; Ülkü, D.; Kurtaran, R.; Aksu, M.; Atakol, O. *Z. Kristallogr. CM* **2004**, *219*, 295–299.

(92) Escuer, A.; Vicente, R.; El Fallah, M. S.; Solans, X.; Font-Bardía, M. *J. Chem. Soc., Dalton Trans.* **1996**, 1013–1019.

(93) Harding, P. A.; Henrick, K.; Lindoy, L. F.; McPartlin, M.; Tasker, P. A. *J. Chem. Soc., Chem. Commun.* **1983**, 1300.

(94) Kapoor, R.; Kataria, A.; Pathak, A.; Venugopalan, P.; Hundal, G.; Kapoor, P. *Polyhedron* **2005**, *24*, 1221–1231.

(95) Lin, H.-W. *Acta Crystallogr. Sect. E, Struct. reports online* **2008**, *64E*, m295.

(96) Naumann, D.; Schulz, F.; Pantenburg, I.; Tyrra, W. *Z. Anorg. Allg. Chem.* **2004**, *630*, 529–534.

(97) Ballmann, J.; Albers, A.; Demeshko, S.; Dechert, S.; Bill, E.; Bothe, E.; Ryde, U.; Meyer, F. *Angew. Chem. Int. Ed.* **2008**, *47*, 9537–9541.

(98) Mayerle, J. J.; Denmark, S. E.; DePamphilis, B. V.; Ibers, J. A.; Holm, R. H. *J. Am. Chem. Soc.* **1975**, *97*, 1032–1045.

(99) Pauling, L. *Proc. Natl. Acad. Sci. U. S. A.* **1976**, *73*, 4290–4293.

(100) Lang, H.; Huttner, G.; Zsolnai, L.; Mohr, G.; Sigwarth, B.; Weber, U.; Orama, O.; Jibril, I. *J. Organomet. Chem.* **1986**, *304*, 157–179.

(101) Sitzmann, H.; Saurenz, D.; Wolmershäuser, G.; Klein, A.; Boese, R. *Organometallics* **2001**, *20*, 700–705.

(102) Campana, C. F.; Lo, F.; Dahl, L. F. *Inorg. Chem.* **1979**, *18*, 3060–3064.

(103) Rheingold, A. L.; Bolinger, C. M.; Rauchfuss, T. B. *Acta Cryst.* **1986**, *C42*, 1878–1880.

(104) Weberg, R.; Haltiwanger, R. C.; Rakowski DuBois, M. *Organometallics* **1985**, *4*, 1315–1318.

(105) Chanaud, H.; Ducourant, A. M.; Giannotti, C. *J. Organomet. Chem.* **1980**, *190*, 201–216.

(106) Brunner, H.; Janietz, N.; Meier, W.; Sergeson, G.; Wachter, J.; Zahn, T.; Ziegler, M. L. *Angew. Chem. Int. Ed. Engl.* **1985**, *24*, 1060–1061.

(107) Yamada, M.; Tobita, H.; Inomata, S.; Ogino, H. *Bull. Chem. Soc. Jpn.* **1996**, *69*, 861–867.

(108) Ogino, H.; Tobita, H.; Inomata, S.; Shimoi, M. *J. Chem. Soc., Chem. Commun.* **1988**, *983*, 586–587.

(109) Cotton, F. A.; Jamerson, J. D.; Stults, B. R. *J. Am. Chem. Soc.* **1976**, *98*, 1774–1779.

(110) Olmstead, M. M.; Power, P. P.; Shoner, S. C. *Inorg. Chem.* **1991**, *30*, 2547–2551.

(111) Dutta, S. K.; Beckmann, U.; Bill, E.; Weyhermüller, T.; Wieghardt, K. *Inorg. Chem.* **2000**, *39*, 3355–3364.

(112) Verma, A. K.; Nazif, T. N.; Achim, C.; Lee, S. C. *J. Am. Chem. Soc.* **2000**, *122*, 11013–11014.

(113) Bart, S. C.; Lobkovsky, E.; Bill, E.; Chirik, P. J. *J. Am. Chem. Soc.* **2006**, *128*, 5302–5303.

(114) Scepaniak, J. J.; Young, J. A.; Bontchev, R. P.; Smith, J. M. *Angew. Chem. Int. Ed.* **2009**, *48*, 3158–3160.

(115) Cowley, R. E.; DeYonker, N. J.; Eckert, N. A.; Cundari, T. R.; DeBeer, S.; Bill, E.; Ottenwaelder, X.; Flaschenriem, C.; Holland, P. L. *Inorg. Chem.* **2010**, *49*, 6172–6187.

(116) King, E. R.; Hennessy, E. T.; Betley, T. A. *J. Am. Chem. Soc.* **2011**, *133*, 4917–4923.

(117) Cowley, R. E.; Holland, P. L. *Inorg. Chem.* **2012**, *51*, 8352–8361.

(118) Blom, R.; Haaland, A. *J. Mol. Struct.* **1985**, *128*, 21–27.

(119) Haddad, T. S.; Aistars, A.; Ziller, J. W.; Doherty, N. M. *Organometallics* **1993**, *12*, 2420–2422.

(120) Odom, A. L.; Cummins, C. C. *Organometallics* **1996**, *15*, 898–900.

(121) Clentsmith, G. K. B.; Bates, V. M. E.; Hitchcock, P. B.; Cloke, F. G. N. *J. Am. Chem. Soc.* **1999**, *121*, 10444–10445.

(122) Herberhold, M.; Dietel, A.; Goller, A.; Milius, W. *Z. Anorg. Allg. Chem.* **2003**, *629*, 871–879.

(123) Hirotsu, M.; Fontaine, P. P.; Epshteyn, A.; Zavalij, P. Y.; Sita, L. R. *J. Am. Chem. Soc.* **2007**, *129*, 9284–9285.

(124) Tonzetich, Z. J.; Schrock, R. R.; Wampler, K. M.; Bailey, B. C.; Cummins, C. C.; Müller, P. *Inorg. Chem.* **2008**, *47*, 1560–1567.

(125) Przyojski, J. A.; Arman, H. D.; Tonzetich, Z. J. *Organometallics* **2012**, *31*, 3264–3271.

(126) Li, B.; Liu, T.; Popescu, C. V.; Bilko, A.; Darensbourg, M. Y. *Inorg. Chem.* **2009**, *48*, 11283–11289.

(127) Kreye, M.; Baabe, D.; Schweyen, P.; Freytag, M.; Daniliuc, C. G.; Jones, P. G.; Walter, M. D. *Organometallics* **2013**, *32*, 5887–5898.

(128) Greenwood, N. N.; Gibb, T. C. *Mössbauer spectroscopy*; Chapman and Hall: London, 1971.

(129) Gütlich, P.; Link, R.; Trautwein, A. *Mössbauer spectroscopy and transition metal chemistry*; Springer: Berlin, 1978.

(130) Han, W.; Liu, T.; Lovell, T.; Noodleman, L. *J. Comput. Chem.* **2006**, *27*, 1292–1306.

(131) Hoggins, J. T.; Steinfink, H. *Inorg. Chem.* **1976**, *15*, 1682–1685.

(132) Ballmann, J.; Dechert, S.; Bill, E.; Ryde, U.; Meyer, F. *Inorg. Chem.* **2008**, *47*, 1586–1596.

(133) Albers, A.; Demeshko, S.; Dechert, S.; Bill, E.; Bothe, E.; Meyer, F. *Angew. Chem. Int. Ed.* **2011**, *50*, 9191–9194.

(134) Albers, A.; Bayer, T.; Demeshko, S.; Dechert, S.; Meyer, F. *Chem. Eur. J.* **2013**, *19*, 10101–10106.

(135) Albers, A.; Demeshko, S.; Pröpper, K.; Dechert, S.; Bill, E.; Meyer, F. *J. Am. Chem. Soc.* **2013**, *135*, 1704–1707.

(136) Fuchs, M. G. G.; Meyer, F.; Ryde, U. *J. Biol. Inorg. Chem.* **2010**, *15*, 203–212.

(137) Fuchs, M. G. G.; Dechert, S.; Demeshko, S.; Ryde, U.; Meyer, F. *Inorg. Chem.* **2010**, *49*, 5853–5858.

(138) Beardwood, P.; Gibson, J. F.; Johnson, C. E.; Rush, J. D. *J. Chem. Soc., Dalton Trans.* **1982**, 2015–2020.

(139) Fee, J. A.; Findling, K. L.; Yoshida, T.; Hille, R.; Tarr, G. E.; Hearshen, D. O.; Dunham, W. R.; Day, E. P.; Kent, T. A.; Münck, E. *J. Biol. Chem.* **1984**, *259*, 124–133.

(140) Kuila, D.; Fee, J. A. *J. Biol. Chem.* **1986**, *261*, 2768–2771.

(141) Geary, P. J.; Dickson, D. P. *Biochem. J.* **1981**, *195*, 199–203.

(142) Vogel, C. S.; Heinemann, F. W.; Sutter, J.; Anthon, C.; Meyer, K. *Angew. Chem. Int. Ed.* **2008**, *47*, 2681–2684.

(143) Hendrich, M. P.; Gunderson, W.; Behan, R. K.; Green, M. T.; Mehn, M. P.; Betley, T. A.; Lu, C. C.; Peters, J. C. *Proc. Natl. Acad. Sci. U. S. A.* **2006**, *103*, 17107–17112.

(144) Danopoulos, A. A.; Braunstein, P.; Wesolek, M.; Monakhov, K. Y.; Rabu, P.; Robert, V. *Organometallics* **2012**, *31*, 4102–4105.

(145) Xiang, L.; Xiao, J.; Deng, L. *Organometallics* **2011**, *30*, 2018–2025.

La vérité de demain se nourrit de l'erreur d'hier.
<Pilote de guerre>
– Antoine de Saint-Exupéry (1900 – 1944)

Chapter 5. Synthesis of [Cp'Fe(η^3-BH_4)] and its conversion to [Cp'Fe(BH_2)]$_3$

Abstract

Salt mehathesis of [Cp'FeI]$_2$ (Cp' = η^5-1,2,4-(Me_3C)$_3$$C_5H_2$) and 2 equiv. $NaBH_4$ yields the low-spin iron complex [Cp'Fe(η^3-BH_4)] (**1**), which is thermally unstable and trimerizes to [CpFe(BH_2)]$_3$ (**2**) under H_2 release. Compounds **1** and **2** have been fully characterized by various spectroscopic methods. An X-ray structure analysis of **2** confirms its nature and reveals rather long B–B distances of 1.883(9) Å.

5.1 Introduction

Iron hydrides are considered as important intermediates in small molecule activations and catalytic transformations, which are performed by such as hydrogenase and nitrogenase.[1] To eluciate the reaction mechanisms and to mimic such reactions, low coordinate iron hydrides were synthesized as model molecules. These are stabilized by various ligands such as β-diketoiminato and trispyrazolyl borate ligands.[2–4]

The previous chapter shows that the 1,2,4-tri(*tert*-butyl)cyclopentadienyl (Cp') ligand is suitable for the stabilization of Fe(II) high-spin molecules which are not 18 valence electron complexes.

Two synthetic pathways to [Cp'FeH]$_n$ complexes can be considered either by salt metathesis of [Cp'FeI]$_2$ with $KHBEt_3$ or KBH_4, or hydrogenation of a [Cp'FeR]$_n$ precursor. Both approaches have been demonstrated in the work by Holland and Peters for the synthesis of low-coordinate Fe–H molecules.[5,6] Therefore, the synthesis of an iron hydrid supported by Cp' ligand was investigated with those approaches and bimetallic iron polyhydrides [Cp'FeH_2]$_2$ and [(Cp'Fe)$_2H_3$] were obtained from the reaction of [Cp'FeI]$_2$ and $KHBEt_3$.[7] The iron monohydride [Cp'FeH]$_n$ was not obtained. To prepare Cp' supported iron hydrid complex *via* [Cp'FeR]$_n$ precursor, the synthesis of stable "[Cp'FeMe]" was tried, however failed despite several attempts. On the other hand, no reaction was observed upon H_2

addition to [Cp'FeCH($SiMe_3$)$_2$].[8]

Now the borohydride anion $[BH_4]^-$ is chosen as a potential precursor to [Cp'FeH]$_n$. In general, tetrahydridoborate complexes can be prepared for transition and f-block metals, and the reactions of tetrahydridoborate with organotransition metal complexes provide a new metallaborane complexes.[9–12] However, these complexes exhibit varying degrees of reactivity and thermal stability.[13–15] For iron, attempts to isolate the homoleptic [Fe(BH_4)$_2$] were unsuccessful because of the thermal instability of this species.[16,17] The replacement of one $[BH_4]^-$ unit by a sterically demanding ancillary ligand increased the thermal stability and allowed the isolation of the low-spin hexahydridoborate-bridged diiron (II)[18,19] and monomeric iron (II)[20,21] tetrahydridoborate complexes. However, the steric hindrance of (C_5Me_5) (Cp*) ligand is not enough to stabilize the metallaboranes of manganese and iron and to prevent the formation of Cp*$_2$Mn and Cp*$_2$Fe[22] with the exception of *arachno*-[Cp*Fe(CO)B_3H_8].[12]

In this chapter, the synthesis of the low-spin complex [Cp'Fe(η^3-BH_4)] (**1**) is reported, which is thermally unstable and trimerizes to the thermally relatively stable complex [Cp'Fe(BH_2)]$_3$ (**2**) and H_2.

5.2 Synthesis and Reaction Chemistry of [Cp'Fe(η^3-BH_4)]

[Cp'Fe(η^3-BH_4)] (**1**), which can also be considered as a ferrocene analogue, since η^3-BH_4 is isoelectronic and isolobal to the η^5-cyclopentadienyl,[23] is prepared by salt metathesis of [Cp'FeI]$_2$ with $NaBH_4$ in tetrahydrofuran. The solution turned purple immediately. After NaI is removed, complex **1** is isolated by bulb-to bulb distillation (0.02 mbar, 28°C) as a purple oil, whose melting point is close to room temperature. The purity of this oil was judged by ^{1}H, ^{13}C and ^{11}B{^{1}H} NMR spectra. Complex **1** is a diamagnetic compound, exhibit a narrow resonance of BH_4 moiety at $\delta = -18.1$ ppm in the ^{1}H NMR and at +2.2 ppm in the ^{11}B{^{1}H} NMR spectra (Figure 1).

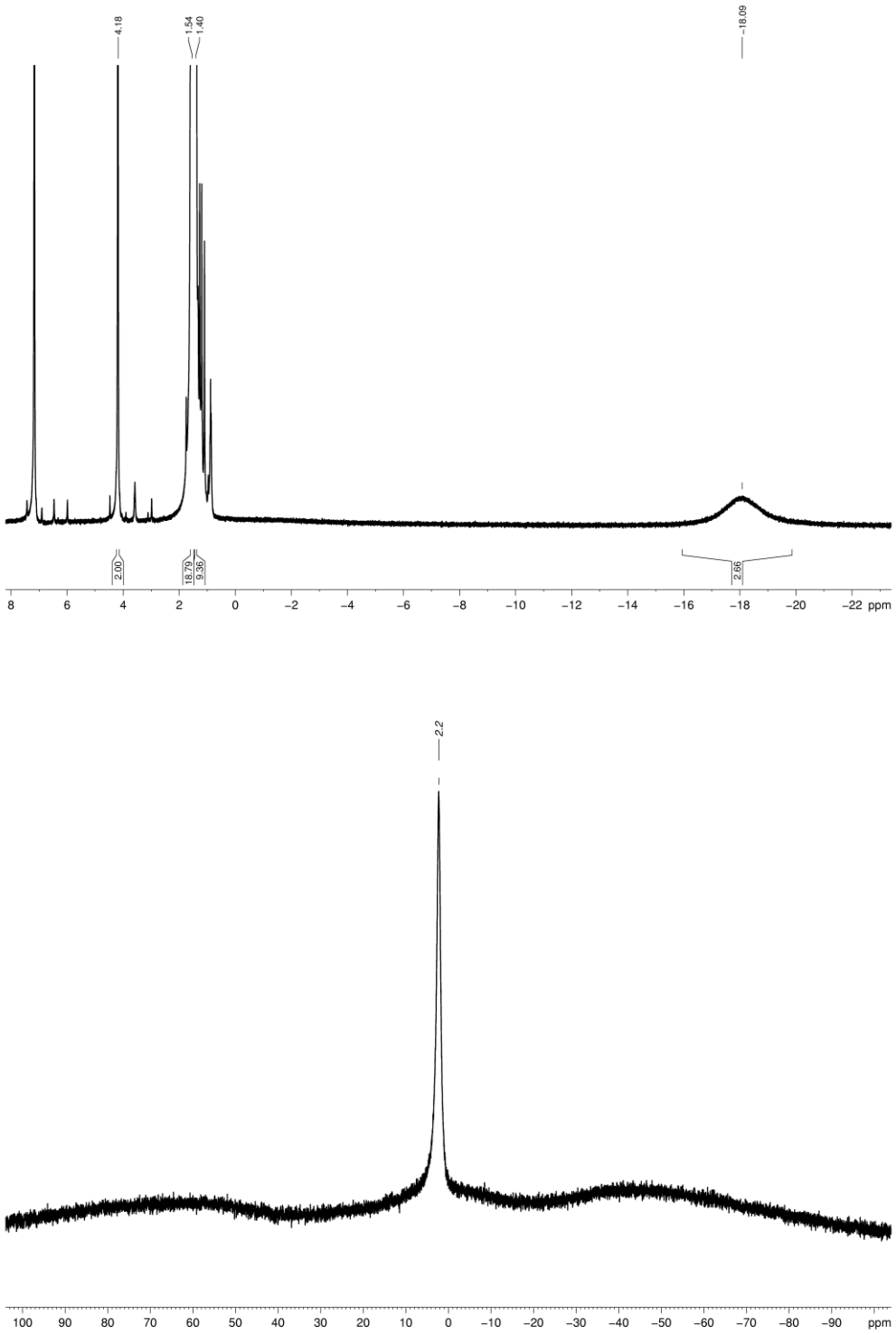

Figure 1. ^{1}H NMR spectrum (top) and ^{11}B{^{1}H} NMR spectrum (bottom) of [Cp'Fe(η^3-BH_4)].

Those chemical shifts are similar to those observed in [($PhBP_3$)Fe(η^3-BH_4)]

($PhBP_3$ = $PHB(CH_2PPh_2)_3$).[21]

The ESI-MS spectrum shows the molecular ion of [Cp'Fe(η^3-BH_4)] at m/z = 304.2020 amu (calcd. 304.2019) and the isotopic distribution agrees the simulated data.

The neat complex **1** solidifies slowly when it is stored under N_2, and the color changes to red-brown. The process is presented by ^{1}H NMR spectroscopy in Figure 2. It converted to the trimer *ca.* 80% within eight days and the conversion completed within two months.

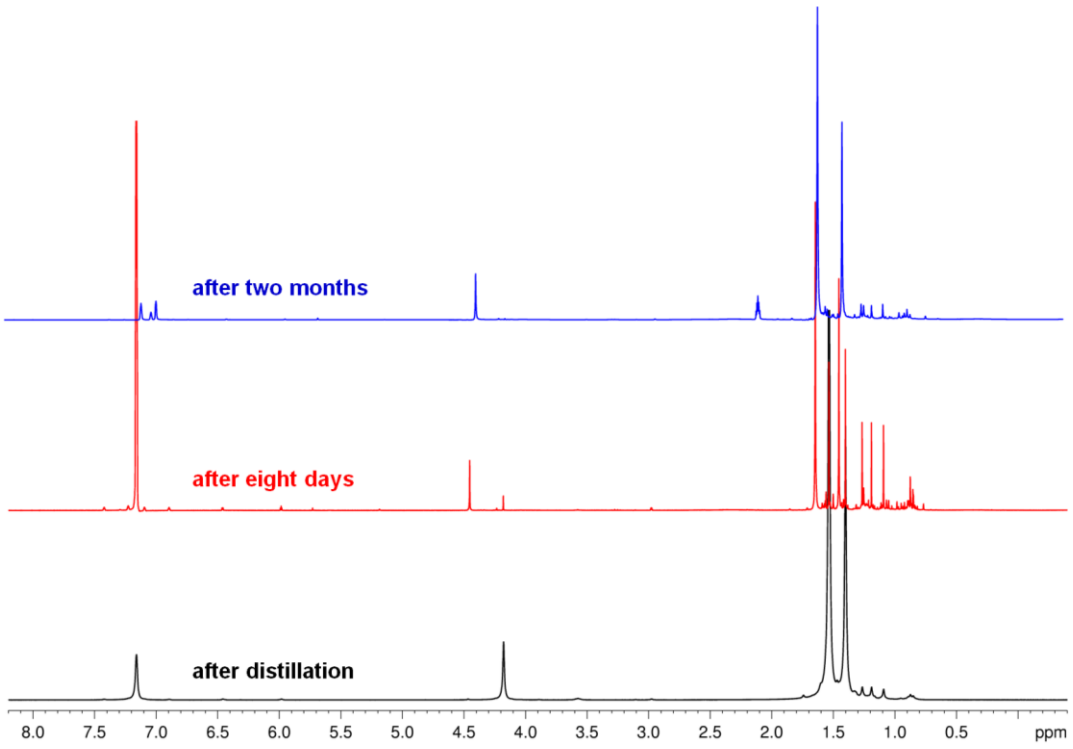

Figure 2. Conversion monitoring from [Cp'Fe(η^3-BH_4)] to [Cp'Fe(BH_2)]$_3$ by ^{1}H NMR spectroscopy.

Pure [Cp'Fe(η^3-BH_4)] is stable in the solution up to fifty days at ambient temperature without any changes, and up to 4% were converted to the trimer after one year according to ^{1}H NMR spectroscopy. However, a brown-black solid was formed when the solution was heated to 55°C (in tetrahydrofuran) or 80°C (in toluene). The identification of this solid was attempted, but was not successful. Although the identification failed, it could be Fe_2B, since the conversion to Fe_2B from diglyme solution of [(diglyme)$_n$Fe(BH_4)$_2$] upon heating was reported.[17]

From unpurified [Cp'Fe(η^3-BH_4)] in any solution, a brown-black solid was precipitated within two weeks, which has also not been successfully identified. A part of complex **1**

converted to the trimer [Cp'Fe(BH_2)]$_3$ (**2**) under H_2 release (yield 17%).

5.3 Reactivity and characterization of [Cp'Fe(BH_2)]$_3$

The trimer [Cp'Fe(BH_2)]$_3$ is stable under EI-MS condition and exhibit the molecular ion at m/z = 906 with the correct isotopic distribution. The trimer **2** is moderately soluble in aromatic and aliphatic hydrocarbons and diethylether, practically insoluble in hexamethyldisiloxane, in which the intermediate is soluble. Unlike [Cp'Fe(η^3-BH_4)], Complex **2** shows no sign of decomposition in solution or in solid state. This complex is also thermally relatively stable, and decomposed only at 224 – 225°C.

The H_2 elimination from [Cp'Fe(η^3-BH_4)] is irreversible and no reaction occurs according to the ^{1}H and the ^{11}B{^{1}H} NMR spectroscopy, when H_2 (1 bar) is added to a C_6D_6 solution of [Cp'Fe(BH_2)]$_3$. The H_2 loss and the formation of [Cp'Fe(BH_2)]$_3$ are induced when [Cp'Fe(η^3-BH_4)] is allowed to stand at ambient temperature. Therefore, this conversion must be thermodynamically favorable. Moreover, this trimerization can not be accelerated, since a brown-black insoluble solid was formed, when complex **1** was exposed to dynamic vacuum for a couple of hours.

Complex **2** is also a diamagnetic compound. In contrast to complex **1**, the resonance of the BH_2 moiety at δ = –14.2 ppm in the ^{1}H NMR is slightly sharper than those of BH_4 in complex **1**. The resonance in the ^{11}B{^{1}H} NMR spectrum is shifted downfield from +2.2 ppm to +61.6 ppm, and exhibit that the BH_2 moieties are magnetically equivalent (Figure 3).

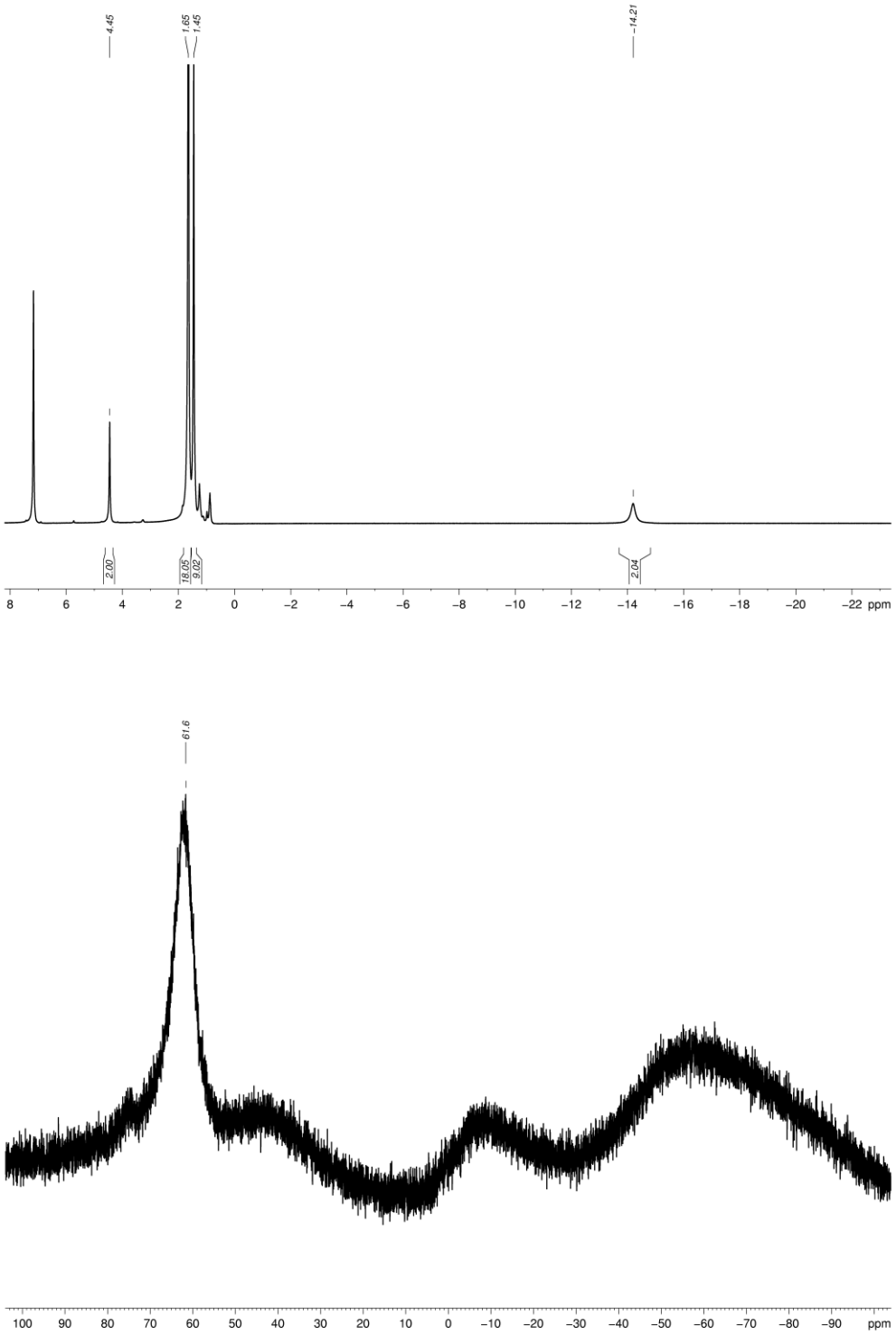

Figure 3. ^{1}H NMR spectrum (top) and $^{11}B\{^{1}H\}$ NMR spectrum (bottom) of $[Cp'Fe(BH_2)]_3$.

$[Cp'Fe(BH_2)]_3$ crystallizes from the concentrated diethyl ether or benzene solution in the

triclinic space group $P\bar{1}$. The solid state molecular structure of [Cp'Fe(BH_2)]$_3$ was determined and exhibits idealized C3 symmetry as shown in Figure 4. The hydrogen atoms of the B_3H_6 moiety were located in the difference Fourier density map and refined isotropically. The average B–B distance of 1.88 Å in compound **2** is considerably longer than typical B–B single bond of 1.72 Å[24] and even longer than the B–B distances in diborane derivatives (1.82 Å). Each centroid of Cp' ring is located on the extension of the sides of the triangle.

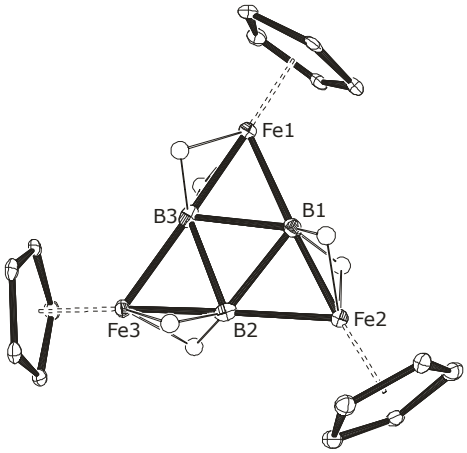

Figure 4. Molecular structure of [Cp'Fe(BH_2)]$_3$ (**2**) in solid state. Thermal ellipsoids are given at the 30% probability level. *t*Bu groups and H atoms on the Cp' rings are omitted for clarity. Selected bond lentehs [Å] and angles [°]: Cp'$_{cent}$–Fe (av.) 1.68, Fe1–B1 1.999(3), Fe1–B3 1.855(4), Fe2–B1 1.855(3), Fe2–B2 2.003(3), Fe3–B2 1.848(3), Fe3–B3 2.001(4), B1–B2 1.873(5), B1–B3 1.881(5), B2–B3 1.896(5), B3–Fe1–B1 58.27(14), B1–Fe2–B2 57.93(14), B2–Fe3–B3 58.85(14), B2–B1–B3 60.68(18), B1–B2–B3 59.86(18), B1–B3–B2 59.46(17), Cp'$_{cent}$–Fe1–B3 178.3, Cp'$_{cent}$–Fe2–B1 175.7, Cp'$_{cent}$–Fe3–B2 175.9.

The molecular structure of [Cp'Fe(BH_2)]$_3$ is peculiar and no other similar structure is known. The $[B_3H_6]^-$ fragment in this complex can be considered as an analogue of the 6π electron aromatic cyclopropenyl trianion $[C_3H_3]^{3-}$, since BH_2 is isolobal and isoelectronic to a CH fragment as has been pointed out in the context of [(Cp*Co)$_3$(η^3-HBH)$_2$].[9] Although $[B_3H_6]^{3-}$ has not yet been isolated, DFT calculations suggest that $Mg_3[B_3H_6]_2$ is a metastable intermediate in the thermal decomposition of $Mg(BH_4)_2$.[25] $[B_3H_6]^+$ is isoelectronic to the smallest 2π electron aromatic compound $[C_3H_3]^+$ and this has recently been synthesized in contrast to $[B_3H_6]^{3-}$.[26]

To further investigate the oxidation states in [Cp'Fe(BH_2)]$_3$, zero-field Mössbauer spectrum was recorded at 77 K and the fits of Mössbauer spectrum were obtained by using Lorenzian

line doublets with isomer shifts δ, quadrupole splittings ΔE_Q and line width Γ_{FWHM}. The isomer shift is 0.22(1) mm s^{-1}, which is in the range observed for low-spin iron(II) (Figure 5).[27,28]

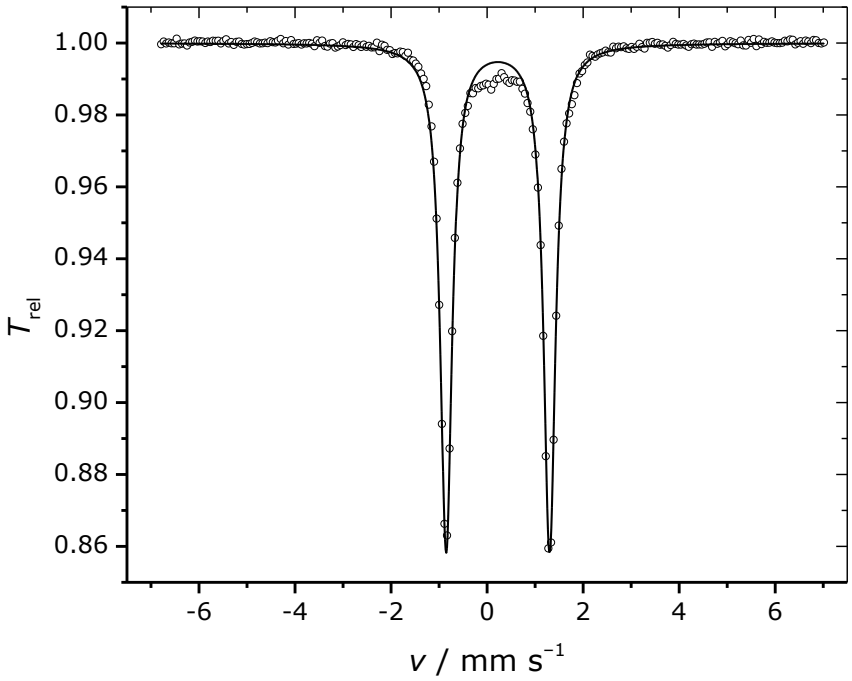

Figure 5. Mössbauer spectrum of [Cp'Fe(BH_2)]$_3$ measured at 77 K. δ = 0.22(1) mm s^{-1}, ΔE_Q = 2.15(1) mm s^{-1}, Γ_{FWHM} = 0.30(1) mm s^{-1}.

UV-vis spectra of [Cp'Fe(η^3-BH_4)] and [Cp'Fe(BH_2)]$_3$ were measured in *n*-hexane at ambient temperature (Figure 6). [Cp'Fe(η^3-BH_4)] has only one band at 540 nm while [Cp'Fe(BH_2)]$_3$ exhibits these at 447 and 766 nm.

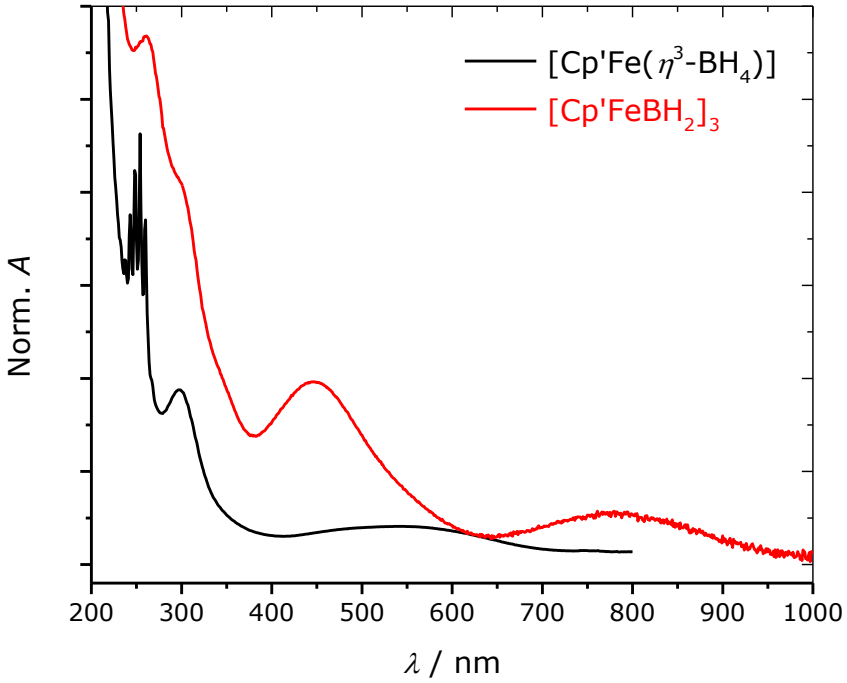

Figure 6. UV-vis spectra of [Cp'Fe(η^3-BH_4)] and [Cp'Fe(BH_2)]$_3$ in *n*-hexane.

5.4 Deuterium labeling experiments

The deuterium labeling was performed for further investigation of molecular properties. The EI-MS spectra show that no H/D-exchange with solvent occurred while the reaction. The ^{1}H NMR spectrum confirmed the BH_4 in [Cp'Fe(η^3-BH_4)] and BH_2 in [Cp'Fe(BH_2)]$_3$ resonances at –18.1 and –14.2 ppm, respectively (Figure 7).

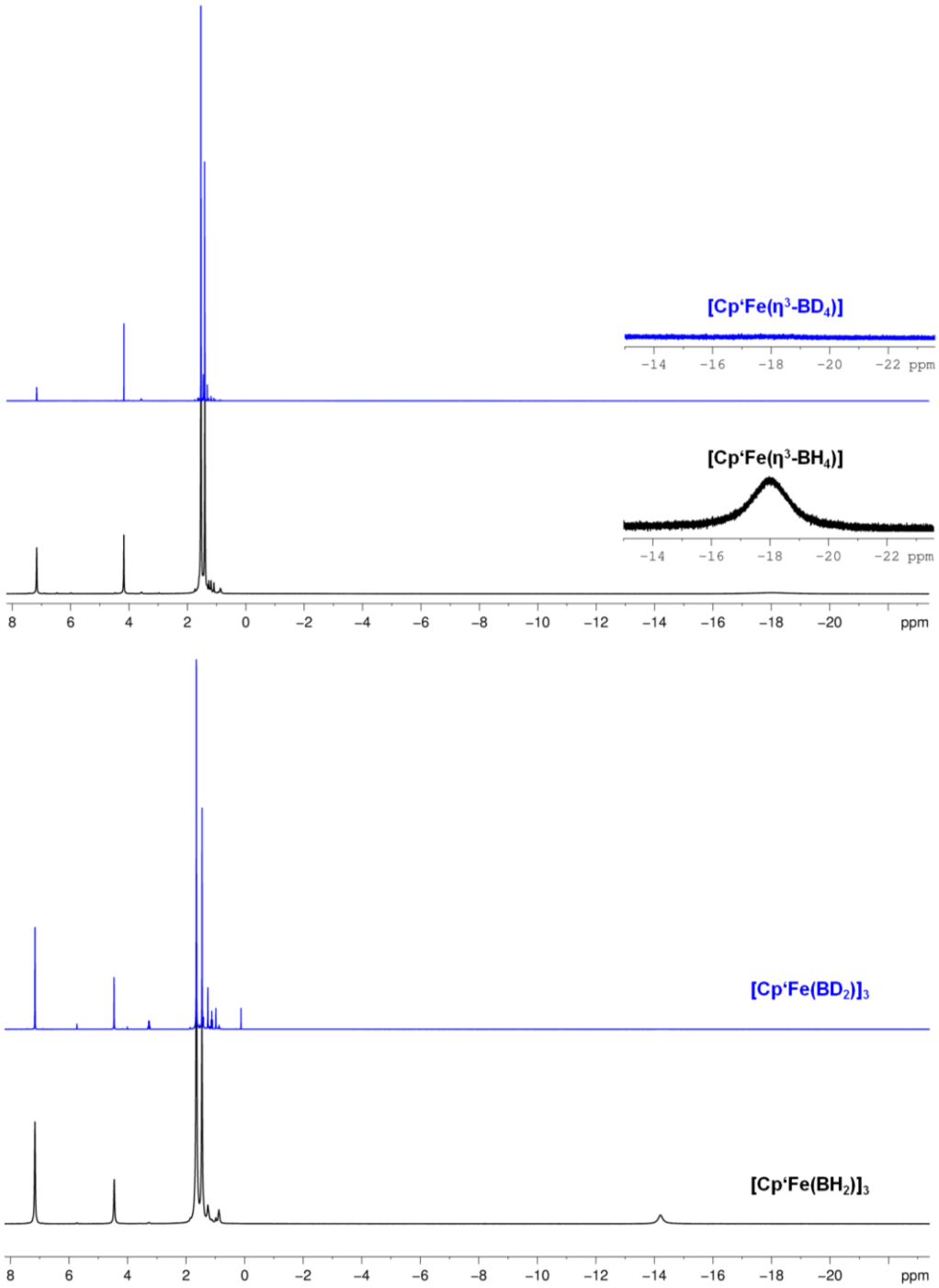

Figure 7. ^{1}H NMR spectra of [Cp'Fe(η^3-BH_4)] (top) and [Cp'Fe(BH_2)]$_3$ (bottom).

IR spectroscopy was also investigated to determinate the hapticity of borohydride ligands in transition metal complexes. The IR spectrum of compound **1** in THF solution shows four broad bands, which are sensitive to isotopic substitution, are observed at 2584, 2408, 2053 and 1307 cm^{-1}. The deuterated species [Cp'Fe(η^3-BD_4)] exhibits reproducible broad features at 1938, 1811 and 1741 cm^{-1}. The mode at 2584 cm^{-1} is tentatively assigned to the ν(B–H)$_{distal}$

stretching mode of a facial η^3-BH_4 moiety, which is in good agreement with published ν(B–H) vibrations.[13,15,21,29] Hooke's law predicts a ν(B–D)/ν(B–H) ratio of 0.74, and a value of 0.75 was observed experimentally for this mode. The broad feature at 2408 cm^{-1} in **1** is split to a doublet at 1811 and 1741 cm^{-1} in [Cp'Fe(η^3-BD_4)] and might be ascribed to the ν(B–H)$_{distal}$ stretching mode (Figure 8). The broad feature at 2053 cm^{-1} disappears on deuteration and is probably masked by the strong ligand absorptions at *ca.* 1500 cm^{-1}. The bands at 1477 and 997 cm^{-1} in the spectrum of [Cp'Fe(BD_2)]$_3$ are corresponding to the bands at 1861 and 1162 cm^{-1} in which may be attributed ν(B–H), however, which stretching mode is unknown.

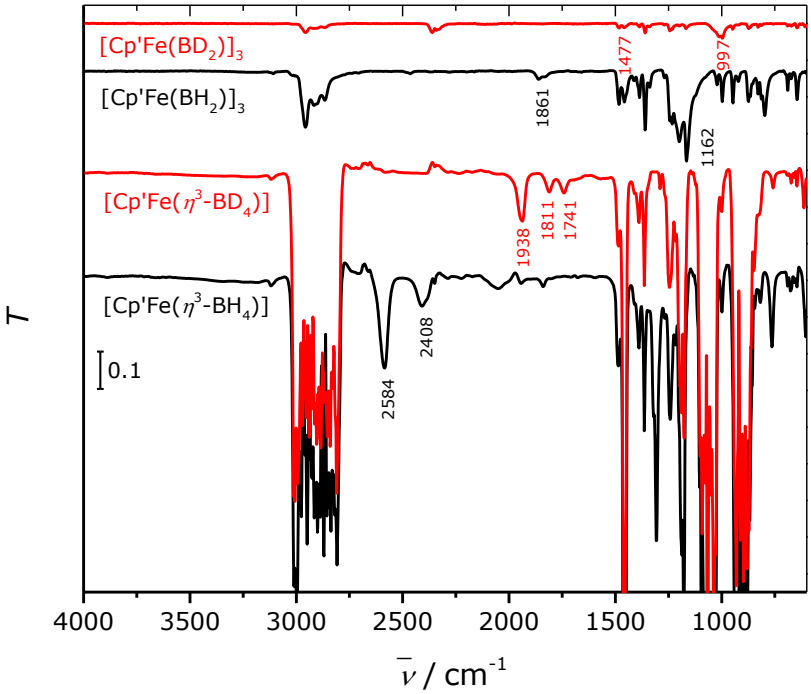

Figure 8. IR spectra of [Cp'Fe(η^3-BH_4)], [Cp'Fe(η^3-BD_4)], [Cp'Fe(BH_2)]$_3$ and [Cp'Fe(BD_2)]$_3$. The measurements for [Cp'Fe(BH_2)]$_3$ and [Cp'Fe(BD_2)]$_3$ were performed in ATR, while the spectra for [Cp'Fe(η^3-BH_4)] and [Cp'Fe(η^3-BD_4)] were recorded in tetrahydrofuran.

5.5 Conclusion

The reaction of [Cp'FeI]$_2$ and $NaBH_4$ yields the diamagnetic tetrahydridoborate iron complex [Cp'Fe(η^3-BH_4)] (**1**) as purple oil, which degrades slowly at ambient temperature to trimeric complex [Cp'Fe(BH_2)]$_3$ (**2**) and H_2. This degradation is irreversible and should be thermodynamically favorable. The molecular structure of complex **2** shows rather long B–B bonds and relating short Fe–B distances. The Mössbauer spectrum of complex **2** showed the low-spin iron(II) center. Deuterium labeling experiments were investigated. In IR spectra of deuterium labeled species, red shifts by isotopic substitution were observed, which corresponds Hooke's law.

5.6 Reference

(1) Lees, N. S.; McNaughton, R. L.; Gregory, W. V.; Holland, P. L.; Hoffman, B. M. *J. Am. Chem. Soc.* **2008**, *130*, 546–555.

(2) Holland, P. L. *Acc. Chem. Res.* **2008**, *41*, 905–914.

(3) Rodriguez, M. M.; Bill, E.; Brennessel, W. W.; Holland, P. L. *Science* **2011**, *334*, 780–783.

(4) Chiang, K. P.; Scarborough, C. C.; Horitani, M.; Lees, N. S.; Ding, K.; Dugan, T. R.; Brennessel, W. W.; Bill, E.; Hoffman, B. M.; Holland, P. L. *Angew. Chem. Int. Ed.* **2012**, *51*, 3658–3662.

(5) Daida, E. J.; Peters, J. C. *Inorg. Chem.* **2004**, *43*, 7474–7485.

(6) Brown, S. D.; Peters, J. C. *J. Am. Chem. Soc.* **2004**, *126*, 4538–4539.

(7) Walter, M. D.; Grunenberg, J.; White, P. S. *Chem. Sci.* **2011**, *2*, 2120–2130.

(8) Walter, M. D.; White, P. S. *Inorg. Chem.* **2012**, *51*, 11860–11872.

(9) Deck, K. J.; Fehlner, T. P.; Rheingold, A. L. *Inorg. Chem.* **1993**, *32*, 2794–2795.

(10) Fehlner, T. P. *Proc. Indian Natl. Sci. Acad.* **2002**, *68A*, 579–596.

(11) Peldo, M. A.; Beatty, A. M.; Fehlner, T. P. *Organometallics* **2003**, *22*, 3698–3702.

(12) Geetharani, K.; Kumar Bose, S.; Pramanik, G.; Kumar Saha, T.; Ramkumar, V.; Ghosh, S. *Eur. J. Inorg. Chem.* **2009**, *2009*, 1483–1487.

(13) Marks, T. J.; Kolb, J. R. *Chem. Rev.* **1977**, *77*, 263–293.

(14) Xu, Z.; Lin, Z. *Coord. Chem. Rev.* **1996**, *156*, 139–162.

(15) Ephritikhine, M. *Chem. Rev.* **1997**, *97*, 2193–2242.

(16) Schaeffer, G. W.; Roscoe, J. S.; Stewart, A. C. *J. Am. Chem. Soc.* **1956**, *78*, 729–733.

(17) Glavee, G. N.; Klabunde, K. J.; Sorensen, C. M.; Hadjipanayis, G. C. *Inorg. Chem.* **1995**, *34*, 28–35.

(18) Hillier, A. C.; Jacobsen, H.; Gusev, D.; Schmalle, H. W.; Berke, H. *Inorg. Chem.* **2001**, *40*, 6334–6337.

(19) Guilera, G.; Sean McGrady, G.; Steed, J. W.; Kaltsoyannis, N. *New J. Chem.* **2004**, *28*, 444–446.

(20) Ghilardi, C. A.; Innocenti, P.; Midollini, S.; Orlandini, A. *J. Chem. Soc., Dalton Trans.* **1985**, 605–609.

(21) Mehn, M. P.; Brown, S. D.; Paine, T. K.; Brennessel, W. W.; Cramer, C. J.; Peters, J. C.; Que, L. *Dalton Trans.* **2006**, 1347–1351.

(22) Fehlner, T. P. *Organometallics* **2000**, *19*, 2643–2651.

(23) Mancini, M.; Bougeard, P.; Burns, R. C.; Mlekuz, M.; Sayer, B. G.; Thompson, J. I. A.; McGlinchey, M. J. *Inorg. Chem.* **1984**, *23*, 1072–1078.

(24) Braunschweig, H.; Dewhurst, R. D. *Angew. Chem. Int. Ed.* **2013**, *52*, 3574–3583.

(25) Zhang, Y.; Majzoub, E.; Ozoliņš, V.; Wolverton, C. *J. Phys. Chem. C* **2012**, *116*, 10522–10528.

(26) Schulenberg, N.; Wadepohl, H.; Himmel, H.-J. *Angew. Chem. Int. Ed.* **2011**, *50*, 10444–10447.

(27) Goodreau, B. H.; Orlando, L. R.; Long, G. J.; Spencer, J. T. *Inorg. Chem.* **1996**, *35*, 6579–6585.

(28) Aldridge, S.; Calder, R. J.; Rossin, A.; Dickinson, A. a.; Willock, D. J.; Jones, C.; Evans, D. J.; Steed, J. W.; Light, M. E.; Coles, S. J.; Hursthouse, M. B. *J. Chem. Soc., Dalton Trans.* **2002**, 2020–2026.

(29) Makhaev, V. D. *Russ. Chem. Rev.* **2000**, *69*, 727–746.

Chapter 6. Attempted syntheses of heavy analogues of diaminocyclopropenylidenes

Abstract

The synthesis of diaminocyclopropenylidenes with heavy analogues of using bis(diehtylamino)-acetylene was attempted. From the reaction of bis(diethylamino)acetylene with $GeCl_2$·(dioxane), the tetra(diethylamino)cyclobutadiene dication (**1**) was obtained, which contains two molecules of $GeCl_3^-$ as anions. The tetra(*N*,*N*-diethylamino)cyclobutadiene monocation (**2**) was prepared using NEt_3·HBr as a starting material to the tetra(*N*,*N*-diethylamino)cyclobutadiene dication. The synthesis of Ge-analogue of a diphosphinocyclopropenylidene was also attempted and a germyl germylene (**3**) was yielded. All compounds were crystallographically analyzed.

6.1 Introduction

Carbens are molecules containing a neutral divalent carbon atom with six valence electrons and they can adopt either a singlet or a triplet state. In singlet carbenes, the carbene carbon atom is sp^2-hybridized and the unhybridized p-orbital remains empty. Thus, the singlet carbenes behave σ-donor and π-acceptor. In contrast, triplet carbenes satisfy Hund's rule and are considered as diradicals. Because of the electron sextett, carbenes are very reactive but can be stabilized by transition metals.

The *N*-heterocyclic (NHC) carbenes belong to the class of persistent carbenes, which are based on the imidazol-2-ylidenes. The imidazol-2-ylidene with adamantyl group is the first "bottleable" and crystallographically characterized carbene. Not only the steric bulky adamantyl group allowed its isolation, but also its electronic features, so that the π donation to the carbene carbon atom and the cyclic conjugated system contribute also to stabilize this compound. Moreover, the energy difference between singlet and triplet states is large (336 kJ mol^{-1}) and the NHC carbenes are more stable in the singlet state than in the triplet state.[1]

If the carbon atom in the NHC is changed by another main group atom, the resulting compounds can be referred as heavy analogues of imidazol-2-ylidenes. Figure 1 shows the heavy analogues that have been already synthesized.[2–9]

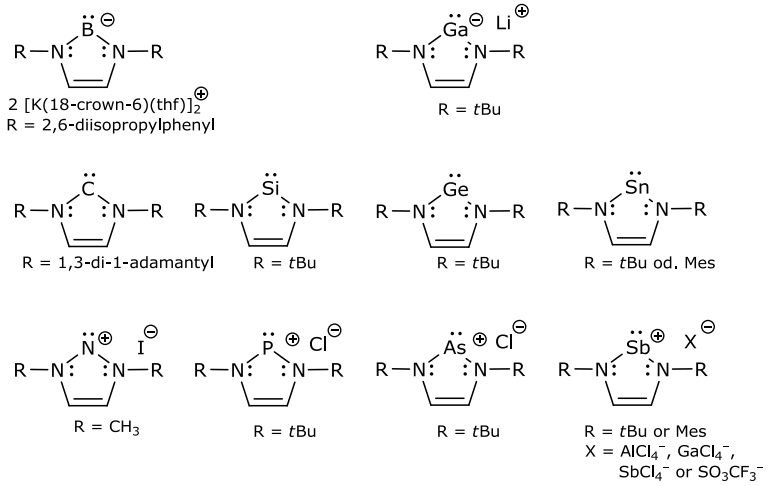

Figure 1. The heavy analogues of imidazol-2-ylidenes.

One type of structural isomers of imidazol-2-ylidenes are the diamino- cyclopropenylidene (Figure 2). This can also be represented as $C_3N_2R_4$ and considered as $2e^-$ aromatic compounds.

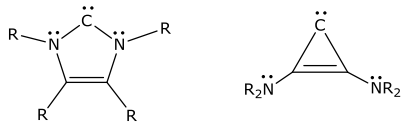

Figure 2. Imidazol-2-ylidene and diaminocyclopropenylidene.

Since the syntheses of the heavy analogues of the imidazol-2-ylidenes were successful, the synthesizability of the heavy analogues of diaminocyclopropenylidenes was theoretically investigated. The three membered rings have a higher energy than the five membered ring due to the ring strain. Furthermore, reduced π conjugation and aromaticity in Si- and Ge-analogues destabilize those. However, theoretical studies showed that the synthesis of heavy analogues of diaminocyclopropenylidenes is theoretically feasible.[10] A β-diketoiminato ligand-supported germylene was successfully synthesized.[11]

In this chapter, the synthesis of diaminocyclopropenylidenes with heavy analogues using bis(*N*,*N*-diethylamino)acetylene was attempted.

6.2 Synthesis of tetra(*N*,*N*-diethylamino)cyclobutadiene dication

In an attempt to synthesize a diaminocyclopropen-2-germylene, bis(*N*,*N*-diethylamino)acetylene was added into a toluene solution of $GeCl_2$·(dioxane) and the solvent was evaporated slowly at ambient temperature. From this solution, however, only small amounts of a cyclobutadiene dication (**1**) were obtained as yellow prisms containing two $GeCl_3^-$ as counter anions. Compound **1** crystallized with imposed inversion symmetry in the monoclinic space group *C*2/*c*. The ORTEP diagram of compound **1** is shown in Figure 3.

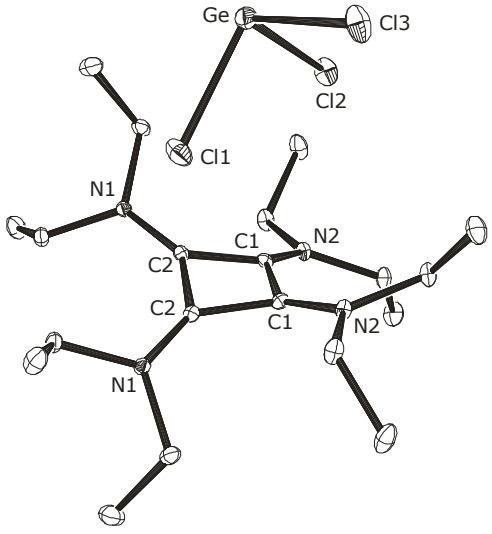

Figure 3. ORTEP diagram of compound **1**. Thermal ellipsoids are given at the 30% probability level. Hydrogen atoms and one of the $GeCl_3^-$ anions are omitted for clarity. Selected bond lengths [Å] and angles[°]: C1–C2 1.4451(16), C1–C1′ 1.478(2), C2–C2′ 1.448(2), C1–N2 1.3301(14), C2–N1 1.3057(14), C1′–C1–C2 88.28(6), C1–C2–C2′ 89.45(6), C1′–C1–C2–C2′ 15.90(12).

Compound **1** adopts a puckered conformation. All of C–C bonds of the ring have similar

bond lengths (av. 1.457(2) Å), suggesting that the electrons are delocalized over the ring. The average C–N distance is 1.3179(14) Å, which is typical for those connecting to a conjugated system. According to the previously published tetra(*N*,*N*-dimethylamino) derivative,[12] the positive charges are expected to be delocalized in the substituents according to ^{1}H NMR spectroscopy as shown in Figure 4, although neither ^{13}C NMR spectroscopy nor single crystal structure analysis was reported.

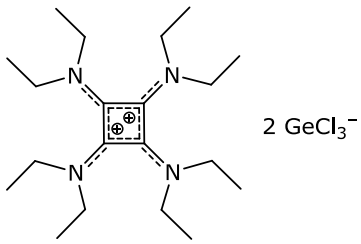

Figure 4. Lewis structure of the tetra(*N*,*N*-diethylamino)cyclobutadiene dication (**1**).

The cyclobutadiene dications or dianions belong to the theoretically smallest Hückel aromatic molecules with n = 0 or n = 1 (Figure 5).

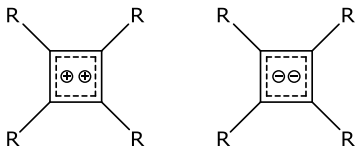

Figure 5. Cyclobutadiene dications (left) and dianions (right).

However, the stability predicted by the Hückel low (4n + 2) may not be applicable to highly charged small ring systems, since the Coulombic repulsion contributes much more than the Hückel aromaticity.[13] Furthermore, recent Hückel calculations predict that the cyclobutadiene dications and dianions are nonaromatic.[14] Removal or addition of two electrons from or to the cyclobutadiene leads to two very different structures, both of which minimize an overlap of their potential π systems.[15] Although the substituents, which donate π electrons to the ring, may change the preferred conformation,[16] the puckered form is preferred over the planar form[15–19] because part of the destabilizing repulsive orbital interactions of C1 and C3 atoms may be relieved through puckering (Figure 6).[17,18]

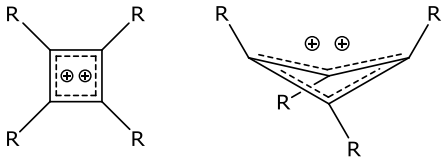

Figure 6. Cyclobutadiene dication in the planar form (left) and in the puckered form (right).

Several cyclobutadiene dianions were synthesized by [2+2] cycloaddition, but they only isolated in the state when coordinated to a metal.[20–23] In contrast to them, cyclobutadiene dications have been mainly predicted by calculations, since their syntheses are difficult. Especially, the cyclobutadiene dications without any substituents ($C_4H_4^{2+}$) have not been successfully isolated, but several di-[24] and tetrasubstituted[25,26] derivatives have been synthesized and characterized. In addition, some neutral tetrasubstituted cyclobutadienes are crystallographically characterized,[27,28] which adopted a planar conformations in contrast to the dications, and the electrons delocalize over the ring to the adjacent nitrogen atoms.

6.3 Synthesis of tetra(*N*,*N*-diethylamino)cyclobutadiene monocation

The synthesis of tetra(*N*,*N*-diethylamino)cyclobutadiene dication *via* the cyclobutadiene monocation (**2**), *i.e.* the proton-adduct of *c*-$C_4(NEt_2)_4$, was carried out according to the previous report of Viehe *et al.*,[12] since the desired product was obtained in only 2% yield *via* the synthesis using $GeCl_2$·(dioxane). The cyclobutadiene monocation was obtained in 70% yield as colorless powder. The single crystal of compound **2** was grown from concentrated ethtyl acetate solution in the monoclinic space group $P2_1/c$ with two independent molecules in the crystal lattice. The following discussion focuses on the molecule shown in Figure 7.

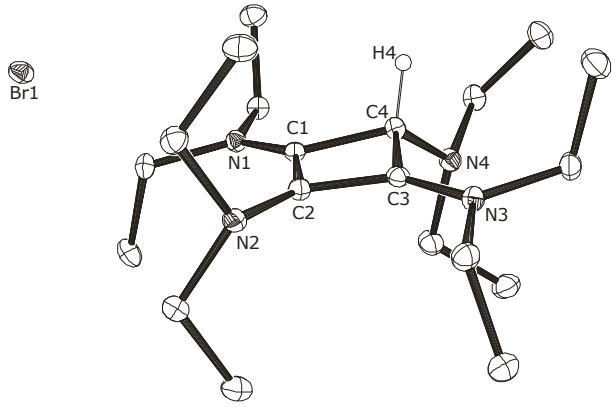

Figure 7. ORTEP diagram of compound **2**. Thermal ellipsoids are given at the 30% probability level. Hydrogen atoms in the ethyl groups are omitted for clarity. Selected bond lengths [Å] and angles [°]:C1–C2 1.421(2), C2–C3 1.412(2), C3–C4 1.537(2), C4–C1 1.5549(19), C21–C22 1.420(2), C22–C23 1.409(2), C23–C24 1.539(2), C24–C21 1.5512(19), C1–N1 1.312(2), C2–N2 1.4150(19), C3–N3 1.312(2), C4–N4 1.4352(19), C21–N5 1.3088(19), C22–N6 1.4105(19), C23–N7 1.311(2), C24–N8 1.4339(19), C4–C1–C2 92.49(12), C1–C2–C3 91.48(12), C2–C3–C4 93.64(12), C3–C4–C1 82.03(11), C24–C21–C22 92.60(12), C21–C22–C23 91.58(12), C22–C23–C24 93.52(12), C23–C24–C21 81.99(11), C1–C2–C3–C4 4.69(12), C21–C22–C23–C24 4.40(12).

Compound **2** adopts a rather flat conformation with average torsion angle of 4.55°. The bond lengths of C1–C2 (1.421(2) Å) and C2–C3 (1.412(2) Å) are much shorter than those of C3–C4 (1.537(2) Å) and C4–C1 (1.5549(19) Å). The Bond lengths of C1–N1 and C3–N3 (1.312(2) Å) are very different from the bond lengths of C2–N2 (1.4150(19) Å) and C4–N4 (1.4352(19) Å). That suggests a π conjugation between the N1–C1–C2–C3–N3 atoms, and a delocalization of the positive charge over them as illustrated in Figure 8. In agreement with this, the N1 and N3 atoms are in equatorial positions, they are nearly coplanar and can this conjugate with the C1–C2–C3 moiety, while the N2 and N4 atoms are in axial positions with respect to the ring.

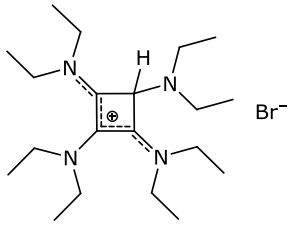

Figure 8. Lewis structure of tetra(*N*,*N*-diethylamino)cyclobutadiene monocation (**2**).

The signals for the C atoms of the cyclobutadiene ring in the ^{13}C NMR spectrum appear at 173.5 ppm for C1 and C3, 115.5 ppm for the C2 and 66.3 ppm for C4, which supports the charge is delocalization. In a fluoro-adduct of the *c*-C_4Me_4 and a bromo-adduct of the *c*-C_4Ph_4 monocations, a similar trend, *e.g.* electron distribution over C1–C3, was observed.[24]

6.4 Attempted synthesis of diphosphinocyclopropenylidene with germanium

Bis(dialkylphosphino)acetylene can also be considered as a heavy analogue of diaminoacetylene and act as a bifunctional ligand. Its coordination chemistry to transition metals has been explored widely,[29–37] however, the coordination behavior to a p-element has not been investigated yet.

In order to synthesize the Ge-analogue of a diphosphinocyclopropenylidene, Bis(diphenylphosphino)acetylene was added into a toluene solution of $GeCl_2$(dioxane) and the solvent was evaporated slowly at ambient temperature. Instead of the desired compound, the germyl germylene complex (**3**) was crystallized as yellow prisms with imposed inversion symmetry in the triclinic space group $P\bar{1}$ from a saturated toluene solution. ORTEP diagram of this compound is shown in Figure 9.

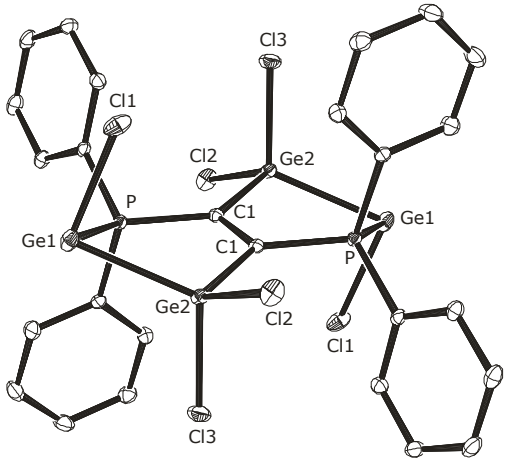

Figure 9. ORTEP diagram of compound **3**. Thermal ellipsoids are given at the 30% probability level. Hydrogen atoms are omitted for clarity. Selected bond lengths [Å]: C1–C1' 1.341(4), C1–P 1.825(2), P–Ge1 2.4605(6), Ge1–Ge2 2.5124(5), Ge2–C1' 2.006(2), Ge1–Cl1 2.2855(7), Ge2–Cl2 2.1537(6), Ge2–Cl3 2.1712(6).

In the solid state, a five membered ring was formed by two carbon atoms, one phosphorous atom and two germanium atoms and the two rings are condensed at the C–C bond, whose length of 1.341(4) Å is typical for a C–C double bond. The bond lengths of C–P and C–Ge bonds are 1.825(2) Å and 2.006(2) Å, respectively, indicating a covalent bond character. The Ge–P bond with a length of 2.4605(6) Å is consistent with a Ge–P coordination bond length reported previously.[38–48] The Ge–Ge distance is 2.5124(5) Å, suggesting a weak interaction. A covalent Ge–Ge bond usually has a bond length of *ca.* 2.4 Å[49–54] and the typical bond length for Ge=Ge bond is *ca.* 2.2 Å.[55–58]

Apparently, these two germanium atoms have different oxidation states. The fact that the bond length of Ge1–Cl1 (2.2855(7) Å) is slightly longer than those of Ge2–Cl2 and Ge2–Cl3 (av. 2.1625(6) Å) supports this inference. Hence, the Ge–Ge bond might have a donor-acceptor-character. Five-membered ring structures with germanium atoms in different oxidation states are known (2.458(1) Å,[41] 2.497(2) Å and 2.536(2) Å[47]), however, condensed ring structures such as that of compound **3** are not found in the literature.

Compound **3** was also characterized by NMR spectroscopy. While the ^{13}C NMR spectrum exhibits the signal for the double bond at 106.5 ppm, a signal was found at 31.4 ppm in the ^{31}P NMR spectrum accounts for the phosphorus atoms. The phosphorus signal in the similar motif appears at 8.1 ppm in CD_2Cl_2,[48] in which the phosphorus atom connects to a carbon atom, has two phenyl groups and forms a coordinative bond to the germanium atom (Figure 10).

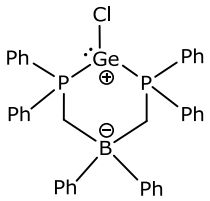

Figure 10. Zwitterionic complex [GeCl(Ph_2PCH_2)$_2$BPh_2].

6.5 Conclusion

The synthesis of diaminocyclopropenylidenes with heavy analogues using diaminoacetylene was attempted. From the reaction of bis(*N*,*N*-diethyl- amino)acetylene with $GeCl_2$·(dioxane), the tetra(*N*,*N*-diethylamino)cyclobutadiene dication (**1**) was obtained, which contains two molecules of $GeCl_3^-$ as anions. The solid state molecular structure of compound **1** adopts a puckered conformation as predicted elsewhere.[15–19] The tetra(*N*,*N*-diethylamino)cyclobutadiene monocation (**2**) was prepared using NEt_3·HBr. In contrast to compound **1**. The molecular structure of compound **2** adopts rather a flat conformation and suggests a π conjugation between the N1–C1–C2–C3–N3 atoms and a delocalization of the positive charge over them. The synthesis of Ge-analogue of a diphosphinocyclopropenylidene was also attempted and a germyl germylene (**3**) was yielded, in whose solid state structure a five membered ring was formed by two carbon atoms, one phosphorus atom and two germanium atoms, two rings are condensed at the C=C bond and the phosphorus atom forms a coordinative bond to the germanium atom.

6.6 References

(1) Arduengo, A. J.; Harlow, R. L.; Kline, M. *J. Am. Chem. Soc.* **1991**, *113*, 361–363.

(2) Segawa, Y.; Yamashita, M.; Nozaki, K. *Science* **2006**, *314*, 113–115.

(3) Schmidt, E. S.; Jockisch, A.; Schmidbaur, H. *J. Am. Chem. Soc.* **1999**, *121*, 9758–9759.

(4) Denk, M.; Lennon, R.; Hayashi, R.; West, R.; Belyakov, A. V.; Verne, H. P.; Haaland, A.; Wagner, M.; Metzler, N. *J. Am. Chem. Soc.* **1994**, *116*, 2691–2692.

(5) Herrmann, W. a.; Denk, M.; Behm, J.; Scherer, W.; Klingan, F.-R.; Bock, H.; Solouki, B.; Wagner, M. *Angew. Chem. Int. Ed. Engl.* **1992**, *31*, 1485–1488.

(6) Gans-Eichler, T.; Gudat, D.; Nieger, M. *Angew. Chem. Int. Ed.* **2002**, *41*, 1888–1891.

(7) Boche, G.; Andrews, P.; Harms, K.; Marsch, M.; Rangappa, K. S.; Schimeczek, M.; Willeke, C. *J. Am. Chem. Soc.* **1996**, *118*, 4925–4930.

(8) Carmalt, C. J.; Lomeli, V. *Chem. Commun.* **1997**, 2095–2096.

(9) Gudat, D.; Gans-Eichler, T.; Nieger, M. *Chem. Commun.* **2004**, 2434–2435.

(10) Pintér, B.; Veszprémi, T. *Organometallics* **2008**, *27*, 5571–5576.

(11) Jana, A.; Nekoueishahraki, B.; Roesky, H. W.; Schulzke, C. *Organometallics* **2009**, *28*, 3763–3766.

(12) Bouvy, A.; Janousek, Z.; Viehe, H. G. *Synthesis* **1983**, 718–720.

(13) Clark, T.; Wilhelm, D.; Schleyer, P. v. R. *Tetrahedron Lett.* **1982**, *23*, 3547–3550.

(14) Hess, B. A.; Schaad, L. J. *Pure Appl. Chem.* **1980**, *52*, 1471–1494.

(15) Hess, B. A.; Ewig, C. S.; Schaad, L. J. *J. Org. Chem.* **1985**, *50*, 5869–5871.

(16) Bremer, M.; Schleyer, P. v. R.; Fleischer, U. *J. Am. Chem. Soc.* **1989**, *111*, 1147–1148.

(17) Krogh-Jespersen, K.; Schleyer, P. v. R.; Pople, J. A.; Cremer, D. *J. Am. Chem. Soc.* **1978**, *100*, 4301–4302.

(18) Krogh-Jespersen, K.; Cremer, D.; Dill, J. D.; Pople, J. A.; Schleyer, P. v. R. *J. Am. Chem. Soc.* **1981**, *103*, 2589–2594.

(19) Chandrasekhar, J.; Schleyer, P. v. R.; Krogh-Jespersen, K. *J. Comput. Chem.* **1981**, *2*, 356–360.

(20) Matsuo, T.; Sekiguchi, A. *Bull. Chem. Soc. Jpn.* **2004**, *77*, 211–226.

(21) Sekiguchi, A.; Matsuo, T.; Tanaka, M.; Watanabe, H.; Nakamoto, M. *Russ. Chem. Bull.* **2004**, *53*, 1109–1115.

(22) Takanashi, K.; Inatomi, A.; Lee, V. Y.; Nakamoto, M.; Ichinohe, M.; Sekiguchi, A. *Eur. J. Inorg. Chem.* **2008**, 1752–1755.

(23) Kottas, G. S.; Brotin, T.; Schwab, P. F. H.; Gala, K.; Havlas, Z.; Kirby, J. P.; Miller, J. R.; Michl, J. *Organometallics* **2014**, in Press.

(24) Olah, G. a.; Staral, J. S. *J. Am. Chem. Soc.* **1976**, *98*, 6290–6304.

(25) Olah, G. A.; Bollinger, J. M.; White, A. M. *J. Am. Chem. Soc.* **1969**, *91*, 3667–3669.

(26) Olah, G. A.; Mateescu, G. D. *J. Am. Chem. Soc.* **1970**, *92*, 1430–1432.

(27) Knunyants, I. L.; Struchkov, Y. T.; Bargamova, M. D.; Espenbetov, A. A. *Bull. Acad. Sci. USSR Div. Chem. Sci.* **1985**, *34*, 1001–1005.

(28) Köhler, K.; Massa, W.; Offermann, G.; Seitz, G.; Sutrisno, R. *Chem. Ber.* **1985**, *118*, 1903–1916.

(29) Carty, A. J.; Efraty, A.; Ng, T. W.; Birchall, T. *Inorg. Chem.* **1970**, *9*, 1263–1268.

(30) Daran, J.-C.; Cabrera, E.; Bruce, M. I.; Williams, M. L. *J. Organomet. Chem.* **1987**, *319*, 239–246.

(31) Nickel, T. M.; Yau, S. Y. W.; Went, M. J. *J. Chem. Soc., Chem. Commun.* **1989**, 775–776.

(32) Powell, A. K.; Went, M. J. *J. Chem. Soc., Dalton Trans.* **1992**, 439–445.

(33) Hong, F.-E.; Chang, R.-E.; Chen, S.-C.; Ko, B.-T. *Organometallics* **2002**, *21*, 961–967.

(34) Arnanz, A.; Marcos, M.-L.; Moreno, C.; Farrar, D. H.; Lough, A. J.; Yu, J. O.; Delgado, S.; González-Velasco, J. *J. Organomet. Chem.* **2004**, *689*, 3218–3231.

(35) Sevillano, P.; Koenig, S.; Himmel, D.; Fuhr, O.; Fenske, D. *Z. Anorg. Allg. Chem.* **2005**, *631*, 2236–2240.

(36) Garon, C. N.; McIsaac, D. I.; Vogels, C. M.; Decken, A.; Williams, I. D.; Kleeberg, C.; Marder, T. B.; Westcott, S. a *Dalton Trans.* **2009**, 1624–1631.

(37) Haehnel, M.; Hansen, S.; Schubert, K.; Arndt, P.; Spannenberg, A.; Jiao, H.; Rosenthal, U. *J. Am. Chem. Soc.* **2013**, *135*, 17556–17565.

(38) Bruncks, N.; du Mont, W.-W.; Pickardt, J.; Rudolph, G. *Chem. Ber.* **1981**, *114*, 3572–3580.

(39) Karsch, H. H.; Deubelly, B.; Riede, J.; Müller, G. *Angew. Chem. Int. Ed. Engl.* **1987**, *26*, 673–674.

(40) Andrianarison, M.; Couret, C.; Declercq, J.; Dubourg, A.; Escudie, J.; Satge, J. *J. Chem. Soc., Chem. Commun.* **1987**, 921–923.

(41) Karsch, H. H.; Hofmann, J.; Müller, G. *J. Chem. Soc., Chem. Commun.* **1988**, 516–517.

(42) Druckenbrodt, C.; du Mont, W.-W.; Ruthe, F.; Jones, P. G. *Z. Anorg. Allg. Chem.* **1998**, *624*, 590–594.

(43) Fedotova, Y. V.; Kornev, A. N.; Sushev, V. V.; Kursky, Y. A.; Mushtina, T. G.; Makarenko, N. P.; Fukin, G. K.; Abakumov, G. A.; Zakharov, L. N.; Rheingold, A. L. *J. Organomet. Chem.* **2004**, *689*, 3060–3074.

(44) Reddy, N. D.; Jana, A.; Roesky, H. W.; Samuel, P. P.; Schulzke, C. *Dalton Trans.* **2010**, *39*, 234–238.

(45) Arii, H.; Nakadate, F.; Mochida, K.; Kawashima, T. *Organometallics* **2011**, *30*, 4471–4474.

(46) West, J. K.; Stahl, L. *Organometallics* **2012**, *31*, 2042–2052.

(47) Hlina, J.; Baumgartner, J.; Marschner, C.; Albers, L.; Müller, T. *Organometallics* **2013**, *32*, 3404–3410.

(48) Weicker, S. a.; Dube, J. W.; Ragogna, P. J. *Organometallics* **2013**, *32*, 6681–6689.

(49) Espenbetov, A. A.; Struchkov, Y. T.; Kolesnikov, S. P.; Nefedov, O. M. *J. Organomet. Chem.* **1984**, *275*, 33–37.

(50) Häberle, K.; Dräger, M. *Z. Naturforsch.* **1987**, *42b*, 323–329.

(51) Mallela, S. P.; Geanangel, R. A. *Inorg. Chem.* **1991**, *30*, 1480–1482.

(52) Renner, G.; Kircher, P.; Huttner, G.; Rutsch, P.; Heinze, K. *Eur. J. Inorg. Chem.* **2000**, 879–887.

(53) Lerner, H.-W.; Schödel, F.; Sänger, I.; Wagner, M.; Bolte, M. *Z. Naturforsch.* **2004**, *59b*, 277–280.

(54) Lee, V. Y.; Yasuda, H.; Ichinohe, M.; Sekiguchi, A. *J. Organomet. Chem.* **2007**, *692*, 10–19.

(55) Hitchcock, P. B.; Lappert, M. F.; Miles, S. J.; Thorne, A. J. *J. Chem. Soc., Chem. Commun.* **1984**, *347*, 480–482.

(56) Snow, J. T.; Murakami, S.; Masamune, S.; Williams, D. J. *Tetrahedron Lett.* **1984**, *25*, 4191–4194.

(57) Tokitoh, N.; Kishikawa, K.; Okazaki, R.; Sasamori, T.; Nakata, N.; Takeda, N. *Polyhedron* **2002**, *21*, 563–577.

(58) Hurni, K. L.; Rupar, P. a.; Payne, N. C.; Baines, K. M. *Organometallics* **2007**, *26*, 5569–5575.

Ce n'est point dans l'objet que réside le sens des choses, mais dans la démarche.
<Citadelle>
– Antoine de Saint-Exupéry (1900 – 1944)

Chapter 7. Summary

In this dissertation, the coordination chemistry of bulky alkyl substituted indenyl and cyclopentadienyl ligand with manganese, iron and cobalt was investigated.

The sterically demanding 1,3-disubstituted indenyl ligands, 1,3-$(Me_3C)_2C_9H_5$ ($^{2t\mathrm{Bu}}$Ind) and 1,3-$(c\text{-}C_6H_{11})_2C_9H_5$ ($^{2\mathrm{Cy}}$Ind), have been synthesized and employed to prepare a series of bis(indenyl)manganese, iron and cobalt complexes (Scheme 1).

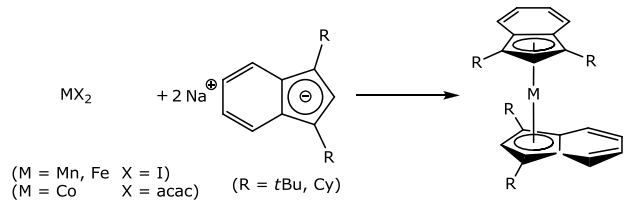

Scheme 1. Synthesis of bulky alkyl substituted indenyl complexes with Mn, Fe and Co.

In the case of iron, indenyl ligand $^{2t\mathrm{Bu}}$Ind stabilizes an iron half-sandwich species at low temperature, which has been confirmed by suitable trapping experiments (Scheme 2).

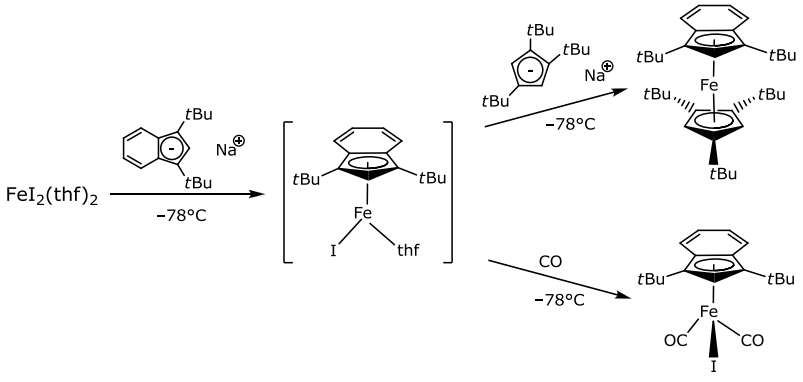

Scheme 2. Trapping experiment of [$^{t\mathrm{Bu}}$IndFeI] half-sandwich species with Cp'Na and CO.

In addition, although $^{2t\mathrm{Bu}}$Ind exhibits similar electronic and steric properties to those of

1,2,4-tri-*tert*-butylcyclopentadienyl (Cp'), the reduced stability of the half-sandwich complex can be attributed to weak metal–carbon bonds in the metal indenyl compounds. The bis(indenyl)manganocenes, [$^{2t\mathrm{Bu}}$Ind$_2$Mn] and [$^{2\mathrm{Cy}}$Ind$_2$Mn], contain high-spin d^5 manganese(II) centers as established by solid state magnetic susceptibility studies, and no spin-cross-over behavior has been observed. Electrochemical studies on [$^{2t\mathrm{Bu}}$Ind$_2$Co] show two reversible redox-processes which suggest that [$^{2t\mathrm{Bu}}$Ind$_2$Co] can be chemically reduced and might offer an interesting entry into the low-valent cobalt half-sandwich chemistry.

A series of halide-bridged Cp'Co half-sandwich complexes [Cp'CoCl]$_2$, [Cp'CoBr]$_2$ and [Cp'CoI]$_2$ were synthesized (Scheme 3) and characterized.

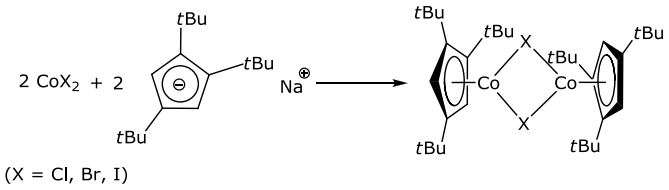

Scheme 3. Synthesis of haliede-bridged Cp'Co half-sandwich complexes (X = Cl, Br, I).

The synthesis of [Cp'CoH]$_2$ from [Cp'CoI]$_2$ was also attempted. Using KHBEt$_3$ as a hydride source, [Cp'CoH]$_2$ was obtained, while the reaction of [Cp'CoI]$_2$ and MeLi yielded methylidyne bridged complex [(Cp'Co)$_2$(μ-CH)(μ-H)].

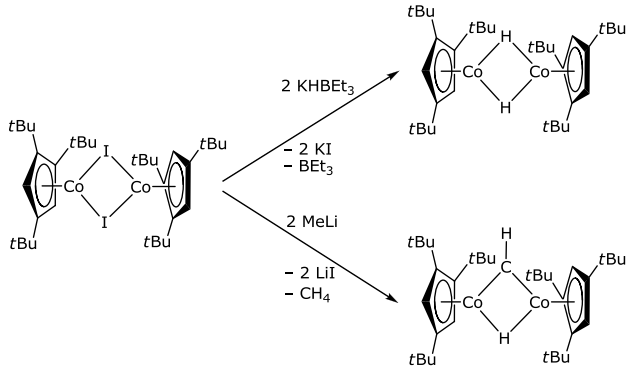

Scheme 4. Reaction of [Cp'CoI]$_2$ with KHBEt$_3$ and MeLi.

Reactions of [Cp'FeI]$_2$ and [Cp'MnI(thf)]$_2$ with pseudohalides were investigated and a series of nitrido-, sulfido-, cyanato-, diselenido- and thiocyanato-bridged iron and manganese complexes [Cp'Fe(NCO)]$_2$, [Cp'Mn(NCS)(thf)]$_2$, [Cp'FeN]$_2$, [Cp'FeS]$_2$ and [Cp'Fe(Se$_2$)]$_2$ were

formed. The pseudohalides either coordinate to the metal centers without participating in a redox reaction, they coordinate in an end-on fashion with splitting of small molecules or coordinate after further reaction (Scheme 5).

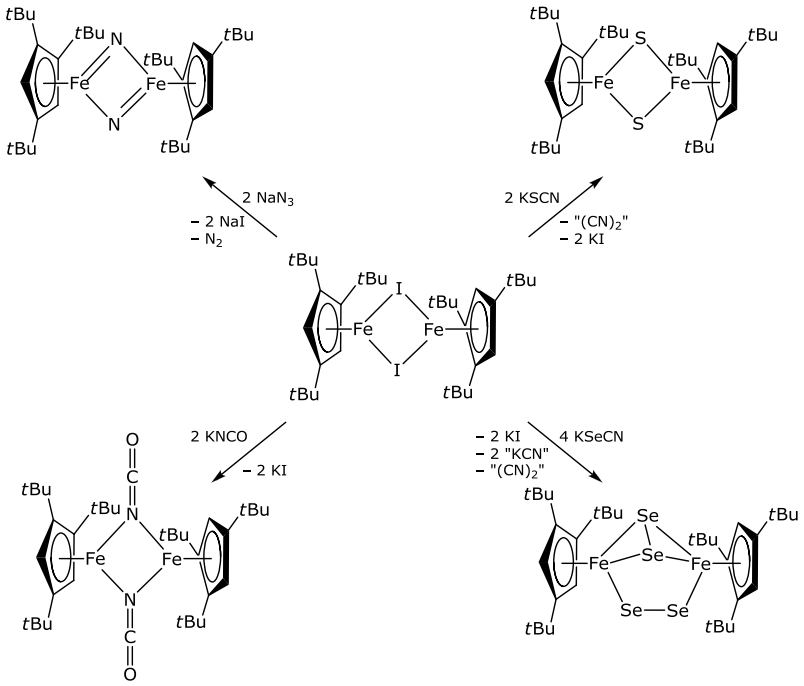

Scheme 5. Reaction of $[Cp'FeI]_2$ toward pseudohalides.

In SQUID magnetometry, $[Cp'FeN]_2$ and $[Cp'FeS]_2$ exhibit a very strong antiferromagnetic coupling whereas $[Cp'FeI]_2$ and $[Cp'Fe(NCO)]_2$ show a weak antiferromagnetic coupling, but no spin-crossover. The Mössbauer spectroscopy was also carried out for the iron complexes. $[Cp'FeI]_2$ and $[Cp'Fe(NCO)]_2$ contain Fe(II) atoms, $[Cp'FeS]_2$ and $[Cp'Fe(Se_2)]_2$ Fe(III) atoms and $[Cp'FeN]_2$ Fe(IV) atom. All complexes contain only one type of iron atoms in the same electronic environment.

The reaction of $[Cp'FeI]_2$ and $NaBH_4$ yields the diamagnetic tetrahydrideborate iron complex $[Cp'Fe(\eta^3\text{-}BH_4)]$ as purple oil, which degrades slowly at ambient temperature to trimeric complex $[Cp'Fe(BH_2)]_3$ and H_2 (Scheme 6).

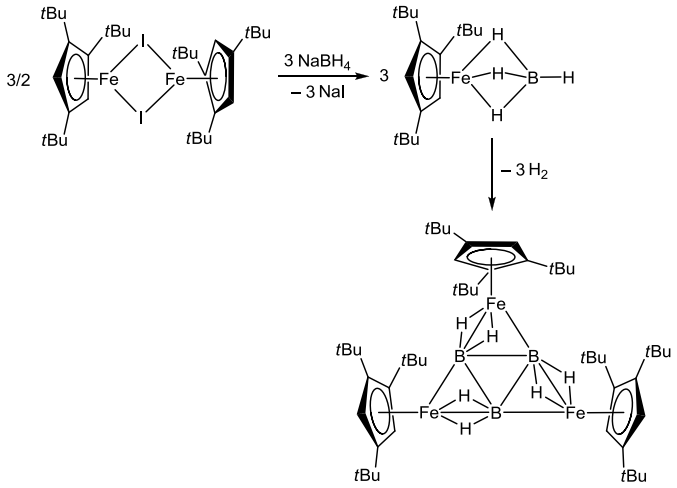

Scheme 6. Synthesis of [Cp'Fe(η^3-BH_4)] and its trimerization to [Cp'Fe(BH_2)]$_3$.

The Mössbauer spectrum of complex [Cp'Fe(BH_2)]$_3$ showed the low-spin iron(II) center. Deuterium labeling experiments were investigated. In IR spectra of deuterium labeled species, red shifts by isotopic substitution were observed, which corresponds Hooke's law.

The synthesis of diaminocyclopropenylidenes with heavy analogues using bis(*N*,*N*-diethylamino)acetylene was attempted. From the reaction of bis(*N*,*N*-diethylamino)acetylene with $GeCl_2$·(dioxane), the tetra(*N*,*N*-diethylamino)cyclobutadiene dication was obtained, which contains two molecules of $GeCl_3^-$ as anions (Scheme 7). The solid state molecular structure of tetra(*N*,*N*-diethylamino)cyclobutadiene dication adopts a puckered conformation.

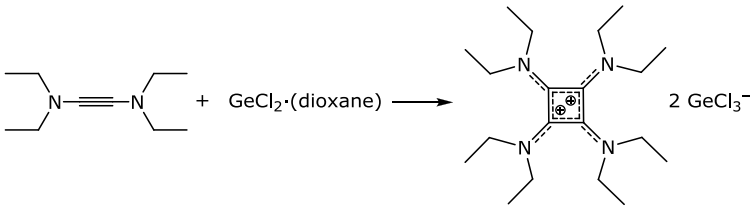

Scheme 7. Formation of tetra(*N*,*N*-diethylamino)cyclobutadiene dication.

The tetra(*N*,*N*-diethylamino)cyclobutadiene monocation was prepared using NEt_3·HBr (Scheme 8). In contrast to tetra(*N*,*N*-diethylamino)cyclobutadiene dication, the solid state molecular structure of tetra(*N*,*N*-diethylamino)cyclobutadiene monocation adopts rather a flat conformation and suggests a π conjugation between the N1–C1–C2–C3–N3 atoms and a delocalization of the positive charge over them.

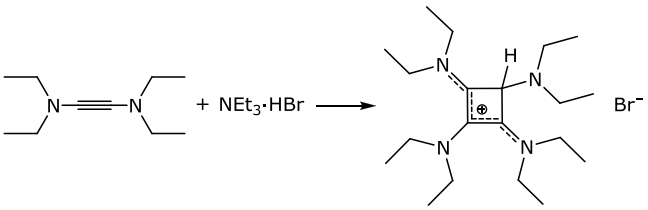

Scheme 8. Synthesis of tetra(*N,N*-diethylamino)cyclobutadiene monocation.

The synthesis of Ge-analogue of a diphosphinocyclopropenylidene was also attempted and a germyl germylene was yielded (Scheme 9), in whose solid state structure a five membered ring was formed by two carbon atoms, one phosphorus atom and two germanium atoms, two rings are condensed at the C=C bond and the phosphorus atom forms a coordinative bond to the germanium atom.

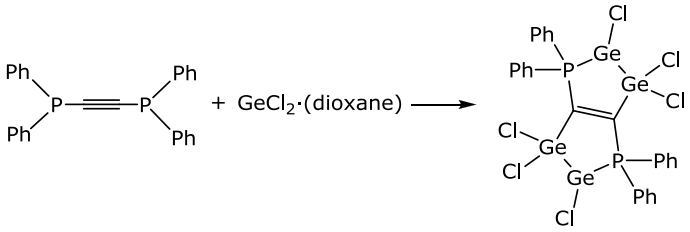

Scheme 9. Formation of the germyl germylene.

Il semble que la perfection soit atteinte non quand il n'y a plus rien à ajouter,
mais quand il n'y a plus rien à retrancher.
<Terre des hommes>
– Antoine de Saint-Exupéry (1900 – 1944)

Chapter 8. Experimental section

General procedures

All operations were performed in a glovesbox (MBraun 200B or MBraun UNIlab, argon or nitrogen atmosphere) or in an atmosphere of dry argon or nitrogen using Schlenk techniques.

^{1}H, $^{13}C\{^{1}H\}$, ^{11}B, $^{11}B\{^{1}H\}$, $^{31}P\{H\}$ and ^{77}Se NMR measurements were performed on Bruker DPX200, Bruker AV300, Bruker DRX 400 and Bruker AV600 spectrometer using tetramethylsilane (for ^{1}H and ^{13}C) as internal standards or $BF_3{\cdot}Et_2O$ (for ^{11}B), H_3PO_4 (for ^{31}P) and Me_2Se (for ^{77}Se) as an external standard. Splitting patterns are indicated as s (singlet), d (doublet), t (triplet), q (quartet), m (multiplet) and br (broad).

Elemental analysis (C, H, N) by combustion and gas chromatography was carried out using an Elementar varioMICRO.

GC analysis was performed on a SHIMADZU GC-2010 using a 30.0-m SGE forte BP5 column (5% phenyl / 95% dimethyl polysiloxane) with FI detection. The temperature program: Initial temperature: 50°C (hold time: 3.0 min), end temperature: 300°C (hold time 5.0 min), equilibration time: 1.0 min and heating rate: 10.0 °C min^{-1}.

GC-MS was carried out on a JOEL AccuTOF, and MS on Thermofinnigan MAT 95 XL (EI), ThermoFischer Scientific LTQ-Orbitrap Velos (ESI) or JEOL JMS-T100GC AccTOF GC (LIFDI) device.

A Bruker Vertex 70 spectrometer was used for recording IR spectra. Absorption patterns are indicated as s (strong), m (medium), w (weak), and sh (shoulder).

UV-vis spectra were collected by Varian Cary 50 Scan. A shoulder is indicated as sh.

Cyclic voltammograms were recorded on a Metrohm μAutolab Type III or Versa Stat II (EG&G Instruments) potentiostat/galvanostat in a dichloromethane or THF solution containing 0.1 M $[n Bu_4N][PF_6]$ as supporting electrolyte. 99.995% gold wire (ϕ 0.5 mm,

Chempur), 99.9% platinum wire (ϕ 0.6 mm, Chempur), or glassy carbon disk (ϕ 2 mm, Metrohm) was used as working and/or counter electrode, respectively, and the potentials were measured against an Ag/AgCl reference electrode (saturated LiCl in EtOH) or 99.9% silver wire (ϕ 1.0 mm, Chempur). The Fc^+/Fe couple displays a reversible cyclic voltammetric trace with a redox potential $E^\circ = +0.46$ V (in dichloromethane) or $E^\circ = +0.56$ V (in THF)[1] under these conditions.

The single crystal X-ray diffraction analyses were measured on XCalibur NovaA and XCalibur EOS from Oxford Diffraction and SMART 1000 CCD from Bruker devices at 100 K. Magnetic susceptibility measurements were carried out in a sealed quartz tube or within a polycarbonate gel capsule on a on a Quantum Design MPMS magnetometer. The program julX written by E. Bill[2] was used for the simulation and analysis of magnetic susceptibility data.

^{57}Fe Mössbauer spectra were recorded on a WissEl Mössbauer spectrometer (MRG-500) at 77 K in constant acceleration mode. ^{57}Co/Rh was used as the radiation source. WinNormos for Igor Pro software has been used for the quantitative evaluation of the spectral parameters (least-squares fitting to Lorentzian peaks). The minimum experimental line widths were 0.20 mm s^{-1}. The temperature of the samples was controlled by an MBBC-HE0106 MÖSSBAUER He/N_2 cryostat within an accuracy of ±0.3 K. Isomer shifts were determined relative to α-iron at 298 K.

EPR spectra were collected on a JEOL continuous wave spectrometer JES-FA200 equipped with an X-band Gunn oscillator bridge, a cylindrical mode cavity, and a helium cryostat. The probes were freshly dissolved in dry toluene in an airtight J. Young quartz EPR tube under dry nitrogen atmosphere.

Materials

Tetrahydrofuran (THF), diethyl ether (Et_2O), hexamethyldisiloxane (HMDSO), dimethoxyethane (DME), hexanes and benzene were distilled over sodium. Dichloromethane was dried over CaH_2. All other solvents were purified and dried by a solvent purification system from MBraun, and stored over a molecular sieve (4 A) under argon or nitrogen.

$[MnI_2(thf)_3]$, $[FeI_2(thf)_2]$, $[CoBr_2(dme)_x]$ and $[CoI_2(thf)_2]$ were synthesized as previously

reported by Job and Earl.[3] According to the crystal structure, $[MnI_2(thf)_3]$,[4] $[Fe(thf)_6][FeI_3(thf)]_2$[5] and $[Co(thf)_6][CoI_3(thf)]_2$[6] are the correct chemical formula of each $[MnI_2(thf)_3]$, $[FeI_2(thf)_2]$ and $[CoI_2(thf)_2]$. In $[CoBr_2(dme)_x]$, the number of coordinated solvent molecule was not able to determine. However, it has no influence on reaction. These salts decompose slowly in dry inert gas atmosphere (argon or nitrogen) under release of coodinated solvent molecules.[3] Cobalt(II) acetylacetonate, $[Co(acac)_2]$, was synthesized as reported starting with cobalt dichloride[7], and purified by two-times sublimation under dynamic vacuum at 120°C prior to use.

$[Cp'FeI]_2$[8] and $[Cp'MnI(thf)]_2$[9] were synthesized as described elsewhere. I*t*Bu,[10] HN=I*t*Bu,[11] I*i*PeMeMe$_2$,[12] IMeMe$_2$,[12] IPr[13] and IMes[13] were prepared according to literature procedures.

NaN_3 (Acros Organics), KSCN (Aldrich), KOCN (Merck), KSeCN (Acros Organics), $NaBH_4$ (Merck) and $NaBD_4$ (Cambridge Isotope Laboratories) were dried over night under dynamic vacuum at 80°C prior to use. Other reagents were used as received.

Synthesis

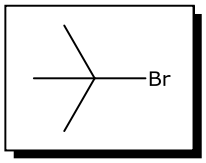

***tert*-Butyl bromide.**[14] *tert*-BuBr was synthesized according to a modified literature procedure:[14] *tert*-BuOH (47.8 mL, 0.50 mol) was added dropwise with vigorous stirring over 25 min to a cold mixture (0°C) of HBr (85.4 mL, 0.75 mol, 48% in H_2O) and H_2SO_4 (32.0 mL, 0.60 mol, 98% in H_2O). During the addition, the temperature was maintained at 0°C. The reaction mixture was then allowed to reach ambient temperature and was stirred vigorously for additional 30 minutes. After the reaction, the organic layer was separated, washed twice with water, and dried over $CaCl_2$. *tert*-BuBr was obtained as a colorless liquid. The product was analyzed by GC and had a typical purity of > 99%. Yield: 57.2 g (0.42 mol, 84%). The use of 2.0 equiv. of HBr and 1.5 equiv. of H_2SO_4 increased the yield to 88%. The product was used without further purification. Pure *tert*-BuBr slowly decomposed and became yellow on storage; and the decomposition appeared to be retarded by the addition of potassium carbonate and storage in the dark at low temperature.

The ^{1}H-NMR spectroscopic data agreed with those reported previously.[15] ^{1}H NMR (200.0 MHz, $CDCl_3$, 300 K, ppm): δ = 1.79 (s, 9H). $^{13}C\{^1H\}$ NMR (50.3 MHz, $CDCl_3$, 300 K, ppm): δ = 63.0 (C_{ipso}, *t*Bu), 36.6 (3C, *t*Bu).

IR (ATR; cm^{-1}): $\tilde{\nu}$ = 2985 (w), 2967 (w), 1473 (sh), 1454 (w), 1369 (m), 1236 (w), 1141 (s), 802 (w). GC retention time: 2.4 min.

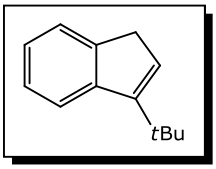

3-*tert*-Butylindene.[16] Adogen 464 (5 mL), indene (50 g, 0.39 mol) and *tert*-BuBr (160 g, 1.17 mol) were added into an aqueous solution of potassium hydroxide (1 kg KOH in 750 mL water). The reaction mixture was stirred vigorously at 80°C for two days and the reaction progress was monitored by GC. The reaction mixture was cooled to ambient temperature and then diluted with diethyl ether (*ca.* 100 mL). The organic layer was separated and washed with 2 M HCl (100 mL). The aqueous layer was extracted twice with diethyl ether (*ca.* 200 mL). The combined organic phases were dried over magnesium sulfate. After filtration the diethyl ether was removed under reduced pressure and the product was distilled at 60°C (0.06 mbar). 3-*tert*-Butylindene was obtained as a light-yellow liquid. Yield: 54.8 g (0.32 mol, 82%).

The ^{1}H[17–19] and $^{13}C\{^{1}H\}$ NMR[19] spectroscopic data agreed with those reported previously. ^{1}H NMR (300 MHz, $CDCl_3$, 297 K, ppm): δ = 7.76 (m, 1H, C(4)-*H*), 7.58 (m, 1H, C(7)-*H*), 7.40, 7.30 (m, 2H, C(5,6)-*H*), 6.31 (t, 1H, C(2)-*H*, J = 2.16 Hz), 3.40 (d, 2H, C(1)-*H*, J = 2.16 Hz), 1.52 (s, 9H, *t*Bu-*H*). $^{13}C\{^{1}H\}$ NMR (75.5 MHz, $CDCl_3$, 298 K, ppm): δ = 153.5, 146.9, 144.1 ($3C_{ipso}$), 126.1, 125.6, 124.1, 124.0, 122.2 (5C, C_9H_6), 37.3 (1C, C_9H_6), 33.2 (C_{ipso}, *t*Bu), 29.5 (3C, *t*Bu). GC-MS: m/z = 172 (M^+), 157 (M^+ – Me), 142 (M^+ – 2 x Me), 116 (M^+ – *t*Bu).

IR (ATR; cm^{-1}): $\overline{\nu}$ = 2961 (m), 1597 (w), 1569 (w), 1477 (m), 1460 (m), 1392 (m), 1363 (m), 765 (s), 721 (s). GC retention time: 14.7 min (indene: 9.4 min).

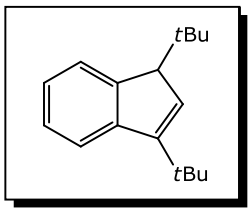

1,3-Di-*tert*-butylindene. EtMgBr used for the synthesis of 1,3-di-*tert*-butylindene was prepared from Mg and EtBr in diethyl ether.

A three-neck 250-mL well-dried round-bottom flask equipped with a dropping funnel and a reflux condenser was charged with Mg turnings (3.40 g, 140 mmol), I_2 (some crystal pieces) and diethyl ether (15 mL). This mixture was stirred until the purple I_2 color faded indicating the activation of the Mg. At this point an ethereal solution of EtBr (11.0 mL, 144 mmol, diluted in 35 mL of diethyl ether) was slowly added under stirring to ensure gentle reflux of the diethyl ether solvent. After complete addition of the EtBr the reaction mixture was heated under gentle reflux for 12 hours. After the reaction mixture was allowed to cool to room temperature and taken to dryness, the crude product was dried for eight hours under dynamic vacuum, and used for further reaction without purification.

3-*tert*-butylindene (24.7 g, 143 mmol) was added dropwise to a suspension of EtMgBr (18.7 g,

140 mmol,) in toluene (40 mL). The reaction mixture was slowly heated to reflux whereby a gas formation was observed, and it was stirred vigorously for eight hours. After this time the reaction mixture was cooled to 0°C, and *tert*-BuCl (15.6 mL, 143 mmol) was added dropwise to this suspension. After complete addition, the temperature was allowed to reach room temperature and the reaction mixture was stirred for eight hours. A saturated aqueous solution of NH_4Cl (50 mL) was mixed with 250 g ice and the reaction mixture was slowly added (very exothermic reaction). The aqueous layer was separated and extracted twice with diethyl ether (*ca.* 150 mL). The ether extracts were combined with the organic layer, washed with water and dried over Na_2SO_4. The solvent was removed under reduced pressure and the residue was purified by distillation (at 70°C under 0.06 mbar) to give the product as a colorless liquid. Yield: 16.3 g (71 mmol, 51%).

The ^{1}H and ^{13}C NMR spectroscopic data agreed with those previously reported for this compound[17,18]. ^{1}H NMR (300 MHz, $CDCl_3$, 297 K, ppm): δ = 7.68 (m, 2H, C(4,7)-*H*), 7.38, 7.25 (m, 2H, C(5,6)-*H*), 6.32 (d, 1H, C(2)-*H*, J = 2.10 Hz), 3.27 (d, 1H, C(1)-*H*, J = 2.10 Hz), 1.51 (s, 9H, *t*Bu-*H*), 1.14 (s, 9H, *t*Bu-*H*). $^{13}C\{^{1}H\}$ NMR (75.5 MHz, $CDCl_3$, 298 K, ppm): δ = 152.7, 147.9, 144.7 ($3C_{ipso}$), 130.2, 125.9, 125.1, 123.6, 122.1 (5C, C_9H_6), 58.7 (1C, C_9H_6), 34.4, 33.2 ($2C_{ipso}$, *t*Bu), 29.7 (3C, *t*Bu), 28.7 (3C, *t*Bu). GC-MS: m/z = 228 (M^+), 172 (M^+ – *t*Bu), 157 (M^+ – *t*Bu – Me), 142 (M^+ – *t*Bu – 2 × Me), 116 (M^+ – 2 × *t*Bu).

IR (ATR; cm^{-1}): $\overline{\nu}$ = 2953 (m), 1602 (w), 1571 (w), 1458 (m), 1391 (m), 1363 (m), 762 (s), 724 (s).

GC retention time: 17.2 min.

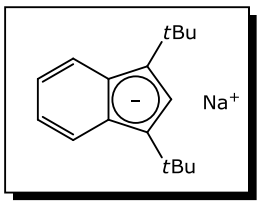

1,3-Di-*tert*-butylindenyl sodium. The sodium salt of 1,3-di-*tert*-butylindene (11.4 g, 50 mmol) was prepared by reaction with $NaNH_2$ (1.87 g, 48 mmol) in THF (120 mL) for 18 hours under reflux. The reaction mixture was allowed to cool to room temperature, filtered and the precipitate was washed with THF (*ca.* 30 mL). The THF-solutions were taken to dryness. The red-brown crude product was suspended in pentane (150 mL) and filtered. The residue was washed with pentane (*ca.* 100 mL) and dried *in vacuo*, affording the product as an ivory solid. Yield: 8.57 g (34 mmol, 71%).

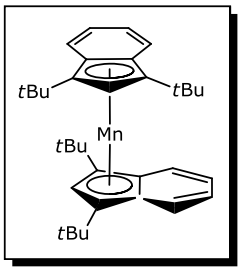

Bis(1,3-di-*tert*-butylindenyl)manganese(II), [($^{2t\mathrm{Bu}}$Ind)$_2$Mn]. [$MnI_2(thf)_3$] (1.43 g, 2.7 mmol) was allowed to react with sodium indenide (1.50 g, 6.0 mmol) in pentane-THF mixture (80 mL : 10 mL) at ambient temperature whereby a orange-brown solution and white precipitate were formed. The solvent was evaporated and the crude product was extracted two times with toluene-THF (70 mL: 35 mL) mixture. The solvent was removed under dynamic vacuum. The remaining solid was extracted with hexanes (4 × 40 mL). Hexanes were distilled off. The obtained solid was washed with hexamethyldisiloxane (15 mL), and then dried under vacuum. Yield: 0.713 g (1.4 mmol, 52%). Diindenylmanganese was crystallized from a pentane solution by slow evaporation of the solvent at room temperature.

Elemental analysis calcd (%) for $C_{34}H_{46}Mn$: C 80.12, H 9.10; found: C 79.86, H 9.19. Mass spectrum (LIFDI, *m*/*z*) calcd for $C_{34}H_{46}Mn$: 509.2980; found: 509.3068.

IR (ATR; cm^{-1}): $\overline{\nu}$ = 3062 (w), 2960 (s), 1459 (s), 1390 (s), 1361 (s), 1201 (m), 1006 (m), 993 (m), 958 (m), 833 (m), 763 (m), 750 (m), 732 (s), 657 (m). UV/vis (*n*-hexane, 22°C, nm): λ (ε, L mol^{-1} cm^{-1}) = 204 (37363), 227 (23363), 242 (26454), 307 (9083), 323 (sh, 7962), 367 (sh, 3092), 414 (sh, 1907). Mp: 207°C.

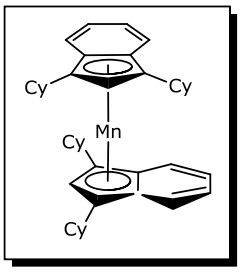

Bis(1,3-dicyclohexylindenyl)manganese(II), [($^{2\mathrm{Cy}}$Ind)$_2$Mn]. [$MnI_2(thf)_3$] (1.50 g, 2.9 mmol) was stirred with sodium indenide (1.73 g, 5.7 mmol) in THF (80 mL) at ambient temperature resulting in a formation of an orange-brown solution. After the complete removal of the solvent, the crude product was extracted with hexanes (5 × 30 mL). The solvent was removed under dynamic vacuum. The residue was washed with hexamethyldisiloxane (5 mL) and then dried. The product was obtained as orange solid. Yield: 0.96 g (1.4 mmol, 55%). Alternatively, diindenylmanganese was crystallized from a pentane solution by slow evaporation of the solvent at room temperature.

Elemental analysis calcd (%) for $C_{42}H_{54}Mn$: C 82.18, H 8.87; found: C 81.70, H 8.87. Mass spectrum (LIFDI, *m*/*z*) calcd for $C_{42}H_{54}Mn$: 613.3606; found: 613.3520.

IR (ATR; cm^{-1}): $\overline{\nu}$ = 3066 (w), 2920 (s), 2849 (s), 1573 (m), 1461 (m), 1445 (s), 989 (m), 888 (m), 819 (m), 775 (s), 742 (s). UV/vis (*n*-pentane, 22°C, nm): λ (ε, L mol^{-1} cm^{-1}) = 207 (sh, 52120), 227 (37400), 237 (sh, 30600), 261 (22560), 310 (4861), 379 (sh, 1975), 438 (1106). Mp: 176°C.

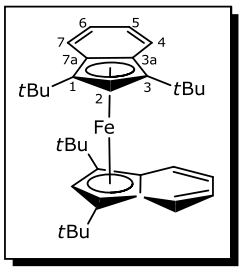

Bis(1,3-di-*tert*-butylindenyl)iron(II), [($^{2t\mathrm{Bu}}$Ind)$_2$Fe]. A Schlenk flask was charged with [FeI$_2$(thf)$_2$] (0.453 g, 1.0 mmol) which was dissolved in THF (10 mL). A solution of sodium indenide (0.500 g, 2.0 mmol) in THF (20 mL) was dropped into it under stirring at ambient temperature. The solvent was completely removed under dynamic vacuum. The remaining solid was extracted with *n*-hexane (3 × 35 mL) and filtrated. *n*-Hexane was distilled off. The residue was rinsed with *n*-pentane (5 mL) and dried under dynamic vacuum. The product was received as blue-green solid. Yield: 0.288 g (0.6 mmol, 56%). Alternatively, bis(1,3-di-*tert*-butylindenyl)iron(II) was crystallized from the concentrated solution at –25°C.

^{1}H NMR (400.0 MHz, C$_7$D$_8$, 299 K, ppm): δ = 7.65 (m, 4H, C(4,7)-*H*), 6.92 (m, 4H, C(5,6)-*H*), 4.19 (s, 2H, C(2)-*H*), 1.32 (s, 36H, *t*Bu-*H*). ^{13}C{^{1}H} NMR (100.6 MHz, C$_7$D$_8$, 299 K, ppm): δ = 130.8 (4C, *C*(4,7)), 123.9 (4C, *C*(5,6)), 87.5 (4C, *C*(1,3)), 86.0 (4C, *C*(3a,7a)), 68.8 (2C, *C*(2)), 32.9 (4C, *t*Bu-C$_{ipso}$), 31.7 (12C, *t*Bu-*C*H$_3$). Elemental analysis calcd (%) for C$_{34}$H$_{46}$Fe: C 79.98, H 9.08; found: C 79.82, H 9.07. The EI mass spectrum showed a molecular ion at *m*/*z* = 510 amu. The parent ion isotopic cluster was simulated: (calcd %, observd %): 508 (6, 8), 509 (3, 2), 510 (100, 100), 511 (41, 38), 512 (9, 8), 513 (1, 1).

IR (ATR; cm^{-1}): $\overline{\nu}$ = 3072 (w), 2952 (m), 1459 (m), 1354 (m), 1306 (m), 1244 (m), 1218 (m), 1000 (m), 962 (m), 730 (s). UV/vis (*n*-hexane, 22°C, nm): λ (ε, L mol^{-1} cm^{-1}) = 204 (36731), 230 (sh, 20317), 261 (16170), 286 (15682), 320 (6774), 342 (5401), 377 (sh, 4196) 471 (232), 639 (328). Mp: 344°C (sublimation at *ca.* 255°C).

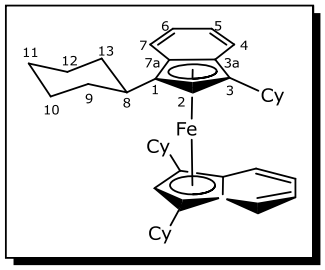

Bis(1,3-dicyclohexylindenyl)iron(II), [($^{2\mathrm{Cy}}$Ind)$_2$Fe]. [FeI$_2$(thf)$_2$] (0.227 g, 0.5 mmol) was allowed to react with sodium salt (0.302 g, 1.0 mmol) in THF (15 mL). The reaction mixture turned deep green and was stirred at ambient temperature for 15 hours. All volatiles were stripped off. The blue green residue was extracted with toluene (15 mL) and filtrated. The dark green toluene extract was concentrated to *ca.* 10 mL and cooled to –30°C to yield dark blue crystals. Yield: 0.157 g (0.3 mmol, 51%).

^{1}H NMR (400.0 MHz, C$_7$D$_8$, 297 K, ppm): δ = 7.17 (m, 4H, C(4,7)-*H*), 6.99 (m, 4H, C(5,6)-*H*), 3.92 (s, 2H, C(2)-*H*), 2.65 (m, 4H, C(13)-*H*$_2$), 2.52 (m, 4H, C(8)-*H*), 2.01 (m, 4H, C(12)-*H*$_2$), 1.83 (m, 4H, C(9)-*H*$_2$), 1.75 (m, 4H, C(11)-*H*$_2$), 1.65 (m, 8H, C(10,12)-*H*$_2$), 1.44 (m, 4H, C(13)-*H*$_2$), 1.40 (m, 4H, C(10)-*H*$_2$), 1.21 (m, 4H, C(11)-*H*$_2$), 0.94 (m, 4H, C(9)-*H*$_2$).

$^{13}C\{^{1}H\}$ NMR (100.6 MHz, C_7D_8, 299 K, ppm): δ = 128.0 (4C, *C*(4,7)), 123.0 (4C, *C*(5,6)), 85.6 (4C, *C*(1,3)), 82.6 (4C, *C*(3a,7a)), 67.0 (2C, *C*(2)), 36.2 (4C, *C*(9)), 35.3 (4C, *C*(8)), 32.7 (4C, *C*(13)), 27.5 (4C, *C*(12)), 27.4 (4C, *C*(10)), 27.1 (4C, *C*11)). Elemental analysis calcd (%) for $C_{42}H_{54}Fe$: C 82.06, H 8.85; found: C 80.95, H 9.03. The EI mass spectrum showed a molecular ion at *m*/*z* = 614 amu. The parent ion isotopic cluster was simulated: (calcd %, observd %): 612 (6, 8), 613 (3, 3), 614 (100, 100), 615 (50, 43), 616 (13, 10), 617 (2, 2).

IR (ATR; cm^{-1}): $\overline{\nu}$ = 3041 (w), 2920 (s), 2847 (s), 1446 (s), 1345 (m), 1260 (m), 990 (m), 889 (m), 836 (m), 730 (s). UV/vis (*n*-hexane, 22°C, nm): λ (ε, L mol^{-1} cm^{-1}) = 203 (sh, 41992), 226 (20140), 264 (sh, 15011), 334 (5545), 450 (sh, 348), 564 (sh, 229), 634 (sh, 205). Mp: 183°C.

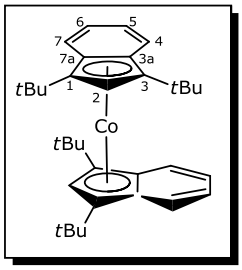

Bis(1,3-di-*tert*-butylindenyl)cobalt(II), [($^{2t\mathrm{Bu}}$Ind)$_2$Co].

[Co(acac)$_2$] (0.257 g, 1.0 mmol) and sodium indenide (0.500 g, 2.0 mmol) were dissolved in THF (100 mL). The temperature was raised until the solvent boiled. The reaction mixture was stirred for 24 hours under reflux. After the stirring THF solvent was evaporated. The residue was extracted with *n*-hexane (3 × 30 mL) and the solvent was removed under vacuum. The product was crystallized from the concentrated solutions of Et_2O or DCM at –25°C. Yield: 0.107 g (0.2 mmol, 21%).

^{1}H NMR (300.1 MHz, C_6D_6, 298 K, ppm): δ = –24.42 (s, br, 2H, C(4,7/5,6)-*H*, $\nu_{1/2}$ = 129 Hz), –22.04 (s, br, 2H, C(5,6/4,7)-*H*, $\nu_{1/2}$ = 144 Hz), 3.51 (s, 18H, *t*Bu-*H*, $\nu_{1/2}$ = 27 Hz). Elemental analysis calcd (%) for $C_{34}H_{46}Co$: C 79.50, H 9.03; found: C 79.04, H 8.94. The EI mass spectrum showed a molecular ion at *m*/*z* = 513 amu. The parent ion isotopic cluster was simulated: (calcd %, observd %): 513 (100, 100), 514 (39, 34), 515 (7, 7), 516 (1, 1).

IR (ATR; cm^{-1}): $\overline{\nu}$ = 3066 (w), 2962 (m), 1458 (m), 1389 (m), 1360 (m), 1298 (m), 1240 (m), 1199 (m), 1000 (m), 959 (m), 727 (s). UV/vis (*n*-hexane, 22°C, nm): λ (ε, L mol^{-1} cm^{-1}) = 255 (13372), 287 (sh, 10907), 334 (8148), 387 (7161), 465 (6181). Mp: 192°C.

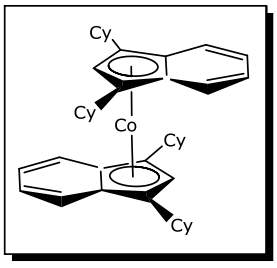

Bis(1,3-dicyclohexylindenyl)cobalt(II), [($^{2\mathrm{Cy}}$Ind)$_2$Co]. A THF (35 mL) solution of [Co(acac)$_2$] (0.514 g, 2.0 mmol) was added dropwise at –78°C very slowly into sodium indenide (1.21 g, 4.0 mmol) which was dissolved in THF (35 mL). The temperature was allowed to rise to room temperature. The reaction mixture was stirred for eight hours. After the reaction all volatile was stripped off in vacuum. The

residue was extracted hexanes (10 × 30 mL). The solvent was removed from the extract. The residue was dissolved in pentane (3 mL) and the solution was stored at –30°C. The product was precipitated from the solution as red crystalline powder. Yield: 0.482 g (0.8 mmol, 39%). [(^{2Cy}Ind)$_2$Co] was crystallized from the saturated benzene solution.

Elemental analysis calcd (%) for $C_{42}H_{54}Co$: C 81.65, H 8.81; found: C 81.08, H 9.00. The EI mass spectrum showed a molecular ion at m/z = 617 amu. The parent ion isotopic cluster was simulated: (calcd %, observd %): 617 (100, 100), 618 (48, 43), 619 (11, 11), 620 (2, 1).

IR (ATR; cm^{-1}): $\overline{\nu}$ = 3081 (w), 2922 (m), 2847 (m), 1585 (s), 1514 (s), 1462 (m), 1447 (m), 1339 (s), 1261 (m), 1016 (m), 923 (m), 772 (m), 740 (s). UV/vis (*n*-hexane, 22°C, nm): λ (ε, L mol^{-1} cm^{-1}) = 204 (sh, 63291), 234 (sh, 24683), 285 (13417), 337 (17683), 455 (8481), 554 (sh, 2367). Mp: 276°C (sublimation at *ca*. 245°C).

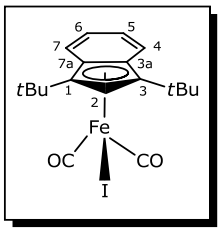

1,3-Di-*tert*-butylindenyl-dicarbonyliron(II)iodide, [($^{2t\text{Bu}}$Ind)Fe(CO)$_2$I]. A Schlenk flask was charged with [FeI$_2$(thf)$_2$] (0.227 g, 0.5 mmol) which was dissolved in THF (10 mL). A solution of sodium indenide (0.125 g, 0.5 mmol) in THF (10 mL) was added dropwise into it under stirring at –78°C within 10 minutes whereby a red-orange solution was formed. It was stirred for 30 minutes at –78°C and then CO was purged for further 30 minutes at this temperature. The solution turned dark red-brown. The temperature was allowed to rise to room temperature during the resulting mixture was stirred for 20 hours. The solvent was evaporated and the residue was extracted with pentane (3 × 10 mL). Cooling concentrated solution to –30°C resulted in dark green crystals. Yield: 0.104 g (0.2 mmol, 44%).

^{1}H NMR (300.0 MHz, C_6D_6, 297 K, ppm): δ = 7.42 (m, 2H, C(4,7)-*H*), 6.68 (m, 2H, C(5,6)-*H*), 5.10 (s, 1H, C(2)-*H*), 1.39 (s, 18H, *t*Bu-*H*). ^{13}C{^{1}H} NMR (75.5 MHz, C_6D_6, 298 K, ppm): δ = 216.3 (2C, *C*O), 128.7 (2C, *C*(4,7)), 127.4 (2C, *C*(5,6)), 100.9 (2C, *C*(1,3)), 100.0 (2C, *C*(3a,7a)), 90.4 (1C, *C*(2)), 32.8 (2C, *t*Bu-C_{ipso}), 32.3 (6C, *t*Bu-CH_3). Elemental analysis calcd (%) for $C_{19}H_{23}FeIO_2$: C 48.96, H 4.97; found: C 48.81, H 5.05. The EI mass spectrum showed a molecular ion at m/z = 466 amu. The parent ion isotopic cluster was simulated: (calcd %, observd %): 464 (6, 6), 465 (1, 1), 466 (100, 100), 467 (24, 23), 468 (4, 3).

IR (ATR; cm^{-1}): $\overline{\nu}$ = 2963 (m), 2870 (m), 2010 (m), 1972 (s), 1944 (m), 1480 (m), 1460 (m), 1365 (m), 1247 (m), 1217 (m), 1200 (m), 1165 (m), 964 (m), 905 (m), 755 (s). Mp: 134.5°C (decomp.).

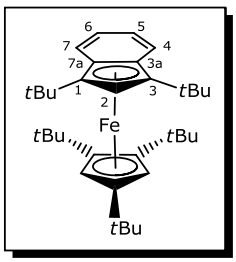

1,3-Di-*tert*-butylindenyl-1,2,4-tri-*tert*-butylcyclopentadienyliron(II), [(2*t*BuInd)(Cp′)Fe]. A THF (10 mL) solution of sodium indenide (0.250 g, 1 mmol) was dropped into a THF (40 mL) solution of $[FeI_2(thf)_2]$ (0.454 g, 1 mmol) at –78°C within 25 minutes and stirred for 40 minutes at this temperature. The solution turned orange. A THF (10 mL) solution of sodium cyclopentadienide (1 mmol, 0.256 g) was added dropwise into the reaction mixture at –78°C within 20 minutes. The temperature was allowed to rise to room temperature within two hours. The solution began to turn brown at –40°C, then slowly into dark green at *ca.* –35°C and became completely green at –8°C. The solvent was evaporated. The residue was washed with HMDSO (10 mL), and then extracted with DCM (20 mL). The extract was filtrated and concentrated to *ca.* 2 mL. HMDSO (3 mL) was added into the solution. The solution was cooled to –25°C. The product was obtained as a dark blue crystalline block. Yield: 0.119 g (0.2 mmol, 23%).

^{1}H NMR (300.1 MHz, CD_2Cl_2, 297 K, ppm): δ = 7.77 (m, 2H, C(4,7)-*H*), 6.85 (m, 2H, C(5,6)-*H*), 4.28 (s, 2H, Cp-*H*), 4.01 (s, 1H, C(2)-*H*), 1.54 (s, 18H, *t*Bu(Ind)-*H*), 1.25 (s, 9H, *t*Bu(Cp)-*H*), 1.15 (s, 18H, *t*Bu(Cp)-*H*). ^{13}C{^{1}H} NMR (75.5 MHz, CD_2Cl_2, 298 K, ppm): δ = 132.0 (2C, *C*(4,7)), 122.3 (2C, *C*(5,6)), 94.0 (2C, ring-C_{ipso}), 91.3 (1C, ring-C_{ipso}), 90.4 (2C, *C*(4,7)), 87.2 (2C, *C*(5,6)), 69.5 (1C, *C*(2)), 65.1 (2C, ring-*C*H), 33.9 (6C, *t*Bu(Cp)-*C*H$_3$), 33.5 (2C, *t*Bu(Cp)-C_{ipso}), 33.0 (6C, *t*Bu(Ind)-*C*H$_3$), 32.8 (2C, *t*Bu(Ind)-C_{ipso}), 32.4 (3C, *t*Bu(Cp)-*C*H$_3$), 31.1 (1C, *t*Bu(Cp)-C_{ipso}). Elemental analysis calcd (%) for $C_{34}H_{52}Fe$: C 79.05, H 10.15; found: C 78.24, H 10.14. The EI mass spectrum showed a molecular ion at m/z = 516 amu. The parent ion isotopic cluster was simulated: (calcd %, observd %): 514 (6, 8), 515 (2, 7), 516 (100, 100), 517 (41, 39), 518 (9, 8), 519 (1, 3).515 (2, 7), 516 (100, 100), 517 (41, 39), 518 (9, 8), 519 (1, 3).

UV/vis (*n*-hexane, 22°C, nm): λ (ε, L mol^{-1} cm^{-1}) = 240 (14655), 272 (14490), 333 (sh, 3720), 579 (214).

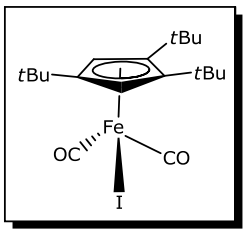

1,2,4-Tri-*tert*-butylcyclopentadienyl-dicarbonyliron(II)iodide, [(Cp′)Fe(CO)$_2$I]. $[FeI_2(thf)_2]$ (1.77 g, 3.9 mmol) and NaCp′ (1.00 g, 3.9 mmol) were stirred in THF (50 mL) for four hours at ambient temperature. Exposure of this solution to CO (1 atm) resulted in a color change to dark brown. After stirring for two days the THF solvent was removed under dynamic vacuum and the residue was extracted with toluene (50 mL). After evaporation of toluene the product was obtained as black solid. Yield: 1.32 g (2.8 mmol, 72%).

^{1}H NMR (300.0 MHz, C_6D_6, 297 K, ppm): δ = 4.87 (s, 2H, ring-C*H*), 1.19 (s, 27H, *t*Bu-*H*). ^{13}C{^{1}H} NMR (75.5 MHz, C_6D_6, 298 K, ppm): δ = 216.1 (2C, *C*O), 108.4 (2C, ring-C_{ipso}), 107.9 (1C, ring-C_{ipso}), 88.6 (2C, ring-*C*H), 33.4 (6C, *t*Bu-CH_3), 32.6 (2C, *t*Bu-C_{ipso}), 32.0 (3C, *t*Bu-CH_3) 31.2 (1C, *t*Bu-C_{ipso}). Elemental analysis calcd (%) for $C_{19}H_{29}FeO_2I$: C 48.33, H 6.19; found: C 48.38, H 6.48. The EI mass spectrum showed a molecular ion at m/z = 472 amu. The parent ion isotopic cluster was simulated: (calcd %, observd %): 470 (6, 7), 471 (1, 1), 472 (100, 100), 473 (24, 22), 474 (4, 4).

IR (ATR; cm^{-1}): $\overline{\nu}$ = 3083 (w), 2959 (s), 2869 (m), 2013 (s), 1966 (m), 1936 (m), 1481 (m), 1462 (m), 1391 (m), 1363 (s), 1245 (m), 1094 (m), 1021 (m), 798 (m), 611 (m). Mp: 115°C (decomp.).

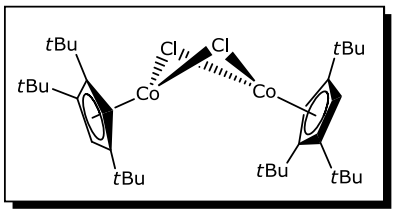

[Cp'CoCl]$_2$. In a schlenk flask [$CoCl_2$] (0.130 g, 1.0 mmol) was dissolved in THF (15 mL). A THF (10 mL) solution of Cp'Na (0.256 g, 1.0 mmol) was added into the flask in one batch and stirred at ambient temperature for three hours. Then the solvent was removed under dynamic vacuum. A dark green solid remained. The solid was extracted with pentane (20 mL). The extract was concentrated to 5 mL. The product was crystallized from the concentrated solution at –25°C as green plates. Yield: 0.052 g (0.08 mmol, 16%).

^{1}H NMR (200.1 MHz, C_6D_6, 300 K, ppm): δ = 9.22 (s, 18H, *t*Bu-*H*, $\nu_{1/2}$ = 81.59 Hz), 6.20 (s, 36H, *t*Bu-*H*, $\nu_{1/2}$ = 78.63 Hz), –4.36 (s, br, 4H, ring-C*H*, $\nu_{1/2}$ = 401.0 Hz). Elemental analysis calcd (%) for $C_{34}H_{58}Cl_2Co_2$: C 62.29, H 8.92; found: C 62.21, H 8.96. EI mass spectrum showed a molecular ion at m/z = 654 amu. The parent ion isotopic cluster was simulated (calc. %, observd. %): 654 (100, 100), 655 (39, 39), 656 (72, 72), 657 (26, 26), 658 (15, 16), 659 (5, 4).

IR (ATR; cm^{-1}): $\overline{\nu}$ = 2957 (s), 2906 (m), 2869 (m), 1482 (m), 1460 (m), 1392 (m), 1360 (s), 1239 (s), 1199 (m), 1022 (w), 977 (w), 942 (w), 924 (w), 862 (m), 828 (m), 684 (m), 655 (w). UV/vis (*n*-hexane, 22°C, nm): λ (ε, L mol^{-1} cm^{-1}) = 203 (43243), 209 (40179), 254 (9403), 301 (5875), 332 (4904), 395 (sh, 1615). Mp: 181–185°C.

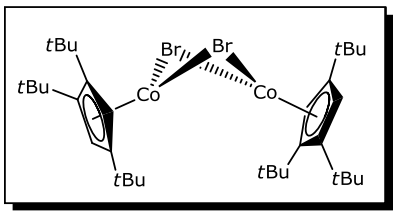

[Cp'CoBr]$_2$. In a Schlenk flask [$CoBr_2$(dme)$_2$] (0.399 g, 1.0 mmol) and Cp'Na (0.256 g, 1.0 mmol) were dissolved in THF (50 mL) and stirred at ambient temperature for 19 hours. Then the solvent was removed under dynamic

vacuum. An oily black solid remained. The solid was extracted with pentane (30 mL). A green-brown solution and turquoise tar were formed. The extract was concentrated to 2 mL. The product was crystallized from the concentrated solution at –25°C as green-brown prisms. Yield: 0.076 mg (0.10 mmol, 20%).

^{1}H NMR (200.1 MHz, C_6D_6, 300 K, ppm): δ = 9.65 (s, 18H, *t*Bu-*H*, $\nu_{1/2}$ = 101.10 Hz), 6.28 (s, 36H, *t*Bu-*H*, $\nu_{1/2}$ = 87.00 Hz). Elemental analysis calcd (%) for $C_{34}H_{58}Br_2Co_2$: C 54.85, H 7.85; found: C 54.80, H 7.86. EI mass spectrum showed a molecular ion at m/z = 742 amu. The parent ion isotopic cluster was simulated (calc. %, observd. %): 742 (49, 51), 743 (19, 20), 744 (100, 100), 745 (38, 37), 746 (54, 56), 747 (19, 19), 748 (4, 3).

IR (ATR; cm^{-1}): $\overline{\nu}$ = 2957 (s), 2903 (m), 2867 (m), 1481 (m), 1458 (m), 1390 (m), 1362 (s), 1239 (m), 1197 (w), 1089 (w), 1021 (m), 866 (m), 829 (m), 652 (w). UV/vis (*n*-hexane, 22°C, nm): λ (ε, L mol^{-1} cm^{-1}) = 210 (sh, 22200), 215 (22830), 218 (22515), 263 (10275), 303 (sh, 7725), 333 (sh, 6603), 406 (sh, 1428), 468 (sh, 831). Mp: 168–171°C.

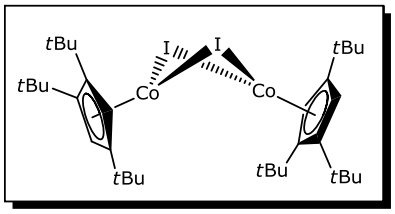

[Cp'CoI]$_2$. In a Schlenk flask [$CoI_2(thf)_3$] (2.65 g, 5.0 mmol) and KCp' (1.36 g, 5.0 mmol) were dissolved in THF (200 mL) and stirred at ambient temperature for six hours. Then the solvent was removed under dynamic vacuum to leave black solid. The solid was extracted with pentane (5 × 40 mL). The extract was concentrated to 40 mL. The product was crystallized from the concentrated solution at –25°C as brown prisms. Yield: 1.26 mg (1.50 mmol, 60%).

^{1}H NMR (300.1 MHz, C_6D_6, 297 K, ppm): δ = 22.05 (s, br, 4H, ring-C*H*, $\nu_{1/2}$ = 365.81 Hz), 9.85 (s, 18H, *t*Bu-*H*, $\nu_{1/2}$ = 58.06 Hz), 6.49 (s, 36H, *t*Bu-*H*, $\nu_{1/2}$ = 55.74 Hz). Elemental analysis calcd (%) for $C_{34}H_{58}Co_2I_2$: C 48.70, H 6.97; found: C 48.24, H 6.96. EI mass spectrum showed a molecular ion at m/z = 838 amu. The parent ion isotopic cluster was simulated (calc. %, observd. %): 838 (100, 100), 839 (39, 40), 840 (7, 4).

IR (ATR; cm^{-1}): $\overline{\nu}$ = 2955 (s), 2915 (m), 2868 (m), 1483 (m), 1459 (m), 1392 (m), 1361 (s), 1241 (s), 1205 (m), 1168 (m), 942 (m), 865 (m), 832 (w). UV/vis (*n*-hexane, 22°C, nm): λ (ε, L mol^{-1} cm^{-1}) = 244(sh, 20899), 248 (21093), 353 (13291), 507 (1234). Mp: 173–182°C.

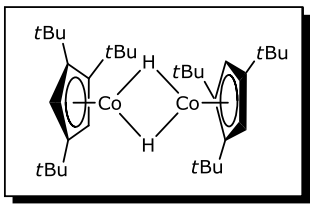

[Cp'CoH]$_2$. In a Schlenk flask [Cp'CoI]$_2$ (0.168 g, 0.2 mmol) was dissolved in pentane (20 mL) and cooled to –78°C. At this temperature KBHEt$_3$ (0.40 mL, 0.4 mmol, 1.0 M solution in THF) was added into the solution and stirred for two hours. After one hour white precipitate was formed and the color of the reaction mixture turned red brown from wine red. The temperature was allowed to rise to room temperature. Then the solvent was removed under dynamic vacuum. A red solid remained. The solid was dissolved in pentane (3 mL) and filtrated. The product was crystallized from the concentrated solution at –25°C as red prisms. Yield: 0.042 g (72 μmol, 36%).

^{1}H NMR (300.1 MHz, C_6D_6, 298 K, ppm): δ = 4.03 (s, 4H, ring-C*H*), 1.72 (s, 36H, *t*Bu-*H*), 1.62 (s, 18H, *t*Bu-*H*), –24.17 (s, 2H, Co-*H*). ^{13}C{^{1}H} NMR (75.5 MHz, C_6D_6, 299 K, ppm): δ = 98.0 (4C, ring-C_{ipso}), 96.9 (2C, ring-C_{ipso}), 66.1 (4C, ring-CH), 33.7 (12C, *t*Bu-CH_3), 31.3 (6C, *t*Bu-CH_3), 30.9 (4C, *t*Bu-C_{ipso}), 29.2 (2C, *t*Bu-C_{ipso}). Elemental analysis calcd (%) for $C_{34}H_{60}Co_2$: C 69.60, H 10.31; found: C 63.31, H 10.14. EI mass spectrum showed a molecular ion at m/z = 586 amu. The parent ion isotopic cluster was simulated (calc. %, observd. %): 586 (100, 100). 587 (38, 90), 588 (8, 26).

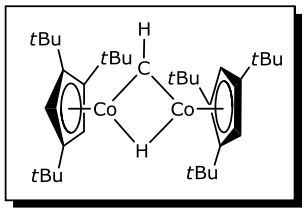

[(Cp'Co)$_2$(μ-CH)(μ-H)]. In a Schlenk flask [Cp'CoI]$_2$ (0.168 g, 0.2 mmol) was dissolved in pentane (20 mL) and cooled to –78°C. At this temperature MeLi (0.25 mL, 0.4 mmol, 1.6 M solution in Et_2O) was added into the solution and stirred for 4 hours whereby the temperature was allowed to rise to room temperature. Then the solvent was removed under dynamic vacuum. A red solid remained. The solid was dissolved in Et_2O (3 mL) and filtrated. The product was crystallized from the concentrated solution at –25°C as red prisms. Yield: 0.014 g (23 μmol, 12%).

^{1}H NMR (200.1 MHz, C_6D_6, 300 K, ppm): δ = 20.61 (d, 1H, μ-C*H*) 5.61 (s, 4H, ring-C*H*), 1.36 (s, 36H, *t*Bu-*H*), 0.79 (s, 18H, *t*Bu-*H*), –1.06 (s, 1H, μ-*H*). ^{13}C{^{1}H} NMR (75.5 MHz, C_6D_6, 299 K, ppm): δ = 127.2 (1C, μ-CH), 107.9 (4C, ring-C_{ipso}), 103.5 (2C, ring-C_{ipso}), 81.0 (4C, ring-CH), 33.5 (12C, *t*Bu-CH_3), 31.1 (4C, *t*Bu-C_{ipso}), 30.4 (6C, *t*Bu-CH_3), 28.2 (2C, *t*Bu-C_{ipso}). Elemental analysis calcd (%) for $C_{35}H_{60}Co_2$: C 70.21, H 10.10; found: C 65.91, H 9.72. EI mass spectrum showed a molecular ion at m/z = 598 amu. The parent ion isotopic cluster was simulated (calc. %, observd. %): 598 (100, 100). 599 (34, 38), 600 (6, 8).

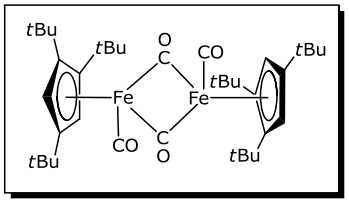

[Cp'Fe(CO)$_2$]$_2$. A Schlenk flask was charged with [Cp'Fe(CO)$_2$I] (0.236 g, 0.50 mmol) which was dissolved in toluene (10 mL). A toluene (10 mL) solution of [Cp$_2$Co] (0.110 g, 0.58 mmol) was added dropwise into the Schlenk flask over five minutes. After 15 minutes the solvent was removed under dynamic vacuum. A mixture of black and colorless solids remained. The residue was extracted with pentane (3 × 15 mL). The wine red extracts were combined, filtered and then pentane was evaporated. The residue was dissolved in toluene (15 mL) and concentrated to 3 mL. The solution was cooled to –30°C and the product was obtained as dark red crystals. Yield: 0.098 g (0.14 mmol, 56%).

^{1}H NMR (300.0 MHz, C$_6$D$_6$, 297 K, ppm): δ = 4.53 (s, 4H, ring-C*H*), 1.52 (s, 36H, *t*Bu-*H*), 1.22 (s, 18H, *t*Bu-*H*). ^{13}C{^{1}H} NMR (75.5 MHz, C$_6$D$_6$, 298 K, ppm): δ = 244.8 (2C, *C*O), 176.6 (2C, *C*O), 108.4 (4C, ring-*C*$_{ipso}$), 107.9 (2C, ring-*C*$_{ipso}$), 88.6 (4C, ring-*C*H), 33.4 (12C, *t*Bu-*C*H$_3$), 32.6 (4C, *t*Bu-*C*$_{ipso}$), 32.0 (6C, *t*Bu-*C*H$_3$), 31.2 (2C, *t*Bu-C$_{ipso}$). Elemental analysis calcd (%) for C$_{38}$H$_{58}$Fe$_2$O$_4$: C 66.09, H 8.47; found: C 66.01, H 8.53. The EI mass spectrum showed no molecular ion of the compound to this complex.

IR (ATR; cm^{-1}): $\overline{\nu}$ = 2958 (m), 2908 (w), 2869 (w), 1953 (m), 1928 (s), 1750 (s), 1524 (w), 1460 (2), 1415 (2), 1361 (m), 1245 (w), 1167 (w), 1108 (w), 1010 (w), 995 (w), 877 (w), 866 (w), 800 (w), 626 (m). UV/vis (*n*-hexane, 22°C, nm): λ (ε, L mol^{-1} cm^{-1}) = 215 (25559), 219 (25647), 306 (sh, 8546), 367 (8871), 439 (2471), 551 (1223). Mp: 201–209°C.

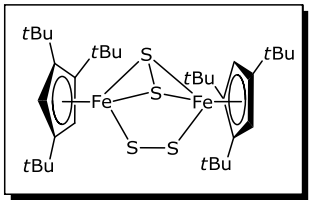

[Cp'FeS$_2$]$_2$. A Schlenk tube was charged with [Cp'Fe(CO)$_2$]$_2$ (0.020 g, 29 μmol) and S$_8$ (0.004 g, 16 μmol), which was sublimed under static vacuum at 80°C prior to use, and dissolved in toluene (0.7 mL). The reaction mixture was heated at 80°C for six days. After the reaction, the solvent was removed under dynamic vacuum. The residue was extracted with pentane (1 mL). The solution was filtrated and cooled to –30°C and the product was obtained as black blocks.Yield: 0.006 g (8 μmol, 28%)

^{1}H NMR (200.0 MHz, C$_7$D$_8$, 300 K, ppm): δ = 5.64 (s, 4H, ring-C*H*), 1.31 (s, 36H, *t*Bu-*H*), 0.88 (s, 18H, *t*Bu-*H*). ^{13}C{^{1}H} NMR (50.3 MHz, C$_7$D$_8$, 300 K, ppm): δ = 105.2 (4C, ring-*C*$_{ipso}$), 103.7 (2C, ring-*C*$_{ipso}$), 84.7 (4C, ring-*C*H), 33.3 (12C, *t*Bu-*C*H$_3$), 32.9 (4C, *t*Bu-*C*$_{ipso}$), 31.4 (6C, *t*Bu-*C*H$_3$), 29.5 (2C, *t*Bu-C$_{ipso}$).

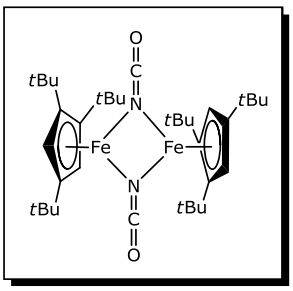

[Cp'Fe(NCO)]$_2$. [Cp'FeI]$_2$ (0.416 g, 0.5 mmol), KNCO (0.081 g, 1.0 mmol) and THF (25 mL) were placed in a Schlenk flask. A green suspension and white precipitate were formed immediately, which separated instantaneously. After 15 minutes the THF solvent was evaporated. The residue was extracted with pentane (20 mL). After filtration, the extract was concentrated to 5 mL and cooled to –30°C. The product was obtained as green plates. Yield: 0.170 g (0.26 mmol, 52%).

^{1}H NMR (400.1 MHz, C_7D_8, 297 K, ppm): δ = 42.47 (s, br, 4H, ring-C*H*, $\nu_{1/2}$ = 508.45 Hz), –4.03 (s, 36H, *t*Bu-*H*, $\nu_{1/2}$ = 74.81 Hz), –7.76 (s, 18H, *t*Bu-*H*, $\nu_{1/2}$ = 74.15 Hz). Elemental analysis calcd (%) for $C_{36}H_{58}Fe_2N_2O_2$: C 65.26, H 8.82, N 4.23; found: C 64.59, H 8.84, N 4.21. The EI mass spectrum showed a molecular ion at m/z = 662 amu. The parent ion isotopic cluster was simulated: (calcd %, observd %): 660 (13, 14), 661 (6, 7), 662 (100, 100), 663 (46, 43), 664 (12, 11), 665 (2, 2).

IR (ATR; cm^{-1}): $\overline{\nu}$ = 2952 (m), 2866 (w), 2176 (s), 2030 (m), 1974 (m), 1460 (m), 1391 (w), 1360 (m), 1236 (m), 1201 (w), 998 (w), 831 (m), 665 (m), 617 (m). UV/vis (*n*-hexane, 22°C, nm): λ (ε, L mol^{-1} cm^{-1}) = 337 (sh, 1711), 408 (sh, 535), 705 (84). Mp: 163°C (sublimation at ca. 215°C).

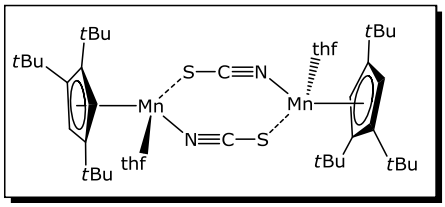

[Cp'Mn(NCS)(thf)]$_2$. [Cp'MnI(thf)]$_2$ (0.186 g, 0.2 mmol), KSCN (0.037 g, 0.4 mmol) and dried THF (30 mL) were put in a Schlenk flask. A pale green suspension with white precipitate was formed immediately. After 20 hours the THF solvent was removed. The residue was extracted with pentane (5 mL). By slowly evaporation of solvent the product was received as pale green crystals. Yield: 0.087 g (0.1 mmol, 58%).

Elemental analysis calcd (%) for $C_{44}H_{74}Mn_2N_2O_2S_2$: C 63.13, H 8.91, N 3.35, S 7.66; found: C 62.52, H 8.58, N 3.86, S 7.09. The EI mass spectrum showed no molecular ion of the compound to this complex.

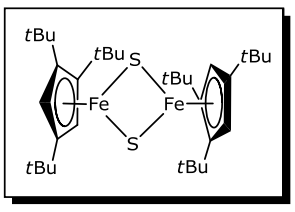

[Cp'FeS]$_2$. A Schlenk flask was charged with [Cp'FeI]$_2$ (0.832 g, 1.0 mmol), KSCN (0.194 g, 2.0 mmol) and THF (50 mL). The suspension was stirred at ambient temperature for 12 hours. The reaction mixture turned black. Then the solvent was evaporated.

After removal of the solvent, the residue was extracted three times with pentane (3 × 20 mL). The extract was filtered and the solvent was removed under dynamic vacuum. The residue was rinsed with HMDSO (2 mL) and then dissolved in Et_2O (3 mL). The solution was cooled to –30°C. The product was separated as dark red crystals. Yield: 0.098 g (0.15 mmol, 15%).
^1H NMR (400.4 MHz, C_6D_6, 296 K, ppm): δ = 10.96 (s, 4H, ring C*H*), 1.01 (s, 36H, *t*Bu-*H*), 0.44 (s, 18H, *t*Bu-*H*). $^{13}C\{^1H\}$ NMR (100.9 MHz, C_6D_6, 298 K, ppm): δ = 235.3 (br, 2C, ring-C_{ipso}, $\nu_{1/2}$ = 58.8 Hz), 199.2 (br, 4C, ring-C_{ipso}, $\nu_{1/2}$ = 41.2 Hz), 98.5 (4C, ring-CH), 53.8 (6C, *t*Bu-CH_3), 46.1 (12C, *t*Bu-CH_3), 21.6 (4C, *t*Bu-C_{ipso}), 9.7 (2C, *t*Bu-C_{ipso}). Elemental analysis calcd (%) for $C_{34}H_{58}Fe_2S_2$: C 63.55, H 9.10; found: C 63.85, H 8.96. The EI mass spectrum showed a molecular ion at m/z = 642 amu. The parent ion isotopic cluster was simulated: (calcd %, observd %): 640 (12, 13), 641 (5, 6), 642 (100, 100), 643 (50, 45), 644 (19, 18), 645 (6, 6), 646 (1, 1).
UV/vis (*n*-hexane, 22°C, nm): λ (ε, L mol^{-1} cm^{-1}) = 256 (22521), 347 (17168), 389 (sh, 12632), 519 (2015).

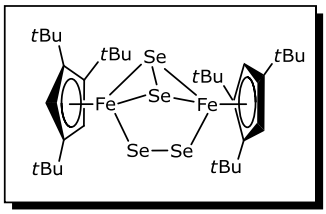

[Cp'FeSe$_2$]$_2$. In a Schlenk flask [Cp'FeI]$_2$ (0.832 g, 1.0 mmol), KSeCN (0.576 g, 4.0 mmol) were dissolved in THF (100 mL). The suspension was stirred at ambient temperature for 15 hours. The reaction mixture turned black. Then the solvent was removed under dynamic vacuum and the residue was extracted with *n*-hexane (3 × 100 mL). The extract was filtered and taken to dryness. The residue was dissolved in Et_2O (15 mL). The solution was very slowly concentrated to 5 mL. The product crystallized as dark orange plates. Yield: 0.132 g (0.15 mmol, 15%).
^1H NMR (300.1 MHz, C_6D_6, 300 K, ppm): δ = 5.89 (s, 4H, ring C*H*), 1.33 (s, 36H, *t*Bu-*H*), 0.81 (s, 18H, *t*Bu-*H*). $^{13}C\{^1H\}$ NMR (75.5 MHz, C_6D_6, 301 K, ppm): δ = 104.5 (4C, ring-C_{ipso}), 102.9 (2C, ring-C_{ipso}), 84.1 (4C, ring-CH), 33.4 (12C, *t*Bu-CH_3), 33.1 (4C, *t*Bu-C_{ipso}), 31.4 (6C, *t*Bu-CH_3), 29.4 (2C, *t*Bu-C_{ipso}). ^{77}Se NMR (76.4 MHz, C_6D_6, 297 K, ppm): δ = 2103.2, 493.2. Elemental analysis calcd (%) for $C_{34}H_{58}Fe_2Se_4$: C 45.66, H 6.54; found: C 46.06, H 6.65. The EI mass spectrum showed a molecular ion at m/z = 896 amu. The parent ion isotopic cluster was simulated: (calcd %, observd %): 886 (6, 5), 887 (8, 8), 888 (18, 16), 889 (21, 20), 890 (41, 42), 891 (41, 41), 892 (72, 74), 893 (59, 57), 894 (97, 98), 895 (63, 62), 896 (100, 100), 897 (49, 47), 898 (72, 70), 899 (30, 26), 900 (32, 29), 901 (12, 9), 902 (8, 7).
IR (ATR; cm^{-1}): $\overline{\nu}$ = 2957 (s), 2910 (m), 2866 (m), 2053 (m), 1999 (m), 1916 (m), 1895 (m), 1484 (s), 1455 (m), 1391 (m), 1359 (s), 1239 (m), 1168 (s), 1198 (w), 1021 (w), 994 (m), 880 (m),

859 (m), 823 (m), 669 (m), 646 (m). Mp: 186.1–186.3°C (decomp.).

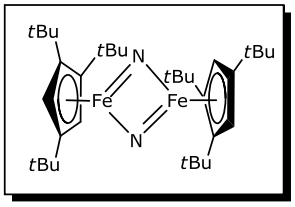

[Cp'FeN]$_2$. A Schlenk flask was charged with [Cp'FeI]$_2$ (0.416 g, 0.5 mmol), NaN_3 (0.065 g, 1.0 mmol) and THF (25 mL). The suspension was stirred at ambient temperature for 10 hours while the mixture gradually turned orange. Then the solvent was removed under dynamic vacuum whereby a color change from orange to green was observed. The residue was extracted with pentane (3 × 15 mL). The extract was filtered and the solvent was evaporated. The residue was dissolved in Et_2O (3 mL). Cooling of Et_2O solution to –30°C gives the product as green crystals. Yield: 0.171 g (0.28 mmol, 56%).

^{1}H NMR (300.1 MHz, C_6D_6, 296 K, ppm): δ = 6.45 (s, 4H, ring C*H*), 1.33 (s, 36H, *t*Bu-*H*), 0.58 (s, 18H, *t*Bu-*H*). ^{13}C{^{1}H} NMR (75.5 MHz, C_6D_6, 297 K, ppm): δ = 114.6 (4C, ring-C_{ipso}), 113.7 (2C, ring-C_{ipso}), 91.3 (4C, ring-*C*H), 33.7 (12C, *t*Bu-*C*H$_3$), 32.7 (4C, *t*Bu-C_{ipso}), 30.7 (6C, *t*Bu-*C*H$_3$), 29.1 (2C, *t*Bu-C_{ipso}). Elemental analysis calcd (%) for $C_{34}H_{58}Fe_2N_2$: C 67.33, H 9.64, N 4.62; found: C 67.17, H 9.52, N 4.81. The EI mass spectrum showed a molecular ion at *m*/*z* = 662 amu. The parent ion isotopic cluster was simulated: (calcd %, observd %): 604 (13, 11), 605 (5, 6), 606 (100, 100), 607 (44, 40), 608 (10, 10), 609 (2, 2).

IR (ATR; cm^{-1}): $\overline{\nu}$ = 3005 (m), 2962 (w), 2907 (w), 1482 (m), 1459 (w), 1418 (m), 1359 (m), 1246 (m), 1169 (m), 997 (w), 947 (w), 858 (4), 828 (m). UV/vis (*n*-hexane, 22°C, nm): λ (ε, L mol^{-1} cm^{-1}) = 255 (sh, 21877), 291 (59826), 386 (12088), 519 (sh, 820).

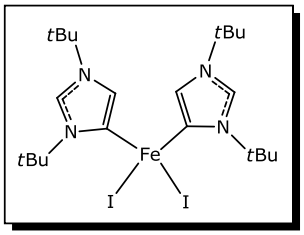

[FeI$_2$(I*t*Bu)$_2$]. A Schlenk flask was charged with [FeI$_2$(thf)$_2$] (0.454 g, 1 mmol) and I*t*Bu (0.361 g, 2 mmol) dissolved in a mixture of THF (10 ml) and pentane (10 ml). The reaction mixture was stirred at ambient temperature for 26 hours. The mixture turned light green and a red-brown precipitate was formed. The solvent was evaporated and the residue was extracted with THF (50 mL). After THF was removed under dynamic vacuum, the product was obtained. Yield: 0.281 g (0.42 mmol, 42%).

Elemental analysis calcd (%) for $C_{22}H_{40}FeI_2N_4$: C 39.42, H 6.02, N 8.36; found: C 38.87, H 6.08, N 7.06.

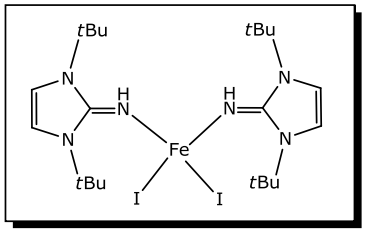

[FeI$_2$(HNI*t*Bu)$_2$]. A Schlenk flask was charged with FeI$_2$(thf)$_2$ (0.113 g, 0.25 mmol) and HN=I*t*Bu (0.098 g, 0.50 mmol) which was dissolved in THF (15 mL). The reaction mixture was stirred at ambient temperature for 15 hours. The mixture turned into light yellow and rose precipitate was formed. The reaction mixture was filtrated and pentane was slowly added so that a pentane layer was formed on the filtrate. The product was received as rose crystals. Yield: 0.099 g (0.13 mmol, 52%). Elemental analysis calcd (%) for $C_{26}H_{50}FeI_2N_6O$: C 40.43, H 6.52, N 10.88; found: C 40.24, H 6.37, N 10.96.

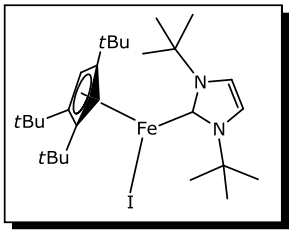

[Cp'Fe(I*t*Bu)I]. Dropwise addition of a pentane (10 mL) solution of I*t*Bu (0.090 g, 0.5 mmol) into a pentane solution of [Cp'FeI]$_2$ (0.208 g, 0.25 mmol) resulted in an immediate precipitation of the product from the reaction solution as yellow crystals. Yield: 0.259 g (0.43 mmol, 86%).

Elemental analysis calcd (%) for $C_{28}H_{49}FeIN_2$: C 56.38, H 8.28, N 4.70; found: C 56.02, H 8.24, N 4.72. The EI mass spectrum showed no molecular ion of the compound to this complex.

IR (ATR; cm^{-1}): $\overline{\nu}$ = 2954 (m), 2903 (m), 2863 (m), 1479 (m), 1460 (m), 1398 (m), 1367 (s), 1354 (m), 1230 (s), 1200 (s), 1146 (m), 837 (m), 740 (s), 680 (m), 626 (m). UV/vis (*n*-hexane, 22°C, nm): λ (ε, L mol^{-1} cm^{-1}) = 462 (sh, 304). Mp: 197–202°C (decomp.).

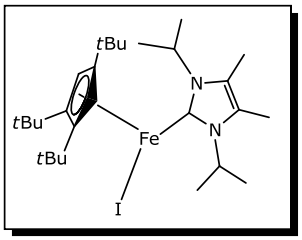

[Cp'Fe(I*i*PrMe$_2$)I]. A pentane (10 mL) solution of I*i*PrMe$_2$ (0.108 g, 0.60 mmol) was added dropwise to a pentane (10 mL) solution of [Cp'FeI]$_2$ (0.208 g, 0.25 mmol). The solution was concentrated and then the product was crystallized and obtained as yellow-green crystals. Yield: 0.122 g (0.20 mmol, 40%).

^{1}H NMR (200.1 MHz, C_7D_8, 300 K, ppm): δ = 32.69 (s, br, 2H, ring-C*H*, $\nu_{1/2}$ = 250.22 Hz), 31.08 (s, 2H, *i*Pr-C*H*, $\nu_{1/2}$ = 21.98 Hz), 29.66 (s, 6H, NHC-backbone-CH_3, $\nu_{1/2}$ = 49.03 Hz), –14.62 (s, br, 18H, *t*Bu-*H*, $\nu_{1/2}$ = 201.83 Hz), –15.80 (s, br, 9H, *t*Bu-*H*, $\nu_{1/2}$ = 185.24 Hz), –17.33 (s, 12H, *i*Pr-CH_3, $\nu_{1/2}$ = 69.12 Hz). Elemental analysis calcd (%) for $C_{28}H_{49}FeIN_2$: C 56.38, H 8.28, N 4.70; found: C 54.56, H 8.05, N 5.07. The EI mass spectrum showed a molecular ion at *m*/*z* = 596 amu. The parent ion isotopic cluster was simulated: (calcd %, observd %): 594 (6, 7), 595 (2, 2), 596 (100, 100), 597 (35, 34), 598 (6, 5), 599 (1, 1).

IR (ATR; cm^{-1}): $\overline{\nu}$ = 2958 (m), 2902 (m), 2868 (m), 1460 (m), 1383 (m), 1356 (s), 1236 (m), 1219 (m), 1134 (m), 1110 (m), 830 (s), 752 (m), 673 (m). UV/vis (*n*-hexane, 22°C, nm): λ (ε, L mol^{-1} cm^{-1}) = 439 (sh, 583), 447 (866), 780 (95). Mp: 184–218°C (decomp.).

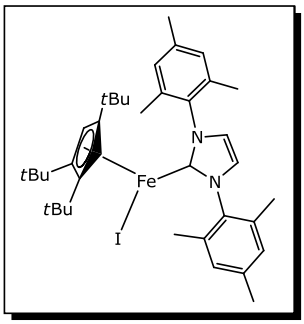

[Cp'Fe(IMes)I]. A pentan (7.5 mL) solution of IMes (0.076 g, 0.25 mmol) was dropped into a pentane solution of $[Cp'FeI]_2$ (0.104 g, 0.13 mmol). The red crystals began to form immediately from the reaction solution. Yield: 0.050 g (0.07 mmol, 55%).

^1H NMR (300.1 MHz, C_7D_8, 300 K, ppm): δ = 101.17 (s, br, 12H, *o*-C*H*$_3$, $\nu_{1/2}$ = 1113.36 Hz), 62.37 (s, br, 4H, *m*-*H*, $\nu_{1/2}$ = 253.82 Hz), 16.86 (s, br, 2H, NHC-backbone-*H*, $\nu_{1/2}$ = 218.52 Hz), –5.67 (s, br, 2H, ring-C*H*, $\nu_{1/2}$ = 521.04 Hz), –20.44 (s, br, 18H, *t*Bu-*H*, $\nu_{1/2}$ = 659.99 Hz), –27.01 (s, br, 9H, *t*Bu-*H*, $\nu_{1/2}$ = 352.87 Hz), –67.68 (s, br, 6H, *p*-C*H*$_3$, $\nu_{1/2}$ = 778.44 Hz). Elemental analysis calcd (%) for $C_{38}H_{53}FeIN_2$: C 63.34, H 7.41, N 3.89; found: C 62.47, H 7.16, N 3.87. The EI mass spectrum showed no molecular ion of the compound corresponding to this complex.

IR (ATR; cm^{-1}): $\overline{\nu}$ = 3167 (w), 3134 (w), 3101 (w), 2949 (s), 2919 (m), 2895 (m), 2862 (m), 1482 (s), 1457 (m), 1395 (m), 1378 (m), 1356 (s), 1266 (s), 1239 (s), 926 (m), 856 (s), 823 (s), 724 (s), 671 (s). UV/vis (*n*-hexane, 22°C, nm): λ (ε, L mol^{-1} cm^{-1}) = 472 (sh, 376), 803 (67). Mp: 168–184°C (decomp.).

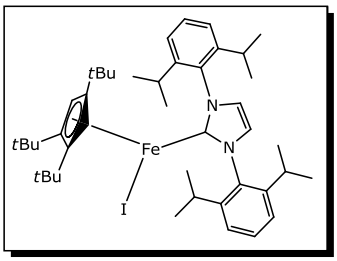

[Cp'Fe(IPr)I]. A pentane (10 mL) solution of IPr (0.117 g, 0.3 mmol) was added dropwise to a pentane (10 mL) solution of $[Cp'FeI]_2$ (0.125 g, 0.15 mmol). The reaction mixture turned into red-orange. After one hour, the product was precipitated directly from the reaction solution as red crystals. Yield: 0.233 g (0.29 mmol, 97%).

Elemental analysis calcd (%) for $C_{44}H_{65}FeIN_2$: C 65.67, H 8.14, N 3.48; found: C 65.86, H 8.26, N 3.41. The EI mass spectrum showed no molecular ion of the compound corresponding to this complex.

IR (ATR; cm^{-1}): $\overline{\nu}$ = 2961 (s), 2925 (m), 2865 (m), 1538 (s), 1457 (s), 1439 (s), 1383 (s), 1356 (s), 1240 (m), 1201 (m), 821 (s), 799 (s), 758 (s), 742 (s), 671 (m). UV/vis (*n*-hexane, 22°C, nm): λ (ε, L mol^{-1} cm^{-1}) = 432 (sh, 509). Mp: 140–180°C (decomp.).

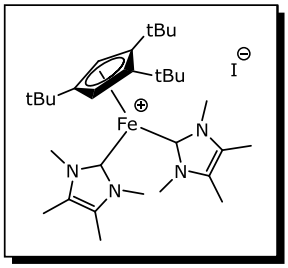

[Cp'Fe(IMeMe$_2$)$_2$]I. A pentane/Et$_2$O (30 mL, 2:1) solution of freshly sublimated IMeMe$_2$ (0.193 g, 1.7 mmol) was added dropwise to a pentane (15 mL) solution of [Cp'FeI]$_2$ (0.291 g, 0.4 mmol). Yellow solid coagulated immediately that was solid was filtered and washed with pantane (10 mL). The product was dried under dynamic vacuum. Yield: 0.368 g (0.6 mmol, 79%).

^{1}H NMR (200.1 MHz, CD_2Cl_2, 300 K, ppm): δ = 15.05 (s, 12H, NHC-backbone-C*H*$_3$, $\nu_{1/2}$ = 12.79 Hz), –2.81 (s, 18H, *t*Bu-*H*, $\nu_{1/2}$ = 50.62 Hz), –6.68 (s, 9H, tBu-*H*, $\nu_{1/2}$ = 55.11 Hz), –14.11 (s, br, 12H, NCH-C*H*$_3$, $\nu_{1/2}$ = 221.32 Hz). Elemental analysis calcd (%) for $C_{31}H_{53}FeIN_4$: C 56.03, H 8.04, N 8.43; found: C 55.56, H 8.01, N 8.41. Mass spectrum (ESI, *m*/*z*) calcd for $C_{31}H_{53}FeN_4^+$: 537.3614; found: 537.3614.

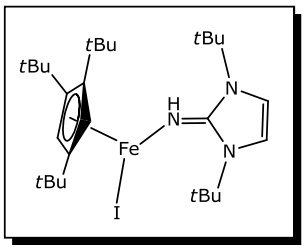

[Cp'Fe(HNI*t*Bu)I]. A Schlenk flask was charged with [Cp'FeI]$_2$ (0.208 g, 0.25 mmol) and HN=I*t*Bu (0.098 g, 0.50 mmol) which was dissolved in THF (15 mL). The reaction mixture was stirred at ambient temperature for 15 hours. The solvent was removed under dynamic vacuum. The product was obtained as a green solid. Yield: 0.185 g (0.31 mmol, 62%). Single crystals suitable for XRD analysis were obtained by recrystallization from concentrated pentane solution at –30°C.

^{1}H NMR (300.1 MHz, C_7D_8, 299 K, ppm): δ = 46.20 (s, br, 2H, NHC-backbone-*H*, $\nu_{1/2}$ = 148.33 Hz), –6.14 (s, br, 18H, NCH-*t*Bu-*H*, $\nu_{1/2}$ = 548.71 Hz), –11.33 (s, br, 18H, ring-*t*Bu-*H*, $\nu_{1/2}$ = 301.41 Hz), –14.31 (s, br, 9H, ring-*t*Bu-*H*, $\nu_{1/2}$ = 363.23 Hz). Elemental analysis calcd (%) for $C_{28}H_{50}FeIN_3$: C 55.00, H 8.24, N 6.87; found: C 54.91, H 8.23, N 6.81. The EI mass spectrum showed no molecular ion of the compound to this complex.

IR (ATR; cm^{-1}): $\overline{\nu}$ = 2954 (m), 2902 (m), 2864 (m), 1538 (s), 1452 (s), 1358 (m), 1238 (m), 1206 (s), 1158 (m), 815 (s), 781 (m), 669 (s). UV/vis (*n*-hexane, 22°C, nm): λ (ε, L mol^{-1} cm^{-1}) = 413 (sh, 509), 783 (63). Mp: 174–184°C (decomp.).

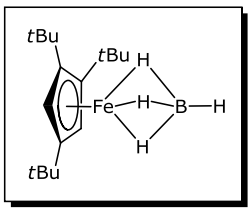

[Cp'FeBH$_4$]. A suspension of NaBH$_4$ (0.019 g, 0.5 mmol) in THF (10 mL) was added to a solution of [Cp'FeI]$_2$ (0.208 g, 0.25 mmol) in THF (10 mL), and stirred at ambient temperature. When the reaction mixture turned violet, the THF solvent was carefully removed under dynamic vacuum into a separate cold trap (without prior filtration).

The product was then isolated as a violet oil by bulb-to-bulb distillation within 20 minutes under dynamic vacuum (0.02 mbar) with gentle heating (*ca.* 50°C). Yield: 0.139 g (0.46 mmol, 92%). B.p. 28°C / 0.02 mbar. Prolonged exposure of the violet oil to dynamic or static vacuum for more than one hour at 50°C induced degradation of [Cp'FeBH$_4$] to [Cp'FeBH$_2$]$_3$. This conversion proceeded *via* one or several intermediates and was accompanied by a color change to dark red brown. [Cp'FeBH$_4$] also degraded to [Cp'FeBH$_2$]$_3$ when stored in pure form under dinitrogen atmosphere at ambient temperature (80% conversion within ten days as judged by ^{1}H and ^{11}B{^{1}H} NMR), but in benzene and THF solution [Cp'FeBH$_4$] was stable for up to 50 days.

^{1}H NMR (300.0 MHz, C$_6$D$_6$, 296 K, ppm): δ = 4.18 (s, 2H, ring-C*H*), 1.54 (s, 18H, *t*Bu-*H*), 1.40 (s, 9H, *t*Bu-*H*), –18.09 (s, br, 4H, B*H*$_4$, $\nu_{1/2}$ = 440.64 Hz). ^{13}C{^{1}H} NMR (75.5 MHz, C$_6$D$_6$, 297 K, ppm): δ = 94.8 (1C, ring-C$_{ipso}$), 93.0 (2C, ring-C$_{ipso}$), 62.9 (2C, ring-*C*H), 34.3 (6C, *t*Bu-*C*H$_3$), 31.9 (3C, *t*Bu-*C*H$_3$), 30.9 (2C, *t*Bu-C$_{ipso}$) 29.2 (1C, *t*Bu-C$_{ipso}$). ^{11}B{^{1}H} NMR (96.3 MHz, C$_6$D$_6$, 297 K, ppm): δ = 2.2. Mass spectrum (ESI, *m*/*z*) calcd for C$_{17}$H$_{33}$BFe: 304.2019; found: 304.2020.

IR (KBr/THF; cm^{-1}): $\overline{\nu}$ = 2584 (m), 2408 (w), 1307 (s). UV/vis (*n*-hexane, 22°C, nm): λ = 237, 243, 248, 254, 260, 297, 540.

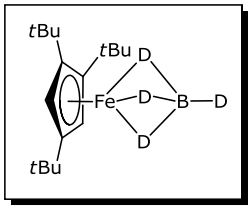

[Cp'FeBD$_4$]. Complex [Cp'FeBD$_4$] was prepared in THF in similar fashion to [Cp'FeBH$_4$] with [Cp'FeI]$_2$ (0.416 g, 0.5 mmol) and NaBD$_4$ (0.042 g, 1.0 mmol). Yield: 0.293 g (0.95 mmol, 95%).

^{1}H NMR (300.0 MHz, C$_6$D$_6$, 266 K, ppm): δ = 4.17 (s, 2H, ring-C*H*), 1.54 (s, 18H, *t*Bu-*H*), 1.40 (s, 9H, *t*Bu-*H*). The corresponding peak at higher field disappeared. Mass spectrum (ESI, *m*/*z*) calcd for C$_{17}$H$_{29}$D$_4$BFe: 308.2271; found: 308.2269.

IR (KBr/THF; cm^{-1}): $\overline{\nu}$ = 1938 (m), 1811 (w), 1741 (s).

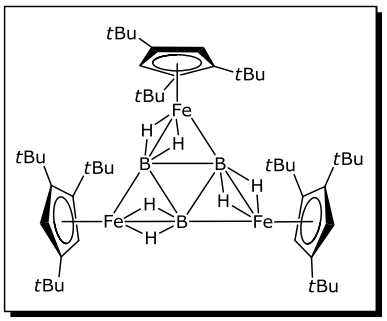

[Cp'FeBH$_2$]$_3$ (dry method). In a Schlenk flask [Cp'FeI]$_2$ (0.208 g, 0.25 mmol) and NaBH$_4$ (0.019 g, 0.5 mmol) were dissolved in THF (20 mL) and stirred at ambient temperature for one hour. During this time the color of the reaction mixture turned deep violet. The solution was filtered, and THF was removed under dynamic vacuum. The purple complex was isolated by bulb-to-bulb distillation and

stored at ambient temperature for one month. During this time, the purple oil solidified and converted into the red-brown compound. The residue was dissolved in Et_2O (*ca.* 3 mL), and slow solvent evaporation yielded small black needles. Yield: 0.114 g (0.12 mmol, 72%).
^1H NMR (400.0 MHz, C_6D_6, 296 K, ppm): δ = 4.45 (s, 6H, ring-C*H*), 1.64 (s, 54H, *t*Bu-*H*), 1.45 (s, 27H, *t*Bu-*H*), –14.22 (s, 6H, BH_2, $\nu_{1/2}$ = 70.74 Hz). $^{13}C\{^1H\}$ NMR (100.7 MHz, C_6D_6, 298 K, ppm): δ = 99.0 (3C, ring-C_{ipso}), 94.9 (6C, ring-C_{ipso}), 73.9 (6C, ring-*C*H), 34.7 (18C, *t*Bu-*C*H_3), 32.6 (9C, *t*Bu-*C*H_3), 32.0 (6C, *t*Bu-C_{ipso}) 30.0 (3C, *t*Bu-C_{ipso}). $^{11}B\{^1H\}$ NMR (128.5 MHz, C_6D_6, 298 K, ppm): δ = 61.8. Elemental analysis calcd (%) for $C_{51}H_{93}B_3Fe_3$: C 67.59, H 10.34; found: C 67.50, H 10.23. The EI mass spectrum showed a molecular ion at m/z = 906 amu and the parent ion isotopic cluster was simulated (calc. %, observd. %): 902 (4, 3), 903 (12, 20), 904 (31, 41), 905 (64, 72), 906 (100, 100), 907 (54, 50), 908 (17, 14), 909 (4, 1).
IR (ATR; cm^{-1}): $\overline{\nu}$ = 2957 (s), 2916 (m), 2866 (m), 2463 (w), 1861 (w, BH_2), 1838 (w, sh), 1483 (m), 1458 (m), 1387 (m), 1360 (s), 1200 (s), 1167 (s, BH_2), 1022 (m), 997 (m), 947 (m), 922 (w), 874 (m), 829 (m), 797 (s), 690 (m), 646 (m). UV/vis (*n*-hexane, 22°C, nm): λ (ε, L mol^{-1} cm^{-1}) = 213 (37493), 261 (27310), 300 (sh, 19689), 447 (9447), 766 (2710). Mp: 224–225°C (decomp.).

[Cp'FeBH$_2$]$_3$ (wet method). In a Schlenk flask [Cp'FeI]$_2$ (3.494 g, 4.2 mmol) and $NaBH_4$ (0.319 g, 8.4 mmol) were dissolved in THF (250 mL) and stirred at ambient temperature for eight hours. During this time the color of the reaction mixture turned deep violet. THF was removed under dynamic vacuum. The remaining violet solid was extracted with pentane (250 mL). The violet extracts were filtered and the pentane solvent was removed under dynamic vacuum. When the solvent was removed, the color of the residue changed to dark brown. The residue was washed with HMDSO until the extracts remained colorless (≈ 100 mL), then dissolved in Et_2O (50 mL). The solution was dark red-brown. Slow solvent evaporation yielded small black needles. Yield: 0.438 g (0.48 mmol, 17%).

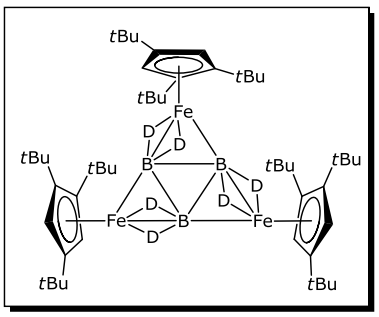

[Cp'FeBD$_2$]$_3$. The same procedure as for synthesis of [Cp'FeBH$_2$]$_3$ (according to wet method) was performed with [Cp'FeI]$_2$ (1.332 g, 1.6 mmol) and $NaBD_4$ (0.136 g, 3.2 mmol) instead of $NaBH_4$. Yield: 0.241 g (0.26 mmol, 24%).
^1H NMR (400.0 MHz, C_6D_6, 297 K, ppm): δ = 4.46 (s, 6H, ring-C*H*), 1.65 (s, 54H, *t*Bu-*H*), 1.46 (s, 27H, *t*Bu-*H*). The

corresponding peak at higher field disappeared. The EI mass spectrum showed a molecular ion at m/z = 912 amu and the parent ion isotopic cluster was simulated (calc. %, observd. %): 907 (1, 2), 908 (3, 10), 909 (12, 16), 910 (31, 37), 911 (64, 69), 912 (100,100), 913 (54, 50), 914 (17, 11), 915 (4, 1).

IR (ATR; cm^{-1}): $\tilde{\nu}$ = 2953 (m), 2921 (w), 2901 (w), 2865 (w), 1483 (w, BD_2), 1458 (w), 1360 (m), 1244 (m), 1231 (w), 1168 (w), 1012 (s), 995 (s, BD_2), 947 (w), 874 (w), 645 (w).

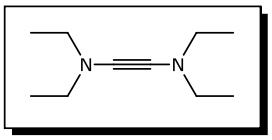

$(Et_2N)_2C{\equiv}C(NEt_2)_2$. A solution of $LiNEt_2$ (3.95 g, 50 mmol) in Et_2O (50 mL) was added dropwise into a solution of trichloroethylene (6.57 g, 4.50 mL, 50 mmol) in Et_2O (50 mL) at –78°C over one hour. The color of the reaction mixture turned from yellow into orange, and a colorless precipitate was formed. After the addition of the lithium amide solution, the mixture was stirred for two hours. Meanwhile the temperature was allowed to rise to room temperature. Then the reaction mixture was cooled to –78°C again and the second lithium amide solution (3.95 g, 50 mmol) in Et_2O (50 mL) was added dropwise into the first step over one hour. The temperature was kept at –78°C during the lithium amide solution was added. The reaction mixture was warmed to room temperature while the mixture was stirred for two hours. The color of reaction mixture turned into red-brown. The reaction mixture was concentrated to 50 mL, and then the reaction mixture was cooled to –78°C. The third lithium amide solution (4.35 g, 55 mmol) in Et_2O (50 mL) was added via dropping funnel into the second step at this temperature over one hour. The temperature was kept at –78°C for two hours and then allowed to rise to room temperature. The precipitate was filtered off and the solvent was removed under dynamic vacuum. The crude product was purified by distillation (27°C, 0.04 mbar) to obtain a colorless fluid. Yield: 4.00 g (24 mmol), 48%.

^1H NMR (200.1 MHz, C_6D_6, 300 K, ppm): δ = 2.75 (q, 4H, CH_2), 1.14 (t, 6H, CH_3). $^{13}C\{^1H\}$ NMR (50.3 MHz, C_6D_6, 300 K, ppm): δ = 74.4 (2C, $C{\equiv}C$), 50.1 (2C, CH_2), 13.5 (2C, CH_3). GC-MS: m/z = 168 (M^+).

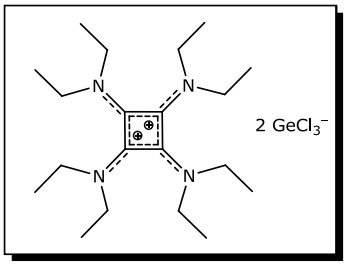

$[(Et_2N)_4C_4][GeCl_3]_2$. Bis(*N*,*N*-diethylamino)acetylene (0.084 g, 0.5 mmol) was dissolved in toluene (2.5 mL). This solution was added into a suspension of $GeCl_2$·dioxane (0.463 g, 2 mmol) toluene (2.5 mL) and stirred over night. Slow evaporation of the solvent at room temperature afforded the product as

yellow crystals. Yield: 0.007 g, (10 μmol, 2%).

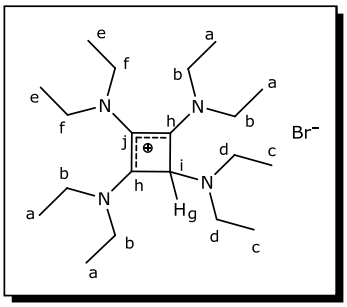

[(Et$_2$N)$_4$C$_4$H]Br. NEt$_3$·HBr (1.18 g, 7 mmol) dissolved in chloroform (6 mL) was added dropwise to bis(*N*,*N*-diethylamino)acetylene (2.19 g, 13 mmol) in chloroform (7 mL) at –50°C within ten minutes. While the reaction mixuture was stirred for fifteen hours, the temperature was arrowed to rize to ambient temperature. All volatile components were removed under reduced pressure. The residue was dissolved in ethyl acetate (1 mL) and cooled to –30°C. The product was obtained as colorless crystals. Yield: 2.08 g (5 mmol, 70%).

^{1}H NMR (600.1 MHz, $CDCl_3$, 301 K, ppm): δ = 5.06 (s, 1H, H_g), 3.76 (m, 2H, H_d, J = 7.24 Hz), 3.64 (m, 4H, $H_{f,d}$, J = 7.17 Hz), 3.42 (m, 2H, H_f, J = 7.22 Hz), 2.78 (q, 8H, H_b, J = 7.20 Hz), 1.27 (t, 6H, H_e, J = 7.34 Hz), 1.25 (t, 6H, H_c, J = 7.34 Hz), 1.02 (t, 6H, H_a, J = 7.14 Hz). ^{13}C{^{1}H} NMR (100.7 MHz, $CDCl_3$, 297 K, ppm): δ = 173.5 (2C, C_h), 115.5 (1C, C_j), 66.3 (1C, C_i), 48.3 (4C, C_b), 44.7 (2C, C_f), 43.5 (2C, C_d), 15.4 (2C, C_a), 14.4 (2C, C_a), 14.0 (2C, C_e), 13.1 (2C, C_c). Elemental analysis calcd (%) for $C_{20}H_{41}BrN_4$: C 57.54, H 9.90, N 13.42; found: C 57.54, H 9.99, N 13.00. Mass spectrum (ESI, *m*/*z*) calcd for $C_{20}H_{41}N_4^+$: 337.3326; found: 337.3319.

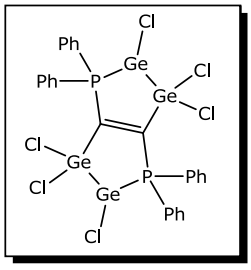

[PPh$_2$(GeCl)(GeCl$_2$)C]$_2$. Bis(diphenylphosphino)acetylene (0.197 g, 0.5 mmol) was dissolved in toluene (2.5 mL). This solution was added into a suspension of GeCl$_2$·dioxane (0.463 g, 2 mmol) toluene (2.5 mL) and stirred over night. During this time, an orange precipitate was formed. This solid was filtered off. Slow evaporation of the solvent at room temperature afforded the product as yellow crystals. Yield: 0.021 g (23 μmol, 12%).

^{1}H NMR (200.1 MHz, C_6D_6, 296 K, ppm): δ = 7.69 (m, 8H, *o*-C*H*), 6.98 (m, 12H, *m*-C*H* and *p*-C*H*). ^{13}C{^{1}H} NMR (50.3 MHz, C_6D_6, 297 K, ppm): δ = 133.2 (8C, *o*-CH), 130.2 (4C, *p*-CH), 129.2 (8C, *m*-CH), 106.5 (2C, *C*=C). ^{31}P{^{1}H} NMR (81.0 MHz, C_6D_6, 297 K, ppm): δ = 31.4. Elemental analysis calcd (%) for $C_{26}H_{20}Cl_6Ge_4P_2$: C 34.79, H 2.25; found: C 35.47, H 2.42. Neither the EI nor ESI mass spectrum showed the molecular ion of the compound to this complex.

References

(1) Connelly, N. G.; Geiger, W. E. *Chem. Rev.* **1996**, *96*, 877–910.

(2) Bill, E. julX http://ewww.mpi-muelheim.mpg.de/bac/logins/bill/julX_en.php.

(3) Job, R.; Earl, R. *Inorg. Nucl. Chem. Lett.* **1979**, *15*, 81–83.

(4) Stolz, P.; Pohl, S. *Z. Naturforsch.* **1988**, *43b*, 175–181.

(5) Pohl, S.; Saak, W. *Z. Naturforsch.* **1984**, *39b*, 1236–1240.

(6) Schneider, J. J.; Goddard, R.; Krüger, C. *Z. Naturforsch.* **1995**, *50b*, 448–459.

(7) Ellern, J. B.; Ragsdale, R. O.; Allen, R. J.; Chatterjee, A. B.; Martin, D. F. *Inorg. Synth.* **1968**, *11*, 82–89.

(8) Walter, M. D.; White, P. S. *New J. Chem.* **2011**, *35*, 1842–1854.

(9) Maekawa, M.; Römelt, M.; Daniliuc, C. G.; Jones, P. G.; White, P. S.; Neese, F.; Walter, M. D. *Chem. Sci.* **2012**, *3*, 2972–2979.

(10) Arduengo, A. J.; Bock, H.; Chen, H.; Denk, M.; Dixon, D. A.; Green, J. C.; Herrmann, W. A.; Jones, N. L.; Wagner, M.; West, R. *J. Am. Chem. Soc.* **1994**, *116*, 6641–6649.

(11) Tamm, M.; Petrovic, D.; Randoll, S.; Beer, S.; Bannenberg, T.; Jones, P. G.; Grunenberg, J. *Org. Biomol. Chem.* **2007**, *5*, 523–530.

(12) Kuhn, N.; Kratz, T. *Synthesis* **1993**, 561–562.

(13) Hintermann, L. *Beilstein J. Org. Chem.* **2007**, *3*, 22.

(14) Bryce-Smith, D.; Howlett, K. E. *J. Chem. Soc.* **1951**, 1141–1142.

(15) Masada, H.; Murotani, Y. *Bull. Chem. Soc. Jpn.* **1980**, *53*, 1181–1182.

(16) Walter, M. D.; Sofield, C. D.; Booth, C. H.; Andersen, R. A. *Organometallics* **2009**, *28*, 2005–2019.

(17) Möller, A. C.; Blom, R.; Heyn, R. H.; Swang, O.; Görbitz, C.-H.; Seraidaris, T. *Eur. J. Inorg. Chem.* **2005**, 1759–1769.

(18) Honzíček, J.; Romão, C. C.; Calhorda, M. J.; Mukhopadhyay, A.; Vinklárek, J.; Padeľková, Z. *Organometallics* **2011**, *30*, 717–725.

(19) Ready, T. E.; Chien, J. C. W.; Rausch, M. D. *J. Organomet. Chem.* **1996**, *519*, 21–28.

On ne découvre pas la vérité : on la crée.
<Terre des hommes>
– Antoine de Saint-Exupéry (1900 – 1944)

Crystallographic data

	[($^{2t\text{Bu}}$Ind)$_2$Mn]	**[($^{2\text{Cy}}$Ind)$_2$Mn]**	**[($^{2t\text{Bu}}$Ind)$_2$Fe]**
Identification code	mima14	mima17	mima13
Empirical formula	$C_{34}H_{46}Mn$	$C_{42}H_{54}Mn$	$C_{34}H_{46}Fe$
Formula weight	509.65	613.79	510.56
Color	red	orange	dark green
Description	prism	prism	prism
Crystal system	monoclinic	triclinic	monoclinic
Space group	$P\,2_1/c$	$P\,\bar{1}$	$P\,2_1/c$
a/Å	17.9709(4)	13.3587(6)	18.3520(4)
b/Å	9.6949(2)	15.8419(6)	9.6436(2)
c/Å	18.0377(2)	16.6358(6)	17.7391(4)
α/°	90	99.248(4)	90
β/°	114.575(2)	92.509(2)	116.946(4)
γ/°	90	101.347(4)	90
Unit cell volume/Å^3	2857.97(9)	3396.6(2)	2798.62(11)
No. of formula units per unit cell, Z	4	4	4
Temperature/K	100(2)	100(2)	100(2)
Absorption coefficient, μ/mm^{-1}	3.875	3.346	0.559
Radiation Type	Cu Kα	Cu Kα	Mo Kα
Theta range/°	4.93 – 75.85	3.60 – 76.19	2.30 – 27.88
No. of reflections measured	37822	35598	109058
No. of independent reflections	5934	13623	6673
R_{int}	0.0337	0.0869	0.0526
Final R_1 values ($I > 2\sigma(I)$)	0.0285	0.0742	0.0266
Final $wR(F^2)$ values (all data)	0.0774	0.2185	0.0626
Goodness of fit on F^2	1.074	1.022	0.933
Structure solved by	C. G. Daniliuc	C. G. Daniliuc	C. G. Daniliuc

	[(^{2Cy}Ind)$_2$Fe]	**[(^{2fBu}Ind)$_2$Co]**	**[(^{2Cy}Ind)$_2$Co]**
Identification code	mima05	mima29a	mima51
Empirical formula	$C_{42}H_{54}Fe$	$C_{34}H_{46}Co$	$C_{60}H_{54}D_{18}Co$
Formula weight	614.70	513.64	870.22
Color	dark blue	red	red-orange
Description	prism	prism	prism
Crystal system	monoclinic	monoclinic	monoclinic
Space group	*P* $2_1/c$	*P* $2_1/c$	*P* $2_1/c$
a/Å	10.1411(2)	18.1912(12)	13.0890(5)
b/Å	15.4986(2)	9.6645(4)	14.2424(5)
c/Å	21.3658(4)	17.7952(10)	13.4791(7)
α/°	90	90	90
β/°	101.712(2)	116.869(8)	110.734(5)
γ/°	90	90	90
Unit cell volume/Å^3	3288.21(10)	2790.8(3)	2350.03(17)
No. of formula units per unit cell, *Z*	4	4	2
Temperature/K	100(2)	100(2)	100(2)
Absorption coefficient, μ/mm^{-1}	3.870	4.943	3.135
Radiation Type	Cu Kα	Cu Kα	Cu Kα
Theta range/°	3.55 – 75.88	4.97 – 74.47	3.61 – 72.98
No. of reflections measured	45481	31069	31069
No. of independent reflections	6830	5697	4662
R_{int}	0.0454	0.0359	0.1048
Final R_1 values ($I > 2\sigma(I)$)	0.0341	0.0283	0.0497
Final $wR(F^2)$ values (all data)	0.0888	0.0734	0.1297
Goodness of fit on F^2	1.086	1.069	1.030
Structure solved by	C. G. Daniliuc	C. G. Daniliuc	M. Freytag

	[(^{2fBu}Ind)Fe(CO)$_2$I]	**[(Cp′)(^{2fBu}Ind)Fe]**	**[(Cp′)Fe(CO)$_2$I]**
Identification code	mima53	mima34	mima52
Empirical formula	$C_{19}H_{23}FeIO_2$	$C_{34}H_{52}Fe$	$C_{19}H_{29}FeIO_2$
Formula weight	466.12	516.61	472.17
Color	yellow-dark brown dichroic	dark violet	brown-violet dichroic
Description	prism	prism	needle
Crystal system	orthorhombic	monoclinic	orthorhombic
Space group	$P\ 2_12_12_1$	$P\ 2_1/n$	$P\ c\ a\ 2_1$
a/Å	8.49836(10)	12.5774(2)	15.3534(3)
b/Å	13.6127(2)	15.1552(2)	10.4548(2)
c/Å	16.3850(2)	15.4685(2)	12.3471(3)
α/°	90	90	90
β/°	90	96.108(2)	90
γ/°	90	90	90
Unit cell volume/Å^3	1895.50(4)	2931.76(7)	1981.92(7)
No. of formula units per unit cell, Z	4	4	4
Temperature/K	100(2)	100(2)	100(2)
Absorption coefficient, μ/mm^{-1}	19.210	0.534	18.373
Radiation Type	Cu Kα	Mo Kα	Cu Kα
Theta range/°	4.22 – 75.77	2.21 – 27.87	4.23 – 75.87
No. of reflections measured	58426	112119	49188
No. of independent reflections	3948	6986	3932
R_{int}	0.0655	0.0532	0.0983
Final R_1 values ($I > 2\sigma(I)$)	0.0193	0.0322	0.0277
Final $wR(F^2)$ values (all data)	0.0501	0.0816	0.0712
Goodness of fit on F^2	1.078	1.022	1.039
Structure solved by	M. Freytag	C. G. Daniliuc	M. Freytag

	[Cp′CoCl]$_2$	**[Cp′CoBr]$_2$**	**[Cp′CoI]$_2$**
Identification code	mima59	mima60	mima55
Empirical formula	$C_{34}H_{58}Cl_2Co_2$	$C_{34}H_{58}Br_2Co_2$	$C_{34}H_{58}Co_2I_2$
Formula weight	655.56	744.48	838.46
Color	brown/dark-turquoise dichroic	dark red	black
Description	block	needle	black
Crystal system	monoclinic	triclinic	monoclinic
Space group	*P n*	$P\bar{1}$	$P\,2_1/c$
a/Å	12.0706(2)	10.3508(10)	13.9563(3)
b/Å	10.2866(2)	12.1789(12)	18.6294(2)
c/Å	27.7809(6)	13.8739(14)	15.1111 (2)
α/°	90	87.656(8)	90
β/°	91.751(2)	89.234(8)	115.551(2)
γ/°	90	89.238(8)	90
Unit cell volume/Å^3	3447.82(12)	1747.2(3)	3544.59(5)
No. of formula units per unit cell, *Z*	4	2	4
Temperature/K	100(2)	100(2)	100(2)
Absorption coefficient, μ/mm^{-1}	1.137	3.256	2.698
Radiation Type	Mo Kα	Mo Kα	Mo Kα
Theta range/°	2.46 – 30.03	2.18 – 26.37°	2.65 – 30.94
No. of reflections measured	126765	32504	253662
No. of independent reflections	19773	6333	10847
R_{int}	0.0567	0.1240	0.0481
Final R_1 values ($I > 2\sigma(I)$)	0.0401	0.0366	0.0228
Final $wR(F^2)$ values (all data)	0.0848	0.0552	0.0440
Goodness of fit on F^2	1.037	0.720	1.070
Structure solved by	M. Freytag	M. Freytag	M. Freytag

	[(Cp′Co)$_2$(CH)(H)]	**[Cp′CoH]$_2$**	**[Cp′Fe(CO)$_2$]$_2$**
Identification code	mima58	mima61	mima54
Empirical formula	$C_{35}H_{60}Co_2$	$C_{34}H_{60}Co_2$	$C_{38}H_{58}Fe_2O_4$
Formula weight	598.69	586.68	690.54
Color	black	black	black
Description	fragment	fragment	tablet
Crystal system	tetragonal	tetragonal	triclinic
Space group	$P\,4_32_12$	$P\,4_12_12$	$P\,\bar{1}$
a/Å	8.99363(10)	9.0208(2)	11.0245(7)
b/Å	8.99363(10)	9.0208(2)	12.0149(7)
c/Å	40.6602(8)	40.167(2)	14.7311(8)
α/°	90	90	93.174(5)
β/°	90	90	91.734(5)
γ/°	90	90	113.619(6)
Unit cell volume/Å^3	3288.81(8)	3268.60(19)	1782.11(18)
No. of formula units per unit cell, Z	4	4	2
Temperature/K	100(2)	100(2)	100(2)
Absorption coefficient, μ/mm^{-1}	8.025	1.034	6.809
Radiation Type	Cu Kα	Mo Kα	Cu Kα
Theta range/°	4.35 – 76.36	2.31 – 28.51	4.03 – 76.07
No. of reflections measured	86262	24106	49198
No. of independent reflections	3434	3882	7386
R_{int}	0.0675	0.0461	0.0740
Final R_1 values ($I > 2\sigma(I)$)	0.0236	0.0313	0.0329
Final $wR(F^2)$ values (all data)	0.0539	0.0614	0.0873
Goodness of fit on F^2	1.053	1.088	1.054
Structure solved by	M. Freytag	M. Freytag	M. Freytag

	[Cp′FeS$_2$]$_2$	**[Cp′Fe(NCO)]$_2$**	**[Cp′Mn(NCS)(thf)]$_2$**
Identification code	mima62	mima21	mima40
Empirical formula	$C_{34}H_{58}Fe_2S_4$	$C_{18}H_{29}FeNO$	$C_{44}H_{74}Mn_2N_2O_2S_2$
Formula weight	706.74	331.27	837.05
Color	black	green	yellow
Description	block	prism	prism
Crystal system	triclinic	monoclinic	monoclinic
Space group	$P\,\bar{1}$	$P\,2_1/n$	$P\,2_1/c$
a/Å	10.0731(3)	10.3424(4)	14.2094(2)
b/Å	12.2254(3)	9.2633(2)	8.9328(2)
c/Å	16.5630(5)	18.3885(6)	18.3244(2)
α/°	80.822(3)	90	90
β/°	77.884(3)	91.346(2)	96.406(2)
γ/°	66.822(3)	90	90
Unit cell volume/Å^3	1826.57(9)	1761.22(10)	2311.39(7)
No. of formula units per unit cell, Z	2	4	2
Temperature/K	100(2)	100(2)	100(2)
Absorption coefficient, μ/mm^{-1}	1.044	6.839	0.671
Radiation Type	Mo Kα	Cu Kα	Mo Kα
Theta range/°	2.23 – 30.91°	4.81 – 75.76	2.24 – 29.13
No. of reflections measured	139454	17685	96748
No. of independent reflections	10910	3658	6212
R_{int}	0.0491	0.0335	0.0452
Final R_1 values ($I > 2\sigma(I)$)	0.0373	0.0270	0.0335
Final $wR(F^2)$ values (all data)	0.0924	0.0701	0.0829
Goodness of fit on F^2	1.042	1.078	1.029
Structure solved by	M. Freytag	C. G. Daniliuc	C. G. Daniliuc

	[Cp′FeS]$_2$	**[Cp′Fe(Se$_2$)]$_2$**	**[Cp′FeN]$_2$**
Identification code	c09311	mima45	c07223
Empirical formula	$C_{34}H_{58}Fe_2S_2$	$C_{34}H_{58}Fe_2Se_4$	$C_{34}H_{58}Fe_2N_2$
Formula weight	642.62	894.34	606.52
Color	red-brown	dark orange	green
Description	block	plate	block
Crystal system	monoclinic	monoclinic	tetragonal
Space group	*P n*	*P* $2_1/n$	*P* 4_12_12
a/Å	11.8379(7)	13.0954(4)	8.9474(3)
b/Å	10.3374(6)	18.8412(6)	8.9474(3)
c/Å	27.9872(19)	15.8088(6)	41.253(4)
α/°	90	90	90
β/°	91.744(4)	107.643(4)	90
γ/°	90	90	90
Unit cell volume/Å^3	3423.3(4)	3717.1(2)	3302.6(4)
No. of formula units per unit cell, *Z*	4	4	4
Temperature/K	100(2)	100(2)	100(2)
Absorption coefficient, μ/mm^{-1}	8.066	4.718	0.902
Radiation Type	Cu Kα	Mo Kα	Mo Kα
Theta range/°	3.16 – 68.44	2.16 – 26.37	2.33 – 24.43
No. of reflections measured	54891	126169	19222
No. of independent reflections	9986	7605	2957
R_{int}	0.0577	0.1059	0.0486
Final R_1 values ($I > 2\sigma(I)$)	0.0406	0.0356	0.0356
Final $wR(F^2)$ values (all data)	0.0992	0.0741	0.0741
Goodness of fit on F^2	1.056	1.039	1.039
Structure solved by	M. D. Walter	C. G. Daniliuc	M. D. Walter

	[$FeI_2(ItBu)_2$]	**[$FeI_2(HNItBu)_2$]**	**[Cp′Fe(I*t*Bu)I]**
Identification code	mima28	mima23	mima32
Empirical formula	$C_{22}H_{40}FeI_2N_4$	$C_{26}H_{50}FeI_2N_6O$	$C_{28}H_{49}FeIN_2$
Formula weight	670.23	772.37	596.44
Color	yellow	pale violet	yellow
Description	prism	prism	plate
Crystal system	monoclinic	monoclinic	monoclinic
Space group	*P* $2_1/n$	*C* 2/*c*	*C* 2/*c*
a/Å	12.5890(2)	23.6876(14)	26.809(5)
b/Å	16.9877(4)	9.0347(2)	15.1557(16)
c/Å	13.1820(4)	19.0810(12)	16.959(3)
α/°	90	90	90
β/°	92.311(2)	127.139(8)	120.93(2)
γ/°	90	90	90
Unit cell volume/$Å^3$	2816.78(12)	3255.3(3)	5910.8(15)
No. of formula units per unit cell, *Z*	4	4	8
Temperature/K	100(2)	100(2)	100(2)
Absorption coefficient, μ/mm^{-1}	2.742	2.388	12.397
Radiation Type	Mo Kα	Mo Kα	Cu Kα
Theta range/°	2.19 – 27.48	2.20 – 29.13	3.49 – 70.07
No. of reflections measured	84096	44001	39142
No. of independent reflections	6454	4380	5623
R_{int}	0.0321	0.0289	0.1274
Final R_1 values ($I > 2\sigma(I)$)	0.0190	0.0159	0.0544
Final $wR(F^2)$ values (all data)	0.0436	0.0352	0.1304
Goodness of fit on F^2	1.082	1.072	1.036
Structure solved by	C. G. Daniliuc	C. G. Daniliuc	C. G. Daniliuc

	[Cp′Fe(I*i*PrMe$_2$)I]	**[Cp′Fe(IMes)I]**	**[Cp′Fe(IPr)I]**
Identification code	mima31	mima33	mima44
Empirical formula	$C_{28}H_{49}FeIN_2$	$C_{38}H_{53}FeIN_2$	$C_{44}H_{65}FeIN_2$
Formula weight	596.44	720.57	804.73
Color	olive green	orange	orange
Description	prism	prism	prism
Crystal system	monoclinic	monoclinic	orthorhombic
Space group	*P* $2_1/n$	*P* $2_1/c$	*P b c a*
a/Å	9.35317(12)	9.7691(4)	18.4790(4)
b/Å	18.27596(18)	38.5982(14)	16.7584(2)
c/Å	17.01417(16)	9.6194(4)	26.7961(4)
α/°	90	90	90
β/°	95.7372(8)	99.676(4)	90
γ/°	90	90	90
Unit cell volume/Å^3	2893.80(5)	3575.6(2)	8298.2(2)
No. of formula units per unit cell, *Z*	4	4	8
Temperature/K	100(2)	100(2)	100(2)
Absorption coefficient, μ/mm^{-1}	1.605	1.312	8.970
Radiation Type	Mo Kα	Mo Kα	Cu Kα
Theta range/°	2.23 – 28.28	2.18 – 27.48	3.30 – 74.49
No. of reflections measured	141565	139395	101789
No. of independent reflections	7192	8201	8484
R_{int}	0.0359	0.0748	0.0607
Final R_1 values ($I > 2\sigma(I)$)	0.0175	0.0582	0.0267
Final $wR(F^2)$ values (all data)	0.0406	0.0978	0.0649
Goodness of fit on F^2	1.051	1.329	1.034
Structure solved by	C. G. Daniliuc	C. G. Daniliuc	C. G. Daniliuc

	[Cp′Fe(IMeMe$_2$)$_2$]I	**[Cp′Fe(HNI*t*Bu)I]**	**[Cp′Fe(BH$_2$)]$_3$**
Identification code	mima50	mima49	mima48
Empirical formula	$C_{39}H_{69}FeIN_4O_2$	$C_{28}H_{50}FeIN_3$	$C_{51}H_{93}B_3Fe_3$
Formula weight	808.73	611.46	906.23
Color	yellow-brown dichroic	yellow	brown
Description	cut prism	plate	plate
Crystal system	triclinic	orthorhombic	triclinic
Space group	$P\bar{1}$	$Pca2_1$	$P\bar{1}$
a/Å	10.5233(3)	20.9140(2)	10.4329(6)
b/Å	11.2527(3)	9.1358(2)	11.8658(8)
c/Å	18.2331(8)	32.0195(4)	21.0042(14)
α/°	104.031(3)	90	93.444(6)
β/°	93.261(3)	90	92.261(6)
γ/°	98.580(3)	90	99.280(6)°
Unit cell volume/Å^3	2061.45(12)	6117.84(16)	2558.4(3)
No. of formula units per unit cell, Z	2	8	2
Temperature/K	100(2)	100(2)	100(2)
Absorption coefficient, μ/mm^{-1}	1.150	12.000	0.870
Radiation Type	Mo Kα	Cu Kα	Mo Kα
Theta range/°	2.31 – 28.28°	4.23 – 74.50	2.25 – 26.73
No. of reflections measured	123110	78666	86448
No. of independent reflections	10196	11133	10850
R_{int}	0.0440	0.0400	0.1162
Final R_1 values ($I > 2\sigma(I)$)	0.0380	0.0495	0.0490
Final $wR(F^2)$ values (all data)	0.0843	0.1307	0.0923
Goodness of fit on F^2	1.081	1.045	1.016
Structure solved by	M. Freytag	C. G. Daniliuc	C. G. Daniliuc

	$[(Et_2N)_4C_4][GeCl_3]_2$	**$[(Et_2N)_4C_4H]Br$**	**$[PPh_2(GeCl)(GeCl_2)C]_2$**
Identification code	mima02	mima07	mima01
Empirical formula	$C_{20}H_{40}Cl_6Ge_2N_4$	$C_{20}H_{41}BrN_4$	$C_{26}H_{20}Cl_6Ge_4P_2$
Formula weight	694.44	417.48	897.42
Color	pale yellow	colourless	yellow
Description	prism	prism	prism
Crystal system	monoclinic	monoclinic	triclinic
Space group	*C* 2/*c*	*P* 2_1/*c*	*P* $\bar{1}$
a/Å	19.8137(4)	19.5545(2)	9.6191(6)
b/Å	14.4608(2)	13.9938(2)	9.6583(6)
c/Å	11.6559(2)	16.9296(2)	10.6653(6)
α/°	90	90	115.299(6)
β/°	110.862(2)	98.87	90.763(4)
γ/°	90	90	113.880(6)
Unit cell volume/Å^3	3120.72(9)	4577.21(10)	798.06(8)
No. of formula units per unit cell, *Z*	4	8	1
Temperature/K	100(2) K	100(2)	100(2)
Absorption coefficient, μ/mm^{-1}	2.456	2.502	4.350
Radiation Type	Mo Kα	Cu Kα	Mo Kα
Theta range/°	2.20 – 27.48	3.90 – 75.99	2.38 – 26.37
No. of reflections measured	58252	64372	19917
No. of independent reflections	3570	9486	3255
R_{int}	0.0332	0.0322	0.0305
Final R_1 values ($I > 2\sigma(I)$)	0.0177	0.0311	0.0208
Final $wR(F^2)$ values (all data)	0.0401	0.0882	0.0543
Goodness of fit on F^2	0.931	1.097	1.013
Structure solved by	C. G. Daniliuc	C. G. Daniliuc	C. G. Daniliuc

Der liebe Gott steckt im Detail.

– Abraham Moritz Warburg (1866 – 1929)

Miyuki MAEKAWA, Dipl.-Chem.

miyuki.maekawa@alumni-uni-hannover.de